THE PHYSICAL REVIEW

A journal of experimental and theoretical physics established by E. L. Nichols in 1893

Published by the American Institute of Physics
for the
AMERICAN PHYSICAL SOCIETY

Officers

President

F. W. Loomis
University of Illinois
Urbana, Illinois

Vice-President

I. I. Rabi
Columbia University
New York, New York

Secretary

K. K. Darrow
Bell Telephone Laboratories
Office:
Columbia University
New York 27, New York

Treasurer

G. B. Pegram
Columbia University
New York 27, New York

Local Secretary
for the Pacific Coast

J. Kaplan
University of California at Los Angeles
Los Angeles, California

Managing Editor

John T. Tate
University of Minnesota
Minneapolis, Minnesota

BOARD OF EDITORS

Associate Editors

S. A. Goudsmit — W. E. Lamb, Jr.
E. M. Purcell — R. G. Sachs
V. F. Weisskopf — J. Schwinger

Papers for publication should be submitted to John T. Tate, [illegible] University of Minnesota, Minneapolis, Minnesota. The authors' Institutions are asked to pay a publication charge of $4 per page which, if honored, entitles them to 100 free reprints. Instructions will be sent with galley proofs.

All other correspondence concerning papers in the process of publication should be addressed to the Publication Manager, American Institute of Physics, Inc., Suite 55 Series, New York 22, New York.

Subscription Price

United States and Canada $25.00
Foreign $27.00

Back Numbers[1]

Back number rate when complete year is available:
Prior to 1949: $20.00
Thereafter: $27.00
Single issues: $2.00 each, prior to July, 1929;
$3.00 each, July, 1929–December, 1941;
$2.00 each, January, 1942–December, 1946;
$3.00 each, January, 1947–December, 1949.
Single issues, 1950: $1.25 each.
Volumes, 1893–1930: $4.00.

Orders and claims for back numbers should be addressed to Physical Review, Lancaster, Pennsylvania, or to the American Institute of Physics, Suite 55 Series, New York 22, New York.

Claims for missing numbers will be allowed (1) if received within sixty days from the date of issue, (2) if the notice states that the publication has been lost in the mails, and (3) if the claimant is a subscriber in the territory served by the publication office. Claims for missing numbers in the case of members of the American Physical Society should be addressed to the Treasurer; in the case of other subscribers to the Secretary, American Institute of Physics.

Address changes should reach the Physical Review Business Office, Cornell University, Ithaca, New York, by the first of the month preceding the month of issue. Please give both old and new addresses.

The Physical Review is published monthly by the American Institute of Physics and Lancaster Press, Inc., Lancaster, Pennsylvania.

Entered as second-class matter March 26, 1918, at the Post Office at Lancaster, Pennsylvania, under the Act of March 3, 1879.

Acceptance for mailing at special rate of postage provided for in Section 1103, paragraph 4, section 538, P. L. & R., authorized January 17, 1925.

THE
PHYSICAL REVIEW

A journal of experimental and theoretical physics established by E. L. Nichols in 1893

SECOND SERIES, VOL. 76, NO. 4 AUGUST 15, 1949

The Elastic Scattering of Electrons by Neutral Hydrogen Atoms by the Variational Method

SU-SHU HUANG
Yerkes Observatory, University of Chicago, Williams Bay, Wisconsin
(Received April 30, 1949)

Two variational methods are proposed for computing the phase shifts for an electron scattered by a neutral atom. These methods are shown to be different formulations of the same physical principle, i.e., the stationary property of the phase shift. By applying one of these methods to the S scattering of an electron by a hydrogen atom, the phase shifts are computed for various kinetic energies. A comparison is finally made with the results which Morse and Allis have derived from the solution of the Fock equation.

I. INTRODUCTION

THE problem of the elastic scattering of electrons by hydrogen atoms has been considered by Chandrasekhar and Breen,[1] Massey and Mohr,[2] McDougall,[3] and Morse and Allis.[4] While the latter authors solved the appropriate Fock equations[5] and determined the phase shifts, the others used the Hartree field. As both the Fock equation and the Hartree field are derived from a variational principle on the assumption that the coordinates of the free and the bound electron are separable, it would be of interest to see if one can formulate a similar principle without such an assumption. For the case of S states, the author has shown that[6] such a formulation is feasible. And the use of this later variation method has the further advantage that the numerical work involved is much less than is required for the solution of the Fock equation.

The method we shall adapt is an extention of the work done by Hulthén[7] and by Tamm.[8] Both of these authors have treated nuclear scattering and consequently limited the problem to the encounter of two particles. In the problem which we propose to consider, three particles are involved in each encounter; a more general formulation of the variational principles of Hulthén and Tamm is necessary. We shall formulate the necessary generalization. It may also be stated here that of the two formulations, that of Hulthén appears to be the more general while Tamm's has the merit of being more simple and direct.

We shall first present these two formulations in their generalized forms and then show their equivalence. Finally, we shall illustrate the principles by considering the S-scattering of free electrons by a neutral hydrogen atom in the ground state.

II. THE VARIATIONAL PRINCIPLE

If we adopt the Bohr radius and Rh as the unit of length and of energy, respectively, the wave equation corresponding to a free electron in the field of a neutral hydrogen atom is

$$(L-E)\psi=0, \tag{1}$$

where

$$L=-\nabla_1^2-\nabla_2^2-2/r_1-2/r_2+2/r_{12}. \tag{2}$$

The effect of the term in r_{12} has been mostly neglected; and we are particularly interested in it. However, this term does not affect the formulation of the variational principle. Insofar as the potential field in which the free electron is moving tends to zero faster than $1/r^p$ (where $p>1$) for $r\to\infty$ (this is evidently the case for motion of an electron in the field of a neutral atom), we can write

[1] S. Chandrasekhar and F. H. Breen, Astrophys. J. **103**, 41 (1946).
[2] H. S. W. Massey and C. B. O. Mohr, Proc. Roy. Soc. **A136**, 289 (1932).
[3] J. McDougall, Proc. Roy. Soc. **A136**, 549 (1932).
[4] P. M. Morse and W. P. Allis, Phys. Rev. **44**, 269 (1933).
[5] V. Fock, Zeits. f. Physik **61**, 126 (1930).
[6] S. S. Huang, Phys. Rev. **75**, 980 (1949).
[7] L. Hulthén, K. Fysiogr. Sällsk. Lund Förhandl. **14**, No. 21 (1944).
[8] E. E. Tamm, J. Exper. Theor. Phys. (Russian) **18**, No. 4 (1948).

the asymptotic form for the wave function:

$$\psi_l(\infty)=[(2l+1)/(4\pi)]^{\frac{1}{2}}[(e^{-r_1}/r_2) \times P_l(\cos\theta_2)\sin(kr_2-l\pi/2+\eta_l) \pm(e^{-r_2}/r_1)P_l(\cos\theta_1)\sin(kr_1-l\pi/2+\eta_l)], \quad (3)$$

the sign being plus or minus according as the state is symmetrical or antisymmetrical, respectively. This asymptotic form represents a final state in which the bound electron is in its ground state and the free electron is at infinity with a kinetic energy k^2. In addition, the wave function should, of course, not have any singularity at $r_1=0$, or $r_2=0$.

Let

$$\mathfrak{L}=\int_\infty\int\psi_l(L-E)\psi_l d\tau_1 d\tau_2, \quad (4)$$

and consider the variation. By Green's theorem,

$$\int\psi_l\nabla_1^2\delta\psi_l d\tau_1=\int\delta\psi_l\nabla_1^2\psi_l d\tau_1 + \oint[\psi_l(\partial\delta\psi_l/\partial r_1)-\delta\psi_l(\partial\psi_l/\partial r_1)]dS_1. \quad (5)$$

The surface integral in Eq. (5) can be evaluated at $r_1\to\infty$ by using the asymptotic expansion (3) of the wave function. It can, in fact, be shown that

$$\int_\infty\int\psi_l\nabla_1^2\delta\psi_l d\tau_1 d\tau_2=\int_\infty\int\delta\psi_l\nabla_1^2\psi_l d\tau_1 d\tau_2-\pi k\delta\eta_l. \quad (6)$$

The corresponding integral with subscript 2 can be similarly transformed. Thus,

$$\delta\mathfrak{L}=2\int_\infty\int\delta\psi_l(L-E)\psi_l d\tau_1 d\tau_2+2\pi k\delta\eta_l. \quad (7)$$

If ψ_l satisfies the wave equation, we have

$$\delta\mathfrak{L}=2\pi k\delta\eta_l, \quad (8)$$

which will reduce to

$$\delta\mathfrak{L}=0 \quad (9)$$

if the phase shift η_l is stationary. Or, in other words, under the stationary condition of η_l, the wave equation assumes a variational form which is given by Eq. (9). Regarding now

$$\mathfrak{L}=0 \quad (10)$$

as an equation which determines η_l, we can conversely impose the stationary condition by making use of Eq. (9). A practical procedure which this principle suggests is the following. Form an approximate wave function ψ_l which satisfies the required boundary conditions and at the same time contains n parameters. Then Eqs. (9) and (10) will give $n+1$ equations which will determine completely η_l and the n parameters. It is thus seen that the phase shift plays in the continuous spectrum the same role as the energy in the discrete spectrum. It is due to this reason that Hulthén[7] introduced the name "eigenphase" for η_l.

As the wave function should approach the asymptotic expansion (3) when the free electron is at infinity and be finite when it is at the origin, it is natural to write it in the approximate form:

$$\psi_l=[(2l+1)/(4\pi)]^{\frac{1}{2}}[F(r_1,\theta_1,r_2,r_{12})P_l(\cos\theta_2)/r_2 \pm F(r_2,\theta_2,r_1,r_{12})P_l(\cos\theta_1)/r_1], \quad (11)$$

where

$$F(r_1,\theta_1,r_2,r_{12})=(\pi kr_2/2)^{\frac{1}{2}}J_{l+\frac{1}{2}}(kr_2)f(r_1,\theta_1,r_2,r_{12}) +(\pi kr_2/2)^{\frac{1}{2}}J_{-l-\frac{1}{2}}(kr_2)g(r_1,\theta_1,r_2,r_{12}), \quad (12)$$

such that

$$f\to e^{-r_1}\cos\eta_l \quad\text{and}\quad g\to e^{-r_1}\sin\eta_l \quad (13)$$

as $r_2\to\infty$. In Eq. (12), $J_{\pm(l+\frac{1}{2})}(kr)$ represent Bessel functions of order $\pm(l+\frac{1}{2})$, respectively.

III. A RESTRICTED FORM OF VARIATIONAL PRINCIPLE

In spite of the general nature of the method derived in Section II, the mathematical formulas for actually working out the variational integral are very complicated. It would, therefore, seem that a somewhat less general but a mathematically simpler formulation of the principle is more suitable. For states with spherical symmetry and zero angular momentum this can be accomplished in the following way: In this case[9] the wave function can be completely expressed in terms of three coordinates r_1, r_2, and r_{12}.

Transforming Eq. (1) into new coordinates, we get

$$(\partial^2\psi/\partial r_1^2)+(2/r_1)(\partial\psi/\partial r_1)+(\partial^2\psi/\partial r_2^2) +(2/r_2)(\partial\psi/\partial r_2)+2(\partial^2\psi/\partial r_{12}^2)+(4/r_{12})(\partial\psi/\partial r_{12}) +[(r_1^2-r_2^2+r_{12}^2)/r_1r_{12}](\partial^2\psi/\partial r_1\partial r_{12}) +[(r_2^2-r_1^2+r_{12}^2)/r_2r_{12}](\partial^2\psi/\partial r_2\partial r_{12}) +[E+2(1/r_1+1/r_2-1/r_{12})]\psi=0. \quad (14)$$

Similar to Tamm's treatment[8] we make the substitution,

$$\psi(r_1,r_2,r_{12})=(e^{-r_1}/r_2)[\sin kr_2+u(r_1,r_2,r_{12})\cos kr_2]. \quad (15)$$

Equation (14) now becomes

$$[(\partial^2u/\partial r_1^2)+(2/r_1)(\partial u/\partial r_1)-2(\partial u/\partial r_1)+(\partial^2u/\partial r_2^2) +2(\partial^2u/\partial r_{12}^2)+(4/r_{12})(\partial u/\partial r_{12})]\cos kr_2 -2k(\partial u/\partial r_2)\sin kr_2+[(r_1^2-r_2^2+r_{12}^2)/r_1r_{12}] \times[(\partial^2u/\partial r_1\partial r_{12})-(\partial u/\partial r_{12})]\cos kr_2 +[(r_2^2-r_1^2+r_{12}^2)/r_2r_{12}][(\partial^2u/\partial r_2\partial r_{12})\cos kr_2 -(\partial u/\partial r_{12})(\cos kr_2/r_2)-k(\partial u/\partial r_{12})\sin kr_2] +2[(1/r_2)-(1/r_{12})](\sin kr_2+u\cos kr_2)=0. \quad (16)$$

[9] E. A. Hylleraas, Zeits. f. Physik **54**, 347 (1929); H. Bethe, *Handbuch der Physik* (1933), Vol. 24, p. 354.

In making the substitution we have used the energy relation

$$E=-1+k^2, \tag{17}$$

which is true in *Rh* unit.

From Eq. (15) it is apparent that $u(r_1, r_2, r_{12})$ becomes the tangent of phase shift as $r_2\to\infty$. Accordingly, we may call Eq. (16) as the equation for the eigenphase. The boundary conditions on $u(r_1, r_2, r_{12})$ are therefore

$$\left.\begin{aligned} u&=0 \quad \text{as} \quad r_2=0 \\ u&=u(k) \quad \text{as} \quad r_2\to\infty \end{aligned}\right\}. \tag{18}$$

As Eq. (14) is symmetrical in r_1 and r_2, the wave function appropriate to the physical problem can be written in the form

$$\psi_0=\psi(r_1, r_2, r_{12})\pm\psi(r_2, r_1, r_{12}), \tag{19}$$

where $\psi(r_1, r_2, r_{12})$ is defined in Eq. (15). In Eq. (19) we have the plus or minus sign according as we are dealing with the singlet or triplet state.

It can now be shown that Eq. (16) is the Euler equation of the variational integral:

$$\delta\mathfrak{F}=0;$$

$$\mathfrak{F}=\int_0^\infty dr_2\int_0^\infty dr_1\int_{|r_1-r_2|}^{r_1+r_2} dr_{12} \times F(u_1, u_2, u_{12}, u; r_1, r_2, r_{12}), \tag{20}$$

where

$$\begin{aligned} F=e^{-2r_1}\cos^2 kr_2\big[&r_1r_{12}(u_1^2+u_2^2+2u_{12}^2)/r_2 \\ &+(r_1^2-r_2^2+r_{12}^2)u_1u_{12}/r_2 \\ &+r_1(r_2^2-r_1^2+r_{12}^2)u_2u_{12}/r_2^2 \\ &-(2r_1r_{12}/r_2)(1/r_2-1/r_{12})(2u\tan kr_2+u^2)\big] \end{aligned} \tag{21}$$

and

$$u_1=\partial u/\partial r_1, \quad u_2=\partial u/\partial r_2, \quad u_{12}=\partial u/\partial r_{12}. \tag{22}$$

It is of interest to note that the integral $\mathfrak{F}$ reduces to that given by Tamm in the special case where $u=u(r_2)$ only, and where $-2(1/r_2-1/r_{12})$ can be approximated by an expression which involves r_2 only (as for example, by a potential $V(r_2)$ of the Hartree field of the hydrogen atom). For in this special case the integration with respect to r_{12} and r_1 can be effected directly, and the final integral

$$\mathfrak{F}=\int_0^\infty dr_2\big[u_2^2\cos^2 kr_2+Vu^2\cos^2 kr_2 +Vu\sin 2kr_2\big] \tag{23}$$

is identical with what Tamm has given.

To derive the variational principle expressed by Eq. (20) from Eq. (9) is a straightforward matter, although it is quite long and tedious. We may therefore indicate the various steps briefly. Substituting Eq. (15) into Eq. (9) we carry out the variation; one part would be equal to zero on account of Eq. (16); the remaining terms are then reduced by integration by parts; the integrated terms do not contribute anything as the variation vanishes on the boundary surface; most of other terms cancel one another, and we are finally left with

$$\delta\mathfrak{L}=\tfrac{1}{2}\delta\mathfrak{F}. \tag{24}$$

IV. *S*-SCATTERING OF ELECTRONS BY THE HYDROGEN ATOM

Here we shall apply Eq. (20) to derive the phase shift of the *S* waves for the case of a free electron scattered by a hydrogen atom. As our trial function, we shall suppose that

$$u=(1-e^{-r_2})[a+(b+cr_{12})e^{-r_2}], \tag{25}$$

where a, b, and c are three parameters which are to be determined. Substituting the foregoing form for u in Eq. (20) we carry out the integration. In order to express our result simply, it is convenient to define the functions:

$$F_n(\alpha, m; k)=\int_0^\infty (1-e^{-r})^n e^{-\alpha r}r^m\cos^2 krdr \qquad (n\geqq 0,\ m\geqq -n), \tag{26}$$

$$G_n(\alpha, m; k)=\int_0^\infty (1-e^{-r})^n e^{-\alpha r}r^m\sin 2krdr \qquad (n\geqq 0,\ m\geqq -n-1), \tag{27}$$

$$I_n(\alpha; k)=\int_0^\infty (1-e^{-r})^n(1-e^{-2r})(e^{-\alpha r}/r^2)\cos^2 krdr \qquad (n\geqq 1), \tag{28}$$

$$J_n(\alpha; k)=\int_0^\infty (1-e^{-r})^n(1-e^{-2r})(e^{-\alpha r}/r^2)\sin 2krdr \qquad (n\geqq 0), \tag{29}$$

and

$$M(\alpha; k)=\int_0^\infty (1-e^{-2r})(e^{-\alpha r}/r)\cos^2 krdr, \tag{30}$$

where m and n are integers. In terms of these functions $\mathfrak{F}$ is a quadratic function in the parameters a, b, and c.

The variational principle would then give three equations for the three parameters. It is found that these three equations have the following forms.

$$\partial\mathfrak{F}/\partial a=A_1a+B_1b+C_1c-D_1=0, \tag{31}$$

$$\partial\mathfrak{F}/\partial b=A_2a+B_2b+C_2c-D_2=0, \tag{32}$$

$$\partial\mathfrak{F}/\partial c=A_3a+B_3b+C_3c-D_3=0, \tag{33}$$

TABLE I. Coefficients of u.

k	3-parameter approximation a	b	c	2-parameter approximation a	c	1-parameter approximation a
0	0	0	0	0	0	0
0.05	−0.4038	+0.16954	−0.4199	−0.4067	−0.3944	+0.3102
0.10	−0.8499	+0.3572	−0.8938	−0.8576	−0.8425	+0.6066
0.15	−1.3978	+0.5883	−1.4970	−1.4160	−1.4208	+0.8777
0.20	−2.158	+0.9099	−2.368	−2.202	−2.274	+1.1155
0.25	−3.394	+1.4348	−3.840	−3.520	−3.765	+1.3162
0.50	+5.254	−2.246	+7.147	+4.616	+6.146	+1.8280
0.75	+2.037	−0.9067	+2.947	+1.8132	+2.649	+1.8969
1.00	+1.6636	−0.8899	+2.071	+1.4068	+1.7846	+1.8572
1.50	+1.8372	−1.3059	+1.6403	+1.3687	+1.1761	+1.7809
2.00	+2.059	−1.4506	+1.6050	+1.4722	+1.0362	+1.7484
2.50	+2.280	−1.5294	+1.7069	+1.6127	+1.0567	+1.7253
3.00	+2.580	−1.7028	+1.9399	+1.7897	+1.1607	+1.6924
4.00	+3.656	−2.523	+2.909	+2.309	+1.5629	+1.5891
6.00	+25.635	−20.46	+22.87	+5.389	+4.045	+1.3282
8.00	−5.763	+5.076	−5.501	−24.69	−19.758	+1.1004
10.00	−2.743	+2.564	−2.722	−4.098	−3.403	+0.9262
20.00	−0.8622	+0.8841	−0.9083	−0.9303	−0.8192	+0.4983
50.00	−0.3102	+0.3276	−0.3330	−0.3181	−0.2853	+0.2037
100.00	−0.1535	+0.1616	−0.1649	−0.1562	−0.1404	+0.1022

where

$$A_1=F_0(2,0;k)-2F_2(2,0;k)-2F_2(2,-1;k), \tag{34}$$

$$A_2=B_1=F_0(3,0;k)-F_1(2,0;k) -2F_2(3,0;k)-2F_2(3,-1;k), \tag{35}$$

$$A_3=C_1=F_0(3,1;k)-F_1(2,1;k)+F_1(2,0;k) +\tfrac{3}{2}F_1(4,0;k)-\tfrac{1}{2}F_0(5,0;k)-F_1(2,-1;k) +2F_1(3,-1;k)+3F_1(4,-1;k) -2I_2(1;k)-I_1(2;k), \tag{36}$$

$$B_2=F_2(2,0;k)-2F_2(4,0;k)-2F_1(3,0;k) +F_0(4,0;k)-2F_2(4,-1;k), \tag{37}$$

$$B_3=C_2=F_2(2,-1;k)-2F_1(3,-1;k) -F_1(4,-1;k)+7F_1(5,-1;k) -\tfrac{3}{2}F_2(4,0;k)-F_2(2,0;k)+2F_1(5,0;k) +F_1(3,0;k)-\tfrac{1}{2}F_0(6,0;k)+F_2(2,1;k) -2F_1(3,1;k)+F_0(4,1;k)-I_1(2;k), \tag{38}$$

$$C_3=F_2(2,2;k)-2F_1(3,2;k)+F_0(4,2;k) -2F_2(2,1;k)+2F_1(3,1;k)+5F_2(2,0;k) -F_2(4,0;k)-6F_1(3,0;k)+3F_0(4,0;k) -4F_2(2,-1;k)-2F_2(4,-1;k), \tag{39}$$

$$D_1=G_1(2,0;k)+G_1(2,-1;k), \tag{40}$$

$$D_2=G_1(3,0;k)+G_1(3,-1;k), \tag{41}$$

$$D_3=J_1(1;k)-\tfrac{1}{2}G_1(3,-1;k). \tag{42}$$

The formal solution of Eqs. (31)–(33) will be given in terms of determinants as follows:

$$a=(DBC)/(ABC),\quad b=(ADC)/(ABC),\quad c=(ABD)/(ABC). \tag{43}$$

Before we give the result of the calculations, we shall indicate some steps in the evaluation of the functions defined by Eqs. (26)–(30). First we may observe that the following recurrence formula holds,

$$F_n(\alpha,m;k)=F_{n-1}(\alpha,m;k)-F_{n-1}(\alpha+1,m;k), \tag{44}$$

provided every function in the formula is convergent. Similar formulas can be written down for $G_n(\alpha,m;k)$, $I_n(\alpha;k)$, and $J_n(\alpha;k)$. Also there exists the relation between F_n and G_n,

$$\partial F_n(\alpha,m;k)/\partial k=-G_n(\alpha,m+1;k). \tag{45}$$

Another relation which is useful in the numerical work is

$$\partial F_n(\alpha,m;k)/\partial\alpha=-F_n(\alpha,m+1;k). \tag{46}$$

Similar formula exists for $G_n(\alpha,m;k)$.

In order to express $I_n(\alpha;k)$ in terms of other more easily calculable functions, we intergrate by parts, and find

$$\begin{aligned} I_n(\alpha;k)=\int_0^\infty &\{d[(1-e^{-r})^n(1-e^{-2r}) \times e^{-\alpha r}\cos^2 kr]/dr\}(dr/r) \\ &=kG_n(\alpha+2,-1;k)-kG_n(\alpha,-1;k) -\alpha F_n(\alpha,-1;k)+nF_n(\alpha+1,-1;k) +(\alpha+n+2)F_n(\alpha+2,-1;k). \end{aligned} \tag{47}$$

In a similar manner it can be shown that

$$\begin{aligned} J_n(\alpha;k)=&2kF_n(\alpha+2,-1;0)-2kF_n(\alpha,-1;0) +4kF_n(\alpha,-1;k)-4kF_n(\alpha+2,-1;k) -\alpha G_n(\alpha,-1;k)+nG_n(\alpha+1,-1;k) +(\alpha+n+2)G_n(\alpha+2,-1;k). \end{aligned} \tag{48}$$

Also in deriving Eqs. (34)–(42) we have made use of the obvious identity:

$$M(\alpha;k)=F_1(\alpha,-1;k)+F_1(\alpha+1,-1;k). \tag{49}$$

It is therefore sufficient to evaluate only a few fundamental functions occurring in Eqs. (34)–(42). The rest

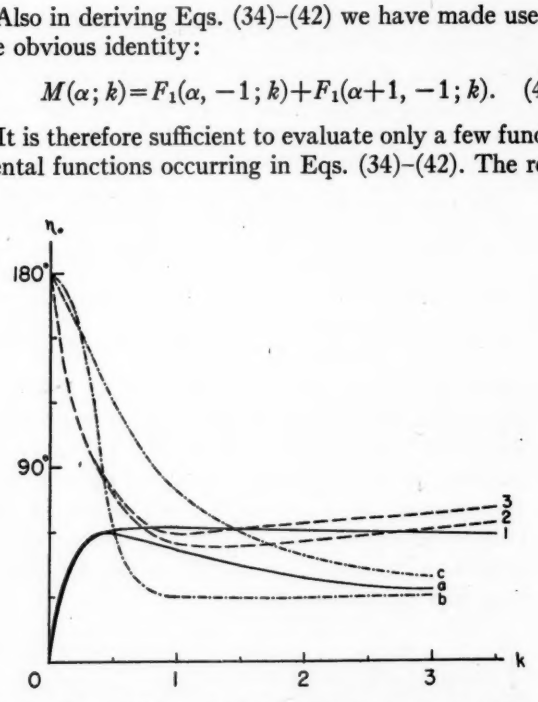

FIG. 1. Phase shifts η_0 of the S wave in degrees against electron velocities k in atomic units. The curves labeled 1, 2, and 3 are computed from the 1-, 2-, and 3-parameter trial functions, respectively, in the present paper. The curves labeled a, b, and c are Morse and Allis' results. Curve a is obtained for an electron moving in the Hartree field. Curves b and c give the phase shifts of symmetrical and antisymmetrical waves, respectively, when the effect of exchange is taken into consideration.

can be obtained by making use of the relations Eqs. (44)–(49). And the basic functions are:

$$F_0(\alpha, 0; k)=1/(2\alpha)+\alpha/[2(\alpha^2+4k^2)], \quad (50)$$

$$F_1(\alpha, -1; k)=\int_\infty^\alpha [\partial F_1(\alpha', -1; k)/\partial\alpha']d\alpha'$$

$$=-\int_\infty^\alpha F_1(\alpha', 0; k)d\alpha'$$

$$=\tfrac{1}{2}\log[(\alpha+1)/\alpha]$$

$$+\tfrac{1}{4}\log\{[(\alpha+1)^2+4k^2]/(\alpha^2+4k^2)\}, \quad (51)$$

$$G_1(\alpha, 0; k)=2k/(\alpha^2+4k^2)-2k/[(\alpha+1)^2+4k^2], \quad (52)$$

$$G_1(\alpha, -1; k)=\int_\infty^\alpha [\partial G_1(\alpha', -1; k)/\partial\alpha']d\alpha'$$

$$=\tan^{-1}[(\alpha+1)/(2k)]-\tan^{-1}[\alpha/(2k)]. \quad (53)$$

That this integral vanishes at the lower limit is as obvious as that of the integral (51), if we combine the two terms into one term according to the trigonometrical identity.

Instead of computing the values of a, b, and c from Eqs. (43) for various values of k, it is simpler to get the numerical solution directly from Eqs. (31)–(33) once their coefficients have been evaluated. The results of the calculation are given in Table I. For comparison, the results for a 2-parameter (a, c) and a 1-parameter (a), trial functions are also included; they are labeled as 2-parameter and 1-parameter approximation, respectively.

As the phase shift η_0 is given by

$$\tan\eta_0=\lim_{r_2\to\infty} u=a, \quad (54)$$

and the cross section of S wave by

$$q_0=4\pi(\sin\eta_0/k)^2,$$

they can be computed directly from Table I; they are given in Table II. The phase shifts are further plotted in Fig. 1 where Morse and Allis's results are also shown.

TABLE II. Phase shifts and cross sections of the S wave.

	3-parameter approximation		2-parameter approximation		1-parameter approximation	
k	η_0	q_0	η_0	q_0	η_0	q_0
0	180°	—	180°	—	0°	—
0.05	158° 0′.7	704.7	157° 52′.3	713.2	17° 13′.9	441.1
0.10	139° 38′.2	527.1	139° 23′.0	532.6	31° 14′.5	338.0
0.15	125° 34′.8	369.4	125° 13′.8	372.7	41° 16′.4	243.0
0.20	114° 52′.0	258.6	114° 25′.2	260.5	48° 7′.5	174.18
0.25	106° 25′.0	185.00	105° 51′.6	186.04	52° 46′.4	127.48
0.50	79° 13′.5	48.51	77° 46′.5	48.01	61° 19′.2	38.69
0.75	63° 51′.2	18.001	61° 7′.4	17.131	62° 12′.2	17.482
1.00	58° 59′.4	9.231	54° 35′.6	8.348	61° 42′.0	9.741
1.50	61° 26′.4	4.309	53° 50′.9	3.642	60° 41′.1	4.246
2.00	64° 5′.7	2.542	55° 48′.8	2.150	60° 13′.9	2.368
2.50	66° 19′.1	1.686	58° 11′.9	1.453	59° 54′.2	1.505
3.00	68° 48′.6	1.214	60° 48′.3	1.064	59° 25′.3	1.035
4.00	74° 42′.2	0.730	66° 34′.9	0.661	57° 49′.1	0.563
6.00	87° 46′.0	0.348	79° 29′.2	0.338	53° 1′.4	0.222
8.00	99° 50′.6	0.191	92° 19′.2	0.196	47° 44′.2	0.108
10.00	110° 1′.8	0.111	103° 42′.9	0.118	42° 48′.3	0.058
20.00	139° 14′.0	0.014	137° 4′.1	0.015	26° 29′.3	0.006
50.00	162° 45′.9	0.0004	162° 21′.2	0.0005	11° 30′.8	0.0003
100.00	171° 16′.4	0.00003	171° 7′.4	0.00003	5° 50′.0	0.00001

Our results are not in agreement with theirs and unfortunately no experimental data are available for comparison. But one common feature between the results of Morse and Allis's and ours is worth noticing. While the 1-parameter trial function which does not contain a term in r_{12} gives a variation of the phase shift, similar to that computed from the Hartree field, approaching 0° as $k\to 0$, the introduction of the r_{12} term (the 3-parameter and the 2-parameter approximations) makes $\eta_0\to 180°$ as $k\to 0$; in this respect it is similar to the introduction of the exchange effect in the manner of Morse and Allis. There is, however, an important difference between these two results. So far as the phase shift is concerned, there is no difference in our formulation for symmetrical and antisymmetrical states, but Morse and Allis give different values of η_0 for these two states.

In a later paper we propose to use the wave functions derived here to the evaluation of the radiative cross sections for the free-free transition of an electron in the field of a neutral hydrogen atom.[10]

I wish to express my sincere thanks to Professor S. Chandrasekhar who suggested this problem and for valuable discussions.

[10] S. Chandrasekhar and F. H. Breen, Astrophys. J. **104**, 430 (1946).

Neutrons from C(d,n)N and Cu(d,n)Zn*

J. C. GROSSKREUTZ
Department of Physics, Washington University, St. Louis, Missouri
(Received April 4, 1949)

The energy distribution among the neutrons emitted from carbon and copper bombarded by 10-Mev deuterons has been investigated by means of proton recoils in photographic emulsions. A description of the method is given. Two excited levels are observed in N^{13} at 2.29±0.12 Mev and 3.48±0.12 Mev, the latter not having been observed previously. Q for the production of N^{13} in the ground state is found to be −0.29 ±0.09 Mev. Both the reactions (d,n) and $(d,2n)$ have been identified in the effects occurring when copper is bombarded by 10-Mev deuterons. Quantitative agreement with the expected energy range of the neutrons from the $(d,2n)$ reaction is found. There is also evidence for some type of level structure in Zn. Discussion is given of a possible interpretation of this structure.

I. INTRODUCTION

THE energy spectrum of the neutrons from the reaction

$$Z^A+H^2\rightarrow(Z+1)^{A+1}+n \qquad (1)$$

yields information as to the energy of the state in which the nucleus $(Z+1)^{A+1}$ is formed. The special emulsions manufactured by Ilford, Ltd., and Eastman Kodak have made it possible to use the photographic plate as a detector of such neutrons. The hydrogen present in the gelatin of the emulsion (1.4 percent by weight) furnishes an adequate supply of protons to be knocked on by impinging neutrons. These protons are then automatically recorded as they render developable the silver bromide grains along their paths. Measurement of the track lengths under magnification gives a measure of the neutron energy. Application of this method to the general reaction (1) has been made by a number of workers.[1]

The energy of the neutrons given out in the reaction

$$C^{12}+H^2\rightarrow N^{13}+n \qquad (2)$$

has been studied by several investigators using deuterons of energy up to 2 Mev.[2] The results of these experiments are all in agreement in reporting a single group of monoenergetic neutrons and a Q-value of −0.27±0.02 Mev (Bennett and Richards). Hornyak and Lauritsen[3] list an excited state of N^{13} at 2.34 Mev. With deuterons of energies no greater than 2 Mev, this state could not have been excited. Using the 10-Mev deuterons available from the Washington University cyclotron, the neutrons from (2) have been studied by means of photographic plate detectors. Deuterons of this energy should be capable of forming N^{13} in several of its excited states.

The neutrons from the reactions

$$Cu^{63,65}+H^2\rightarrow Zn^{64,66}+n, \qquad (3)$$

$$Cu^{63,65}+H^2\rightarrow Zn^{63,65}+2n, \qquad (4)$$

are of interest for two reasons. First, information as to the excited states in the Zn nuclei may be obtained from a study of the energy spectrum of neutrons resulting from reaction (3). Second, neutrons from both reactions are present in profusion near a deuteron-accelerating cyclotron because of the large amount of copper in the dees and associated components of the machine. To plan proper shielding against neutrons originating in the cyclotron, it would be helpful to know their energy distribution. Reactions (3) and (4) have been studied using the 10-Mev deuterons available at this laboratory.

II. EXPERIMENTAL METHOD

A. The Deuteron Source

The fringing field of the cyclotron magnet combined with a specially designed slit system is used to isolate a monoenergetic beam of deuterons[4] for use in the investigation. The beam then passes down a long snout to a point well away from the cyclotron where experimentation can be carried out with adequate shielding. The energy of these deuterons was determined by a photographic method, in which the beam was scattered by a thin platinum foil and allowed to strike an emulsion at a glancing angle. The distribution in range of the recorded deuteron tracks was then determined and converted to an energy scale. In this way, the monoenergetic beam selected for use in these experiments was found to have an energy of 9.93±0.07 Mev with a spread of less than one percent.

B. Apparatus

Figure 1 shows schematically the experimental arrangement. The homogeneous beam of deuterons strikes a thin target, and the neutrons from the resulting reaction are detected at 90° to the incident beam by the

* Assisted by the joint program of the ONR and the AEC.

[1] H. T. Richards, Phys. Rev. **59**, 796 (1941); C. F. Powell, Proc. Roy. Soc. **181**, 344 (1943); R. A. Peck, Phys. Rev. **73**, 947 (1948).

[2] T. W. Bonner, Phys. Rev. **53**, 496 (1938); W. E. Bennett *et al.*, Phys. Rev. **59**, 781 (1941); W. E. Bennett and H. T. Richards, Phys. Rev. **71**, 565 (1947).

[3] W. F. Hornyak and T. Lauritsen, Rev. Mod. Phys. **20**, 191 (1948).

[4] E. C. Creutz and R. R. Wilson, Phys. Rev. **59**, 916 (1941).

proton recoils in the photographic plate as shown. The main beam of deuterons passes on through the thin target and emerges into air through a 1-mil aluminum window. Hence the beam dissipates most of its energy at a considerable distance from the detection plate, thus reducing background fog in the emulsion due to gamma-radiation. This is an important point since the exposures needed to obtain adequate yields of neutrons are quite long.

The plates used for detection are encased in light tight steel holders which are in turn mounted on a rigid support as shown. This support is a circular disk on which several plate holders can be mounted radially with respect to the target. The detecting plates are outside the cyclotron vacuum system.

Adequate collimation of the neutrons results from the fact that the photographic plate is almost tangential to the neutrons leaving the target. The plates are at a mean distance of 10 cm from the center of the target. Shielding from extraneous neutrons from the cyclotron chamber is achieved by the use of large paraffin blocks cast to fit into place on all sides of the photographic plates, leaving a narrow path open between plate and target for the free passage of the neutrons to be studied.

C. Emulsion Technique

The best exposure of a photographic plate to neutrons is one which yields an adequate number of recoil proton tracks with a minimum of background fog to interfere with their measurement. In order to reduce this background to a minimum, one inch of lead shielding was used on that side of the plate nearest the cyclotron. Deuteron beam currents of about 0.25 microampere were used with exposure times of approximately one hour for the target thickness employed.

The plates were developed in the usual manner employed for Ilford C-2 plates and were examined by microscope. For all scanning and measuring, a magnification of 900× was used with bright field illumination. The eyepiece micrometer employed in measurement of the tracks was a special one made by Bausch and Lomb. The divisions were ruled with a diamond point such that the rulings themselves were only two microns in width. This specification was made so that the thickness of the division markings would not interfere in estimating the last significant figure in track lengths. Calibration of the eyepiece micrometer was made with a Bausch and Lomb stage micrometer.

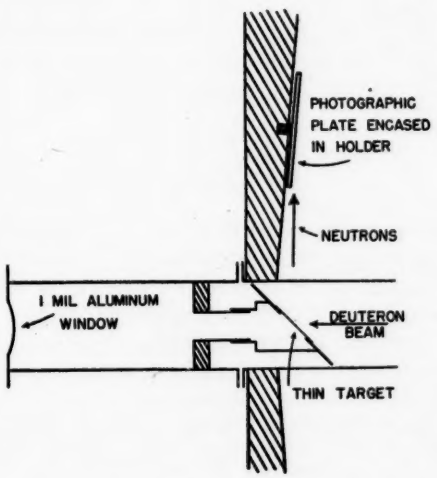

FIG. 1. Schematic arrangement for the study of neutrons from (d,n) reactions by means of photographic plates.

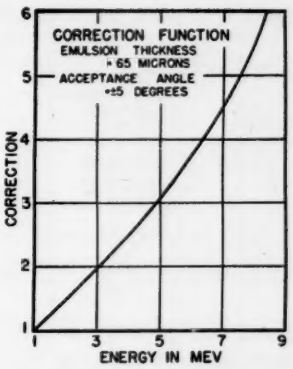

FIG. 2. Correction function consisting of geometric and cross-section corrections applied to the proton recoil spectra obtained experimentally in order to infer the correct neutron distribution.

The criteria for accepting a track for measurement were: (1) the direction of the track should be within 5° of the forward direction of the neutrons in both the horizontal and vertical planes; (2) a track should clearly begin and end within the emulsion. Tracks were measured by scanning across the plate in the direction of the incident neutrons, taking swaths at 0.2-mm intervals.

III. EXPERIMENTAL RESULTS AND CONCLUSIONS

A. Carbon

A thin carbon target (165-kev thickness for 10-Mev deuterons), was prepared by depositing soot from burning camphor on to a sheet of 0.1-mil platinum. This target was subjected to deuteron bombardment and the neutrons from reaction (2) recorded photographically. The raw data, as obtained from the measurement of recoil proton track lengths, must be altered in order to yield the neutron energy spectrum. To transform the range distribution to an energy distribution, recourse is made to a range-energy curve for the emulsion. This calibration has been made for Ilford emulsions by Lattes and his co-workers[5] and their results were used in this study.[6] The energy distribution histo-

[5] Lattes, Fowler, and Cuer, Proc. Phys. Soc. **59**, 883 (1947).

[6] Confirmation of the relative constancy in stopping power of Ilford emulsions has been demonstrated by agreement of independent workers in reporting alpha-particle ranges in the emulsions from natural radioactive elements. A batch taken at random at this laboratory yielded an alpha-particle calibration curve differing only by 0.3 percent from that obtained by the Bristol group. It has become the practice here to check the stopping power of a given batch of plates by impregnation with uranium and subsequent measurement of the UI and UII alpha-particle ranges.

TABLE I. Neutron groups from $C^{12}(d,n)N^{13}$ and the assignment of excitation energies to N^{13}.

Group	Mean energy of neutrons (Mev)*	Q (Mev)	Excitation energy of N^{13} (Mev)
A	7.53±0.07	−0.29±0.09	0.00
B	5.40±0.05	−2.58±0.08	2.29±0.12
C	4.30±0.04	−3.77±0.08	3.48±0.12

* Mean energy of neutron groups calculated following the procedure of Bethe and Livingston, Rev. Mod. Phys. 9, 245 (1937).

gram was plotted in 200-kev intervals. In order to overcome any observer bias in measurement and to lend smoothness to the curve, the energy histogram was overlapped, i.e., the number of tracks per 200-kev interval was calculated and plotted every 100 kev. Finally, in order to infer the correct neutron spectrum, two corrections must be applied: (1) one which recognizes that the probability of recording a short track is greater than that of recording a long one, and (2) one which gives the variation of the cross section for neutron-proton scattering as a function of the neutron energy. Calculation of such correction functions have been discussed by other authors[7] and will not be repeated here. A plot of the correction used in this work is given in Fig. 2.

Figure 3 is the corrected neutron spectrum of reaction (2) representing measurement of 1500 recoil proton tracks in 2.3 cm² of plate area. Three groups are clearly resolved. To insure that none of these neutrons were extraneous, a "blank" run was made with only the platinum backing in place. The background so obtained

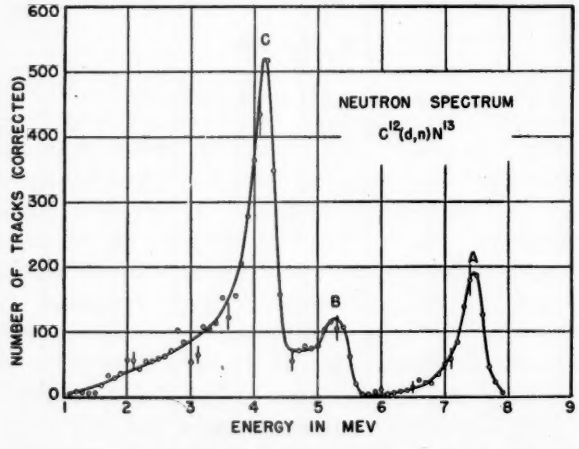

FIG. 3. Energy distribution of neutrons from $C^{12}(d,n)N^{13}$. The number of tracks in each 200-kev interval have been plotted every 100 kev and corrected according to Fig. 2. Background neutrons (see text), amounting to 100 percent of the total number of tracks measured below 1.5 Mev, ~50 percent of those in the interval 2–3 Mev, 5 percent at the peak of group C, 12 percent at group B, and zero at group A, have been subtracted prior to plotting. The standard deviation is shown at several typical points on the curve. The spectrum represents 1500 acceptable recoil proton tracks in 2.3 cm² of plate area.

[7] H. T. Richards, Phys. Rev. 59, 796 (1941); W. M. Gibson and D. L. Livesay, Proc. Phys. Soc. 60, 523 (1948).

was subtracted from the carbon run and the data appearing in Fig. 3 is the resulting pure carbon spectrum. Group A corresponds to the formation of N^{13} in the ground state. The Q of this transition, as calculated from the mean energy of group A, is −0.29±0.09 Mev as compared to −0.27±0.02 Mev as found by Bennett and Richards.[2] Groups B and C correspond to the formation of N^{13} in excited states. For the level associated with group B, the energy of the excited state is found to be 2.29±0.12 Mev which is in satisfactory agreement with that listed by Hornyak and Lauritsen[3] (2.34 Mev). Group C yields a level in N^{13} at 3.48±0.12 Mev, as yet not reported in other reactions involving N^{13}. Results are listed in Table I.

B. Copper

A copper foil, of thickness 0.4 mil, was bombarded by 9.93-Mev deuterons and information as to the energy of the resulting neutrons was recorded as in the case of carbon. Figures 4 and 5 represent the neutron spectrum so obtained from 1300 acceptable tracks.

At the bombarding energies used, neutrons from both the (d,n) and $(d,2n)$ reactions should be present. The threshold of the reaction $Cu^{63}(d,2n)Zn^{64}$ has been reported as 7 Mev by Livingston and Wright.[8] Meitner gives a value of 5.5 Mev as calculated from the end point of the energy spectrum of beta-particles in the decay of Zn^{63}.[9] Neutrons produced by the stripping of deuterons should also be present at this bombarding energy, as predicted by Peaslee.[10] However, a calculation of the mean energy to be expected of these neutrons at 90° to the incident beam can be made. Assuming a momentum distribution for the neutron inside the deuteron as that given by Serber[11] and a Coulomb barrier of 7 Mev for copper, a rigorous evaluation of the mean energy of stripped neutrons gives a value of ~1 Mev at 90°. Examination of Fig. 4 will indicate that these neutrons do not give a serious contribution to the observed spectrum.

A calculation of the spread in energy of the neutrons from the $(d,2n)$ reaction can be made. Following Bethe,[12] we suppose the mechanism, in the case of the most abundant (70 percent) isotope, Cu^{63}, to be

$$H^2+Cu^{63}\rightarrow Zn^{64*}+n+Q_1, \quad (5)$$

$$Zn^{64*}\rightarrow Zn^{63}+n+Q_2. \quad (6)$$

If we assume the neutron in (5) is evaporated with negligible energy, the neutron energy in (6) is found to be 3.9 Mev at 90°. The reverse situation, in which the neutron in (6) comes off with very small energy, can be arrived at if one knows the binding energy of the last neutron in Zn^{64}, and hence the minimum excitation

[8] R. S. Livingston and B. T. Wright, Phys. Rev. 58, 656 (1940).
[9] L. Meitner, Arkiv. f. Mat. Astr. o. Fys. 33A No. 3 (1946).
[10] D. C. Peaslee, Phys. Rev. 74, 1001 (1948).
[11] R. Serber, Phys. Rev. 72, 1008 (1947).
[12] H. Bethe and M. S. Livingston, Rev. Mod. Phys. 9, 245 (1937).

energy needed for evaporation. A consideration of the masses involved yields ~13 Mev for this binding energy. Consideration of the nuclear energy surface by Feenberg,[13] predicts a value of ~12 Mev for this nucleus. Taking a mean value of 12.5 Mev for the excitation of Zn^{64}, reaction (5) will then yield a neutron of 3.5 Mev. Thus the region from zero to about 3.9 Mev in the spectrum will correspond to the production of two neutrons by deuterons on Cu^{63}. Similar calculations for the other target isotope of copper, Cu^{65}, yield the region zero to about 5.6 Mev for double neutron production. An examination of Fig. 4 reveals a Maxwellian appearance of the curve for two particle emission. An end point might well be assigned somewhere in the neighborhood of 4 Mev, in good agreement with the prediction on Cu^{63}, since a majority of the neutrons will come from that more abundant isotope. From Fig. 5 it is seen that after undergoing a slight rise, the curve falls still further to a minimum value at approximately 5.5 Mev. This is in qualitative agreement with the predicted end point of the (d,$2n$) reaction in Cu^{65}.

Above 5.5 Mev, the spectrum shows definite grouping of the neutrons. Neutrons of these energies correspond to a (d,n) reaction and hence some sort of level structure in Zn^{64} or Zn^{66} is indicated. Neutrons arising from production of these isotopes in the ground state would have energies around 16 Mev as calculated from the mass values involved. These were not detected, which is not surprising since the probability is small that Zn be formed in the ground state with the excitation energies available.[14] The probability of detection in the emulsion is also very small at these energies. The fact that a group at 8.6 Mev was the highest observed can be interpreted only by saying that neutrons above this energy are produced too infrequently to be detected by the present method in the length of exposure used.

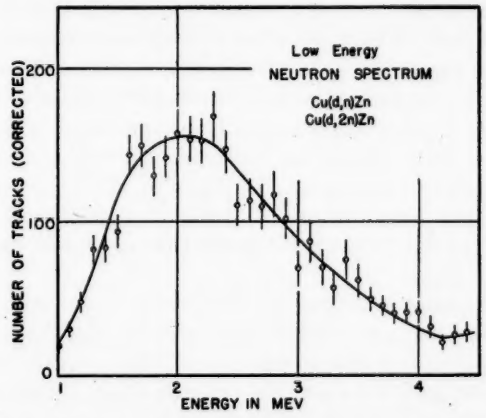

FIG. 4. Low energy distribution of neutrons from Cu(d,n)Zn and Cu(d,$2n$)Zn. The number of tracks in each 200-kev interval have been plotted every 100 kev and corrected according to Fig. 2. The spectrum represents 1000 acceptable recoil proton tracks in 2.0 cm² of plate area.

[13] E. Feenberg, Rev. Mod. Phys. **19**, 239 (1947).
[14] H. A. Bethe, Rev. Mod. Phys. **9**, 100 (1937).

TABLE II. Neutron groups from Cu(d,n)Zn and assignment of a mean energy to "level groups" in Zn^{64} or Zn^{66}. Neutron groups are numbered reading from right to left in Fig. 5. Values of the energy are given to only two significant figures, corrections affecting the third figure having not been applied.

Group	Mean energy of neutrons (Mev)	Mean excitation energy (Mev) Zn^{64}	Zn^{66}
I	8.5	6.3	9.1
II	6.4	8.5	11.3
III	5.7	9.2	12.0
IV(?)	4.6	10.3	—

Existing statistical theories of nuclei in the neighborhood of Zn predict extremely close spacing (a few hundred ev) of the levels whose energy above the ground state (~6–10 Mev) would correspond to the production of the neutrons in Fig. 5. Hence in order to account for the apparently definite grouping observed, one might suppose the compound nucleus, Zn^{65}, to be formed in states with a certain limited range of angular momenta. Transitions might then be made to an allowed range of states in Zn^{64} with the emission of neutrons whose energies are not homogeneous but spread over a finite range. Such a mechanism, with transitions of the compound nucleus to several allowed "ranges of states" in the residual nucleus, would account for the distribution in Fig. 5. Still another interpretation is possible if one assumes the density of highly excited levels in medium-heavy nuclei to vary irregularly with their energy above the ground state. Such assumptions, however, are highly speculative with the limited experimental information at hand.

The mean excitation energy of three "groups of levels" in Zn can be obtained from the mean energy of the neutron groups in Fig. 5. Corrections to these energies, which affect the third significant figure, have not been made, since the peaks in Fig. 5 presumably do not represent homogeneous groups and the usual corrections for straggling, etc., cannot be applied. Hence, only two figures are given in Table II which gives the

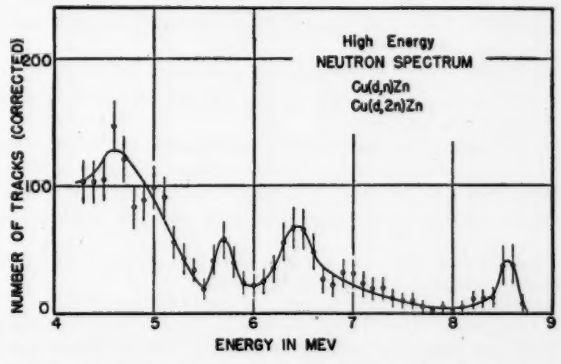

FIG. 5. High energy distribution of neutrons from Cu(d,n)Zn and Cu(d,$2n$)Zn. The number of tracks in each 200-kev interval have been plotted every 100 kev and corrected according to Fig. 2. The spectrum represents 300 acceptable recoil proton tracks in 4.1 cm² of plate area.

mean excitation energies of "level groups" according to whether they be assigned to Zn^{64} or Zn^{66}, unambiguous assignment being possible only if experiments are made with separated Cu isotopes.

The author should like to make acknowledgment to Dr. F. N. D. Kurie for his stimulating interest in the early stages of this problem; to Dr. H. Primakoff and Dr. E. Feenberg for helpful discussions, and to Miss Eileen Denison for measurement of track lengths in the copper spectrum.

PHYSICAL REVIEW VOLUME 76, NUMBER 4 AUGUST 15, 1949

Fading of Proton Tracks in Vacuum*,**

K. B. MATHER
Physics Department, Washington University, St. Louis, Missouri
(Received April 11, 1949)

The fading of the latent images due to protons has been compared for photographic emulsions maintained in air and in vacuum after the exposure was made. The fading in vacuum was found to be approximately 10 percent of that in air indicating a purely chemical origin for the phenomenon of fading. At the present time it is speculative whether the residual 10 percent arises from the same source in which case it could be eliminated by merely improving the vacuum, or comes from an altogether distinct process. Some suggestions are advanced concerning a possible Ag atom evaporation process.

THE fading of tracks caused by charged particles has been well established by the Bristol group *et al.* Although it is improbable that the phenomenon is confined exclusively to latent images formed by charged particles as distinct from photons, in the former case it has proved more consequential by imposing a limit on the effective exposure times which can be utilized (notably in cosmic-ray research).

A significant question arises as to whether the dissipation of the latent image has a chemical or physical origin or involves two distinct processes. There could be a reoxidation of the Ag of the latent image by the atmosphere, possibly involving the water vapor, CO_2, etc. Alternatively the Ag atoms may "evaporate" from the Ag speck[1] constituting the latent image, and rediffuse into the AgBr lattice. The former alternative seems to be favored by the following observations:

(a) The rate of fading of alpha and proton tracks was conspicuously greater in summer than in winter in St. Louis. (Summer temperature $\backsimeq$30°C and relative humidity $\backsimeq$75 percent, winter $\backsimeq$22°C and $\backsimeq$39 percent.)

(b) Under constant temperature conditions ($\backsimeq$30°C) fading was accelerated by artificially raising the humidity and retarded by lowering the humidity.[2]

(c) Elevating the temperature sufficiently, produces rather than destroys a latent image.[3] Evidence for this comes from two sources,—the spontaneous "fogging" of an emulsion which increases rapidly with temperature and also the latent image resulting from frictional contacts[4] with an emulsion, explainable by a thermal mechanism.

A logical *coup de grace* to either theory would be supplied by comparing the rate of fading of tracks in vacuum and in air under the same temperature conditions.

Kodak Nuclear Track Plates NTB and Ilford Nuclear Research Plates C2, both 50μ, were exposed to fast neutrons from the Washington University cyclotron providing abundant proton recoils in each emulsion. Some of these plates were developed immediately. The remainder were divided into two groups and were allowed to stand as follows: (1) In vacuum. The container was evacuated with a mechanical pump every few days. The pressure varied from $\simeq$0.1–10-mm Hg. These plates were exposed to atmospheric pressure only for the initial half hour after bombardment and for the few minutes necessary to occasionally remove a plate for developing. (2) In air. The experiment was performed during the winter (temperature $\simeq$22°C, relative humidity $\simeq$39 percent). Both groups of plates were at the same temperature. A developing technique was standardized to permit identical development of successive plates.

The plates were scanned for proton tracks ending in the emulsion and having a range of at least 300μ (corresponding to a proton energy $\simeq$7 Mev). Grain counts per unit length were made on each track commencing from the end of the track where the protons stopped. However, it was found that the grain density towards the end of the track was too great to permit accurate counting. Less subjective data were obtained by excluding the ends of the tracks. In the final analysis

* A more comprehensive account of fading experiments will be published in *Review of Scientific Instruments*.

** Assisted by the joint program of the ONR and AEC.

[1] Consider the latent image mechanism in this case to comprise at least two competing primary processes—thermal liberation of electrons, and evaporation of Ag atoms from sensitivity specks.

[2] Dependence on seasonal humidity has recently been verified for alpha-tracks: R. Coppens, J. de phys. et rad. **10**, 11 (1949).

[3] However this could well be the net effect of the two primary processes and does not exclude the possibility of fading by evaporation proceeding simultaneously.

[4] K. B. Mather, J. Opt. Soc. Am. **38**, 1054 (1948).

grain counts were summed over only half the track i.e., over the next to last 150μ of range. (The number of grains over this length of track was $\simeq$180 in the unfaded Kodak plates.) Between six and ten tracks were counted on each plate. Figure 1 compares the results of (1) and (2) in terms of relative grain counts normalized to unity at zero time.

The rate of fading in vacuum is $\simeq$0.55 percent per week as compared with an average rate of fading (averaged over 76 days) $\simeq$4.8 percent per week in air. On this basis it appears that at least $\simeq$90 percent of the fading had a chemical origin. The rate of fading of Ilford plates in vacuum was almost the same as for the Kodak, but the fading in air was somewhat less rapid. It is evidently profitable to maintain nuclear emulsions in vacuum whenever fading may be deleterious. The result is more significant for meson and electron tracks which can be expected to fade more rapidly than proton tracks. It is suggested that cosmic-ray exposures be made in vacuum vessels maintained at $\simeq$1-mm Hg.

The physical interpretation of Fig. 1 is still somewhat in question. While the experiments were in progress it was found that emulsions placed in a vacuum of 10^{-4}–10^{-5} mm Hg became much more brittle and generally peeled off completely indicating that with vacua used in the fading work an appreciable amount of moisture was retained by the emulsion. In view of the reduction in the rate of fading effected by excluding $\simeq$99 percent of the atmosphere it would be interesting to know the result of a similar test in high vacuum.[5] It is quite possible that no fading exists in an isolated emulsion. Until this is established discussion is necessarily speculative.

However, if indeed there is a small residual fading even in high vacuum its magnitude is indicative of the true stability of the latent image against escape of Ag atoms. The problem is then to reconcile the existence of an evaporation process with the observed fact that a positive latent image builds up with increasing temperature. It is conceivable that Ag atoms be evaporated from shallow traps at temperatures too low for appreciable production of electrons. However this state of affairs implies that the atom-evaporation process be much less temperature-dependent than the electron-liberation process allowing the latter to predominate, as it seemingly does, at higher temperatures. From this point of view an investigation of the temperature dependence of the residual fading should be highly illuminating. With decreasing temperature, residual fading could be expected to decrease more or less rapidly depending on the exact picture of the evaporation mechanism. Similarly with increasing temperature the rate of fading presumably increases but becomes subordinate to the process of electron-liberation which evidently increases more rapidly. This seems to imply that true fading could be frozen out by maintaining the emulsion at a sufficiently low temperature, or at some higher temperature a state of equilibrium could be found at which the evaporation process balanced the thermally liberated electrons. Above this temperature the emulsion should fog by domination of the latter process.

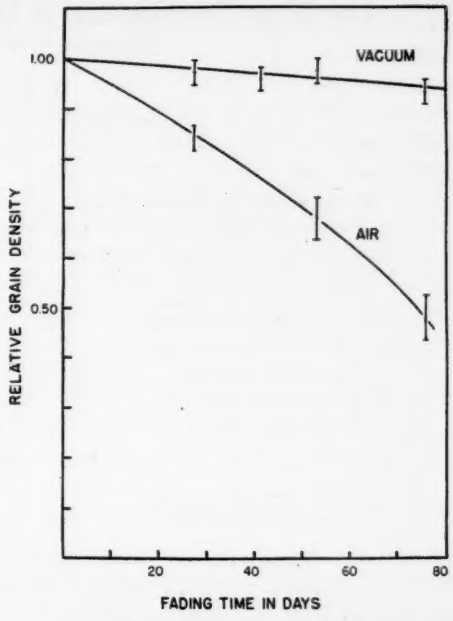

FIG. 1. Comparison of rates of fading of Kodak NTB plates in air and in vacuum.

The writer acknowledges his Studentship from the Science and Industry Endowment Fund, Commonwealth of Australia.

[5] Such an experiment would not be easy to carry out because of the peeling of the emulsion. It should be added that in the present tests with Kodak plates a large percentage of each emulsion flaked off even in this comparatively poor vacuum. Tracks were examined on the patches of undisturbed emulsion still adhering to the glass. Ilford emulsions did not peel off in the fading tests but did at 10^{-4} mm Hg. It was chiefly the latter circumstance which convinced us that the emulsions were not being dehydrated sufficiently by the present tests for a categorical verdict to emerge.

The Time Distribution of Decay Electrons from Mesons Stopped in Magnesium at 3500 Meter Altitude*

A. H. BENADE AND R. D. SARD
Department of Physics, Washington University, St. Louis, Missouri
(Received April 15, 1949)

The time distribution of decay electrons from the natural mixture of positive and negative mesons stopped in 13.2 g/cm² magnesium at Climax, Colorado has been measured. The apparatus recorded delayed coincidences in ten contiguous 0.6 μsec. channels covering delays from 0.5 to 6.5 μsec. The time distribution of false delayed coincidences due to G-M tube lags was also measured. These lags are shown to affect only the data from the first delay channel (0.5 to 1.1 μsec.), and an approximate correction for this effect can be made. Corrections for accidental delayed coincidences are also applied. The results (based on 2869 delayed coincidences) lie on a smooth differential decay curve, closely fitting the composite decay curve calculated on the assumption of competition between capture and decay for negative mesons. The effective mean life of the negative mesons is definitely less than 2.15 μsec., and appears to be approximately one μsec. The results can also be fitted by a single exponential of mean life 1.7±0.1 μsec.

I. INTRODUCTION

THE aim of this experiment[1] was to study the capture of stopped negative mesons through its competitive effect on the distribution in time of the decay electrons emerging from a material in which mesons are stopped. Conversi, Pancini, and Piccioni[2] had interpreted their discovery that decay electrons result from the stopping of negative mesons in graphite but not in iron by means of a capture probability depending on Z; and Wheeler[3] had pointed out that this probability would be expected to vary roughly as Z^4. Sigurgeirsson and Yamakawa[4] had shown that the yield of decay electrons from various materials agreed roughly with this prediction, the capture and decay probabilities being equal in the neighborhood of $Z=10$. Ticho[5] had pointed out that his low value for the mean lifetime of mesons stopped in aluminum at 3500-meter altitude could be explained as the effect of competition between capture and decay in the disappearance of the negative mesons. The decay curve observed with the natural mixture of positive and negative mesons should be a superposition of two exponentials of different mean life. It should appear in first approximation as a simple exponential of intermediate mean life; with greater experimental precision its composite character should become apparent. Our experiment was essentially the same as Ticho's,[5] differing only in the absorber used (magnesium rather than aluminum) and in geometrical arrangement and circuitry. The limitation of the range of measurable time delays, by G-M tube lags at short times and accidentals at long times, prevented us from establishing the composite character of the decay curve, but we did get a smooth differential decay curve of apparent mean life 1.7±0.1 microseconds (μsec.), definitely less than the 2.15±0.1 μsec.[6] obtained with absorbers of higher Z at sea-level.

Meanwhile Valley[7] and Ticho[8] have independently measured the decay curves of mesons of known charge, and the assumption of a negative meson capture probability comparable with the decay probability in the region $Z=9$–16, and increasing rapidly with Z, can now be regarded as experimentally established.[9] Our experimental points are well fitted by a curve computed for a 55–45 mixture of positive mesons of mean life 2.15 μsec. and negative mesons of mean life 1.0 μsec. (Fig. 4). Our data are in qualitative agreement with the results obtained by Ticho[8] and Valley[7] for magnesium ($Z=12$), who find respectively for the effective mean lives of the negatives 1.0±0.1 μsec. and 1.1±0.2 μsec.

II. APPARATUS

The experiment was carried out in the High Altitude Laboratory of the University of Chicago at Climax, Colorado. This laboratory is at an altitude of 3500 m; its light roof is made of one layer of pulpboard and one layer of sheet iron about 0.04 cm thick.

The arrangement of G-M tubes and absorbers is shown in Fig. 1. The meson-stopper was a 7.6 cm thick

* Assisted by the joint program of the ONR and AEC.

[1] A condensed report on this experiment was given at the Washington Meeting of the American Physical Society, May 1, 1948: R. D. Sard and A. H. Benade, Bull. Am. Phys. Soc. **23** (3), 43 (1948); Phys. Rev. **74**, 1237 (1948).

[2] Conversi, Pancini, and Piccioni, Phys. Rev. **71**, 209 (1947).

[3] J. A. Wheeler, Phys. Rev. **71**, 462 (1947); Phys. Rev. **71**, 320 (1947).

[4] T. Sigurgeirsson and A. Yamakawa, Phys. Rev. **71**, 319 (1947).

[5] H. K. Ticho, Phys. Rev. **72**, 255 (1947); H. K. Ticho and M. Schein, Phys. Rev. **72**, 248 (1947).

[6] B. Rossi and N. Nereson, Phys. Rev. **64**, 199 (1943); M. Conversi and O. Piccioni, Phys. Rev. **70**, 859 (1946); Maze, Chaminade, and Fréon, J. de phys. **6**, 202 (1945). See also references 7 and 8.

[7] G. E. Valley, Chicago Meeting of the American Physical Society, Dec. 30, 1947; G. E. Valley and B. Rossi, Phys. Rev. **73**, 177 (1948); G. E. Valley, Phys. Rev. **73**, 1251 (1948); G. E. Valley, Pasadena Cosmic Ray Symposium, June 21, 1948.

[8] H. K. Ticho, Chicago Meeting of the American Physical Society, Dec. 30, 1947; H. K. Ticho and M. Schein, Phys. Rev. **73**, 81 (1948); H. K. Ticho, Phys. Rev. **74**, 492 (1948); H. K. Ticho, Phys. Rev. **74**, 1337 (1948).

[9] The alternative hypothesis of accelerated decay seems to be disproved by the numbers of decay electrons found by Ticho (reference 8) and Valley (reference 7) and by the discovery of neutrons resulting from the stopping of μ mesons in lead (Sard, Ittner, Conforto, and Crouch, Phys. Rev. **74**, 97 (1948)).

(13.2 g/cm²) block of magnesium, of purity 99.86 percent. The three G-M tube trays, labeled $I-A$, $I-B$, and $I-C$, were used to select incoming charged particles. Each of these trays contained 5 tubes of effective length 25.4 cm and inner diameter 2.38 cm. On the underside of the absorber were placed three G-M tube trays, labelled $II-A$, $II-B$, and $II-C$, whose function was to detect decay electrons emerging downward from the magnesium. These trays each contained seven tubes, identical with those above the absorber except for having an effective length of 50.8 cm. A group of ten 50.8-cm tubes, labeled B, was placed around the sides of the absorber; this group was connected in the circuit so that it reduced the frequency of accidental delayed coincidences. Underneath the tubes of group II was a 2.9-cm lead slab, below which was a group of five 25.4-cm G-M tubes, labeled C. The lead slab and tray C were needed for the determination of the frequency of long lags in the discharges of the G-M tubes of groups I and II.

Each group of G-M tubes connected in parallel was held in a box made of 0.16-cm aluminum sheet. The tubes had 0.079-cm brass walls, and were filled to a pressure of 10 cm Hg with a 9:1 mixture of argon and ethyl alcohol. They were operated at about 70 volts above threshold, the circuit responding to pulses greater than 1 volt.

Figure 2 is a functional diagram of the circuit, which is based essentially on an earlier design of M. L. Sands.[10] The pulses from trays $I-A$, $I-B$ and $I-C$ went to a special coincidence circuit, α, which gave an output 0.5 μsec. after the time of occurrence of the *earliest* of the three pulses, provided that all three occurred within 0.5 μsec. of one another. This output will be referred to as pulse I. This timing from the first (rather than the last) pulse had the aim of reducing the effect of fluctuating time delays in the G-M tube discharges. In effect, the delay depends on the initial positions of the ions, and is least when the ions are formed close to the wire and near its central portion.[11] By using three trays of counters, we increased the probability of obtaining a short delay in at least one of the three tubes traversed. The staggering of the trays, both cross-wise and lengthwise, should have somewhat further increased this probability.

The same technique was used for the pulses of trays $II-A$, $II-B$, and $II-C$. Here, too, the special coincidence circuit, β, gave an output 0.5 μsec. after the time of occurrence of the earliest of the three pulses provided that all three occurred within 0.5 μsec. We shall refer to this output as pulse II.

Pulse I, delayed an additional 0.5 μsec. by delay unit γ, and pulse II, delayed an additional 1.0 μsec. by delay unit δ, entered an eleven-channel double-coincidence unit, ϵ. In this unit, pulse I produces a sequence of eleven "gate" pulses, one on the heels of the other. The first lasted 1.0 μsec., while the succeeding ten were each about 0.6 μsec. long. Each of the eleven gate pulses went to one input of eleven corresponding double-coincidence circuits. Pulse II was applied as a narrow "spike" to the other (paralleled) inputs of the eleven double-coincidence circuits. Only that coincidence circuit gave an output whose input gate was "on" at the time of arrival of pulse II. The counts of the eleven double-coincidence circuits were recorded on eleven electro-mechanical counters ("message registers"). Consideration of the time relationships in the complete circuit shows that the first message register recorded "prompt" coincidences, in which counter group II discharged between 0.5 μsec. before and 0.5 μsec. after counter group I; the second message register recorded delayed coincidences in which II discharged between 0.5 and 1.1 μsec. after I; the third message register recorded delayed coincidences in which II discharged between 1.1 and 1.7 μsec. after I; and so on, out to a maximum delay of about 6.5 μsec. The apparatus thus recorded continuously a differential time-distribution curve, the time scale being divided up into segments of about 0.6 μsec.

The essential features of the circuits just described are due to M. L. Sands.[10] We added several refinements designed to reduce spurious effects. The two main sources of false delayed coincidences were accidental delayed coincidences of two unrelated particles, and the occasional large delays of the counters of group II with respect to those of group I when actuated simultaneously. The special coincidence circuits had a feature (pointed out in reference 10) which reduced the frequency of accidental coincidences. A pulse, on any of its three inputs, paralyzed the circuit for about 14 μsec. Thus, if the particle which triggered group I also triggered any one of the counters of group II, a second particle which triggered group II could not give rise to an accidental delayed coincidence (the maximum measurable delay,

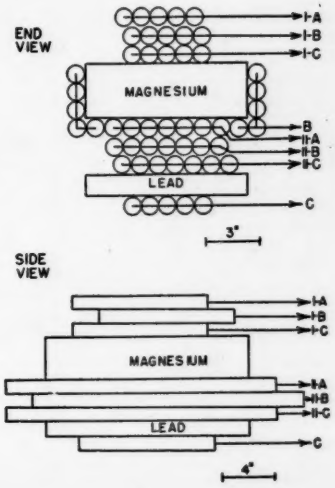

FIG. 1. Geometrical arrangement of the absorbers and G-M tubes.

[10] Rossi, Sands, and Sard, Phys. Rev. **72**, 120 (1947). It is to be hoped that the designer of these ingenious and reliable circuits will find time to publish a detailed description of them.

[11] See, for references, D. R. Corson and R. R. Wilson, Rev. Sci. Inst. **19**, 207 (1948).

ca. 6.5 μsec., being less than 14 μsec.). In our experiment we strengthened this protection by adding the G-M tubes of group B. These were connected to the special coincidence circuit, β, in such a way that any pulse from B paralyzed the circuit for the next 14 μsec. but did not give rise to an output pulse II unless it was followed within 0.5 μsec. by pulses from $II-A$, $II-B$, and $II-C$. A coincidence (within 0.5 μsec.) of $II-A$, $II-B$, and $II-C$ produced, on the other hand, an output pulse II whether or not there was a pulse from B. The expected rate of accidental coincidences in the i-th channel is, therefore,

$$\{(I-A\cdot I-B\cdot I-C) - (I-A\cdot I-B\cdot I-C:II-A+II-B+II-C+B)\} \times(II-A\cdot II-B\cdot II-C)\tau_i,$$

where the first term in curly brackets represents the rate of triple coincidences of $I-A$, $I-B$, and $I-C$, the second term in curly brackets represents the rate of triple coincidences of $I-A$, $I-B$, and $I-C$ accompanied by a pulse from $II-A$ or $II-B$ or $II-C$ or B; the second factor is the rate of triple coincidences of $II-A$, $II-B$, and $II-C$, while τ_i is the width of the channel in question. Addition of the counters B reduced the magnitude of the expression in curly brackets. Even so, the latter was about one-third of $(I-A\cdot I-B\cdot I-C)$, a result which can be ascribed to the large amount of soft radiation present at 3500 m altitude. By means of a toggle switch, circuit β could be altered to give a pulse II whenever a pulse from $II-A$ or $II-B$ or $II-C$ or B entered it. The prompt $(I:II)$ coincidence rate in this case gave the second term in curly brackets.

The effect of fluctuating counter lags on the delayed coincidence rates is discussed in the next section. It is shown there that the effect can be calculated with good accuracy if one knows how often a particle (or simultaneous particles) traversing $I-A$, $I-B$, $I-C$, $II-A$, $II-B$ and $II-C$ produces a coincidence in each of our delayed coincidence channels. In order to determine this frequency experimentally, we added the lead slab, G-M tubes C, the gate generating circuit ζ, and the coincidence gating circuit η. The lead slab was of ample thickness to stop any decay electron coming from above. Thus, when there was a prompt coincidence of group I and C, group II must have been traversed simultaneously, and any delayed coincidence recorded must have been due to the shortest counter lag in group II exceeding by this recorded delay time the shortest counter lag in group I. In the gate generating circuit, ζ, pulses from C produced 0.5 μsec. (or 1.0 μsec., depending on the throw of a switch) rectangular pulses which entered the gating circuit, η. The narrow pulse I, delayed an additional 0.5 μsec. by circuit γ (for a total delay of 1.0 μsec. from the earliest of the pulses of group I) also entered the gating circuit. It could only pass through to the multiple coincidence unit ϵ if the gate from C was on. Thus ϵ could only function if there was a pulse from C within 0.5 μsec. (or 1.0 μsec.) after the earliest pulse from group I. The readings of ϵ in this case gave us the frequency of delayed coincidences due to counter lags from prompt events. When we wished to measure true delayed coincidences due to meson disintegrations, we permanently opened the gate η by throwing a switch. Measurements of true delays and of counter lags were alternated.

The circuit also contained a scaler and message-register for monitoring various counting rates. The scaler could be connected to any one of six points, enabling us to determine the following rates: $(I-A\cdot I-B\cdot I-C:C)$, $(I-A\cdot I-B\cdot I-C)$, $(I-A+I-B+I-C)$, $(II-A\cdot II-B\cdot II-C)$, $(II-A+II-B+II-C+B)$, C. The first expression represents the rate

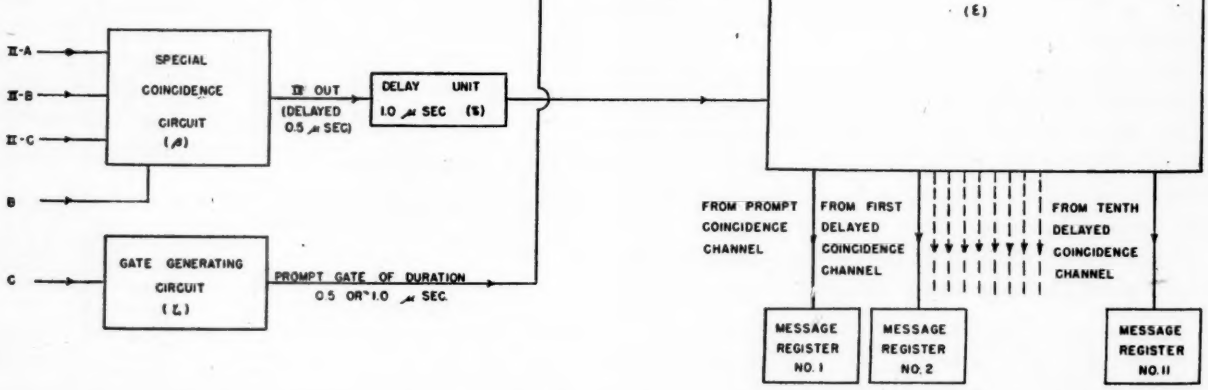

FIG. 2. Functional diagram of the circuit.

of events in which $I-A$, $I-B$, and $I-C$ discharge within 0.5 μsec. and C discharges within 0.5 (or 1.0) μsec. of the earliest of them; the second the rate at which $I-A$, $I-B$, and $I-C$ discharge within 0.5 μsec. of each other; the third the rate at which $I-A$ and/or $I-B$ and/or $I-C$ discharge, being recorded through a mixer of 14 μsec. insensitive time; the fourth the rate at which $II-A$, $II-B$, and $II-C$ discharge within 0.5 μsec. of each other; the fifth the rate at which $II-A$ and/or $II-B$ and/or $II-C$ and/or B discharge, as recorded through a mixer of 14 μsec. insensitive time; and the sixth the rate at which C discharges. The monitor was switched between the six positions during the experiment. The reading in the first position had the meaning stated only when the circuit η was switched to perform its gating function; when the gate was thrown open, the readings in the first and second positions coincided.

Periodic calibrations of the circuit were made, using three artificial pulses whose time of occurrence with respect to a trigger pulse could be continuously and independently adjusted by fifteen-turn helical potentiometers ('helipots') whose settings were reproducible to within ±0.01 μsec. This "sliding pulser" was copied from an unpublished design of Sands'; we added a circuit for synchronizing the trigger with a 2.500-Mc crystal-controlled oscillator which was also used to provide marker pips 0.4 μsec. apart. These marker pips were used to calibrate the helipots. The pulses were shaped to simulate G-M tube pulses, and their amplitudes were adjusted to equal those of the smallest pulses from the particular G-M tube groups. We feel that the determination of time differences was very accurate; the zero point of our time scale may, however, be somewhat off, because of the varying rise rates of the G-M tube pulses as contrasted with the uniformity of the artificial pulses.

III. THEORY OF THE EFFECT OF COUNTER LAGS

As has been pointed out by Rossi and Nereson,[12] the effect of variable G-M tube delays and of an error in the location of the zero of the time scale is to make each measured delay differ from the true delay by a variable amount t' independent of the delay. Let $f(t')dt'$ be the probability of an error in the interval dt' at t', $N(t)$ be the number of coincidences in which counter group II is actuated by a particle arriving more than t seconds after its parent has actuated counter group I, and $N_{obs}(t)$ be the measured number of coincidences in which the pulse from group II occurs more than t seconds after the pulse from group I. The smearing of the time distribution is given by[12]

$$N_{obs}(t)=\int_{t'=-\infty}^{+\infty} N(t-t')f(t')dt'. \qquad (1)$$

As illustrated in Fig. 3a, $N(t)$ has the large constant

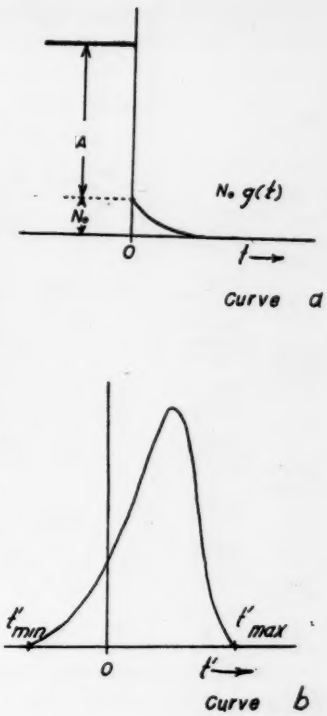

FIG. 3. a. Plot of $N(t)$, the true distribution of coincidences with delay greater than t. A is the number of prompt coincidences due to penetrating particles and showers; N_0 is the number of delayed coincidences due to decay electrons. b. Plot of $f(t')$, the differential probability distribution of the difference between the measured delay and the true delay. For no distortion of the time distribution, $f(t')$ would have to be a delta-function.

value $A+N_0$ for negative t, and the small diminishing value $N_0g(t)$ for positive t. A is the true number of "prompt" coincidences caused by penetrating particles and showers and N_0 is the true number of delayed coincidences due to meson decays; $g(t)$ would be $\exp(-t/\tau)$ for a simple exponential decay. As illustrated in Fig. 3b, $f(t')$ is expected to be a peaked but not necessarily symmetrical function, differing appreciably from zero only for several tenths of a microsecond to either side of the origin. It is clear physically that $f(t')$ is essentially zero everywhere outside a finite interval $t'_{min}<t<t'_{max}$. If the shortest delay measured, t, is greater than the longest lag, t'_{max}, (this is the case for all delayed channels after the first), (1) becomes

$$N_{obs}(t)=N_0\int_{t'_{min}}^{t'_{max}} g(t-t')f(t')dt'. \qquad (2)$$

For a mixture of positive and negative mesons, $g(t)$ is a linear combination of two exponentials

$$g(t)=a\exp(-t/\tau_+)+b\exp(-t/\tau_-)$$

and

$$N_{obs}(t)=N_0a\exp(-t/\tau_+)\int_{t'_{min}}^{t'_{max}}\exp(t'/\tau_+)f(t')dt'$$

$$+N_0b\exp(-t/\tau_-)\int_{t'_{min}}^{t'_{max}}\exp(t'/\tau_-)f(t')dt'. \qquad (3)$$

The number of counts in a delay channel extending from

[12] B. Rossi and N. Nereson, Phys. Rev. 62, 417 (1942).

TABLE I. Calibration of delayed coincidence channels.*

		Nov. 17	Dec. 3	Dec. 16	Dec. 30	Jan. 4	Mean value, weighted according to duration of decay measurements between successive calibrations
First channel	Delay to midpoint of channel	0.75	0.74	0.80	0.80	0.80	0.76
	Width of channel	0.71	0.73	0.64	0.69	0.59	0.67
Second channel	Delay to midpoint of channel	1.37	1.36	1.38	1.39	1.35	1.37
	Width of channel	0.63	0.62	0.58	0.59	0.63	0.61
Third channel	Delay to midpoint of channel	1.94	1.92	1.98	1.98	1.96	1.95
	Width of channel	0.60	0.62	0.63	0.64	0.63	0.62
Fourth channel	Delay to midpoint of channel	2.51	2.51	2.55	2.59	2.56	2.54
	Width of channel	0.61	0.63	0.66	0.66	0.66	0.64
Fifth channel	Delay to midpoint of channel	3.08	3.10	3.15	3.19	3.15	3.13
	Width of channel	0.58	0.57	0.66	0.65	0.64	0.61
Sixth channel	Delay to midpoint of channel	3.68	3.68	3.76	3.81	3.78	3.72
	Width of channel	0.65	0.63	0.67	0.65	0.67	0.65
Seventh channel	Delay to midpoint of channel	4.27	4.29	4.37	4.42	4.39	4.33
	Width of channel	0.60	0.61	0.65	0.62	0.63	0.62
Eighth channel	Delay to midpoint of channel	4.87	4.88	4.95	5.01	4.97	4.92
	Width of channel	0.66	0.67	0.66	0.64	0.66	0.66
Ninth channel	Delay to midpoint of channel	5.45	5.46	5.55	5.64	5.61	5.51
	Width of channel	0.64	0.65	0.68	0.70	0.67	0.66
Tenth channel	Delay to midpoint of channel	6.05	6.05	6.18	6.24	6.21	6.11
	Width of channel	0.60	0.61	0.65	0.62	0.63	0.62

* The numbers are times in microseconds.

t_i to t_{i+1} ($t_i > t'_{max}$) is then,

$$N_{obs}(t_i)-N_{obs}(t_{i+1}) = N_0 a[\exp(-t_i/\tau_+)-\exp(-t_{i+1}/\tau_+)] \times \int_{t'_{min}}^{t'_{max}} \exp(t'/\tau_+)f(t')dt' + N_0 b[\exp(-t_i/\tau_-) -\exp(-t_{i+1}/\tau_-)] \int_{t'_{min}}^{t'_{max}} \exp(t'/\tau_-)f(t')dt'. \quad (4)$$

The relative weights in the linear combination are distorted by the lags, but by a factor independent of t_i and t_{i+1}. A series expansion of the exponential in the integrands shows that the distortion is small if, as in the present experiment, the mean and root-mean-square values of t' are small compared to both τ_+ and τ_-. For the limiting case of a single exponential ($\tau_+=\tau_-$) the distortion vanishes, the only effect of the lags being to change the number of decays observed.[12]

When t can be smaller than t'_{max}, (1) becomes

$$N_{obs}(t)=N_0\int_{t'-t'_{min}}^{t} g(t-t')f(t')dt'+(A+N_0) \times \int_{t'=t}^{t'_{max}} f(t')dt'. \quad (2')$$

For our first delay channel, $t_1<t'_{max}<t_2$, and

$$\begin{aligned} N_{obs}(t_1)-N_{obs}(t_2) &= N_0 a \exp(-t_1/\tau_+)\int_{t'_{min}}^{t_1} \exp(t'/\tau_+)f(t')dt' \\ &\quad - N_0 a \exp(-t_2/\tau_+)\int_{t'_{min}}^{t'_{max}} \exp(t'/\tau_+)f(t')dt' \\ &\quad + N_0 b \exp(-t_1/\tau_-)\int_{t'_{min}}^{t_1} \exp(t'/\tau_-)f(t')dt' \\ &\quad - N_0 b \exp(-t_2/\tau_-)\int_{t'_{min}}^{t'_{max}} \exp(t'/\tau_-)f(t')dt' \\ &\quad + (A+N_0)\int_{t_1}^{t_2} f(t')dt', \quad (4') \\ &= N_0 a[\exp(-t_1/\tau_+)-\exp(-t_2/\tau_+)] \times \int_{t'_{min}}^{t'_{max}} \exp(t'/\tau_+)f(t')dt' \\ &\quad + N_0 b[\exp(-t_1/\tau_-)-\exp(-t_2/\tau_-)] \times \int_{t'_{min}}^{t'_{max}} \exp(t'/\tau_-)f(t')dt' \\ &\quad + (A+N_0)\int_{t_1}^{t_2} f(t')dt'. \quad (4'') \end{aligned}$$

In going from (4') to (4''), we have used the fact that only a very small fraction of the lags (of the order of 1.6×10^{-4}) occurs beyond t_1. The last term of (4'') is the number of prompt coincidences thrown into the first delay channel by the lags. This can be calculated with the help of the data obtained when group I is required to be in prompt coincidence with tray C. In effect, the integral is very closely the ratio of the number of counts

in the first delay channel to the number in the prompt channel when C is in control, while $(A+N_0)$ is very closely the number of counts in the prompt channel when C is not controlling.

The effect of variable lags and of an error in the location of the zero of the time scale is seen to be twofold: a small distortion of the relative weight of the two exponential components (smearing of the true decay curve) and a throwing of some truly prompt coincidences into the first delay channel. As we shall show in the next section, only the second effect is serious in our experiment.

IV. RESULTS

The meson decay measurements (C not controlling), which were made at intervals between November 22, 1947 and January 1, 1948, had a total duration of 466.6 hours. Lag measurements (C controlling) were interspersed throughout the period December 3 to January 3, and lasted 214.65 hours. Time calibrations of the circuit were made on November 17, December 3, December 16, December 30, and January 4. Tests of the individual G-M tubes were made at more frequent intervals, and during the runs the counting rates were checked two or three times a day.

The calibration data relative to the delayed coincidence channels are shown in Table I. While the calibrations could be made with good precision and repeatability (± 0.01 μsec.), there were appreciable variations in the results obtained on different days. These are thought to be due in large part to bias changes resulting from changes in the room temperature and aging of circuit components. The widths of the different channels are not expected to be exactly the same, each being determined by the effective length of its own section of delay line.

In an effort to take into account the systematic changes in the positions and widths of the delay channels, we have divided the decay data into four groups, each comprising the data obtained between successive calibrations. The data in each group are assumed to refer to channel widths and midpoints obtained by averaging the results of the calibrations which began and ended the period. The weight of each group in the final result is taken to be proportional to the duration of the decay measurements included in it. In this way, we arrive at the numbers in the last column of Table I, the weighted means of the widths of the channels and the delays to their centers.

TABLE II. Delayed coincidence data.

Counts in 466.6 hours (Nov. 22–Jan. 1)

Delayed coincidence channel	Raw data	Corrected for effect of lags	Reduced to standard channel width of 0.63 μsec.	Corrected for accidental coincidences	Final corrected data (number for first channel multiplied by 1.959)	Estimated statistical standard error
First	2241 (849 in the 238.2 hours between Dec. 3 and Jan. 1)	— 474±40 (in 238.2 hours)	— 445±40 (in 238.2 hours)	— 421±40 (in 238.2 hours)	825	±83 (= [849+78²]^½)
Second	571	571	590	549	549	±24
Third	374	374	380	339	339	±19
Fourth	275	275	271	230	230	±17
Fifth	212	212	219	178	178	±15
Sixth	174	174	169	128	128	±13
Seventh	136	136	138	97	97	±12
Eighth	108	108	103	62	62	±10
Ninth	92	92	88	47	47	±10
Tenth	78	78	79	38	38	± 9

TABLE III. Coincidences with lag-measuring arrangement (C controlling).

Counts in 261.77 hours in the interval Dec. 3–Jan. 3

Prompt coincidences	Delay channels									
	First	Second	Third	Fourth	Fifth	Sixth	Seventh	Eighth	Ninth	Tenth
523,104	83	1	0	1	0	1	0	1*	1*	0*

* For only 174.45 hours, in which the number of prompt coincidences was 410,704.

The data obtained in the meson-decay measurements (C not controlling) are shown in the second column of Table II. The numbers given there have to be corrected for the effect of lags and for accidental delayed coincidences.

The data obtained in the lag measurements (C controlling) are totalized in Table III. Almost all of the measurements were made with the gate pulse from circuit ζ 0.5 μsec. long, requiring that C discharge between 0 and 0.5 μsec. after the earliest discharge of counter group I. For 26.03 of the 261.77 hours, the gate was made 1.0 μsec. long; as this change had no significant effect on the results, the data from this period are included in the total. The lag counts in the delay channels beyond the first are suspected to be of accidental origin. Unfortunately no lag measurements were made with the switch in circuit β thrown to give $(I-A\cdot I-B\cdot I-C:II-A+II-B+II-C+B)$, so that we are unable to calculate the expected number of accidental coincidences (which would have been produced by side showers striking IA, IB, IC and C but missing counter group II). Whether or not the counts in these later channels are true lags or accidentals has, at any rate, a negligible effect on the results.

The ratio of the lag counts in the first delay channel to the prompt counts is seen to be $83/523{,}104=(1.59\pm0.17)\times10^{-4}$. This is the value of the integral in the last term on the right-hand side of Eq. (4″), representing the probability of a truly prompt coincidence being thrown into the first delay channel. In this connection it is worth noting that the starting time of the first delay channel ranged from 0.37 μsec. (December 3) to 0.50 μsec. (January 4).

As the number of counts obtained in the first delay channel in the decay-measuring arrangement was large, it is thought wiser to use only those (numbering 849)

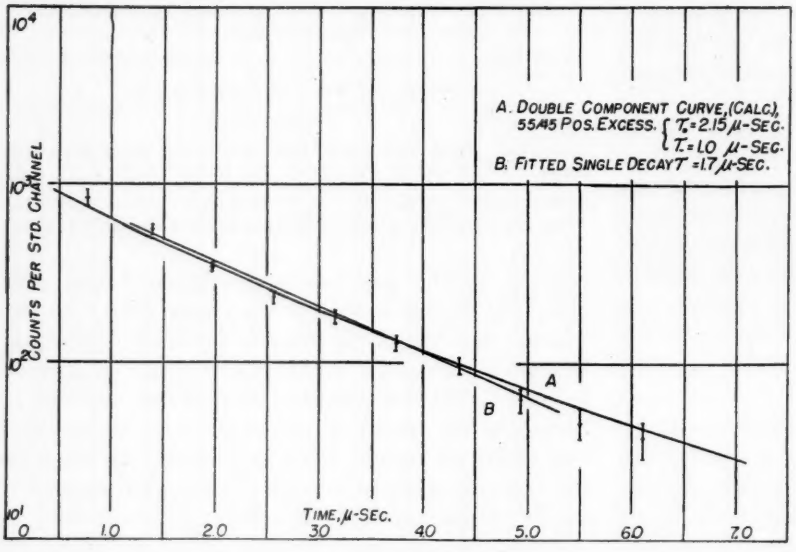
A. DOUBLE COMPONENT CURVE, (CALC), 5545 POS. EXCESS. $\tau_+ = 2.15\ \mu$-SEC. $\tau_- = 1.0\ \mu$-SEC.
B. FITTED SINGLE DECAY $\tau = 1.7\ \mu$-SEC.
COUNTS PER STD. CHANNEL
TIME, μ-SEC.
A
B

FIG. 4. The differential decay curve from mesons stopped in magnesium. The number of counts per 0.63 μsec. time interval is plotted against the delay to the center of the interval. The experimental points are estimates of the mean numbers, derived from our data, the vertical lines representing estimated statistical standard deviations. Also plotted for comparison is a calculated composite curve, as well as a single exponential fitted to the data by the method of Peierls (see text).

which were obtained in the period (December 3–January 1) during which frequent lag measurements were made. In this period the number of prompt coincidences (A in (4″)) was 2,358,672, so that the last term in (4″) becomes 375±40. Subtracting this correction, we obtain the figure in the third column of Table II, 474±40.

It is seen that the lag correction is appreciable for the first delay channel. Unfortunately, the frequency of the lags is so small that the correction itself has a considerable statistical inaccuracy. An even greater uncertainty results from the fact that the C tray did not completely cover the cone defined by counter groups I and II. Hence the lag distribution measured refers only to cases in which particles passed through the central portion of counter group II.

It remains to correct for the accidental delayed coincidences. The number of these as well as of true delays (to a good approximation) is proportional to the channel width. We therefore now reduce the number of counts in each channel to a standard channel width of 0.63 μsec. The results are given in the fourth column of Table II. Measurements with the switch in circuit β thrown so as to give ($I-A\cdot I-B\cdot I-C$:$II-A+II-B+II-C+B$) were made on December 12–13, simultaneously with measurements of the ($I-A\cdot I-B\cdot I-C$) rate. The difference of these two was 99.9/min. (i.e. 433.9/min.–334.0/min.). Immediately afterwards (December 13–14) the ($II-A\cdot II-B\cdot II-C$) rate was measured as 1483/min. The expression in Section II for the mean accidental rate gives then 9.33×10^{-2}/hr. for a 0.63 μsec. channel. The average ($I-A\cdot I-B\cdot I-C$) rate in the period November 22–January 1 was 412.5/min. Assuming that the accidental rate is proportional to this rate, we use 8.87×10^{-2}/hr. for the mean accidental rate, giving 41 as the expected number of accidentals per standard channel width in 466.6 hours. A similar calculation for the 238.2 hour period between December 3 and January 1 gives 24 as the expected number of accidentals in the first delay channel (reduced to standard width). The fifth column of Table II shows the corrected numbers of counts per standard channel, the expected number of accidentals having been subtracted off. The sixth column gives the final results: our estimate of the mean number of true delayed coincidences in each channel during 466.6 hours. The number of counts in the first delay channel has been scaled up to correspond to a duration of 466.6 hours. It is seen from Table II that the result for the first delay channel is strongly affected by the rather uncertain lag correction, while the correction for accidentals has a large effect on the results for the last delay channels. In fitting curves to the data we have, therefore, ignored the first, ninth, and tenth delay channels.

If the mean accidental rate were known with high precision, the standard error of one of our estimates, e.g. 230 for the fourth channel, could be fairly estimated as simply the square root of the number of observed delays,[13] e.g. $(275)^{\frac{1}{2}}=17$. These estimated standard errors, which are purely statistical, are given in the last column of Table II. In the first delay channel the statistical error in the lag correction (±78) is compounded with the statistical error in the decay measurement ($\pm(849)^{\frac{1}{2}}$) to give ±83.

There were, of course, systematic errors over and above the statistical uncertainties. There were changes of as much as 20 percent in the prompt coincidence rates, which seemed to be correlated with weather conditions. These could affect only the accidental correction (41 per channel), so that the corresponding systematic errors in the corrected numbers of delayed coincidences would be negligible compared to the statistical uncertainties, though approximately equal to the estimated statistical standard errors in the last three delayed channels. The shifting of the channel widths and positions (Table I)

[13] A. Sard and R. D. Sard, to be published.

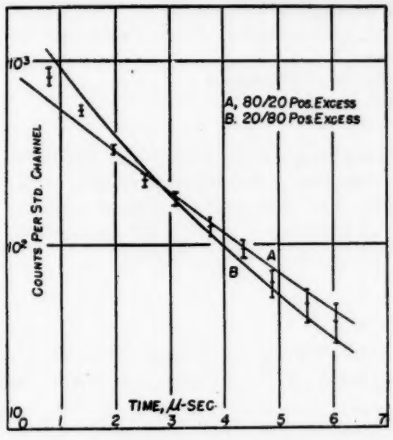

FIG. 5. Comparison of the results with composite decay curves calculated for positive-negative stopped meson ratios of 80–20 and 20–80. The effective mean lives of the positives and negatives are assumed to be 2.15 and 1.0 μsec. respectively.

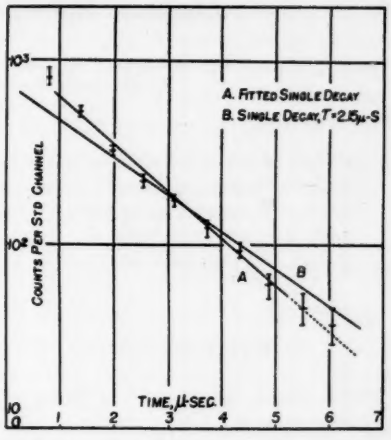

FIG. 6. Comparison of data and its equivalent single decay curve of mean life 1.7 μsec. with a single decay curve of 2.15 μsec.

introduced systematic errors in both the corrected numbers of counts per standard channel width and in the weighted mean values of the delays of the channel midpoints.

The results (last two columns of Table II, last column of Table I) are plotted semilogarithmically in Fig. 4. These are points of the differential decay curve of the mixture of positive and negative mesons stopped in magnesium at 3500 m. altitude. As the systematic errors are not large enough to have an appreciable effect on the fitting of curves, we have not indicated them in Fig. 4.

We have calculated the differential decay curves to be expected on the assumption that competition between capture and decay results in a lower effective mean life for the negative meson and a smaller number of decay electrons from negative mesons. The curve for a 55–45 mixture of positives and negatives and a mean life for the negatives of 1.0 μsec. is shown in Fig. 4. It is seen to fit the experimental results. Even with our relatively small experimental uncertainties, it is, unfortunately, impossible to pin down these two parameters within narrow limits. Figure 5 shows that it is necessary to go to such extreme values of the positive-negative ratio as 80–20 and 20–80 in order to get a poor fit. This justifies, incidentally, our neglect of the effect of counter lags on the relative weight of positives and negatives in the mixture.

The expected composite curve can be approximated by a pure exponential of intermediate mean life. By applying the procedure of Peierls[14] to the results for the second through eighth delay channels, we obtain 1.7 ± 0.1 μsec. for this apparent mean life. The 1.7 μsec. pure exponential is drawn in Figs. 4 and 6 and is seen to give essentially as good a fit as the composite curve. It is clear from Fig. 6 that a pure exponential of 2.15 μsec. mean life would give a poor fit.

V. ACKNOWLEDGMENTS

We are grateful to Professor Marcel Schein of the University of Chicago for permission to use the High Altitude Cosmic Ray Laboratory of the University of Chicago at Climax, Colorado and to the Chicago Branch of the Office of Naval Research for assistance with the material arrangements. Through the kindness of the officers and men of the Naval Air Station, St. Louis, it was possible to test the apparatus in an aircraft at 3500 meters before sending it to Colorado. The work was part of a research program supported by the U. S. Government through the ONR.

We are indebted to Mr. J. D. Miller for his fine work in building and testing the electronic equipment used in this experiment.

[14] R. Peierls, Proc. Roy. Soc. **A149**, 467 (1935).

Absolute Speed Gauge for High Voltage Particles*

W. ALTAR AND M. GARBUNY
Westinghouse Research Laboratories, East Pittsburgh, Pennsylvania
(Received February 21, 1949)

A precision method has been devised to measure nuclear reaction voltages, and equipment has been built capable of measuring reaction energies of charged heavy particles in the Mev range with accuracies of ~0.1 percent. Limitations of the operation are discussed and the possibility of a direct determination of the electronic charge-to-mass ratio and related fundamental constants is pointed out. To verify the conclusions reached, test runs have been carried out with electron beams, and performance was as expected.

INTRODUCTION

THE need for a direct and precise method for measuring speeds of fast charged particle beams arises in the study of nuclear reactions because the precise threshold and resonance energies at which these reactions occur form the basis of evaluation of nuclear constants besides being significant in their own right. Existing instruments such as the generating voltmeter are valuable for linear interpolation between reference voltages but are inherently unsuited for absolute calibration. Consequently, energy quotations from different observers are frequently found difficult to correlate even though different measurements by the same observer may be quite consistent relative to each other. It is fortunate that the threshold and resonance energies are extremely sharp and so will themselves provide the most convenient scale, once their values are established with commensurate precision.

For instance, the half-width of the 985 kv Al(p, γ) reaction is only 300 volts or less when a thin target[1] is used, and other reactions occur with comparable sharpness. Equipment described in the following had for its immediate purpose a determination of the Li(p, n) threshold at 1.89 Mev, described in the companion paper.[2] We were content with an accuracy of 0.1 percent, in view of more stringent limitations arising in the present application from the voltage constancy attainable with the Van de Graaff generator. But this is by no means the highest accuracy of the speed gauge. Given a constant voltage source, a precision-built r-f cavity and a carefully focused electron or ion beam, the accuracy can probably be increased by a factor of the order 10.

For the present purpose the charge-to-mass ratio, which enters into the evaluation of the measurements, is known for protons, deuterons and electrons with sufficient accuracy. It is possible to reverse the procedure, however, and thus to obtain a precise value for the electronic charge-to-mass ratio, of an accuracy at least comparable to the most accurate non-direct methods, and far exceeding the accuracy of direct e/m determinations heretofore used. Besides, in view of a slight discrepancy now existing between the two non-direct methods it is interesting and practicable to design a speed gauge precision-built for the purpose of obtaining e/m within 0.01 percent.

A typical application of the new device would be e.g., the determination of the proton-neutron mass difference by combining the results from (p, n) reactions with those of other suitable reactions.

Perhaps more interesting from a fundamental viewpoint, the device offers an absolute determination of speed and kinetic energy of the particle just before entering into a reaction. Unlike the electrostatic analyzer which compares voltages in the Mev region with much lower known voltages, the r-f speed gauge establishes an absolute voltage scale directly related to the fundamental atomic constants.

II. DESCRIPTION OF OPERATING PRINCIPLE

The principle on which the method is based, has been reported earlier.[3] Transit of the charged particle through two successive, accurately spaced r-f gaps is timed in terms of the period of an r-f oscillation of accurately known frequency. Thus one finds the particle speed as the ratio of the two most accessible and most direct data. Among several possible schemes for effecting the experiment[4] the one best suited provides for exceedingly tight coupling between gaps by means of a high frequency resonator cavity of high Q, of which the two gaps form a part. The high cavity-Q assures one of a high degree of phase synchronism at the two gaps, in addition to the obvious gain in power economy which results in higher signal voltage; thus a high Q is necessary for the required accuracy (0.1 percent in voltage) and also advantageous for sensitivity (beam currents of the order of 10^{-6} amp. or less).

The beam current is modulated at the source with 70 megacycles/second (Fig. 1a), and after acceleration passes in succession through the two gaps which are separated by a field-free drift space. The cavity is capable of electromagnetic resonance at the modulation frequency, in a mode which energizes both gaps in the same field directions at any instant. A particle will

* Assisted by the joint program of the ONR and the AEC.
[1] Bender, Shoemaker, and Powell, Phys. Rev. 71, 905 (1947).
[2] Shoupp, Jennings, and Jones, Phys. Rev., this issue.
[3] Altar, Garbuny, and Coltman, Phys. Rev. 72, 528 (1947).
[4] Coltman, Shoupp, and Altar, HV Ion Speed Gauge and Voltmeter. U. S. Patent appl. In particular, the operating scheme finally adopted was suggested to us by Dr. Coltman.

generally contribute net energy at the two gaps toward excitation of the mode, and the resulting r-f power is fed to an indicator. Only when transit time between gaps is exactly an odd multiple (preferably 11, 13) of half-cycles, will the two contributions from a given particle cancel each other exactly. The resulting null at the indicator serves as the timing criterion. To make impulses, contributed by all particles toward mode excitation, most effectively additive, it would be best to modulate the particle beam in very short pulses which would enter the cavity an integral number of cycles apart. It suffices, however, to modulate the beam periodically at the operating frequency, in which case the amplitude of the fundamental Fourier component is indicative of the excitation effect.

If the two gap fields are symmetric and have identical geometries, particles at the second gap will encounter an exact repetition of the field interacted with at the first gap; it will then clearly be permissible to identify effective gap spacing L with the relative displacement between two identical field configurations. Drift distance can then be ascertained with a very small error, considerably less than the longitudinal extension of the fields encountered and, indeed, much smaller than the gap width.

The beam voltage V corresponding to the n-th indicator minimum is related to drift length L, frequency f and speed $s=2fL/n$ as follows:

$$V=\frac{m_0c^2}{e}\left[\frac{1}{\left(1-\frac{s^2}{c^2}\right)^{\frac{1}{2}}}-1\right]$$

$$\cong\frac{2m_0}{e}\frac{f^2L^2}{n^2}\left(1+\frac{3f^2L^2}{n^2c^2}+\cdots\right) \quad (1)$$

where kinetic energy is represented by its relativistically corrected value. This correction, amounting to 0.3 percent for 2 Mev-protons, cannot be ignored.

Least accurate factor in (1) is the length L. If the drift distance is about 1 meter, L has to be measured with an accuracy of 0.05 cm or better to be satisfactory.

Frequency measurements and fundamental constants involved offer no problem at the currently attempted accuracy level.

III. SIGNAL AND NOISE CONSIDERATIONS

The probable error incurred in the presence of noise may be computed as the smallest deviation from the timing criterion (1) which results in a detectable signal-to-noise ratio. Signal power for given transit angles (differing from π by small amounts δ) is fixed by the condition of energy balance; the gap voltage will build up to a steady-state amplitude v such that power transfer P_{in} from the beam to the gap fields equals P_{out} lost by dissipation and other causes. Thus:

$$P_{\text{in}}=\int dt[i_0+i\cos\omega t][v\sin(\omega t-\varphi)$$

$$+v\sin(\omega\{t+L/s\}-\varphi)]$$

$$=iv\sin\delta/2\cos(\delta/2+\varphi)$$

in view of

$$\omega L/s=n\pi-\delta.$$

If both gaps contribute equally to the build-up, the phase of the excited electromagnetic oscillation is halfway between the two phases of the (sinusoidal) beam current when entering and, respectively, when leaving the cavity. This is true because interaction with the two fields may be represented as the vector sum of two a.c. vectors of equal magnitude, representing the respec-

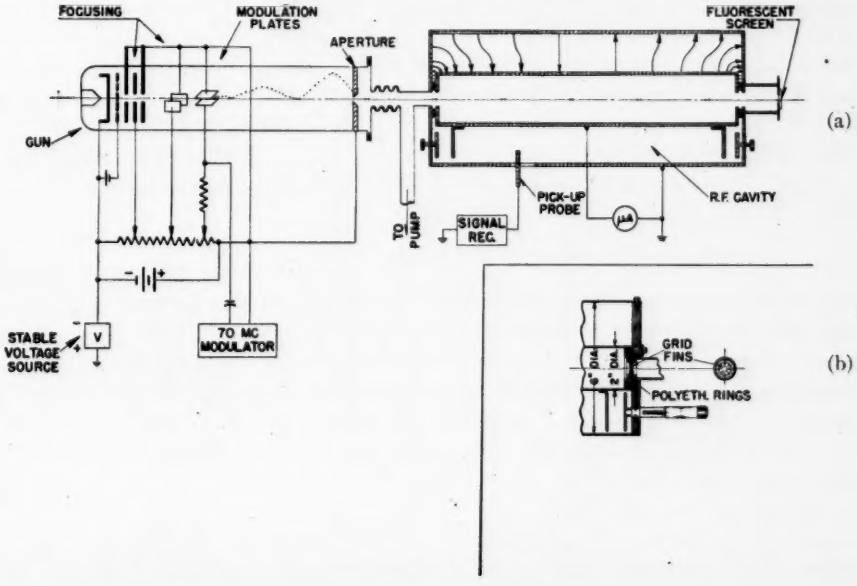

FIG. 1. (a) Schematic diagram of speed gauge. Experimental arrangement to measure particle speeds shown for the case of electron beams using a preferred method of deflection modulation. Spacings between bunches drawn for $n=9$ near minimum cavity response. Arrowed lines in cavity indicate electric field of the excited mode. (b) Design of cavity gap.

tive contribution at each gap. Hence:

$$\varphi = -\delta/2, \tag{2}$$

so

$$P_{\text{in}} = iv\cos(\omega L/2s) \cong (n\pi iv/2)(\Delta s/s), \tag{3}$$

where Δs is the deviation from the due value s_0 satisfying the timing criterion. If we define shunt resistance r_{sh} as that resistance which, when shunted across one of the two gaps will simulate the entire power loss in the cavity, we have for the steady-state condition

$$P_{\text{out}} = v^2/2r_{sh} = P_{\text{in}}; \tag{4}$$

hence from (3) and (4)

$$v = n\pi i r_{sh}(\Delta s/s). \tag{5}$$

Of course, under loaded conditions r_{sh} is considerably less than the purely dissipative value R_{sh} obtained when there is no power transfer to an indicator. If power is fed through a transformer of suitable "turns" ratio k, to an amplifier offering an effective resistance r across the first amplifier grid, it will be seen that the grid voltage is given by

$$V^2_{\text{grid}} = \frac{v^2}{k^2} = \frac{2r_{sh}}{k^2}P_{\text{out}} = \frac{2R_{sh}r}{R_{sh}+k^2r}P_{\text{out}}, \tag{6}$$

which can be maximized by making $k^2 = R_{sh}/r$. Comparing this with Eq. (3) one has

$$V_{\text{grid, opt}} = \frac{n\pi i}{2}r\left(\frac{v}{V_{\text{grid, opt}}}\frac{\Delta s}{s}\right) = \frac{n\pi i}{2}(R_{sh}r)^{\frac{1}{2}}\frac{\Delta s}{s}. \tag{7}$$

For instance, if the cavity has a shunt resistance $r_{sh} = 150{,}000$ ohms (300,000 ohms/gap) and operates into an amplifier showing an input resistance $r = 20{,}000$ ohms at the first grid, a signal of about 50 microvolts can be derived from a beam with a modulated component of 10^{-7} A operating at $n = 11$, for a deviation of 0.05 percent in speed (0.1 percent in particle voltage). Total r-f power generated would be 65×10^{-13} watt, half of which is dissipated in the cavity. The gap voltage is 130 microvolts for optimal loading, just half the value obtained if the cavity were unloaded.

Since the cavity represents in effect two tuned circuits, thermal noise originates to the extent

$$P_{\text{noise}} = 8ktf/Q \sim 4\times10^{-16} \text{ watt},$$

clearly far below the signal level. Noise originating in the first amplifier tube is larger but not objectionable. Since there is no limitation on the time available for completion of a measurement, receiver bandwidth can be reduced almost at will. If a 6AK5 tube were used for the first amplifier stage, the noise component in the plate current would be $2.5\times10^{-14}\Delta f$ amp. The receiver bandwidth Δf actually used was 10 kc and since the signal at this level of amplification is 2×10^{-7} amp., noise from extraneous sources is not a limitation.

Another—intrinsic—limitation is more interesting because it arises directly from the statistical nature of the beam current itself. As a consequence of beam density fluctuations, the frequency of the cavity oscillations is not defined with absolute precision but has statistical uncertainty. The attending spectral width can be narrowed by using a cavity of high Q. If the driving force were strictly sinusoidal or otherwise periodic, its period would be identical with the response period, and the frequency would be defined regardless of the cavity-Q. In the other extreme, if the cavity has an extremely high Q, there would be no need for periodicity of modulation except for the purpose of securing a higher sensitivity of the cavity response. Each particle, or sharp pulse of particles, could serve individually to show deviations from the timing criterion, and the frequency of the signal would be the resonance frefiuency of the cavity. The practical case lies between the two extremes, in that strict periodicity of the beam current is marred by statistical fluctuations, and that the cavity Q is high but finite.

To analyze this case, we may consider the steady state as resulting from many transient impulses set up by the consecutive half-cycles of the modulated beam. Each impulse results in an oscillation at the natural cavity frequency which decays exponentially, but owing to the slight uncertainty $(\Delta I)_\tau$ (this suffix indicates that average has been taken over one half-cycle) the beam modulation frequency fluctuates around the due value with a probable deviation given by $(\Delta f/f)_{\text{resp.}} = 1/(2\pi)(\Delta I/I)$. Here, the steady-state value of current I and its fluctuation ΔI can be computed from the build-up process as follows:

$$\frac{\Delta I}{I} = \left(\frac{\Delta I}{I}\right)_\tau \frac{(\frac{1}{2}(1+e^{-\pi/Q}+e^{-2\pi/Q}\ldots))^{\frac{1}{2}}}{1+e^{-\pi/2Q}+e^{-2\pi/2Q}+e^{-3\pi/2Q}\ldots} = \left(\frac{\Delta I}{I}\right)_\tau \left(\frac{\pi}{8Q}\right)^{\frac{1}{2}}.$$

In the numerator, the square root represents the r.m.s. value of all random fluctuations, subject to the natural circuit decay, and the factor $\frac{1}{2}$ takes into account the fact that these fluctuations take place in the two dimensions of the a.c. vector plane. This results in

$$(\Delta f/f)_{\text{resp.}} = (\Delta I/I)_\tau 1/4(2\pi Q)^{\frac{1}{2}}. \tag{8}$$

In the present application, using current amplitudes of order 10^{-7} amp. at $f = 10^7$ c.p.s., the number of particles per half-cycle is around 5000 so statistical fluctuations amount to about 1.5 percent. With a cavity of $Q = 6000$, statistical fluctuations of signal frequency should be restricted to around 0.002 percent which is safe for the present purpose.

IV. DESIGN OF CAVITY

Choice of a relatively low modulation frequency seemed indicated on two counts. For high precision,

a long drift distance is important because the fractional error in determining its length is the most stringent limitation of attainable over-all accuracy for the method. This requires that one keep the frequency low and the order number as high as possible. Secondly, by choosing the lowest frequency at which microwave techniques are still practicable, one combines the latter's advantage of high Q and shunt resistance with the advantage of high receiver sensitivity, all of which decrease at still higher frequencies. The order number n is more or less fixed by the intended beam voltage; since the length of the cavity is around 0.30λ one finds easily $ns/c \cong 0.60$. Around 2 Mev, this means $n \sim .60/0.065 \sim 9$. The frequency was chosen at 70 megacycles/sec., giving a cavity length of 125 cm.

The exact length of the cavity (Fig. 1a) is of course dependent on the gap width, about 1.5 mm in the present design. A certain freedom of choice existed between long and slender cavities and short cavities of large diameter. It was felt that the former offered the advantage of a higher accuracy (see Eq. (1), (5)), which outweighed the advantage of somewhat higher Q and R_{sh} values which might have been obtained by shortening the length. Most important, the longer cavity can be built from commercially available copper tubing which would have been impossible for larger diameters. The inner and outer diameters used were 5.0 and 15.0 cm, respectively.

Polyethylene rings separating the end plates of the two cylinders served as insulating spacers and at the same time as vacuum gaskets between the vacuum in the drift space and the normal pressure in the cavity proper (Fig. 1b).

Two variable plate condensers provide a means for adjusting the resonance frequency and for symmetry between the two gaps. For perfect canceling of r-f inputs at the two gaps, it is important that the gap voltages be equal to each other. Beyond this, it is feasible to compensate for loss of particles between the two gaps, by increasing the second gap voltage inversely in relation to the current. Incomplete compensation of these two effects results in a minimum instead of a null, and the accuracy of the timing criterion suffers as the curvature of the response curve goes down with increasing residual signal.

Grids at the gaps, in the form of thin radial fins, served to improve the electric field configuration at the gaps. Care had to be taken to hold to a minimum the cross section offered to the approaching particles by the fins. About 2 percent of the beam particles were intercepted, and the resulting disturbance through production of secondaries or scattering proved negligible upon investigation.

The unloaded cavity Q was measured to be 6000 which compares well with a previously computed value of 9200 representing copper loss but not dielectric losses in spacers, washers, etc. Tuning to the exact resonance frequency by means of the variable condensers provided no difficulties. The final Q-value was obtained only after elimination of unsuitable spacer components. By frequency modulating the input signal and rectifying the pick-up voltage, the frequency response of the resonator could be conveniently demonstrated, and the Q measured, by means of an oscilloscope. Thus reciprocal Q contributions could be assigned to various component parts and unsuitable specimens were eliminated.

A potential disadvantage of longer drift distances is an increase in the number of particles which get lost between the two gaps by collision with gas molecules or other causes. The attending unbalance between impulses contributed at the two gaps tends to flatten the response curve from a null to a shallower minimum and thus reduces the accuracy with which the latter can be read. It is possible to compensate largely for loss of particles by introducing an asymmetry into the cavity such that the second gap executes proportionately larger voltage oscillations. Still, since the statistical nature of the loss of particles adds to the random noise, it is probably best for high accuracy to maintain a good vacuum (10^{-5} mm or better) and to improve the beam focusing, minimize stray fields, etc.

V. EXPERIMENTAL RESULTS OBTAINED WITH ELECTRONS

Preliminary to applying the speed gauge to high energy protons, test runs were performed using electron beams of relatively low energy. Since generation of the r-f signal depends on the charge and speed, not on the mass of the particles used, these preliminary runs served to test the device under conditions approximating actual operation, yet without the complications of operating the Van de Graaff generator and of the low yield of ion sources. In particular, since particle velocities remain unchanged if beam voltage is reduced in the same proportion as the rest mass, the speed gauge could be tested with electrons against known voltages of the order of 1000 volts.

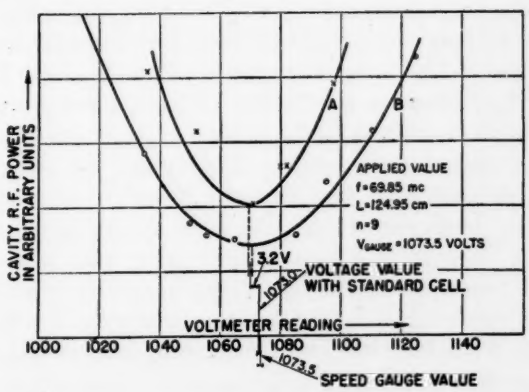

FIG. 2. Response of cavity energy build-up to beam voltage. Measured on the scale of comparing voltmeter. Curve A for more intense and better focused electron beam than in curve B. Contact potential of 3.2 volts has to be added to applied voltage for comparison value of speed gauge formula.

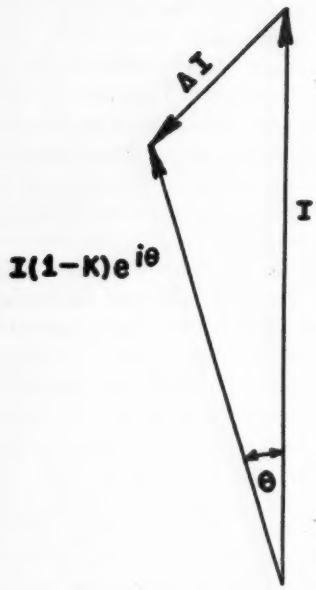

FIG. 3. Diagram for computing the theoretical curves for Fig. 2.

An electron gun of the type used in the RCA cathode-ray tube 5BP1A was carefully lined up along the axis of the speed gauge. Shielding against the earth's magnetic field is necessary with electrons to avoid curvature of the paths. This was effected by wrapping $\frac{1}{32}$-in. Hypernik ribbons around the outer cylinder.

Modulation was provided in the preliminary runs by sweeping the electron beam transversely back and forth by means of a 70-mc voltage applied to one pair of deflecting plates of the electron gun. The gun was first adjusted carefully to be coaxial with the gauge cylinders so that in the absence of transverse fields a focused electron beam impinged on a fluorescent screen mounted at the far end of the cavity. A biasing d.c. voltage equal to the amplitude of the r-f voltage was next applied to the deflecting plates, permitting the beam to enter the cavity through a centered aperture only at the extreme end of the swing. This has the advantage of highest modulated yield for given aperture size, because of the relatively long time intervals spent by the beam at positions near sweep reversal. The aperture diameter was chosen 2.8 mm, a compromise between conflicting requirements of high modulated yield and of good focusing. The number of particles lost between grids was measured by means of an ammeter connected between the inner and the grounded outer cylinder. The total beam current was measured with the same ammeter by means of magnetic deflection of all beam particles into the inner conductor. The fraction of particles lost was thus determined to be about 30 percent of the total. This can only in a small part be attributed to scattering and dispersion of the beam. The air pressure inside the cavity, estimated to be 5×10^{-5} mm Hg, implies a mean free path for 1kv electrons which must be around 20 times the drift length[5] so gas collisions account for only a fraction of the observed particle loss.

Dispersion caused the beam to spread to twice its diameter at the exit diaphragm of the cavity, and the first diaphragm was small enough to keep this source of particle loss in small bounds. Inaccurate focusing as well as defocusing by stray fields must thus be held accountable for most of the loss of particles, and will have to be avoided in future experiments aiming at a better accuracy. With the yield from the gun already cut down to 2 or 3 microamps., it seemed inappropriate with the present limited equipment to try for better focusing conditions in these electron experiments. It would have necessitated replacing our simple crystal rectifier with a detector-amplifier stage.

Figure 2 shows r-f response of the cavity in arbitrary power units as a function of the kinetic energy of the electrons. The theoretical shape of these curves was derived for parameter values k indicating the fraction of particles lost between gaps. Experimental points were then analyzed for a determination of k to give the best fit with a theoretical curve.

R-f power can be expressed in terms of beam current, shunt resistance, transit angle and characteristic resonator impedance $(L/C)^{\frac{1}{2}}$

$$\text{Power}=[(\Delta I)^2/2r_{sh}]L/C$$

where ΔI is the length of the vector difference shown in Fig. 3 between two vectors of length I and, respectively, $(1-k)$I embracing the net transit angle θ between them. This leads to

$$\text{power}\sim k^2+2(1-k)(1-\cos\theta).$$

For best fit, the values $k=0.32$ and $k=0.37$ had to be assigned to the curves A and B (Fig. 2), respectively. With these high k-values a good fit was obtained; also, they are well consistent with the direct determination of k by means of the ammeter. With this procedure, one ascertains the minimum of the theoretical curve with an accuracy far exceeding that obtainable from individual points themselves.

It is seen from Fig. 2 that the minimum can be read with 0.1 percent accuracy. Several runs of these curves taken on various days gave a total spread of 0.2 percent for the position of the minima. The average reading of the two minima shown is 1069.8 ± 1.0 volts as measured on the scale of the calibrated comparing instrument. The contact potential of the copper of the cavity and the BaO-surface of the gun had to be added to this value. This correction amounts to 3.2 volts and was arrived at in two ways with an accuracy sufficient for these measurements. First, the contact potential equals the difference of the work functions of the two materials concerned, except for a negligible contribution due to thermal effects. The work function of copper is 4.3

[5] Knoll, Ollendorf, and Rompe, *Gasentladungstabellen* (Verlag. Julius Springer, Berlin, 1935), pp. 115 and 116.

volts,[6] that of the BaO surface 1.1 volts,[7] yielding a contact potential of 3.2 volts. Secondly, the difference of speed gauge measurements of electron energy taken at other points and the corresponding voltage drop was found consistently to be 3.9 ± 1.0 volts. The only conceivable error might have been the lengthening of the electron path due to curvature in a magnetic field. The latter had, however, been effectively shielded, and such an effect could have increased the difference only by a very small amount. The total energy applied to the electrons therefore amounts to $1069.8+3.2=1073.0$ ±2.0 volts. The absolute voltage value as determined by Eq. (1), with $L=124.95$ cm, $f=69.85$ megacycles, $n=9$ and an $e/m_0=1.7592\times10^7$ (emu) g^{-1} is 1073.5 ± 0.3 volts in good agreement with the value above. However, the real test for the accuracy of the method lies in the precision with which the minimum can be located, and this is determined by the factor k, not by Eq. (1) in which all variables were measured to far better than 0.1 percent. The voltage was compared to a standard cell through precision resistances. The frequency was heterodyned against a secondary frequency standard.

VI. APPLICATION TO ION BEAMS

The accuracy attained in the electron runs was taken to give reassurance that at least equal accuracy would be attained with ion beams of several million volts. As described in the companion paper,[2] the ion beam which enters the cavity is already well focused, the small current strength being largely due to elimination of all badly focused beam portions, and the stiffness of the HV beam guards against much further particle loss within the cavity proper so k should be very small. This seems to be born out by the appearance of the minima in Fig. 4 of reference 2 which shows much stronger curvature at the minima.

[6] J. A. Becker, Rev. Mod. Phys. **7**, 95 (1935).
[7] J. B. Blewett, J. App. Phys. **10**, 831 (1939).

VIII. POSSIBILITY OF REVISING FUNDAMENTAL CONSTANTS

The best existing determinations of e/m have a probable error of 0.02 percent but other determinations are in poor agreement with this, giving a total spread of 0.2 percent of values used for determining the weighted average now accepted.[8,9] If the accuracy of our method is improved by a factor of 10, it will be possible to determine the electronic charge-to-mass ratio with greater accuracy, and more directly, than has been possible so far. To this end, the following improvements will be necessary:

1. For sharper definition of the gap spacing L, it will be advisable to reduce all gap dimensions to a fraction of the present values. Gap fields may be sharply localized between conical electrodes or other shapes designed for low capacity and high Q. Provision will have to be made for measurement of L after the cavity has been assembled.
2. Focusing and absence of stray fields will be very important to reduce particle loss between the gaps to a minimum. To obtain stiff electron beams, the accelerating voltage should have the highest possible value that can still be conveniently compared with a standard cell.
3. Modulation by sideways deflection will be even more important than in the present tests for keeping the forward velocity of the particles unchanged.

It will also be possible to determine h/e more accurately by measuring the electron energy exactly just before hitting an x-ray target. Once e/m has been determined, there is no further limitation on magnitude of accelerating voltage except the constancy with which it can be maintained.

Several discussions with Dr. J. W. Coltman proved exceedingly helpful in the course of this investigation, and our appreciation of his cooperation is gratefully acknowledged.

[8] J. W. M. DuMond and E. R. Cohen, Rev. Mod. Phys. **20**, 82 (1948).
[9] *Note added in proof.*—A very accurate value has been published recently by Thomas, Driscoll, and Hipple (Phys. Rev. **75**, 992 (1949)) using yet another indirect method.

An Absolute Calibration of the $Li^7(p,n)$ Threshold Voltage*

W. E. Shoupp, B. Jennings, and W. Jones
Westinghouse Research Laboratories, East Pittsburgh, Pennsylvania

(Received February 21, 1949)

The $Li^7(p,n)$ threshold has been the most generally accepted secondary voltage standard for nuclear experiments done with an electrostatic generator. Recent measurements of this threshold by electrostatic analyzer methods have given a result about 2 percent higher than the older value made by an extrapolation of a resistor measurement of the $Li(p,\gamma)$ resonance at 440 kv. The $Li^7(p,n)$ threshold has now been measured by a third method, the radio frequency ion speed gauge. The calibration by this method is absolute in that the kinetic energy of the particle is determined in terms of its known mass to charge ratio and two easily measurable parameters: a length and a frequency. The results of this calibration place the threshold at (1.8812±0.1 percent) Mev, in good agreement with values obtained from the electrostatic analyzer measurements.

BECAUSE of its sharpness and easy reproducibility the energy threshold of the $Li^7(p,n)$ reaction has become generally accepted as a secondary standard reference voltage for many nuclear experiments. The absolute calibration of this standard is consequently of considerable importance since its value, and other measurements made relative to it, enter in the determination of the masses of several atomic nuclei,[1] the neutron, the neutrino,[2] and the absolute value of many nuclear energy levels and resonances.

The most commonly used value of this secondary standard is based on the measurement of the $Li^7(p,n)$ threshold made by the Westinghouse group[3] in 1940, wherein they extrapolated the resistor measurement of the $Li^7(p,\gamma)$ resonance at 440 kv by Hafstad, Heydenburg and Tuve[4] to the $Li^7(p,n)$ threshold at 1.85 Mev using a compensated generating voltmeter of known linearity. This result was considered to be in error by as much as 1 percent or 2 percent because of the accuracy and corona characteristics of the resistor measurement and the long extrapolation involved. In 1944 Hanson and Benedict[5] measured the threshold by electrostatic deflection methods and obtained a value of 1.883 Mev for this threshold. The recent measurements of Herb, Snowdon and Sala[6] using a refined electrostatic analyzer yield a value of 1.882 Mev. The present measurement has been done by a method experimentally very different from either of the previous measurements and should serve as an independent calibration of this threshold.

EXPERIMENTAL

Method

The radio frequency ion speed gauge was used to make an absolute measurement of the velocity or voltage of the ion beam from the Westinghouse electrostatic generator at a point about 0.5 percent above the expected $Li^7(p,n)$ threshold. This voltage calibration point was interpolated to the threshold by a compensating generating voltmeter using a linear interpolation over this short voltage range. The generating voltmeter was also used as a source of error signal to stabilize the electrostatic generator voltage to better than 0.1 percent by the biased corona point method.

Absolute Voltage Calibration

The radio frequency speed gauge,[7] which is described in the accompanying article by W. Altar and M. Garbuny, permits one to establish a number of calibration points on the nuclear voltage scale. The calibration is absolute in the sense that the kinetic energy of a particle is determined in terms of its known mass plus directly and accurately measurable parameters: length and frequency. The ion beam of the electrostatic generator (Fig. 1) is intensity modulated by a defocusing electrode placed below the ion source probe and supplied from a 50V, 70 mc crystal controlled oscillator, mounted within the high voltage electrode of the electrostatic generator. After acceleration by the high voltage field of the generator, the modulated beam was analyzed into its various mass components by a deflection magnet and the desired beam sent through the two gaps in the resonant cavity. The cavity (Fig. 2) is of the coaxial type with the inside of the center conductor used as a field free beam drift tube. The two tuning condensers are adjusted simultaneously to bring the resonant frequency of the cavity to 70 mc, while keeping the *RF* voltages across the two gaps equal. The ion beam, as it passes through the first gap in the *RF* cavity, induces a 70 mc voltage in the cavity because of its density modulation. As it passes through the second gap, the voltage induced in this gap will either add or subtract from that of the first gap depending on the phase difference of the 70 mc modulation cycle between the two gaps. If the transit angle $\Delta\theta$ is equal $n\pi$, where n is an

* Assisted by the Joint Program of the ONR and the AEC.
[1] W. E. Stephens, Rev. Mod. Phys. **19**, 19 (1947).
[2] Shoupp, Jennings, and Sun, Phys. Rev. **75**, 1 (1949).
[3] Haxby, Shoupp, Stephens, and Wells, Phys. Rev. **58**, 1035 (1940).
[4] Hafstad, Heydenburg, and Tuve, Phys. Rev. **50**, 504 (1936).
[5] A. O. Hanson and D. L. Benedict, Phys. Rev. **65**, 33 (1940).
[6] Herb, Snowdon, and Sala, Phys. Rev. **75**, 246 (1949).
[7] Altar, Garbuny, and Coltman, Phys. Rev. **72**, 528A (1947).

odd integer, the excitation from the second gap will cancel that of the first and a minimum in the *RF* signal from the cavity will result. Whence,

$$\Delta\theta = n\pi = 2\pi f \Delta t, \tag{1}$$

where Δt is the time of transit of any group of ions of velocity v through the length L between the gaps, and f is the frequency so that:

$$\Delta t = n/2f = L/v. \tag{2}$$

The velocity of the ions will therefore be:

$$v = 2fL/n, \tag{3}$$

and the equivalent voltage, V, of a beam of particles of velocity v and mass to charge ratio M_0/e considering the relativistic correction is:

$$V = \frac{M_0c^2}{e}\left[\frac{1}{(1-\beta^2)^{\frac{1}{2}}} - 1\right], \quad \beta = \frac{v}{c}, \tag{4}$$

where c is the velocity of light. To an approximation sufficiently accurate for this experiment, the voltage at which a minimum occurs is:

$$V = \frac{2M}{e}\frac{f^2L^2}{n^2}\left(1 + \frac{3f^2L^2}{n^2c^2}\right). \tag{5}$$

The voltage of the ion beam or of the electrostatic generator at the point where the *RF* signal is a minimum can therefore be calculated from the modulation frequency f and the length L between the gaps. The following atomic constants are used:[8]

Ratio charge/mass of electron $e/m = (5.2741 \pm 0.0005) \times 10^{17}$ e.s.u./g.
Ratio mass proton/electron $= M/m = 1836.57 \pm 0.20$.
Velocity of light $= c = (2.99776 \pm 0.00004) \times 10^{10}$ cm/sec.

The value L for the spacing between midpoints of the two gaps, measured with a special inside micrometer calibrated against the laboratory shop standard, was:

$$L = (1.2488 \pm 0.0002) \text{ meters.}$$

The error assigned to this measurement includes nonparallelism of the gap end plates and differences between the two gap widths.

The frequency f of the beam modulation oscillator was measured by using an intermediate crystal controlled secondary standard, the frequency of which was adjusted to within a few cycles of the 5 mc standard frequency signal from *WWV*. It was possible to beat a 70 mc harmonic of this oscillator against the modulation oscillator in the electrostatic generator electrode resulting in an audible beat note of less than 2 kc. The frequency f was therefore:

$$f = (70 \pm 0.0020) \times 10^6 \text{ cycles.}$$

A number of calibration points are available with the radio frequency ion speed gauge by using various values of the order number n and beam mass number M. Since the *RF* signal generated in the cavity is proportional to the square of the ion current, it is advantageous to use the hydrogen molecular ion beam ($M=2$) as it has about twice as much current as the proton beam. Also the voltage at which a minimum occurs with $M=2$ and $n=13$ is closer to the $Li^7(p,n)$ threshold, thereby requiring a shorter interpolation by the generating voltmeter. The mass of the molecular ion, mass 2, beam is that of two protons plus an electron, so that the voltage of the minimum of mass=2 and order number $n=13$ is calculated to be 1.8915 ± 0.05 percent Mev from Eq. (5).

The 70 mc beam modulator was in turn amplitude modulated with a 1000 cycle signal to allow the use of audio amplifiers in the *RF* receiver whose function is to measure the induced voltage in the cavity. The signal induced by the modulated ion beam in the cavity was picked up by a voltage probe and fed to a preamplifier and impedance matching tube adjacent to the probe. The signal was further amplified and detected by a S-27 communication receiver with a 1000 cycle narrow-band filter in the output. This filter reduced the receiver bandwidth to about 100 cycles and thus considerably increased the signal to noise ratio. The *RF* signal from the cavity could be read on a meter or oscilloscope.

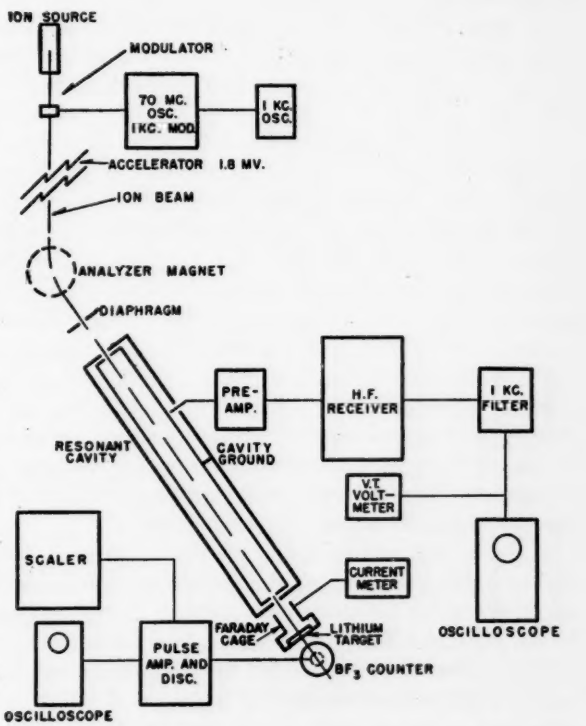

FIG. 1. *RF* ion speed gauge assembly. The magnetic analyzer permits rapid switching from the proton beam used for threshold measurement to the mass 2 beam used for the speed measurement, the mechanical geometry remaining fixed.

[8] J. W. DuMond and E. R. Cohen, Rev. Mod. Phys. **20**, 82 (1948).

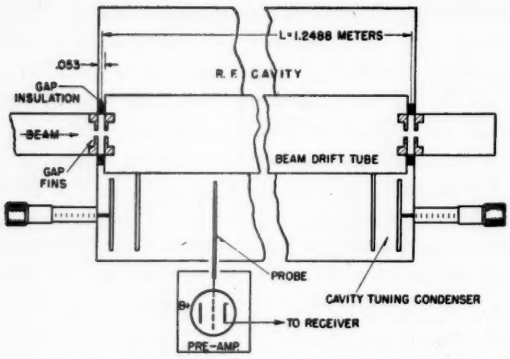

FIG. 2. Schematic section of the speed gauge cavity, giving essential dimensions.

Voltage Comparison and Stability

A compensated generating voltmeter[3] has previously been successfully used as means of voltage comparison on the Westinghouse electrostatic generator and its use was extended to stabilizing the generator operating voltage. In this voltmeter a rotating pick-up plate produces a 120 cycle error signal, the magnitude and phase of which is a measure of the inhomogeneities in the field behind a reference voltage plate. Voltage is applied to this plate until it coincides with an equipotential surface of the field of the high potential electrode. This condition is indicated by a minimum in the 120 cycle signal and a phase shift in the neighborhood of the minimum.

By demodulating this a.c. signal in a phase demodulator against a standard phase, a d.c. voltage can be derived whose sign depends on whether field due to electrode voltage is above or below the reference voltage and is, of course, zero at balance. This d.c. is amplified and is used to bias the grid of a transmitting tube in series with the corona point in the usual manner. In the Westinghouse electrostatic generator this biased corona point is on the end of a movable rod whose position can be mechanically changed. When the corona point is biased off completely by the voltage control system, some of the corona is transferred to the sharp edges of the grounded support rod with reduction of the over-all discharge current. This fortunately allows for a dual type of control, one by rod position and the other by bias voltage, so that the system can give continuous regulation. Thus the voltage is stabilized to about 0.1 percent or less at voltage levels of 2 Mev.

The d.c. null voltage from the demodulator is used also to indicate balance of the generating voltmeter at which point the reference plate voltage is proportional to the generator electrode voltage. The reference plate voltage, about 1 kv, is divided by an uncalibrated but very stable resistor divider by a factor of 0.001 and measured to an accuracy of one part in 10^5 by a type K potentiometer. When the electrostatic generator voltage is standardized by some other process such as the radio frequency speed gauge, or $Li^7(p,n)$ threshold, the voltage reading of the type K potentiometer becomes a measure of the electrode voltage, and all intermediate measurements in the generating voltmeter system are eliminated. Departure from linearity of the generating voltmeter is known to be small over ranges of at least 1 Mev, and errors over a range of about 100 kv are negligible compared to errors in determining the minimum from the cavity, or the $Li^7(p,n)$ threshold.

Threshold Measurement

The $Li^7(p,n)$ threshold was measured in a target chamber (Fig. 3) with a thick metallic lithium target which was heated at all times to prevent deposition of oil from the diffusion pumps. A large spiral dry ice trap in the vacuum line to the diffusion pumps also helped to prevent oil deposits on the target. No sign of carbon discoloration of the target was found after hours of operation. The neutrons produced by the reaction were measured by a large enriched $B^{10}F_3$ proportional counter with appropriate amplifier and scaling circuits, and oscilloscopes. Enough neutrons were produced in the reaction to permit determination of the threshold by the "spot check method," correlating the appearance on the oscilloscope of pulses due to the neutrons during voltage fluctuations of the generator. This method, although requiring some personal judgment on the part of the experimenter, allows the threshold to be more exactly matched with the generating voltmeter reference plate reading.

Experimental Data

The electrostatic generator voltage was stabilized by the error signal from the generating voltmeter, and the

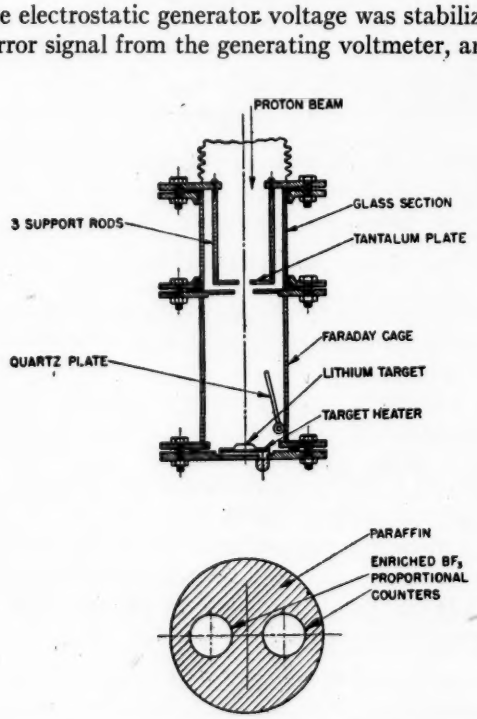

FIG. 3. Arrangement of target, paraffin, and BF_3 proportional counters.

RF signal from the speed gauge cavity was plotted against the generating voltmeter type K potentiometer reading over a region of about 100 kv above and below the expected minimum, as shown in Fig. 4, and a value for the minimum was selected from the resulting curve by inspection. Vertical lines are shown instead of points, representing the variation in *RF* cavity voltage due largely to residual fluctuation in the stabilized electrostatic generator voltage. A spot check of the $Li^7(p,n)$ threshold was made before, after, and in the middle of such a run and the type K potentiometer readings averaged and used as the threshold. The threshold voltage in Mev was calculated from these results by simple proportion.

$Li^7(p,n)$ threshold

$$= 1.8915 \frac{\text{threshold type } K \text{ reading}}{\text{cavity min. type } K \text{ reading}} \text{ Mev.}$$

The results of 10 such curves selected only on the basis of known defects in the taking of the data have been averaged and the standard deviation calculated. Including the error in the calculation of the voltage equivalent to the cavity minimum the $Li^7(p,n)$ threshold is (1.8812±0.0019) Mev in absolute volts.

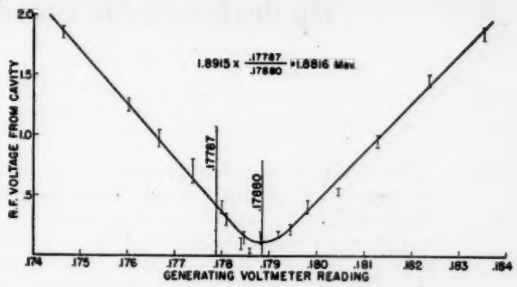

FIG. 4. Typical results of a single calibration run showing relation of $Li^7(p,n)$ threshold to $M=2$, $n=13$ cavity minimum. Average of ten such runs yields a value of 1.8812±0.0019 Mev for the threshold.

DISCUSSION

Experimental Results

This method for measuring the absolute voltage of the ion beam in the megavolt range has the advantage that the physical parameters necessary to determine the voltage equivalent to a minimum in the *RF* cavity signal are easy to measure. The frequency can be measured to an accuracy much higher than needed in this experiment and the length of the drift space is a simple physical measurement. The values of the necessary atomic constants are known to be at least a factor of five better than the accuracy required by this experiment.

Probably the largest source of error in this experiment is in the precise location of the minimum of cavity excitation due to the remaining fluctuations of the high voltage generator in spite of the control. However, it is hard to believe that this process can conceal any systematic error so that treatment of enough data by standard statistical methods should be valid.

An increase in the experimental accuracy by a factor of about five might be accomplished with the radio frequency ion velocity gauge by using an electrostatic generator equipped with an electrostatic analyzer to more closely define the voltage of the ion beam.

Previous experimental measurements of nuclear thresholds and resonances whose values are based on one of the older measurements of the $Li^7(p,n)$ threshold should be corrected by the appropriate factor:

Old value of $Li^7(p,n)$ threshold	Correction factor
1.85 Mev	1.0168
1.856 Mev	1.0136
1.883 Mev	0.999

We wish to express our appreciation to Mr. William Gueir, Mr. Kenneth Richmond, and Mr. Kenneth Fromm for their help in solving some of the experimental problems involved in use of the *RF* cavity with the electrostatic generator.

On the Knock-On Secondaries of Penetrating Particles

W. W. BROWN, A. S. MCKAY, E. D. PALMATIER*
Cornell University, Ithaca, New York

(Received March 29, 1949)

The knock-on secondaries of penetrating particles emerging from Pb plates (15 g cm^{-2}) have been investigated by cloud chamber and by counter telescope. The frequency of occurrence and the observed spatial distribution of the secondaries with respect to the primary penetrating particles have been found to be in agreement for the two different methods. Further data are presented on the back scattering of secondaries in Pb plates and on the emergence of secondaries from thin pieces of wood and counter walls. The possible effects on counter experiments are discussed briefly.

INTRODUCTION

DURING the course of a recent measurement by one of us on the total intensity of cosmic radiation, it was observed that a large fraction of the so-called side shower correction (obtained by the usual method of displacing the center counter out of the solid angle of the telescope) appeared to originate in the walls (0.11 g cm^{-2} of Al) of the top counter of the telescope and in the thin wooden roof (0.4 g cm^{-2}) over the telescope. In order to correct for this effect, we have investigated the frequency of occurrence and the spatial distribution, relative to the primary penetrating particle, of secondaries emerging from various materials. The investigation was made with both cloud chamber and counter telescope in an attempt to reduce the possibility of misinterpretation of the data.

A. CLOUD-CHAMBER MEASUREMENT

1. Experimental Method

A cylindrical argon-filled cloud chamber of 11-inches diameter and $3\frac{1}{4}$-inches depth was operated at 1.2 atmospheres and contained five lead plates (7 inches $\times 3\frac{1}{4}$ inches $\times \frac{1}{2}$ inch) in which the production of the secondaries was observed. The expansion of the chamber was counter controlled by a threefold coincidence telescope consisting of one counter (A) immediately above the chamber, a second counter (B) immediately below the chamber and a tray of counters (C) under five inches of lead placed below the second counter. The disposition of the chamber, counters, and lead is shown to scale in Fig. 1. The effective areas of the counters A, B, and the tray C are 1 inch $\times$ 5 inches, 1 inch $\times 2\frac{3}{4}$ inches, and 3 inches $\times$ 16 inches respectively. The telescope defines a beam of penetrating particles, mostly mesons at sea level, lying within the well illuminated portion of the cloud chamber. The photographs were not stereoscopic, hence only the projection of each track on the plane of the cloud chamber could be observed. The small maximum angular deviation of a meson path from the plane of the chamber, indicated by the dashed lines in the side view (Fig. 1) ensures that all secondaries making true angles of 75° or less with their primary will have visible tracks of sufficient projected length for a good measurement of the projected angle between primary and secondary. Furthermore it allows us to consider the primaries as lying in this plane without introducing any appreciable error.

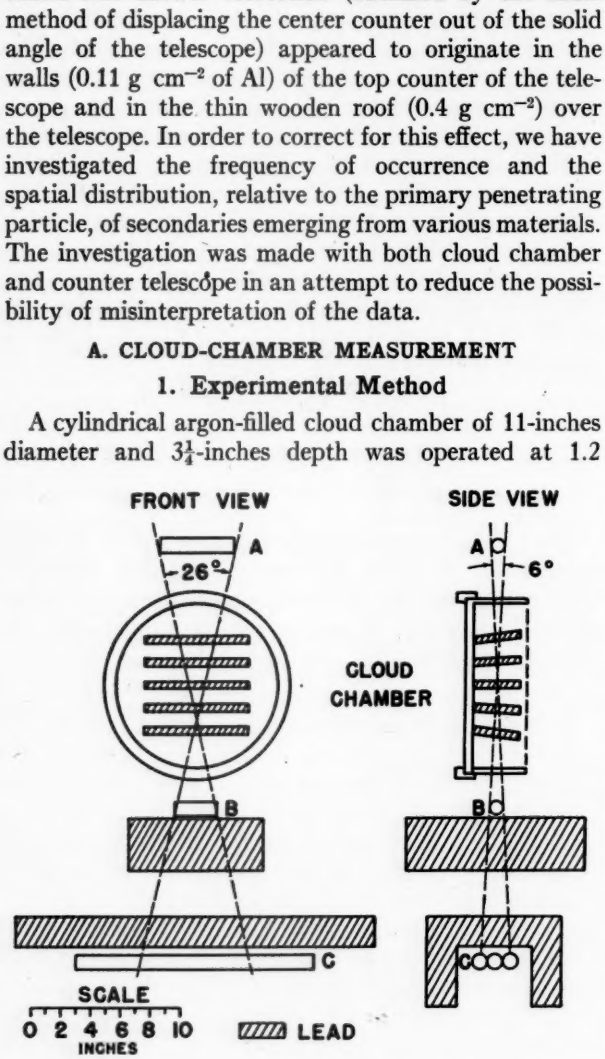

FIG. 1. Arrangement of cloud chamber and triggering telescope used in Part A.

It is expected that secondaries lying in a small cone around the line of sight of the camera and making an angle greater than 75° with the primary will be missed, as well as secondaries whose projections are superimposed on that of the primary. However, it will be apparent from the observed distribution and the geometry of the telescope that these effects are insignificant.

2. Results and Discussion

Out of 1200 photographs taken at an elevation of 260 m, 900 showed single mesons free from the extraneous electrons of local or extensive showers and suitable for measurement. The events observed were classified in accordance with the headings of Table I, the arbitrary division into high and low energy secondaries (columns 4 and 5 of Table I) being arrived at by defining as a low energy secondary any secondary which in the interval between two plates deviated by 10° or more from

* Now at University of North Carolina, Chapel Hill, North Carolina.

its initial direction of emergence. Since an electron with an r.m.s. projected deviation of 10° has about 1 Mev energy, this may be taken as the energy boundary between the two groups.

The observed total number of knock-ons accompanying mesons emerging from lead is in close agreement with the results of Hazen who used 0.7 cm of Pb.[1] Hazen has shown that of the secondaries emerging from 0.7 cm of Pb only a few percent are capable of penetrating an additional 0.7 cm of Pb; hence equilibrium has essentially been reached at this thickness and the comparison is valid.

Whenever a secondary did occur, the projected angle between its direction and that of its primary was measured to the nearest degree. The latter data are summarized (by 10° intervals) for penetrating particles emerging from or entering into a $\frac{1}{2}$-inch lead plate, in Figs. 2 and 3 respectively. The histograms do not represent the angular distribution at the point of production, but rather the distribution resulting after each secondary has undergone an amount of scattering in the lead, depending on its initial energy, direction, and position of production. If $N_1(\theta)d\omega$ is the probability that a knock-on will emerge from the lead into the solid angle $d\omega$, making an angle θ with its primary, then the probability of its occurring in the projected angular interval β to $\beta+d\beta$ is given by

$$N_2(\beta)d\beta=4\int_0^{\pi/2} N_1(\theta)\cos\alpha d\alpha d\beta$$

where $\cos\theta=\cos\alpha\cos\beta$ (see Fig. 4A). If we assume that $N_1(\theta)\sim\cos^n\theta$ then $N_2(\beta)=k\cos^n\beta$ where k is a constant depending on n. The curves of Fig. 2 are plots of $\cos^n\beta$ for $n=2$, 2.5, and 3, normalized so that the area

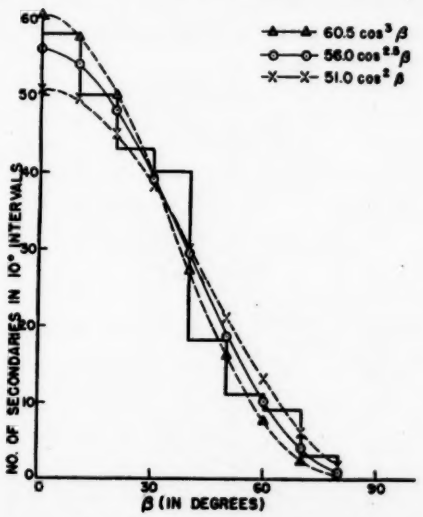

FIG. 2. Distribution in projected angle, β, between mesons (of energy >200 Mev) and the knock-on secondary electrons they produce in a $\frac{1}{2}$-inch lead plate which are capable of emerging in the forward direction.

[1] W. E. Hazen, Phys. Rev. 64, 7 (1943).

TABLE I. Knock-on electrons of mesons observed in cloud chamber.

Event	Number of events observed	Number of accompanying knock-ons observed	High Energy knock-ons per meson	Low Energy knock-ons per meson	Total number of knock-ons per meson
Emergence of a meson from a lead plate	3364	232	0.065	0.004	0.069±0.005*
Entry of a meson into a lead plate	3304	59 (back scattered)	0.014	0.004	0.018±0.002
Traversal of gas between 2 lead plates	3523	119	0.0035	0.0305	0.034±0.003

* Errors quoted are statistical standard deviations only.

under each curve is equal to that under the histogram. It is apparent that $n=2.5$ gives a satisfactory fit for an empirical relationship of this form.

Some further observations concerning the nature and behavior of the secondaries follow.

(a) The 232 knock-ons observed, occurred as 201 singles, 11 pairs emerging from the same plate and 3 triplets, a distribution not differing significantly from what would be expected if the events were independent of one another.

(b) Three of the singly occurring knock-ons had sufficient energy to produce a small cascade through the next three plates with a maximum of 3 to 6 electrons after traversing $\frac{1}{2}$ to $1\frac{1}{2}$ inches of Pb. In one of the triplet cases, an electron produced a small cascade containing 4 electrons after $\frac{1}{2}$ inch of lead. In all of these instances the direction of the shower-producing electron made a projected angle of less than 10° with that of its primary.

(c) 140 of the knock-ons produced by emerging mesons were observed to impinge on the next lead plate and of these, 43 were scattered back into the gas. The large number of back-scattered knock-ons occurring when a meson enters a lead plate is thus understandable.

(d) Of the knock-ons produced in the gas, the shortest delta-ray tracks counted were of about 3-mm length (equivalent to 0.59 g cm^{-2} of Al). Since a beta-ray of this range in aluminum has an energy of about 20 Kev[2] we have this rough lower limit of the energies of the secondaries produced in the gas that were counted. In traversing the gas between two plates a meson travels through approximately 3.0 cm of argon at 90 cm Hg and 30°C. The 119 knock-ons produced in the total observed path length (21.0 g cm^{-2} of argon) is, in view of the uncertainty of the low energy limit, in agreement both with Seren's[3] value of 143 knock-ons with tracks longer than 2 mm produced in 24.2 g cm^{-2} of argon and a value of 3.4 knock-ons per g cm^{-2} with tracks longer than 3 mm calculated from the Rutherford formula.

B. COUNTER TELESCOPE MEASUREMENT

1. Experimental Method and Results

The arrangement of counters, counter shields and material (S) for the production of secondaries is shown in Fig. 5. All the counters were of a standard construction described elsewhere,[4] h, b and c were of brass, while the remainder were of aluminum with a wall thickness of 0.11 g cm^{-2}, an external diameter of one

[2] F. Rasetti, *Elements of Nuclear Physics* (Prentice-Hall, Inc., New York, 1936).

[3] L. Seren, Phys. Rev. 62, 204 (1942).

[4] D. R. Corson and R. R. Wilson, Rev. Sci. Inst. 19, 225 (1948).

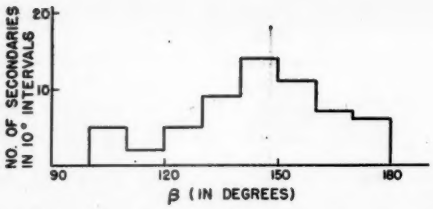

FIG. 3. Distribution in projected angle, β, between mesons (of energy >200 Mev) and the knock-on secondary electrons they produce in a $\frac{1}{2}$-inch lead plate which, through scattering, emerge in the backward direction.

inch and an effective length of sixteen inches. Counters labelled identically in the diagram were connected in parallel. In the main series of measurements the following coincidences were recorded concurrently.

Fourfold—abch (referred to as T from now on)—arising mainly from passage of single mesons through the telescope.

Fivefolds—Td, Te, Tf, Tg—arising mainly from mesons and accompanying secondaries generated in S.

Sixfolds—Tde, Tef—arising mainly from showers (local as well as extensive).

With no material at S the 5 fold and 6 fold rates were found to be appreciable, and arose apparently from showers (local and extensive) as well as secondaries of mesons generated in the counter walls and in the air. These rates ($S=0$) were decreased considerably by:

(a) housing the telescope in a wooden hut with thin walls (0.4 g cm^{-2}) and a thin plastic roof (0.0125 g cm^{-2}).

(b) placing the bottom of the curved collecting tray d, e, f, and g on the same level as the top counter of the telescope rather than below it.

A further effect which is highly undesirable is that of secondaries being scattered in the counter walls so as to pass through more than one counter of the tray. Since the magnitude of this effect will depend on the material and dimensions of S in an unknown manner, we have attempted to eliminate it by inserting strips of lead and iron as indicated in the diagram. Very few of the secondaries scattered through large angles in the counter walls would be expected to traverse these strips (thickness of approximately 0.3 cm). Now the presence of this shower generating material between counters may well introduce further local effects, but these new effects may be considered as remaining constant as S is changed.

From the observed number of the coincidences listed above, the number of 5 folds per 4 fold, and the 6 folds per 4 fold can be calculated. These results, obtained with various absorbers at S and in some cases with shields over the counters d, e, f, and g, are shown in Table II.

2. Discussion of Results

The 5 fold coincidences without S are interpreted as background effects and these rates (coincidences per event T) are subtracted from the observed 5 fold coincidences rates with S present. The remaining 5 fold events are assumed to be due to mesons accompanied by knock-ons generated in S. The corrected 5 fold coincidences per meson are shown in Table III. The subtraction of the 5 fold rates with S absent is justified by the following arguments.

(a) The equality of all 6 fold counting rates (within the statistical error) in columns 9 and 10 of Table II, in the cases where shields are absent, shows that the 6 fold counting rates, taken concurrently with the 5 folds in each case, are independent of the presence of S and show no marked dependence on the angular position β of the counters (see Fig. 4*B*). When S is present, the expected contribution of multiple knock-ons from S to the 6 fold rate, calculated from the cloud chamber observations, is only 4 percent of the observed rate. This indicates that the 6 fold rate is due to air showers.

(b) In the cloud chamber with considerably smaller counters and a slightly greater thickness of lead over the bottom counter, the rate for events observed in the small thickness of the cloud chamber and appearing as showers originating outside the cloud chamber was 0.4 per hour. In view of the differing geometry this may be considered as in rough agreement with the shower rate of 0.65 per hour indicated by the 6 fold coincidences.

(c) The five fold coincidences (Td, Te, Tf, Tg) for S of zero thickness, after subtracting the average 6 fold shower background of 0.0044 ± 0.0002 per T event then appear as 0.0043 ± 0.0008; 0.0013 ± 0.0007; 0.0013 ± 0.0006; 0.0000 ± 0.0005 per T event, respectively. These residual counts may be attributed to the following causes: (i) the production of knock-ons in the air by mesons passing through the telescope (the cloud chamber re-

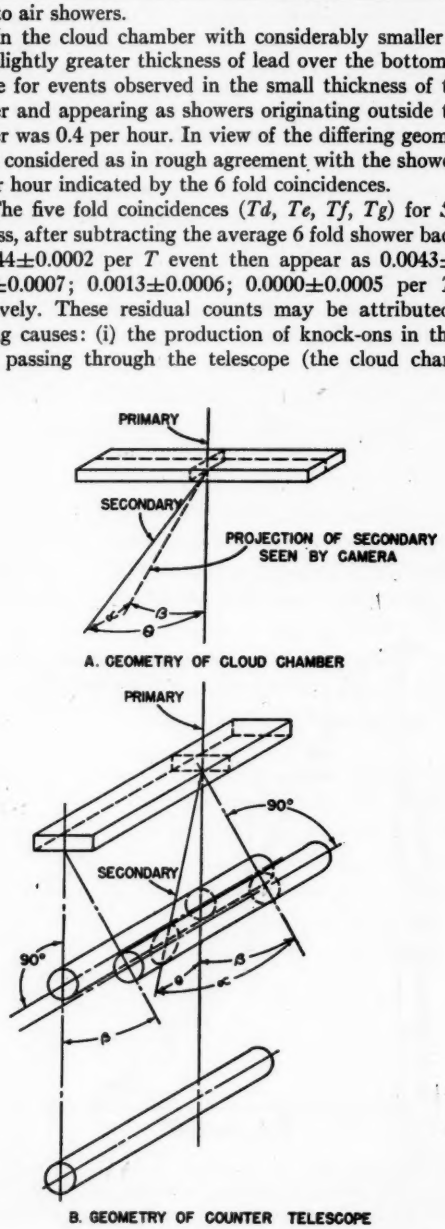

FIG. 4. Meaning of the angles α, β, and θ in the cloud chamber and counter telescope experiments.

TABLE II. Observed 4 fold coincidences T, 5 folds per T, 6 folds per T, for various materials at S. (Fig. 5).

Case	Material at S	Shields***	T	5 Folds per T				6 Folds per T	
				$(Td/T)\times10^3$	$(Te/T)\times10^3$	$(Tf/T)\times10^3$	$(Tg/T)\times10^3$	$(Tde/T)\times10^3$	$(Tef/T)\times10^3$
1	None	absent	15236	8.7±0.8*	5.7±0.7**	5.7±0.6	4.4±0.5	4.0±0.6**	3.9±0.6**
2	15 g cm^{-2} Pb	absent	17348	28.3±1.3	18.6±1.0	12.1±0.8	7.4±0.65	4.4±0.5	5.6±0.6
3	15 g cm^{-2} Pb	2.0 g cm^{-2} Pb	4782	24.4±2.3	12.1±1.6	9.8±1.4	6.9±1.2	6.1±1.1	7.3±1.2
4	3.8 g cm^{-2} Pb	absent	14379	22.3±1.2	13.1±1.0	9.2±0.8	5.2±0.6	3.3±0.5	4.2±0.5
5	3.8 g cm^{-2} Pb	2.0 g cm^{-2} Pb	3986	17.3±2.1	7.0±1.3	6.8±1.3	6.0±1.2	5.0±1.1	5.3±1.1
5*a*	3.8 g cm^{-2} Pb	0.4 g cm^{-2} Al	4862	21.8±2.1	12.7±1.6	7.6±1.3	6.4±1.1	4.3±0.9	4.7±1.0
6	0.45 g cm^{-2} Pressed wood	absent	8006	16.0±1.4	10.1±1.1	7.2±1.0	6.5±0.9	4.1±0.7	4.1±0.7
7	2 Al counters (identical to *a*) placed side by side	absent	8102	14.2±1.3	9.0±1.1	7.3±0.95	6.0±0.9	3.3±0.6	3.8±0.7

* Errors quoted are statistical standard deviations only.
** Te, Tde, and Tef in this case obtained with only 11900 coincidences in T as e counters were inoperative during a portion of the run. Chance coincidences in the worst case above were less than 2 percent of the observed rate and have been neglected.
*** In some instances small strips of Pb and Al were placed over counters d, e, f, and g as indicated.

corded .0035 high energy knock-ons per meson in traversing 3 cm of argon at 1.2 atmospheres—see Table I), (ii) the production of electrons in the material around the counters coincident with a T event.

The data of Table III, with the standard statistical errors, are shown in Fig. 6. It is apparent from this figure that quite small thicknesses of material may be the source of relatively large numbers of secondaries which are able to penetrate thin counter walls, while a considerable fraction of the secondaries produced may penetrate quite thick counter walls. It is of interest to note that the large angle secondaries are more markedly reduced than the small angle secondaries by the presence of a Pb shield over the counters.

A comparison of the results obtained by the cloud chamber and counter coincidence methods has been made for a Pb thickness of 15 g cm^{-2} and is shown in Fig. 7. The blocks indicate the statistical error and counter widths as well as the number of secondaries per meson for the counters of the counter telescope. The

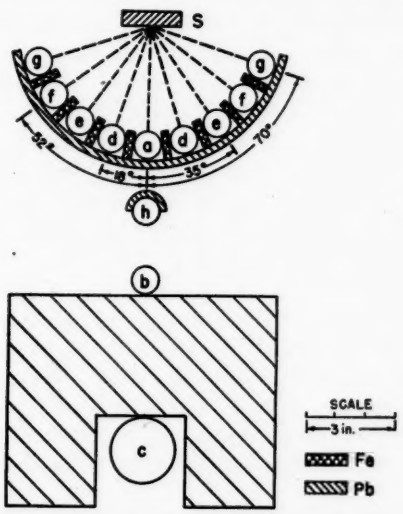

FIG. 5. Arrangement of meson counter telescope *ahbc*, secondary detecting counter pairs *d*, *e*, *f*, and *g*, and counter shields used in Part B. The production of secondaries in S is observed.

TABLE III. Single knock-ons generated in S per meson and counted by the counter pairs *d*, *e*, *f*, and *g*.

Case	Knock-ons per meson detected by counter pair			
	$d\times10^3$	$e\times10^3$	$f\times10^3$	$g\times10^3$
2	19.6±1.5*	12.9±1.2	6.4±1.0	3.0±0.9
3	15.7±2.4	6.4±1.8	4.1±1.5	2.5±1.3
4	13.6±1.5	7.4±1.2	3.5±1.0	0.8±0.8
5	8.6±2.2	1.3±1.5	1.0±1.5	1.6±1.3
5*a*	13.1±2.2	7.0±1.8	1.9±1.3	2.0±1.2
6	7.3±1.6	4.4±1.3	1.5±1.2	2.1±1.0
7	5.5±1.8	3.3±1.3	1.6±1.2	1.6±1.0

* Errors quoted in table are statistical standard deviations only.

solid line is the calculated distribution in β for the counter telescope (see Fig. 4) based on the results of Part A where a total number of 0.069 knock-ons per meson and an angular distribution of $\cos^{2.5}\beta$ for the secondaries were observed. An end loss of 10 percent was estimated for this particular counter geometry. The curve has been plotted without normalization at any point. It can be shown in a manner similar to the treatment of the projected distribution for the cloud chamber that the distribution in $\beta\sim\cos^n\beta$ if the distribution in θ follows the same law. The agreement of the two methods is perhaps better than might be expected in view of small factors which we have neglected in the interpretation of the counter telescope data, e.g., absorption in the counter walls, materialization of photons, increase in the effective widths of the counters owing to the presence of the thin Fe strips between the counters. However, these effects are small, and as the first one will tend to compensate for the latter ones, it is possible that no appreciable error, outside the statistical error, has been introduced.

GENERAL CONCLUSIONS

(1) The cloud chamber and counter telescope methods both give a total number of 0.07 secondaries per meson emerging from a ½-inch Pb plate in the forward direction and indicate a distribution of $\cos^{2.5}\theta$, where θ is the angle between a secondary and its primary. The

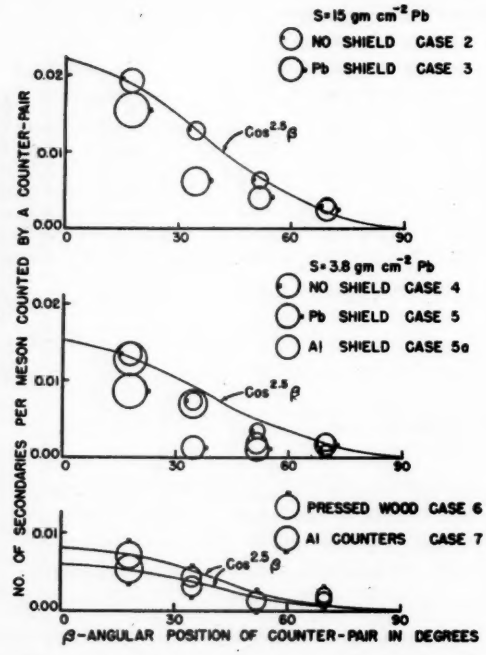
S=15 gm cm⁻² Pb
NO SHIELD CASE 2
Pb SHIELD CASE 3
S=3.8 gm cm⁻² Pb
NO SHIELD CASE 4
Pb SHIELD CASE 5
Al SHIELD CASE 5a
PRESSED WOOD CASE 6
Al COUNTERS CASE 7
Cos^2.5 β
NO. OF SECONDARIES PER MESON COUNTED BY A COUNTER-PAIR
β-ANGULAR POSITION OF COUNTER-PAIR IN DEGREES

FIG. 6. Single knock-on secondaries generated in the material S per meson and counted by the counter-pairs d, e, f, and g.

results for the total number of secondaries per meson also agree, within statistical error, with the measurements of others where conditions were most similar to ours.[1,5]

(2) Thin sections of material produce appreciable numbers of secondaries which appear to follow a similar distribution in θ.

[5] S. N. Nassar and W. E. Hazen, Phys. Rev. **69**, 298 (1946).

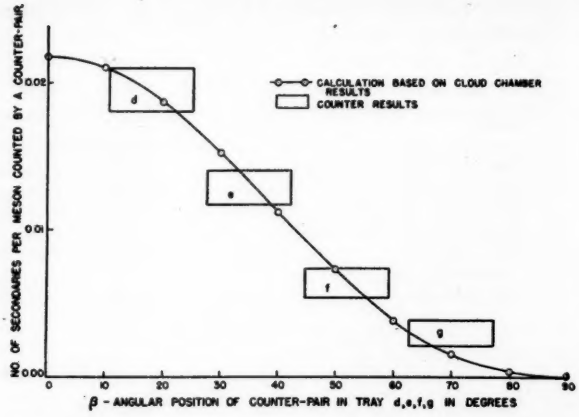
CALCULATION BASED ON CLOUD CHAMBER RESULTS
COUNTER RESULTS
NO. OF SECONDARIES PER MESON COUNTED BY A COUNTER-PAIR
β - ANGULAR POSITION OF COUNTER-PAIR IN TRAY d,e,f,g IN DEGREES

FIG. 7. Comparison of the expected number of knock-ons per meson counted by the counter geometry of Fig. 5 (calculated from the cloud chamber results) with the observed number counted.

(3) Some of the difficulties inherent in the interpretation of counter coincidence experiments are readily apparent; e.g., backscattering of secondaries, in the case of a tray of coincidence counters with absorber above and below, may introduce an appreciable contribution to 3 fold and higher coincidence rates, while the production of secondaries in the counter walls or in the surrounding air may also give rise to errors. We shall discuss these effects further at a later date, in their application to the correction of measurements on the total intensity of cosmic radiation.

The authors are indebted to Professor K. I. Greisen for helpful discussion and criticism of the work. The apparatus used had been built under a contract with the Office of Naval Research.

Penetrating Showers*

W. B. FRETTER
Department of Physics, University of California, Berkeley, California
(Received April 26, 1949)

Penetrating showers produced in lead have been observed in a large cloud chamber at sea level and 3027 meters. Observations made on the showers include frequency of occurrence, multiplicity, angular distribution, and production of high energy electrons. An attempt is made to compare the numerical data obtained with predictions of various meson theories, assuming that the events are produced by high energy nucleons.

I. INTRODUCTION

THE penetrating showers produced in lead by high energy particles can be observed in cloud chambers. Several experimenters[1] have been able to photograph these rather rare events and draw from them conclusions about the nuclear interactions which they probably represent. Recently[2,3] multi-plate cloud chambers have been used to make detailed analyses of the various types of events which can occur. The present paper will report measurements on penetrating showers observed in a large cloud chamber at sea level and at 3027 meters elevation at Tioga Pass in Yosemite National Park.

The penetrating showers observed have been divided into two main categories, those produced by isolated particles to be called *local* showers, and those produced by particles which are *accompanied* by extensive showers. The types of data obtained from analysis of these showers include: frequencies of occurrence, multiplicity of penetrating particles produced, identification of particles, angular distribution of penetrating particles produced, and simultaneous production of electronic radiation.

II. THE APPARATUS

The cloud chamber, shown schematically in Fig. 1, contained 16 lead plates each ½ inch thick, separated at the center of the illuminated region by approximately 0.8 inch. Photography was with a stereoscopic camera using flash tubes FT-422 (G. E.) with parabolic reflectors for right-angle illumination.

The chamber was counter-controlled, the coincidence arrangement requiring at least one particle through the upper counters and two below the cloud chamber, a fourfold coincidence (Fig. 1) being required. The result of this loose selection of events was that at sea level 75 percent of the pictures showed single tracks, presumably mesons which made knock-on electrons near the lower counters. The remaining pictures were mostly air showers or not identifiable. At 3027 meters, however, the air showers made up 57 percent of the pictures, the single penetrating particles only 28 percent. The frequencies of these and other events will be discussed in the next section.

In addition to the counters used to trigger the cloud chamber, auxiliary counter trays and circuits were used which provided information on whether or not the event observed in the cloud chamber occurred simultaneously with an air shower. An unshielded tray of area of about 1200 cm² was located at a distance of about 6 meters from the cloud chamber. If a pulse from this tray occurred coincidentally with a fourfold coincidence of the counters controlling the chamber, a neon light on the side of the chamber flashed and was photographed. Four other counter trays being used in an experiment performed by John Ise, Jr., were similarly connected to neon lights. During the course of the summer, these four other trays were covered with various amounts of lead

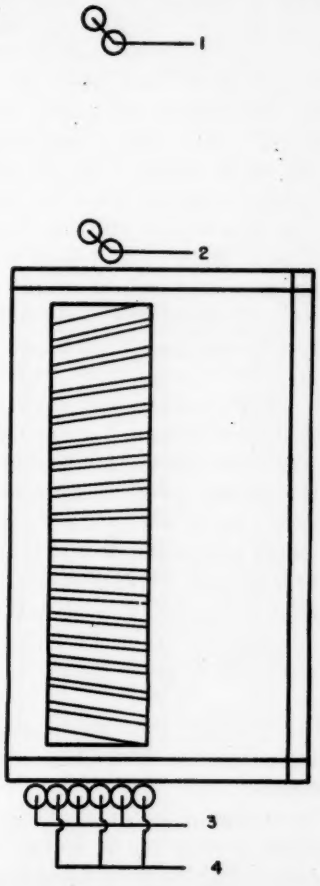

FIG. 1. Experimental arrangement.

* Assisted by the Joint Program of the ONR and the AEC.
[1] W. B. Fretter, Phys. Rev. **73**, 41 (1948) (bibliography).
[2] W. B. Fretter, Am. J. Phys. **17**, 148 (1949).
[3] C. Y. Chao, Phys. Rev. **75**, 581 (1949).

TABLE I. Frequencies of events (all rates per hour).*

Event	Single penetrating particles	Electron showers	Local penetrating showers	Accompanied penetrating showers
Sea level	2.33 ±0.035	0.503 ±0.016	0.016 ±0.003	0.018 ±0.003
3027 m	2.56 ±0.05	5.15 ±0.07	0.192 ±0.013	0.130 ±0.011

* The probable errors are from statistics only.

and some information was obtained about coincidence of penetrating showers in the cloud chamber with extensive penetrating showers. A separate paper will be devoted to this study and to the study of the air showers observed in the cloud chamber.

The cloud chamber was housed in a thermally insulated trailer with a thin sheet steel roof under which were ¼ inch of plywood and 2 inches of glass wool insulation.

III. ANALYSIS OF DATA

A. Frequencies of Occurrence

The total number of penetrating showers observed was: 133 local showers and 93 accompanied showers. In many cases the events were successive, so the total number of penetrating events observed was much larger. In a few cases the accompanied showers did not register a count in one of the extensive shower trays, but the presence of electronic radiation or other penetrating particles simultaneously present in the chamber permitted their classification as "accompanied."

The frequencies of various types of events at sea level and at 3027 meters are given in Table I.

The small increase in the number of penetrating particles is probably not to be taken too seriously. The photographs at high altitudes were not as good quality as those at sea level and there was a higher proportion of pictures in which identification of the event was difficult. Each of the penetrating particles observed must have penetrated more than 20 cm of Pb and made a knock-on in order to be observed, so that only very high energy penetrating particles are observed, and these do not increase very fast with altitude. There is an additional effect of hardening of the energy spectrum as the mesons proceed through the atmosphere; the relatively higher energy mesons at sea level will produce a greater proportion of knock-on electrons than those at 3027 meters. Another important effect is the simultaneous occurrence in a picture of electrons and penetrating particles; these were classed as electron showers and are not included in the rate of penetrating particles.

The electron showers increase by a factor of 10 between the two altitudes, in agreement with other observers.

The penetrating showers accompanied by electron showers increase by a factor of 7.2±1.3. Since the accompanying electron showers are usually responsible for tripping the counters, the factor of increase for these accompanied penetrating showers should be very nearly the same as that for electron showers, and it is believed that the difference is not significant.

The local penetrating showers increase by a factor of 12±2.4. If the particles producing them have an exponential absorption between 3027 meters and sea level, the mean free path for absorption is 123±10 g/cm². This is in agreement with the results of Tinlot[4] and indicates we are probably observing the same phenomena.

Tinlot and Gregory[5] concluded from auxiliary counter measurements, however, that a negligible proportion of penetrating showers are accompanied by air showers, whereas we observed almost as many accompanied showers (93) as local showers (133). The number of accompanied showers observed when actual frequencies were being taken was 84, compared to a total number of electron showers identified under the same conditions as 3229. Thus, for our particular detection equipment, one electron shower in 38 showed a penetrating shower produced in our apparatus. The uncertainties of solid angle and density of electrons make it impossible to

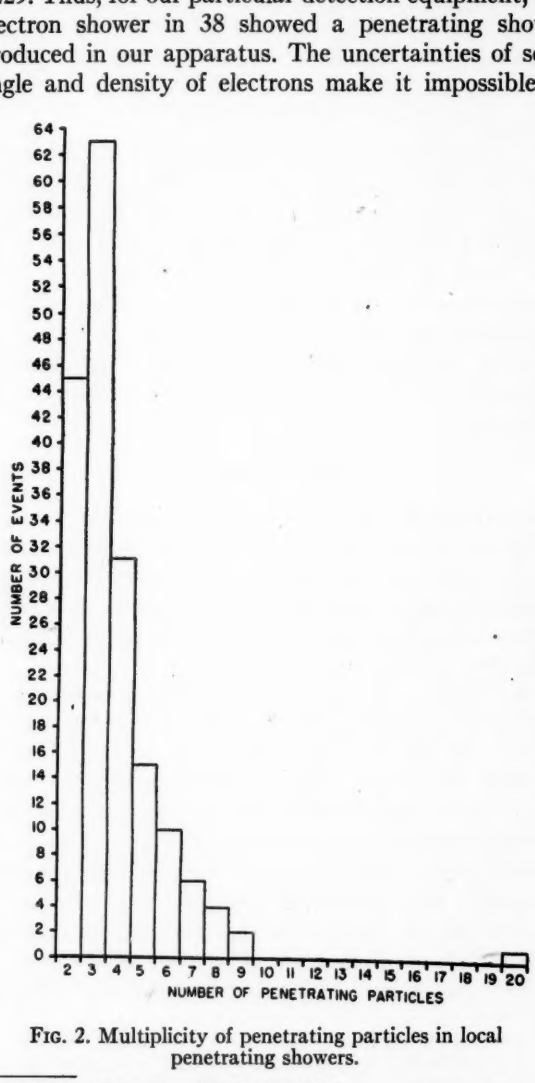

FIG. 2. Multiplicity of penetrating particles in local penetrating showers.

[4] J. Tinlot, Phys. Rev. **73**, 1476 (1948).
[5] J. Tinlot and B. Gregory, Phys. Rev. **75**, 520 (1949).

calculate from this a density of penetrating shower producing particles in an air shower, but the presence of particles capable of producing penetrating showers in air showers is clearly demonstrated. In addition, it might be remarked that the areas of extended counters used by Tinlot and Gregory[5] were such as to record only high density showers whereas some of the penetrating showers detected in the cloud chamber were accompanied by relatively few particles.

B. Multiplicity

The multiplicity of production of charged penetrating particles is shown for local showers in Fig. 2, and for accompanied showers in Fig. 3. These were obtained simply by counting the number of penetrating particles produced to each event. To be classified as penetrating, a particle had to go through one ½-inch lead plate without producing secondaries; thus protons and mesons are included. These are minimum values, undoubtedly some particles were missed because of poor illumination or unfortunate location in the chamber. The peak at three particles in the local shower curve is probably instrumental; with the counter arrangement used it is, of course, more probable to detect highly multiple events than those containing only two particles. This is borne out by the curve for accompanied showers which shows no such peak since in most cases the counters were tripped by particles in the air shower.

The multiplicities are, however, mostly fairly low, averaging about four particles per event. Twelve showers are omitted from these graphs because their electronic density was so high that no count of penetrating particles could be made.

Using the criteria of ionization and scattering developed by Powell,[6] it was possible to identify 35 mesons and 21 protons which stopped in the chamber after traversing one or more lead plates. Further classification of the mesons (into π- or μ-types) was not possible. Some cases of anomalously large scattering of the produced particles will be discussed later.

Slow protons and mesons were produced abundantly in these showers. These were evidenced by heavy tracks found at the beginning and throughout the shower. About half the initial events showed production of slow protons or mesons (not distinguishable in these pictures), the average number being two per event when they were observed at all. It seems likely that slow mesons or protons are produced in nearly every penetrating shower and that whether or not they are observed depends on the position of the event in the lead plate.

In addition to the heavy tracks produced in the initial event, heavy tracks are frequently observed scattered at random through the shower. On the average, 1.5 heavy tracks are observed per shower which are not associated with the original event. In one case fifteen such tracks were observed and in another, where there was a twelve-particle star, twenty heavy tracks were found. These are probably produced by the neutrons which Cocconi, Tongiorgi, and Greisen[7] have found to be produced in penetrating showers in large numbers.

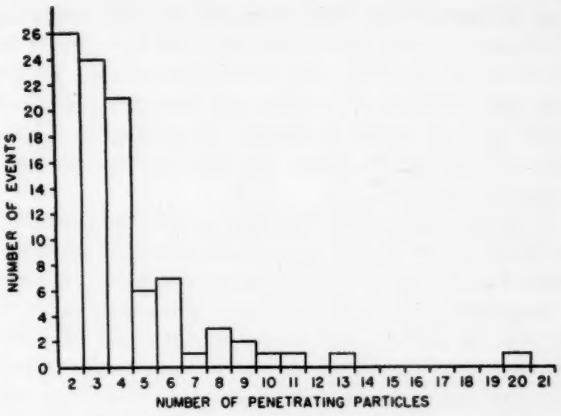

FIG. 3. Multiplicity of penetrating particles in accompanied penetrating showers.

C. Angular Distribution

The projected angle between the initiating particle and the charged penetrating particles produced has been measured for local and accompanied penetrating showers and the results plotted in Figs. 4 and 5. Again the counter selectivity must be considered; showers with very wide angular dispersion will not be detected. The local and accompanied showers show very little difference in angular distribution, however, so the counter selection could not have been too rigorous. The similarity in angular distribution lends support to the idea that the two types of penetrating showers are probably similar in their mechanisms.

With the information on multiplicity and angular distribution at hand, we can compare the experimental results with theoretical calculations. Lewis, Oppenheimer, and Wouthuysen[8] have made calculations of multiplicities and angular distributions of mesons according to various theories. In the energy range where most of the showers observed in the present investigation lie the asymptotic solution for very high energies does not apply. Professor Lewis[9] has very kindly made calculations to cover the lower energy range.

It should be noted that any conclusions about multiplicity and angular distributions from this experiment are uncertain because of lack of identification of particles and lack of knowledge of energies.

The *average projected* angle for the charged penetrating particles in this experiment is 18.6°. The average

[6] W. M. Powell, Phys. Rev. **69**, 385 (1946).

[7] Cocconi, Cocconi-Tongiorgi, and Greisen, Phys. Rev. **74**, 1867 (1948).

[8] Lewis, Oppenheimer, and Wouthuysen, Phys. Rev. **73**, 127 (1948).

[9] H. W. Lewis, Phys. Rev. **76**, 566 (1949).

angle is related to the root-mean-square angle (assuming a Gaussian distribution which may not be correct) by $\langle\theta^2\rangle_{Av}^{\frac{1}{2}}=(\pi/2)^{\frac{1}{2}}\langle\theta\rangle_{Av}$ and the true angle related to the projected angle by $\sqrt{2}$ so that the true r.m.s. angle is about 33°, or about $\frac{1}{2}$ radian. According to Lewis, $\langle\theta^2\rangle_{Av}^{\frac{1}{2}}=[2/(1+\gamma_0)]^{\frac{1}{2}}$, thus the average γ_0 for these primaries is about 7.

If we now compare the average γ_0 with the curves for multiplicity, we see that for an average multiplicity of about 4 and a γ_0 of 7 the factor α must be of the order of magnitude 1.5, and this seems quite reasonable. It can also be noted that energies of the order of 7-Bev are very common in the primary cosmic rays. Thus, although the agreement between the theory and this experiment may in this case be completely coincidental, it is seen that at least the order of magnitude given must be correct.

D. Production and Penetration of Electronic Radiation

It is now well established by ionization-chamber[10] and cloud-chamber[1] work that high energy electronic radiation is often produced simultaneously with the penetrating particles. The rapid interaction of high energy γ-rays and electrons with lead makes it impossible to say whether the radiation which initiates the observed electron showers has the character of γ-rays or electrons. Some information can be obtained, however, from a study of the electron showers produced.

The production and penetration of these electron showers is plotted in Fig. 6. Since no difference in production of electrons was noticed in local and accompanied showers, the electron production for all showers is given. The value given for zero plates penetrated does not mean that *no* electrons or γ-rays were produced; it simply means that such radiation was not energetic enough to create an electron shower capable of penetrating $\frac{1}{2}$ inch of lead. It must also be remarked that the production and penetration of electrons is not always a clear-cut visible phenomenon, especially for small penetrations, and some judgment had to be used in classifying these events. The peak in the region of three plate penetration is instrumental; if showers occurred near the bottom of the chamber the *minimum* penetration was observed and plotted on the graph. The actual penetration, or energy, in many cases was higher.

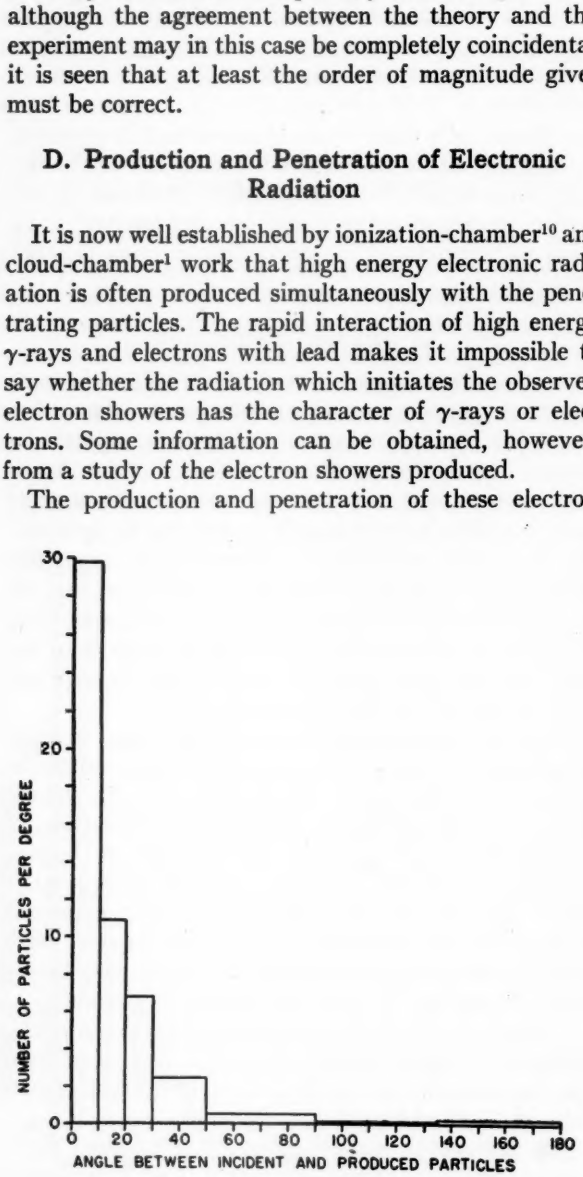

FIG. 4. Projected angle between the initiating particle and the charged penetrating particles produced in local penetrating showers.

FIG. 5. Projected angle between the initiating particle and the charged penetrating particle produced in accompanied penetrating showers.

The most satisfactory way of estimating the energy of an electron shower is to count the number of particles at its maximum.[11] In most of the present cases this procedure was impossible because of the large number of particles present. Thus, only a rough idea can be had of the energy of the shower by observing its penetration in lead. The thickness of each plate corresponds to 1.27 cm or 2.44 shower units (one shower unit=0.52 cm). Four plates correspond very nearly to ten shower units and a shower that has died out while penetrating four plates should have had roughly about 200 Mev, while one capable of penetrating eight plates, or twenty shower units, may have had an energy of the order of 1000 Mev. The most energetic electron shower observed penetrated twelve plates, or thirty shower units and must have had an energy of the order of 5×10^{10} Mev.

In considering the origin of these electron showers it is of interest to observe whether single or multiple cores or cores at angles occur. Table II gives the angle from the incident particle and penetration in the case where

[10] Bridge, Hazen, Rossi, and Williams, Phys. Rev. **74**, 1083 (1948).

[11] S. Nassar and W. E. Hazen, Phys. Rev. **69**, 298 (1946).

the angle was large or the shower simple enough to make the effect noticeable.

From these pictures and those of Chao[3] it is clear that for low energy events the electrons sometimes come off at appreciable angles from the initiating particle. The energies are relatively low in most cases; in the case of the two cores which penetrated 7 plates each, the angle between them was small. With more data, a study of the angular distribution of the electron showers and their energy might reveal details of the production process.

Another observation which may be of interest is the correlation of multiplicities of penetrating particles with production of electrons. Table III gives data for all showers which could be analyzed.

If we assume that the relative probability of obtaining charged penetrating particles is twice as great as obtaining uncharged particles (neutral mesons) or γ-rays we can write:

$(\frac{2}{3})^N$ = probability of getting N charged particles only.

$(\frac{1}{3})^N$ = probability of getting N uncharged particles only.

For $N=9$, for example, $(\frac{2}{3})^9=1/38.4$, or one shower in 38.4, with total multiplicity 9 should show only charged particles. At first glance, the probability of observing a nine-particle shower with no electrons seems very small, since only four showers were observed with multiplicity 9. However, it must be remembered that some of the other showers with lower multiplicity of charged particles might actually have had a total multiplicity of 9. If we take the factor $1/(\frac{2}{3})^N$, and multiply it by the actual number of showers of corresponding multiplicity from $N=2$ to 9 in which no electrons were observed, and sum all these numbers, we find that a total of 144 showers should have been recorded in order to record the numbers seen without electrons. A total of 255 showers were actually counted in this survey. This rough calculation leaves out all energy dependence considerations, and was made only to determine whether, under the assumptions made, it was at all reasonable to find as many showers without electrons as we did. Since electron showers of less than 100 Mev may easily have been missed, it seems reasonable to conclude that an assumption of 2:1 probability for production of charged and neutral particles will explain the results.

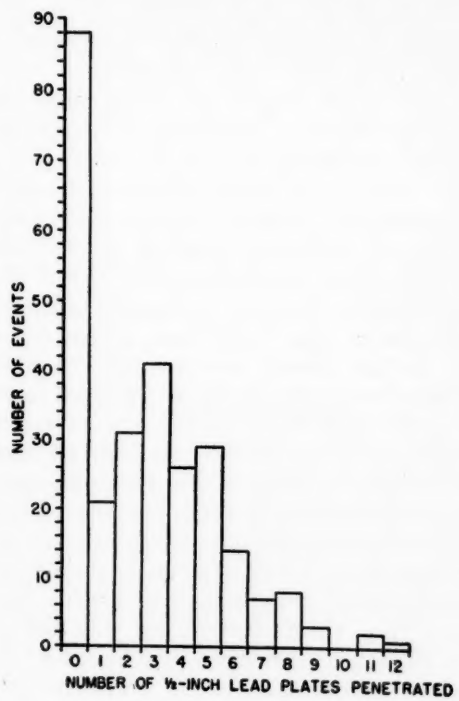

FIG. 6. Production and penetration of electrons in penetrating showers.

TABLE II. Angles from the incident and penetration.

Picture No.	Angle θ_1	Penetration (1)	Angle θ_2	Penetration (2)
3490	−3°	7 plates	+6°	7 plates
10640	28°	3 plates	no other core	
11977	46°	2 plates	no other core	
12292	0°	2 plates	+24°	2 plates
12759	−16°	4 plates	+16°	3 plates
13325	−4°	5 plates	+22°	4 plates
13980	+10°	4 plates	+22°	3 plates

TABLE III. Correlation of multiplicities with the production of electrons.

Multiplicity N	2	3	4	5	6	7	8	9	>9
Number of showers with no high energy electrons	20	37	15	4	3	1	2	1	0
Total number observed with this multiplicity	71	87	42	21	17	7	7	3	4

E. Free Path and Flux of Primaries

The distribution of single events through the cloud chamber is shown in Fig. 7. In consideration of these data two factors must be taken into account: the free path of the primaries in lead and the selection bias of the counters. If we assume that the primaries are absorbed exponentially we can write that the number which have not made a penetrating shower after traveling a distance x through the lead is $n=n_0e^{-x/L}$ where L is the mean free path for shower production. The number which collide between x and $x+dx$ is $dn=-(n_0/L)e^{-x/L}dx$. The probability of detecting the event will depend on the position of the event in the cloud chamber, the multiplicity N, and the counter arrangement. We can write the probability of detection $P(r,\ N)=k(N)A/r^2$, where $k(N)$ depends on the multiplicity and the counter arrangement; A/r^2 represents the solid angle of the counters subtended at a distance r from the event.

Thus, the number observed in dx will be proportional to

$$(n_0/L)e^{-x/L}(k(N)A/r^2)dx,$$

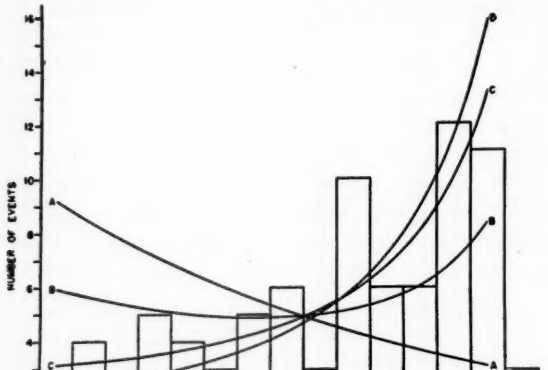

FIG. 7. Distribution of single local showers in the cloud chamber, and calculated distribution for $L=170$ g cm^{-2} with no counter bias (curve A). The calculated distributions including counter bias are given by $L=86$ g/cm^{-2} (curve B), $L=170$ g/cm^2 (curve C) and $L=350$ g/cm^{-2} (curve D).

r and x are related by the geometry of the counters and cloud chamber, A is constant, and $K(N)$ can be considered to have a constant value for some average multiplicity. Thus a fraction proportional to $f=e^{-x/L}/r^2$ can be calculated which gives the fraction of observed events occurring in each plate. This is calculated for various assumed values of L and the results normalized to the total number of events occurring in plate 1 to 14. Plate 15 is omitted because of difficulty of identification of showers.

Curves are drawn for $L=86$ g/cm^2 (curve B), 170 g/cm^2 (curve C), and 350 g/cm^2, (curve D), Fig. 7.

It is seen that the data are reasonably well fitted by $L\sim170$ g/cm^2 but that a longer mean free path would not be excluded. A free path as short as 86 g/cm^2 in lead, however, seems too small. Thus the recent values of 160–300 g/cm^2 obtained by various observers are in agreement with the present results.

The total flux of primaries at 10,600 feet has been estimated by Hazen, Randall, and Tiffany[12] to be $1.1\pm0.3\times10^{-4}$ cm^{-2} sec.$^{-1}$ steradian^{-1}. In the present experiment, the solid angle was 0.145 steradian, the active area of counters 103 cm^2, so the expected rate of primary particles is about 0.59/hr. The observed rate of local penetrating showers was 0.192/hr. at 3027 meters. If the mean free path, as used by Hazen, is 180 g/cm^2 of Pb, and we assume that 7 in. or 202 g/cm^2 Pb are useful in this case to produce observable showers, $(1-e^{-202/180})=0.67$, so 67 percent of the particles should have made showers in the chamber. This would give a rate of 0.4/hr. The lower observed rate of 0.192/hr. means that some showers were lost due to the geometry, spreading, and low multiplicity, but taking these into account, the present experiment agrees in order of magnitude with the value given by Hazen. The expected distribution of events in the chamber with no counter bias (curve A, Fig. 7) shows that a great number of events which occurred near the top of the chamber were not observed because of the arrangement of the lower counters.

[12] Hazen, Randall, and Tiffany, Phys. Rev. **75**, 694 (1949).

SUCCESSIVE EVENTS

Free Path of Secondaries

In fifty-eight photographs of penetrating showers, successive production of penetrating particles was observed, sometimes as many as three successive events. Most of these events occured more or less in line with the original particle, but in several cases, particles which were definitely secondaries produced additional penetrating showers. It is of interest to analyze these events to see if a free path for successive events can be calculated.

A minimum free path can be calculated by measuring the distance between two events and taking the weighted average distance. The weight must be taken according to (1) the inverse of the distance between events (it is more probable to observe short distances than long ones simply because of the limited size of the cloud chamber), and (2) the position of the second event in the cloud chamber. If the second event occurs near the lower counters it is more likely to be recorded than if it is near the top of the chamber. The second weight was calculated according to solid angle considerations similar to those used in consideration of position of single events in the cloud chamber. The minimum free path thus calculated comes out about 80 g/cm^2. The actual free path must be larger than this, because many secondaries made no successive events.

The total track length of penetrating particles emerging at minimum ionization from the showers would give some information on the free path. A count has been made of the total number of traversals of charged secondary particles through the $\frac{1}{2}$-inch lead plates. 4675 traversals were observed. These include not only the secondary particles produced, but also the primary particle if it was not absorbed catastrophically. The secondaries may have been either mesons or protons. In this number of traversals, 78 additional penetrating events and stars were observed to be produced by the charged secondaries, and twelve cases of large single scattering ($>15°$) were observed. Assuming that the single scattering is also due to nuclear interaction, the mean free path for total nuclear interaction of the secondaries comes out to be 750 g/cm^2 of lead. This represents a maximum free path, since other stars and possibly penetrating showers occurred in the cores of large events where identification was difficult and energies of particles concerned may have been too low to produce nuclear events. The corresponding cross section is 5.3×10^{-25} cm^2 per lead nucleus. If we consider the anomalous scattering only, the cross section

for scattering through an angle greater than 15° is $\sim 3\times 10^{-28}$ cm² per *nucleon*.

It is not very meaningful to compare the observed scattering cross section with the cross sections calculated from various meson theories, since the energies of the particles are not known and the calculated values are quite energy dependent. It seems, however, that most meson theories, coupled with reasonable estimates of the energies, give scattering cross sections which are an order of magnitude or more greater than the observed cross section.

Experiments by Piccioni[13] indicate that the particles produced in penetrating showers are mostly π-mesons. We are thus confronted with too few scatterings, according to present theories, by a factor of ten or so. It may be that when these particles scatter they nearly always produce a nuclear disruption, and thus count, not as an anomalous scattering, but as a nuclear event. Most of the nuclear events were high energy, however, and the question of the low cross section for scattering remains unresolved.

[13] O. Piccioni, Phys. Rev. **75**, 1281 (1949).

A final remark should be made concerning the comparisons which have been made between the observed data and the various meson theories. Because of the uncertainties in the meson coupling constants, none of the numerical comparisons can be considered as rigorous. In addition to this uncertainty, it is often necessary to jump from one meson theory to another in order to get any kind of agreement at all between theory and experiment. Thus, any numerical comparisons which have been made in this paper have been for illustrative purposes only, and cannot be considered as proof that any particular theory is correct.

ACKNOWLEDGMENTS

We are indebted to Mr. Carl P. Russell, Superintendent, Yosemite National Park, and to the National Park Service men who were so helpful to us during the summer at Tioga Pass, and without whose cooperation our work would have been impossible. Professor R. B. Brode's continuing interest and support, and the help of John Ise, Jr., and Andrew Yeiser in taking the pictures, are also gratefully acknowledged.

PHYSICAL REVIEW VOLUME 76, NUMBER 4 AUGUST 15, 1949

On the Mechanism of Production of the Neutron Component of the Cosmic Radiation

VANNA COCCONI TONGIORGI
Laboratory of Nuclear Studies, Cornell University, Ithaca, New York

(Received April 22, 1949)

Experiments have been performed on the neutron component of the cosmic radiation, with a system of BF_3 proportional counters embedded in paraffin, capable of recording neutrons in the energy range between ~2 and ~15 Mev. The neutron rate recorded with such a detector is due to both neutrons locally produced inside the detector and neutrons produced outside the detector, i.e., in the surroundings and in the atmosphere.

The local neutron production is due to a radiation which in the great majority does not consist either of photons or μ-mesons.

The intensity of such a radiation increases with altitude with a mean free path in air of 120–130 g/cm², which is confirmed by the fact that it shows a barometric coefficient ≈ -11 percent per cm Hg. At mountain elevation (4000 m) the intensity of this radiation is close to that of the total ionizing cosmic radiation. This suggests that it consists principally of fast neutrons.

The locally produced neutrons are mostly produced in multiples, with multiplitiy depending upon the material. In lead the average multiplicity observed was close to 8, in carbon smaller than 2.

The rates of neutron production in different materials are satisfactorily described by a cross section proportional to the $\frac{2}{3}$ power of the mass number of the material.

The results indicate that the main source of all the neutrons present in the cosmic radiation are "stars," though high energy processes like penetrating and extensive showers do contribute to neutron production.

I. INTRODUCTION

FOR more than ten years neutrons have been known to exist in the atmosphere as a component of the cosmic radiation and many experiments have been performed to study their properties.

In the last few years the importance of the strongly interacting radiations (neutrons, protons, heavy mesons) for the general understanding and interpretation of the cosmic-ray phenomena has been steadily growing. Recently the phenomena concerning the neutron component have been framed in a picture in which stars, penetrating showers, bursts and extensive showers also find their places.

According to this picture, the presence of neutrons in the atmosphere can be justified somewhat as follows. As neutrons have a finite lifetime, they cannot be primaries, hence they must originate within the atmosphere. The primary radiation (say protons and heavy ions), when it collides with air nuclei, produces fast neutrons in association with fast protons, heavy mesons and photons. High energy processes of this kind can be thought of as the origin of extensive showers, bursts and penetrating showers. The fast neutrons and

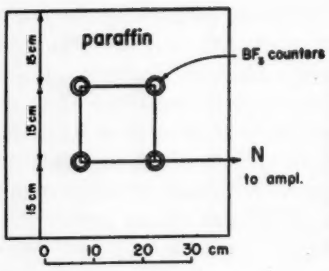

FIG. 1. Construction of the neutron detector. The paraffin block is 45×50×45 cm³. Four BF_3 proportional counters (2.5×45 cm²) connected in parallel are embedded in it. The paraffin block is completely covered with aluminum foil to provide electrical shield to the counters.

protons produced in these phenomena are eventually capable of giving rise to further nuclear disintegrations, as a result of which more neutrons are produced, either through one of the processes listed above or through the occurrence of stars. Nuclear evaporations with consequent emission of neutrons can be produced also by both π- and μ-mesons undergoing capture and, finally, neutrons can be ejected from a nucleus through photonuclear processes ((γ,qn) reactions) induced by the photons of the soft component.

Whatever is the nature of the nuclear process occurring, a neutron has a small probability of being emitted from a nucleus with kinetic energy lower than about 1 Mev. The great majority of the neutrons are likely produced with energies of several Mev. In the following we shall call "moderate energy neutrons" the particles, whose energies lie between 0.5 and 50 Mev and "fast neutrons" those with energies higher than 50 Mev.

The neutrons produced are then slowed down in the atmosphere by inelastic and elastic collisions with nuclei in the air and eventually undergo capture mostly by nitrogen nuclei through (n,p) processes. The average energy at which the capture occurs is about 0.07 ev and the root mean square distance traveled by neutrons with energies of the order of 10 Mev from their point of origin to the capture point is of the order of 100 g/cm².[1] Hence, as a result of this diffusion process, an equilibrium energy distribution is reached, in which slow neutrons predominate, though neutrons at thermal energies represent (in the free atmosphere) only ~15 percent of the neutron component.

This picture is based on many pieces of information collected from experiments on neutrons, stars, etc.[2] The most significant result is that the altitude variations of penetrating showers, extensive showers, stars and neutrons seem to be all described by an exponential law, $e^{-x/\lambda}$, with roughly the same mean free path λ.

However, no *direct* experimental evidence for the picture given above is so far available, as we lack *direct* experimental information about the characteristics of the processes in which neutrons are produced, and about the behavior of the neutron producing radiation. This lack of information arises from the fact that cloud chambers and photographic plates cannot give information about neutrons, while neutron counter experiments have not been developed enough to supply consistent data. The counter experiments on thermal and slow neutrons, which are the easiest to interpret, are not probably the most suitable ones to throw light on the processes in which neutrons originate, since, as pointed out before, the great majority of neutrons are produced as either fast or moderate energy particles.

Moderate energy neutrons can be detected by the same devices capable of recording slow and thermal particles provided that a proper layer of hydrogenate material is put around them to slow the neutrons down to energies such as to make their detection probable. A system like that, however, gives results which are surely affected by scattering and local production of neutrons in the detector itself. Proper experimental arrangements must be chosen to make a sound interpretation of the results possible and still unavoidable uncertainties are left in the deductions. So far, no systematic sets of data have been taken with arrangements of this kind to study the origin of the neutrons present in the cosmic radiation.

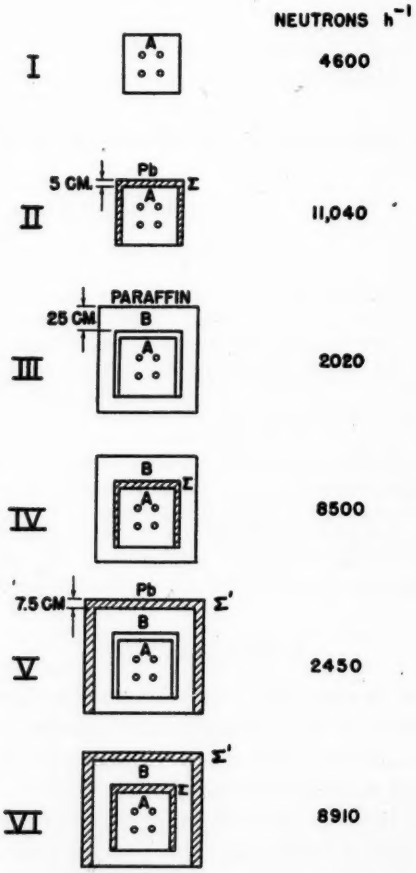

FIG. 2. Sketches of the six arrangements of paraffin and lead absorbers put around the neutron detector. Arrangement I is the naked neutron detector as drawn in Fig. 1. At the right side of the sketches are given the recorded neutron rates (h^{-1}) corrected for Cd-background.

[1] Bethe, Korff, and Placzek, Phys. Rev. **57**, 573 (1940).
[2] See e.g., B. Rossi, Rev. Mod. Phys. **20**, 537 (1948).

The aim of this paper is to present some information about the mechanism of neutron production and about the nature of the neutron producing radiation as it can be derived from experiments we have performed on neutrons of moderate energies.

II. EXPERIMENTAL ARRANGEMENT

The data we are going to report are in part the by-product of experiments performed during the spring and summer of 1948 intended to study the neutrons associated with extensive air showers, and in part the results of further experiments made during the winter of 1949 designed to complete the information acquired.

In all the experiments, the neutron detector consisted of a paraffin block ($45\times50\times45$ cm^3) in which four BF_3 proportional counters (2.5×45 cm^2) were embedded (see Fig. 1). Details concerning the construction of the detector and the operation of the counters have been fully given in a previous article concerning neutrons in the extensive showers,[3] that we shall quote in the following as paper I.

The neutrons that our detector is capable of recording are those whose energies lie between ~2 and ~15 Mev, hence the results obtained refer to moderate energy neutrons.

The over-all efficiency ϵ of the detector is given by the product of the efficiency η of the BF_3 counters to record slow neutrons (for our counters $\eta=0.3$), times the probability α that a neutron falling on the paraffin block is slowed down to detectable energies and crosses the counters. From tests with a (Ra+Be) neutron source we estimated $\alpha_4=0.1$ when the four BF_3 counters were all connected in parallel. Hence we assume $\epsilon=\eta\cdot\alpha_4=0.03$. This estimate is considered reliable within a factor 2.

The pulses of the neutron counters, amplified as described in paper I, have been recorded through a scaler circuit.

The cadmium-difference, i.e., the difference between the rates recorded without and with Cd shields (0.75 mm Cd foil) around the BF_3 counters, has been measured in all experiments and assumed as the neutron counting rate. The Cd-background was always smaller than 5 percent of the rates recorded without Cd.

All the data have been taken under roofs of a few g/cm^2 of light materials with the detector placed as far as possible from walls and other materials. In detecting moderate energy neutrons the effect of the back scattering of the ground was thought to be negligible.

As in the course of this discussion we shall often quote results given in paper I concerning neutrons coherent with extensive showers, we shall use the expression "incoherent neutrons" to identify the particles constituting the *total* neutron component of the cosmic radiation, which we are dealing with in the present paper.

TABLE I. Neutron rates (h^{-1}) (corrected for Cd-background and barometric effect) recorded with the arrangement in Fig. 3 with different thicknesses t of the lead absorber.

	$t=0$ (h^{-1})	$t=\frac{1}{2}$ in. (h^{-1})	$t=1$ in. (h^{-1})	$t=3$ in. (h^{-1})	$t=6$ in. (h^{-1})
N_t	553±4	596±4	645±5	722±5	778±5
N_t-N_0	0	43±0.5	92±1	169±1.7	225±2.3

III. NATURE OF THE NEUTRON PRODUCERS

Since neutrons are produced in the atmosphere, it is reasonable to expect that neutron production takes place also in condensed materials, hence experiments in which proper absorbers are put around a neutron detector can supply information about the mechanism of local production of neutrons.

With the aim of studying the origin of neutrons, a group of experiments have been performed at Echo Lake (3260-m altitude). The six arrangements of absorbers surrounding the neutron detector, drawn in Fig. 2, have been used. Arrangement I is the naked detector as it was shown in Fig. 1. The nature and the thickness of the absorbers are indicated in the drawings. The lead absorbers Σ and Σ' in arrangements II, IV, V, and VI were put on top and on four sides of the detector. The extra paraffin B in arrangements III, IV, V, and VI shielded the detector on all six sides.

The numbers given at the right side of the sketch of each arrangement are the neutron rates recorded per hour (Cd-background subtracted). The statistical errors are not given as they are smaller than 1 percent, while changes in the barometric pressure surely caused a larger uncertainty. We think that the errors that should be attributed to our data are smaller than 10 percent.

From our results the following qualitative conclusions can be derived:

(a) The large increase in the counting rates when the arrangement is varied from I to II, as well as from III to IV; hence, whenever lead is put in the vicinity of the detector, shows that a strong local production of neutrons of moderate energies occurs in lead. This means that a radiation is present capable of producing neutrons.

(b) The comparison of the difference (II–I) = 6440 with the difference (V–III) = 430 shows that the great majority of the neutrons produced in lead cannot cross 30–40 cm paraffin; hence

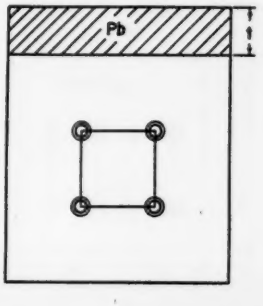

FIG. 3. Arrangement used to study the transition curve air-lead for the neutron producing radiation. The area of the lead was 45×50 cm^2. The thickness t was varied from 0 to 6 in. Pb.

[3] V. Cocconi Tongiorgi, Phys. Rev. 75, 1532 (1949).

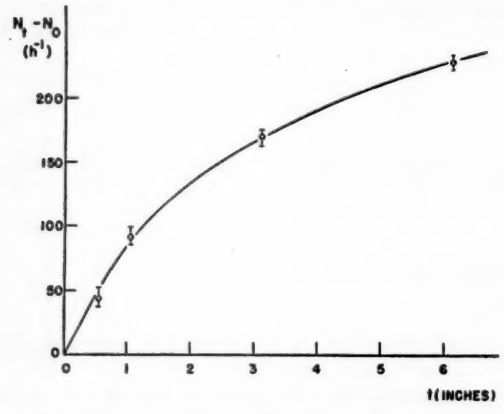

FIG. 4. Transition curve air-lead for the neutron producing radiation.

indicates that the energies of the neutrons locally produced are, on the average, smaller than 10–20 Mev.

(c) Deduction (b) implies that the mean contribution to rate VI is due to neutrons generated in the lead Σ, not in Σ'. Now, the comparison of rates IV and VI indicates that the addition of layer Σ' (7.5 cm Pb on top, 5 cm on the sides) to arrangement IV does not cause a reduction in the rates, but actually a small increase. To justify such an increase one may think that a small fraction of the neutrons produced in Σ' reaches the counters and/or that the neutron producing radiation undergoes a multiplication in lead: both effects could mask the absorption of the neutron primaries. Anyhow this result rules out the possibility that the neutron producing radiation is strongly absorbed in lead.

As pointed out in Section I, nucleonic particles, π- and μ-mesons and photons can be thought capable of producing neutrons. On the basis of the results given above we think that photons are ruled out as substantial contributors to neutron production. The layer Σ', in fact, is equivalent to $\sim$15 radiation lengths and would produce a reduction in the intensity of the photon component probably greater than 90 percent.

It is interesting to note that the same behavior observed in the series of measurements reported in Fig. 2 has been found when the same six arrangements of absorbers have been used to study the origin of neutrons coherent with extensive air showers (see paper I). In the extensive showers, electrons and photons represent more than 99 percent of the radiation present, while in the total incoherent radiation at 3260 m elevation electrons and photons are less than 70 percent of the total radiation. Furthermore, the average energy of the soft component is larger in the extensive showers than in the incoherent radiation. Then, the fact that the same absorbers affect in the same manner neutrons both incoherent and coherent with extensive showers supports the deduction that the soft component of the cosmic radiation does not contribute substantially to neutron production. This conclusion is consistent also with the fact that stars (in which neutrons are surely emitted besides the ionizing heavy particles observed) appear to be hardly ever correlated with occurrence of a cascade shower,[4,5] as well as with the fact that neutrons are also produced in penetrating showers[6] where the originating particles are known not to be photons.

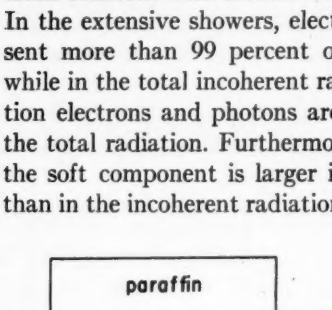

FIG. 5. Arrangement of the neutron detector used to study the multiplicity of neutron production. Pulses n_1 and n_2 were fed into two identical amplifier-discriminator channels.

An attempt at quantitative interpretation of the data given in Fig. 2 has been made by using the method of analysis developed by Levinger.[7] The hypothesis that this procedure requires and the limitations it possesses are indicated in Levinger's paper to which we refer the reader for details.

The results obtained are the following ones:

Transmission of the neutrons through 25 cm paraffin = 0.045,
Transmission of neutron producers through 25 cm paraffin = 1.02,
Transmission of neutron producers through 7.5 cm Pb = 0.997,
Counting rate due to neutrons produced in 1 cm paraffin = 45.7 h^{-1},
Counting rate due to neutrons produced in 1 cm lead = 1285 h^{-1},
Counting rate due to neutrons present in the atmosphere or produced in materials outside the paraffin-lead arrangement = 3229 h^{-1} (with arrangement I).

These results are in agreement with the deductions derived before from the qualitative discussion of the data. The fact that the transmissions through both 25 cm paraffin and 7.5 cm Pb are close to unity for neutron producers confirms that this radiation behaves differently from electrons and photons.

The low value of the transmission of the neutrons through 25 cm paraffin confirms that the neutrons recorded are of moderate energies, roughly 3 Mev, on the average. It is interesting to note that the same transmission has been found at the same altitude for neutrons coherent with extensive showers.[7]

The analysis shows that production of moderate energy neutrons occurs not only in lead but also in paraffin. Roughly $\frac{1}{3}$ of the rate recorded with the naked detector (arrangement I) is due to neutrons locally generated in the paraffin, while about $\frac{2}{3}$ of that rate is due to neutrons entering the detector from the outside, produced in the atmosphere and in materials surrounding the detector.

In order to check and increase the information derived from the measurements taken at Echo Lake, a further experiment has been performed at Ithaca, intended to study the air-lead transition curve for the neutron producing radiation.

Data have been taken with different thicknesses t of lead covering the top of the neutron detector (see

[4] W. E. Hazen, Phys. Rev. **65**, 67 (1944).
[5] W. M. Powell, Phys. Rev. **69**, 385 (1946).
[6] Cocconi, Cocconi-Tongiorgi, and Greisen, Phys. Rev. **74**, 1867 (1948).
[7] J. Levinger, Phys. Rev. **75**, 1540 (1949).

Fig. 3). The neutron rates recorded per hour, N_t, corrected both for Cd-background and for barometric effect (see Section VIII), are reported in Table I.

The differences $N_t - N_0$ (rate with absorber *t minus* rate with no absorber) are also given in the table and plotted in Fig. 4. Besides confirming the occurrence of neutron production in lead, the graph of Fig. 4 indicates that the mean free path in lead, λ_{Pb}, of the neutron producers must be larger than ~ 100 g/cm^2. This experiment, however, can give only a lower limit of such a mean free path, as scattering, absorption in lead of neutrons both present in the air and locally produced, as well as variation with the thickness t of the mean distance of the point in which the neutrons originate from the detector cause an apparent decrease of λ_{Pb}. In our opinion these effects cannot change the order of magnitude of the mean free path; however, they can easily make it appear too low by a factor two or three.

The behavior of the curve in Fig. 4 is consistent with the deduction derived from the experiments made at Echo Lake, i.e., that photons do not play an important role in neutron production; in fact, the large increase in the counting rate when the lead is increased from 7.5 to 15 cm is hardly understandable if the contribution due to photo-nuclear reactions is substantial.

On the basis of the results so far reported, there is no ground for ruling out that a considerable fraction of the neutrons recorded under lead arise from processes induced by μ-mesons. However, the order of magnitude of the contribution due to capture in lead of negative μ-mesons can be estimated and put in comparison with the data plotted in Fig. 4. We shall calculate the number of neutrons expected to be produced by μ-mesons in the lead absorber when the thickness t is 1-in. Pb. Let $N_0 \cos^n\theta$ ster^{-1} sec^{-1} g^{-1} be the number of negative slow μ-mesons stopped in one gram of air at sea level per time unit, arriving in unit solid angle, with zenith angle θ. Then the number N of negative μ-mesons stopped for time unit, in the thickness t of a lead absorber whose surface is S, is:

$$N = 2\pi(S \cdot t \cdot \rho/n+1)(N_0/\alpha) \text{ sec}^{-1},$$

where ρ is the density of the lead and α is the relative stopping power of air and lead.

With $N_0 = 2\times 10^{-6}$ g^{-1} sec^{-1} ster^{-1},[7] $n = 3.3$,[8] $\alpha = 1.7$,[9] $t = 2.5$ cm, $S = 2250$ cm^2 and $\rho = 11.2$ g/cm^3, one has: $N = 0.11$ sec^{-1}. If 0.03 is the over-all efficiency of the neutron detector and 0.5 the probability that a neutron produced in the lead enters the detector, one gets that the effective neutron rate to be expected is 5.8 ν neutrons/h, where ν is the average number of neutrons produced in one act by the meson. This estimate is an upper limit, as the losses of neutrons due to the geometry and to the scattering make the probability that a neutron produced in the absorber enters the detector surely smaller than 0.5.

[8] W. Kraushaar (unpublished result).
[9] G. C. Wick, Nuovo Cimento 1, 310 (1943).

TABLE II. Rates (h^{-1}) corrected for Cd-background of the neutron coincidences n_1+n_2 and average n of the rates n_1 and n_2 for arrangements III and IV.

	n (h^{-1})	n_1+n_2 (h^{-1})
Arr. III	1250	2.39
Arr. IV	5100	36.0

The figure obtained above must be compared with 92 h^{-1} neutrons actually recorded for the difference $N_{2.5} - N_0$. No satisfactory determination of ν has been made so far. The experimental evidence and the theoretical expectation, however, agree in indicating that ν is of the order of a few units. We think, therefore, that at sea level no more than 10–15 percent of the rates recorded can be accounted for by neutrons produced in capture of negative μ-mesons. If this is the case at sea level, at higher elevations the relative importance of the contribution due to μ-mesons is, of course, strongly reduced, as neutrons increase with altitude much faster than μ-mesons (see Section VII).

No appreciable contribution due to neutrons arising from μ-mesons capture has to be expected in light materials like paraffin and graphite.

IV. NEUTRON PRODUCTION IN DIFFERENT MATERIALS

The analysis of the experiments performed at Echo Lake, reported in Section III, indicates that local production of moderate energy neutrons occurs in lead as well as in paraffin.

In the course of those experiments a test measurement was made to confirm the occurrence of neutron production in materials of low atomic number.

In arrangement IV of Fig. 2 the 2-in. Pb constituting the absorber has been substituted with 2-in. graphite.

The difference between the rate recorded (corrected for Cd-background) and rate III in Fig. 2 is 430 h^{-1}. It essentially represents the neutron production in the graphite absorber. This number can be compared with the neutron production in lead, namely with the difference (IV–III) = 6400 h^{-1} (see Fig. 2), provided that a 25 percent increase is made of the production in graphite to take into account the fact that the surface of the detector covered with graphite was 25 percent smaller than that covered with lead. With this cor-

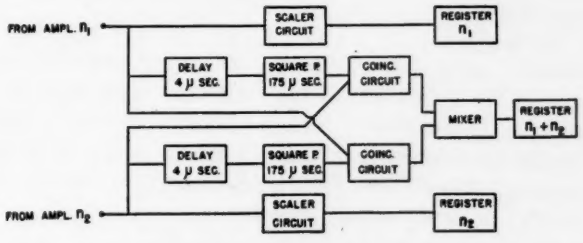

FIG. 6. Circuit used to study the multiplicity of neutron production. Pulses n_1, n_2 and coincidences n_1+n_2 were recorded.

TABLE III. Neutron rates (h^{-1}) corrected for Cd-background recorded in arrangements I, II, III and IV at Ithaca (260 m), Echo Lake (3260 m) and Mt. Evans (4300 m).

	I (h^{-1})	II (h^{-1})	III (h^{-1})	IV (h^{-1})	IV-III (h^{-1})
Ithaca	520	1230	285	1190	805
Echo Lake	4600	11040	2020	8500	6480
Mt. Evans	12510	25000	4780	20630	15850

rection, the rates of production in graphite and lead are respectively 108 h^{-1} cm^{-1} and 1296 h^{-1} cm^{-1}.

These figures agree very satisfactorily with the estimates made through the quantitative analysis of the data in Section III, which gave 1285 h^{-1} cm^{-1} neutrons produced in lead and 45.7 h^{-1} cm^{-1} neutrons produced in paraffin. With the assumption that the neutron production in paraffin is all due to the C-nuclei, the last figure corresponds to a neutron production in graphite $=45.7\times1.7/0.76=102$ h^{-1} cm^{-1}. Our results indicate a ratio ~2 between the production per gram in lead and carbon. However, one has to keep in mind that our detector was sensitive only to neutrons in a finite energy range, hence that the comparison between production in different materials requires assumption of constant energy spectrum of the neutron produced from different nuclei.

Recently Tobey[10] reported an experiment designed to measure the absolute rates of neutron production per gram of different materials. His detector can be considered as energy independent. The rates of neutron production obtained at sea level are: 6×10^{-5} neutron sec^{-1} g^{-1} in lead and 2.3×10^{-5} neutron sec^{-1} g^{-1} in carbon. This indicates a ratio neutron production in lead/neutron production in carbon ≈2.6, which is in fair agreement with our result.

Our experiments were not designed to supply information about the *absolute* intensity of the neutron production. However, an order of magnitude estimate can be made from the data recorded at sea level for the transition curve given in Fig. 4, Section III. If one assumes that the neutron production is isotropic, then a recorded rate N_t-N_0 indicates a neutron production per gram of lead per sec equal to:

$$(N_t-N_0)\cdot1/M\cdot1/\epsilon.\ 4\pi/\omega,$$

where ω is the solid angle subtended by the paraffin at the detector, ϵ the over-all efficiency of the detector and M the mass of the lead absorber.

With $N_t-N_0=N_{2.5}-N_0=92$ neutron $h^{-1}=2.57\times10^{-2}$ neutron sec^{-1} (see Table I), $M=2.5\times2250\times11.2$ g $=6.3\times10^4$ g, $\epsilon=0.03$, $\omega/4\pi=0.3$, one finds that the neutron production in lead is 4.5×10^{-5} sec^{-1} g^{-1}. This is slightly smaller than Tobey's figure, which is to be expected owing to the finite range of neutron energies to which our detector was sensitive.

The agreement is therefore satisfactory.

[10] A. R. Tobey, Phys. Rev. **75**, 894 (1949).

V. MULTIPLICITY OF THE NEUTRON PRODUCTION

For the interpretation of the data on neutron production in different materials, it is essential to know whether neutrons are produced mostly singly or in multiples, and, in the second case, how the multiplicity of neutron production depends upon the material in which such a production takes place.

Some evidence in favor of multiple neutron production has been obtained by Korff and Hamermesh.[11] However, the geometry of their experiment is such that it does not allow quantitative interpretation of the results.

At 3260 m an experiment has been performed to get information about the multiplicity of neutron production. We shall call multiplicity, ν, the average number of neutrons simultaneously produced with energies lying in the energy range to which our detector is sensitive.

The four counters inside the detector have been connected in two groups of two counters each, as shown in Fig. 5. Their pulses, n_1 and n_2, amplified and discriminated through two identical channels, were fed into the coincidence circuit schematically drawn in Fig. 6. The delays of 4-μsec were introduced to reduce the background due to spurious phenomena. The reresolving time was 175-μ sec. Coincidences n_1+n_2 as well as pulses n_1 and n_2 were recorded.

Paraffin and lead absorbers have been put around the detector as in the arrangements III and IV in Fig. 2.

The results are given in Table II. The rates n are the averages of the counts recorded for n_1 and n_2, corrected for Cd-background. Coincidences n_1+n_2 are corrected for chance events, which constitute 13 percent of the rates recorded in arrangement III and 3 percent of the rates recorded in arrangement IV. The ratio $(n_1+n_2)/n$ gives the probability that a neutron occurs within 4 and 179-μsec after the occurrence of a first neutron. With the assumption that the neutrons emitted from a nucleus are isotropically distributed, one may write:

$$(n_1+n_2)/n=1-e^{-(\nu-1)\epsilon'\cdot\omega/4\pi},$$

where ω is the solid angle subtended by the detector at the absorber. The efficiency has been estimated by assuming that the system (paraffin+2 counters) has over-all efficiency $\frac{1}{2}$ of the system (paraffin+4 counters) used in the other experiments, and that the loss of neutrons due to the delay introduced in the circuit and to the finite duration of the coincidence pulse causes a further reduction in the efficiency by a factor ≈0.7. Hence $\epsilon'=\frac{1}{2}\times0.03\times0.7\approx0.01$.

In order to deal only with neutrons locally produced in the lead, we shall consider the differences between the rates recorded in arrangements IV and III. With

[11] S. Korff and B. Hamermesh, Phys. Rev. **70**, 429 (1946).

the assumption $\omega/4\pi=0.3$ we have:

$$83.6/3850=1-e^{-(\nu-1)\times 0.01\times 0.3}$$

and then $\nu\approx 8$. This means that, on the average, eight neutrons of energies between 2 and 15 Mev are produced simultaneously in lead by a *single* neutron producer. In fact, the possibility that two or more incoherent neutron producers fall by chance simultaneously on the lead is taken into account by the correction of the rates n_1+n_2 for chance events. The possibility that a "shower" of neutron producers falls on the detecting system is, of course, not ruled out, but it is reasonable to assume that the frequency of such an event is small enough as to make its effect negligible.

It is interesting to note that an analogous experiment on the neutrons coherent with extensive showers, performed at the same altitude, with the same apparatus (actually the two sets of data have been taken simultaneously) yielded ≈ 60 as the average multiplicity of the neutron production in lead (see paper I). A very high multiplicity in lead has been found also for neutrons produced in association with penetrating showers.[6]

The considerably smaller figure obtained for incoherent neutrons can probably be accounted for by an average energy of the neutron producers smaller in the incoherent radiation than in the showers, as well as by different relative intensities of the processes in competition in neutron production.

The multiplicity observed for incoherent neutrons suggests that most of these neutrons arise from stars of the same average size as observed in cloud chambers and in photographic plates.

From the data taken with arrangement III one deduces that the multiplicity of the neutron production in paraffin, and hence also in carbon, is close to unity ($\nu\approx 1.6$). The same result had been obtained from the data concerning neutrons coherent with extensive showers. These results on the multiplicity of neutron production in different materials must be considered as first approximation ones. It would be desirable to determine how the multiplicity depends upon the thickness of the absorber in which the neutron production takes place.

VI. CROSS SECTION FOR NEUTRON PRODUCTION

The estimate made in Section III of the mean free path in lead of the neutron producers, as well as the results concerning the absorption mean free path in air that will be given in Sections VII and VIII agree in indicating that the cross section for neutron production is of the order of magnitude of the geometrical cross section of nuclei. This leads to expect that the cross sections σ for neutron production is proportional to the $\frac{2}{3}$ power of the mass number A of the nuclei.

The information about the average multiplicity of the neutron production in lead and carbon obtained in Section V allows a check of whether or not such an assumption is consistent with the experimental results. In fact, if $\sigma\sim A^{\frac{2}{3}}$, the observed rate of production of neutrons under a given thickness of material, n_{obs}, must be proportional to: $(\rho/A)\cdot A^{\frac{2}{3}}\cdot\nu$ where ρ is the density of the material and ν the multiplicity of neutron production in it. Therefore, one must have

$$\frac{n_{\text{obs}}\cdot A^{\frac{1}{3}}}{\rho\nu}=K=\text{const. in different materials.}$$

With the figures obtained in Section IV for the neutron production in Pb and in C ($n_{\text{obs}}=1290\ h^{-1}\ \text{cm}^{-1}$ in Pb and $n_{\text{obs}}=105\ h^{-1}\ \text{cm}^{-1}$ in C) and in Section V for the multiplicity ($\nu=8$ in Pb and $\nu=1.6$ in C), one obtains for Pb $K=86.4$ and for C $K=88.5$. This result strongly supports the assumption that the $A^{-\frac{1}{3}}$ law holds for neutron production in different materials.

As the same law has been found to hold for production of stars,[12–14] the hypothesis that stars are the source of the great majority of the neutrons observed receives further strength.

VII. ALTITUDE VARIATION OF THE NEUTRON PRODUCERS

Measurements with the neutron detector surrounded by absorbers as in arrangements I, II, III, and IV of Fig. 2 have been taken at three different altitudes above sea level, namely at Ithaca (260 m; 1007 g/cm²), at Echo Lake (3260 m; 708 g/cm²) and at Mt. Evans (4300 m; 616 g/cm²). The recorded rates (h^{-1}) corrected for Cd-background are given in Table III.

The errors in these data are smaller than 10 percent.

As shown in Section III, the rates recorded with arrangement I result from a contribution due to

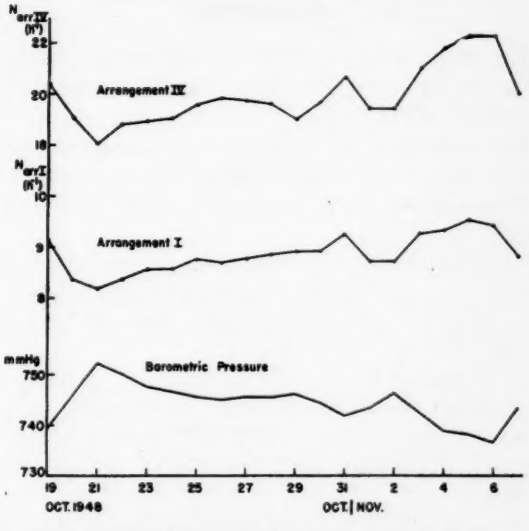

FIG. 7. Example of the correlation observed between neutron rates and barometric pressure.

[12] D. H. Perkins, Nature **160**, 707 (1947).
[13] G. Bernardini, Phys. Rev. **74**, 845 (1948).
[14] E. P. George and A. C. Jason, Proc. Phys. Soc. **A62**, 243 (1949).

neutrons produced in the paraffin and a contribution due to neutrons produced outside the detector, both in the atmosphere and in the surrounding materials. As the effect of the surroundings cannot be maintained the same in different stations we do not attribute great significance to comparison of data taken in different stations with arrangements I and II. This is not the case for arrangements III and IV in which the large thickness of paraffin made the detector practically insensitive to the effect of the surroundings. We shall consider the differences between the rates IV and III, reported in the last column of the table, which refer essentially to neutrons produced in the lead Σ. If one assumes that the efficiency for detection of neutrons is the same at all stations (which implies constant average multiplicity in the neutron production, as well as constant energy distribution of the neutrons produced), then the altitude variation of the difference IV–III is proportional to the altitude variation of the neutron producing radiation interacting with the absorber Σ. The rates (IV–III) vary by a factor 19.7 from Ithaca to Mt. Evans. If the absorption in air of the neutron producers is described by the law $I(x)=I_0e^{-x/\lambda}$, this result indicates for such a radiation an absorption mean free path $\lambda=132\pm15$ g/cm^2. This value is in good agreement with the mean free path observed for slow neutrons, stars, bursts, and penetrating showers.

This strong altitude variation of the neutron producers rules out conclusively the possibility that μ-mesons contribute substantially to the neutron production observed, which is consistent with the estimate made in Section III.

VIII. BAROMETRIC EFFECT OF NEUTRON PRODUCERS

The mean free path in air of the neutron producing radiation can be determined also by measuring its barometric effect.

The barometric effect of the rates recorded both in arrangement I and in arrangement IV has been studied at Ithaca during the winter of 1949, over a period of ten weeks.*

A very definite and strong correlation between the fluctuations in the rates recorded and the variations of the barometric pressure has been observed, as shown by the example given in Fig. 7.

By following the method indicated by Janossy and Rochester[15] we have obtained the barometric coefficients α given below, which are the averages of five partial calculations, each covering a period of two weeks:

$$\alpha_{\text{arr IV}}=-(11.2\pm0.6) \text{ percent per cm Hg},$$
$$\alpha_{\text{arr I}}=-(10.6\pm0.6) \text{ percent per cm Hg}.$$

The dependence on the barometric pressure of the Cd-background can be disregarded as the Cd-background is only 3 percent of the rates recorded without Cd.

Consider first the results obtained with arrangement IV. As indicated by the comparison between the rates III and IV in Table III, Section VII, ~75 percent of the rates recorded with arrangement IV are due to neutrons produced in the lead, while the remaining 25 percent are mostly due to neutrons generated in the paraffin. It is reasonable to expect that both the neutrons produced in lead and the neutrons produced in paraffin have the same barometric effect. This has been checked over a period of two weeks by removing the lead, hence recording the rates in arrangement III. We found $\alpha_{\text{arr III}}=\alpha_{\text{arr IV}}$ within the errors.

We are, therefore, led to conclude that the barometric coefficient obtained with arrangement IV, $\alpha_{\text{arr IV}}=-11.2$ percent per cm Hg, represents the barometric effect of the radiation that causes the local neutron production observed.

The corresponding mean free path in air is then $\lambda=13.59/11.2=121\pm7$ g/cm^2, which is in agreement with the result obtained in Section VI from the experiments at different altitudes.

We want to recall that roughly the same barometric coefficient, actually $\alpha=-(11.7\pm2.7)$ percent per cm Hg has been found by Janossy and Rochester[15] for the radiation that produces penetrating showers. This is interesting both because penetrating showers are thought to be phenomena initiated by nucleonic radiation and because penetrating showers are known to be one of the sources of moderate energy neutrons.[6]

The interpretation of the barometric coefficient obtained for neutrons recorded with arrangement I is more uncertain. As pointed out in Section III, the rates recorded with the naked detector are due both to neutrons produced locally and to neutrons produced in the atmosphere, the two contributions being of the same order of magnitude. If one assumes that the radiation which produces neutrons locally in any material has barometric coefficient $\alpha=-11.2$ percent per cm Hg, the fact that we obtained $\alpha_{\text{arr I}}=\alpha_{\text{arr IV}}$ inside the errors, leads one to think that also the neutrons present in the atmosphere have a barometric effect of the same order of magnitude. This supports the hypothesis, which is, however, quite reasonable, that neutrons in the atmosphere are produced mostly through the same processes as those that cause the local neutron production.

IX. INTENSITY OF THE NEUTRON PRODUCING RADIATION

From our data a tentative estimate can be derived of the intensity of the neutron producing radiation at different altitudes.

Consider again the arrangement drawn in Fig. 3 and the result reported in Fig. 4 for the neutron production

* We thank Mrs. Mildred Shapiro for help in performing this experiment.

[15] L. Janossy and G. D. Rochester, Proc. Roy. Soc. **183**, 186 (1944).

in 1-in. Pb at 260-m elevation, namely $N_t - N_0 = 92$ neutrons h^{-1}. If N neutrons per time unit are recorded, generated with average multiplicity ν in a thickness x of an absorber in which the mean free path of the neutron producers for neutron production is λ, then the number of neutron producers falling per time unit on the surfaces S of the absorber is

$$\mathfrak{N} = N \cdot \frac{1}{(1-e^{-\nu\epsilon\cdot\omega/4\pi})} \cdot \frac{1}{(1-e^{-x/\lambda})}$$

where ω has here the same meaning as in Section V.

The information about the mean free path in lead for production of neutrons is meager. The transition curve reported in Section III sets a lower limit at $\lambda = 100$ g/cm² for total absorption mean free path in lead of the neutron producers. The discussion developed in Section V indicates that the cross section for neutron production in different materials is likely proportional to $A^{\frac{1}{2}}$, hence that the corresponding mean free paths obey the $A^{\frac{1}{2}}$ law. Several experiments[12–14] indicate that the mean free path of the star producing radiation is ~150 g/cm² in air and ~300 g/cm² in Pb, which is consistent with the $A^{\frac{1}{2}}$ law.

As a tentative assumption we shall use in our calculation $\lambda = 300$ g/cm^{-2}. This is likely correct within a factor 1.5. By substituting in the formula written above $\nu = 8$, $\epsilon = 0.03$, $\omega = 0.3$, $x = 1$-in., Pb = 28 g/cm² and $N = 92/3600$ sec^{-1}, one has $\mathfrak{N} = 4$ sec^{-1}. At the same altitude, ~78 ionizing particles belonging to the total cosmic radiation fall in a second on the same surface ($S = 2250$ cm²). This indicates, therefore, a ratio neutron producers/total ionizing cosmic radiation close to 0.05 at 260-m altitude.

By using the absorption mean free path in air of the neutron producers obtained in Section VII, $\lambda = 130$ g/cm², one finds that the intensity of the neutron producers falling on the same surface is

at 3260 m	$\mathfrak{N} = 40$ sec^{-1}
at 4300 m	$\mathfrak{N} = 76$ sec^{-1}.

At those altitudes the ionizing particles of the total cosmic radiation falling on the surface S are respectively 148 and 175 sec^{-1}. Then, the ratio neutron producers/total ionizing radiation is close to 0.2 at 3260 m and to 0.4 at 4300 m.

As our neutron detector is sensitive only to neutrons in a finite energy range, these figures surely err on the low side. Furthermore, because of the uncertainties involved in the calculations they can easily be wrong by a factor two in either direction.

Yet, these estimates can supply further information about the nature of the neutron producing radiation. From our previous discussion, we have reached the conclusion that both photons and μ-mesons are ruled out as substantial contributors to neutron production. This left us with σ-mesons, fast neutrons and protons.

Several estimates of the proton intensity in the cosmic radiation[2] indicate that protons at sea level are of the order of 0.1 percent of the total radiation and at altitudes of 3000–4000 m of the order of a few percent.

As for σ-mesons, only very scanty data are available, but it is believed that their intensity is negligible at sea level and at altitudes of 3000–4000 m it is still rather small compared with the total ionizing cosmic radiation. Hence, the result that the intensity of neutron producers at mountain altitudes is of the same order of magnitude as that of the total radiation, leads one to conclude that the neutron producers are predominantly fast neutrons.

It is important to recall that from the analysis of stars in photographic plates and in cloud chamber pictures the conclusion has been reached that also the star primaries are mostly fast neutrons.

Estimates of the ratio star primaries/total ionizing rays can be derived from cloud-chamber and photographic plate data. The comparison with our results is of great interest.

Powell,[5] by comparing the number of stars and penetrating particles simultaneously observed in cloud-chamber pictures obtained at Mt. Evans, deduced that the star primaries are at 4300-m altitude seven times more frequent than penetrating particles, hence roughly three times more abundant than the total ionizing cosmic rays. This figure is likely too high owing to the restrictive criterion used by the author to select penetrating particles (no secondaries produced in two or more lead plates 1-cm thick).

On the other hand, in Powell's estimate a mean free path in lead for star production of ~110 g/cm² has been used. If we introduce the same mean free path $\lambda = 300$ g/cm² as used in our calculations, the ratio star primaries/total radiation becomes ~3 times higher.

Furthermore, in any estimate based on cloud-chamber observations, a difficulty arises from the fact that the sensitive time of the apparatus is somewhat bigger for stars than for the thin tracks of penetrating particles. In Powell's estimate the effect of sensitive time has not been taken into account. We think that a correction must be made for it, and that a reduction by a factor two or so for the ratio in question is probably reasonable. Hence, we think that Powell's data, with the assumptions and the corrections indicated, lead to a ratio star primaries/total radiation at 4300-m altitude close to two.

The cloud-chamber pictures taken by Hazen[4] at Echo Lake can be analyzed in the same way.

With the same assumptions as indicated above, one gets a ratio star primaries/total radiation at 3260 m close to ~0.6. This estimate is based on the observation of 58 stars emerging from the lead plates while *two* stars originate in the gas. The uncertainty in this estimate is consequently very high. Powell's data, based on observation of 156 stars from the lead and 13 originating in the gas are statistically more significant.

TABLE IV. Ratios neutron primaries/total ionizing radiation and star primaries/total ionizing radiation as estimated by various authors at different elevations above sea level.

Neutron primaries/total radiation		Star primaries/total radiation		
260 m	0.05	sea level	0.06	(George)
3260 m	0.20	3260 m	0.60	(Hazen)
		3750 m	0.20	(George)
4300 m	0.40	4300 m	~2	(Powell)

Both these estimates refer to stars in which several ionizing particles are present. In fact, two or more prongs are observed to emerge from the lead, which corresponds to an average number of ionizing particles generated in the stars likely higher than five.

Recently George and Jason[14] have estimated that the radiation (likely fast neutrons) which produces in photographic plates stars with 3 or more prongs is about 0.20 times the total ionizing radiation at 3750-m elevation (Jungfraujoch) and about 0.06 at sea level. As the authors pointed out, this figure errs on the low side, due to stars consisting of particles with energies above the limit of detectability in the emulsion.

The estimates derived from our experiments, as well as the estimates derived from cloud-chamber and photographic plate data are summarized in Table IV. The large uncertainties involved both in the experimental data and in the calculations do not allow one to look in these estimates for more than first approximation information. It is remarkable and satisfactory indeed that these estimates based on such different kinds of experiments and methods of evaluation agree as to the order of magnitude. This gives another strong argument in favor of the conclusion that most of the neutrons of moderate energies observed to be produced in lead are originated in stars induced by fast neutrons.

Furthermore, BF_3 counters, cloud-chamber and photographic plate data agree in indicating that the intensity of the fast neutrons present at an altitude of ~4000 m above sea level is of the same order of magnitude as the intensity of the total ionizing cosmic radiation.

X. CONCLUSIONS

The general picture given in Section I to justify the presence of neutrons in the cosmic radiation is consistent with all the results obtained in our experiments, hence it receives from them a direct confirmation.

On the basis of the results reported in Sections III, IV, V, VI, VII, VIII and IX the following details can be added to it:

(1) Though it is experimentally proved that high energy processes like penetrating showers do contribute to generation of moderate energy neutrons, the great majority of the neutrons of moderate energies produced in absorbers surrounding a detector are originated in less energetic phenomena (stars).

(2) The radiation that causes production of moderate energy neutrons does not consist substantially of photons or of μ-mesons; neither can σ-mesons nor protons give rise to a considerable fraction of the neutrons observed. Hence, fast neutrons are the particles that contribute mostly to the production of moderate energy neutrons.

(3) The radiation capable of producing moderate energy neutrons is, at mountain elevations, roughly as abundant as the total of ionizing particles constituting the cosmic radiation.

(4) Its altitude variation is described by an absorption mean free path in air of 120–130 g/cm², which is confirmed by the fact that it shows a barometric coefficient $\alpha = -11$ percent per cm Hg.

(5) In each process of neutron production in lead, on the average, roughly eight neutrons with moderate energies are simultaneously produced. In carbon the multiplicity of neutron production is close to unity. The average energy of the neutrons produced in lead is close to 3 Mev.

(6) The rates of neutron production observed in different material are satisfactorily described with the assumption that the cross section for neutron production is proportional to the $\frac{2}{3}$ power of the mass number of the material.

Note added in proof.—Recently, measurements have been performed with the equipment located at Ithaca, in a tunnel underground, at a depth equivalent to 2000 g/cm² water. The neutron detector was surrounded with paraffin and lead as in the arrangements III and IV of Fig. 2. The difference (III−IV) corrected for Cd-background was found to be $16.4h^{-1}$. Hence the intensity of the local production of neutrons in Pb at that depth is about 50 times smaller than that at the level of the ground (260-m elevation). With the assumption that the neutrons observed are produced only by fast nucleons, whose mean free path in the rock is 150–200 g/cm², one should expect that the neutron intensity is reduced by a factor larger than 10^4. Our result, therefore, shows that radiations different from nucleons, likely μ-mesons or their secondaries, contribute to neutron production. As the meson intensity at such a depth is reduced by a factor 4, one deduces that at the level of the ground the contribution to the neutron production due to μ-mesons is smaller than 10 percent of the effect observed. This is in agreement with the conclusion reached in Section III.

Absorption of 17.6 Mev Gamma-Rays in C, Al, Cu, Sn, and Pb

R. L. WALKER
Cornell University, Ithaca, New York
(Received May 6, 1949)

The gamma-ray absorption cross sections of C, Al, Cu, Sn, and Pb have been measured for the 17.6 Mev gamma-rays produced in the $Li^7(p, \gamma)Be^8$ reaction. A gamma-ray pair spectrometer was used as a detector for the 17.6 Mev gamma-rays in order to avoid counting lower energy quanta produced either in the $Li^7(p, \gamma)Be^8$ reaction, or as secondary radiation in the absorber. The measured cross sections are compared to the sum of the theoretical cross sections for Compton scattering, pair production in the field of the nucleus and pair production in the field of the atomic electrons. For the light elements, the agreement is within the experimental errors of about one percent, but for lead the theoretical value is ten percent above the measured cross section. This discrepancy probably results from the use of the Born approximation in the Bethe-Heitler calculation of pair production. The present results are in good agreement with recent measurements of Adams at 11.04, 13.73, and 19.10 Mev, and of Lawson at 88 Mev.

INTRODUCTION

THE importance of accurate measurements of the absorption coefficients of high energy gamma-rays in various elements as a means of checking the theoretical predictions concerning pair production and Compton scattering, has long been recognized.[1] Until very recently, however, no very accurate measurements have been made because of difficulties introduced by the production of degraded secondary radiation accompanying the absorption of the primary radiation. This secondary radiation makes it necessary to use for an absorption measurement an energy selective detector which can discriminate between the primary gamma-rays and the lower energy secondary quanta.

The first measurement performed with such a detector was that of Delsasso, Fowler, and Lauritsen,[2] in 1937. They determined the quantum energy of the gamma-rays produced in the $Li^7(p, \gamma)Be^8$ reaction, by measuring the total energy of electron pairs produced by the gamma-rays in a thin lead plate in a cloud chamber. They then used the same technique of counting pairs in a cloud chamber to measure the absorption coefficient for these gamma-rays in lead. Their result was about ten percent below the theoretical value, but the statistical uncertainty was also ten percent. Later McDaniel, von Dardel, and Walker[3] used a magnetic pair spectrometer to measure the absorption of the 17.6 Mev lithium gamma-rays in lead and aluminum. The results were roughly in agreement with the theory within statistical errors of 5 to 10 percent.

Recently, accurate measurements of the absorption of betatron radiation in various elements have been made by Adams, and by Lawson. Adams[4] used threshold detectors to measure the absorption in Al, Fe, Cu, and Pb of 11.04, 13.73, and 19.10 Mev betatron x-rays. Lawson[5] used a magnetic pair-detecting spectrum analyser to measure the absorption of 88 Mev gamma-rays in Be, Al, Cu, Sn, Pb, and U. The experimental results of Adams and of Lawson, as well as those reported in the present paper, show rather good agreement with the theory for light elements (except for Lawson's Be measurement) but discrepancies of the order of 9 to 13 percent for the heaviest elements. These discrepancies for very heavy elements are believed to result from a failure of the Born approximation used in the Bethe-Heitler calculation of pair production.[6] Unfortunately, no more exact calculations are available at present.

The gamma-rays used in the present experiments were those emitted from the 440-kev proton resonance of the $Li^7(p,\gamma)Be^8$ reaction. The spectrum of these gamma-rays consists of a sharp line at 17.6 Mev, and a broad line near 14.8 Mev with a relative intensity about half that of the 17.6 Mev line.[7] The gamma-ray detector was a magnetic pair spectrometer. By adjusting the spectrometer to be sensitive only to gamma-rays in a narrow energy band near 17.6 Mev, one can avoid counting either the lower energy gamma-rays from the source (near 14.8 Mev), or lower energy secondary radiation produced in the absorber. Thus the gamma-rays investigated have a very sharply defined energy rather than a narrow band from a continuous spectrum, as is the case when betatron radiation is used. This advantage is rather unimportant, however, since the absorption cross sections investigated do not vary rapidly with energy.

II. APPARATUS

The gamma-ray spectrometer used in these experiments has been described previously in some detail.[7] It measures the total energy of electron pairs produced by the gamma-rays in a thin radiator. In the absorption experiments, a comparatively thick radiator of 0.006-inch Pb was used in order to obtain a high counting rate, and thus good statistical accuracy.

[1] For example, see W. Heitler, *Quantum Theory of Radiation* (Oxford University Press, London, 1936).
[2] Delsasso, Fowler, and Lauritsen, Phys. Rev. **51**, 391 (1937).
[3] B. D. McDaniel, Guy von Dardel, and R. L. Walker, Phys. Rev. **72**, 985 (1947).
[4] G. D. Adams, Phys. Rev. **74**, 1707 (1948).
[5] J. L. Lawson, Phys. Rev. **75**, 433 (1949).
[6] H. A. Bethe and W. Heitler, Proc. Roy. Soc. **146**, 83 (1934).
[7] R. L. Walker and B. D. McDaniel, Phys. Rev. **74**, 315 (1948).

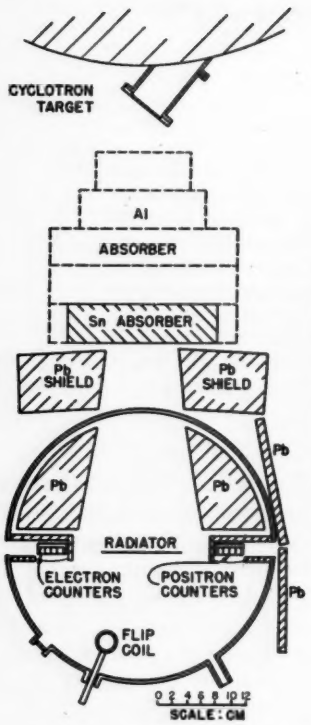

FIG. 1. Geometrical arrangement of the spectrometer, the absorber, and the cyclotron target. The actual positions occupied by the Sn and Al absorbers are shown. The Pb and Cu absorbers occupied a space about like the Sn, whereas the graphite had a configuration similar to that shown for Al.

The geometrical arrangement of the spectrometer, absorber, and cyclotron target is shown in Fig. 1. The transmission of each absorber was measured in the usual way by observing alternately the counting rates with and without the absorber in position. (Because of the wide radiator used in the spectrometer, some of the gamma-rays traverse the absorber at small angles from its normal. Thus the effective thickness of the absorber is slightly greater than its actual thickness, but this effect has been neglected since it amounts to only 0.2 percent.)

In order to monitor the gamma-ray intensity, two small Geiger counters were mounted in lead shields, one 65 cm above and one 21 cm below the cyclotron target. Precautions were taken to insure that the counting rates of the monitors were not affected by the presence of the absorbers, since the graphite and aluminum absorbers extented rather close to the cyclotron target, and might scatter gamma-rays into the monitors. For example, the positions of the monitors were such that radiation reaching them from the absorber must have been scattered through angles $\gtrsim 90°$. Thus most of this scattered radiation had very low energies ($\lesssim 0.5$ Mev) and would be more strongly absorbed in the 4.5 cm lead monitor shield than the primary gamma-rays from the cyclotron target.

A rough calculation indicates that the effect on the monitor counting rates of radiation scattered from the absorber was probably much less than 0.5 percent. This question was also investigated by observing the monitor counting rates relative to the spectrometer counting rate when large blocks of aluminum were placed on both sides of the cyclotron target in such a position that they did not shield the spectrometer radiator, but might be expected to scatter about twice as much radiation into the monitors as the aluminum or graphite absorbers. An effect of 2.2 ± 1.1 percent in the wrong direction was found, which probably has no significance.

III. PROCEDURE

As described in a previous paper[7] the gamma-ray spectrometer records data simultaneously in seven different energy intervals, separated in energy by about 4 percent. In the absorption experiments, the magnetic field of the spectrometer was adjusted so that the center of the 17.6 Mev lithium gamma-ray peak fell midway between the central channel, No. 4, and an adjacent channel, No. 3. The counts in these two channels were then added (after correcting for a difference in statistical weight arising from the fact that channel 4 is fed by coincidences from four counter pairs, whereas channel 3 is fed by only 3 counter pairs). This procedure makes the final "spectrometer counting rate" insensitive to small variations in the magnetic field, since *e.g.* a drop in the counting rate of channel 4, caused by a slight increase in the magnetic field, is closely compensated by an increase in the counting rate of channel 3.

The transmission of each absorber for 17.6 Mev gamma-rays was measured by counting alternately with and without the absorber in position. For each transmission measurement from six to fifteen measurements were made with the absorber, and a like number without. The time required to obtain one percent statistical accuracy in the determination of the cross section for one absorber was usually from eight to fifteen hours, with a proton current of about 100 μa, and a fresh Li target. The proton energy used in these experiments was approximately 460-kev, just above the 440-kev Li resonance. The thick Li targets used were made by evaporation of lithium metal in a vacuum.

A small background of counts obtained with no radiator in the spectrometer was subtracted from the counting rates with and without absorber before calculating the transmission. This background was 0.1 percent of the counting rate without absorber, and about 2.3 percent of the counting rate for the thickest absorber used. The resulting correction to the transmis-

TABLE I. Experimental cross sections.

Absorber element	Thickness (cm)	Thickness (g/cm^2)	Transmission T	$1/N \log(1/T)$ (10^{-24} cm^2)	Resolution correction (10^{-24} cm^2)	Experimental absorption cross section (10^{-24} cm^2)
C	29.90	46.15	0.477	0.320	+.003	0.323±0.0045
Al	25.65	69.60	0.2231	0.965	+.007	0.972±0.011
Cu	6.367	56.76	0.1418	3.631	+.016	3.65 ±0.027
Cu	6.367	56.76	0.1456	3.582	+.016	3.60 ±0.029
Cu (Av)						3.62 ±0.020
Sn	4.976	36.27	0.1932	8.93	+.027	8.96 ±0.09
Pb	1.659	18.78	0.3271	20.46	+.04	20.50 ±0.26
Pb	2.746	31.10	0.1563	20.53	+.04	20.57 ±0.17
Pb	4.405	49.88	0.0509	20.54	+.04	20.58 ±0.21
Pb (Av)						20.56 ±0.12

TABLE II. Theoretical cross sections.

Element	Compton cross section (10^{-24} cm²)	Pair production (nucleus unscreened) (10^{-24} cm²)	Screening correction (percent)	Pair production (nucleus screened) (10^{-24} cm²)	Pair production (electrons) (10^{-24} cm²)	σ (theory) (10^{-24} cm²)
C	0.2004	0.1100	−1.4	0.1085	0.0124	0.3213
Al	0.434	0.516	−2.1	0.505	0.027	0.966
Cu	0.968	2.569	−3.1	2.489	0.060	3.517
Sn	1.67	7.64	−4.0	7.33	0.10	9.10
Pb	2.74	20.54	−5.0	19.51	0.17	22.58*

* The total cross section of lead includes a contribution of 0.16×10^{-24} cm² (0.7 percent) for the atomic photoelectric effect.

sion alters the cross section by only 0.8 percent. To obtain confidence that no errors might occur from some unknown and unmeasured background, three quite different thicknesses of lead were used as absorbers. All gave the same result for the absorption cross section, as may be seen in Table I.

Because gamma-rays in a finite energy interval near 17.6 Mev may be recorded by the spectrometer, Compton scattered gamma-rays which have lost only a small fraction of their energy will not appear to have been "absorbed." A "resolution correction" has been made in the absorption cross sections to take account of this effect. This resolution correction has been calculated on the assumption that the Compton scattering is correctly described by the differential Klein-Nishina formula.[1] It is simply the cross section for scattering of a 17.6 Mev gamma-ray in which the scattered quantum has an energy greater than or equal to 16.9 Mev. This correction is 1.6 percent of the total Compton cross section.

IV. EXPERIMENTAL RESULTS

The transmission, T (corrected for background), observed for each of the absorbers is shown in Table I. The column headed $(1/N)\log(1/T)$ then gives the uncorrected absorption cross sections, where N is the thickness of the absorber in atoms per cm². After adding the small resolution correction, one obtains the experimental absorption cross section, σ, in the last column of Table I. The errors listed are statistical standard errors obtained either from the total number of counts, or from the root mean square deviations of the individual runs from their average, whichever was larger. (The two measurements of Cu shown in Table I were made with the same Cu absorber, but slightly different geometrical arrangements. In the second measurement the Cu absorber was nearer to the cyclotron target than in the first.)

The purity of the absorbers was checked by obtaining standard, qualitative spectrographic analyses from the New England Spectrochemical Laboratories of Ipswich, Massachusetts. Any impurities reported in amounts which might be significant were then measured quantitatively in our laboratory by Dr. D. R. Miller. No impurities were found in sufficient amounts to warrant making a correction in the data. (The largest correction for impurities would have been only −0.3 percent, for the aluminum absorber.)

V. THEORETICAL CROSS SECTIONS

In Table II are given the theoretical values of the absorption cross sections for 17.6 Mev gamma-rays, assuming that this absorption takes place only by Compton scattering and by pair production in the field of the nucleus or of the atomic electrons. In addition, the cross section of lead includes a small contribution from the atomic photoelectric effect.

The Compton cross section is given directly by the Klein-Nishina formula.[1,8]

The cross section for pair production in the field of the nucleus has been calculated from the theory of Bethe and Heitler.[6] The unscreened pair cross sections have been obtained from the high energy integral formula given by Hough.[9] The effect of screening is not entirely negligible at 17.6 Mev, since it amounts to 5 percent for lead, for example. Therefore, screening corrections have been calculated from the low energy formula of Bethe and Heitler[6] involving the function $C(\gamma)$. These corrections, and the final screened pair cross sections are shown in Table II.

The cross section for pair production in the field of the atomic electrons is unfortunately not known very certainly at 17.6 Mev, although several calculations have been made for various energy regions.[10] The values given in Table II are obtained from the results of Borsellino, who gives for the ratio of the pair cross section of an electron to that of the proton the (interpolated) value of 0.68 at 17.6 Mev. (Perhaps a ratio nearer 1.0 should be used, according to the calculations of Wheeler and Lamb. However, this change would not make much difference in the total cross sections used.)

The last column of Table II, headed σ(theory), gives the sum of the three cross sections discussed above, except for the lead cross section, which includes a contribution of 0.7 percent for the atomic photoelectric effect.[1] The photoelectric effect is not significant for the other elements. Another process which might contribute

TABLE III. Comparison between theory and experiment.

Element	σ (theory) (10^{-24} cm²)	σ (experiment) (10^{-24} cm²)	Difference (%)
C	0.3213	0.323±1.4%	+0.5
Al	0.966	0.972±1.1%	+0.6
Cu	3.517	3.62 ±0.6%	+2.9
Sn	9.10	8.96 ±1.0%	−1.5
Pb	22.58	20.56 ±0.6%	−9.8

[8] O. Klein and Y. Nishina, Zeits. f. Physik **52**, 853 (1929).

[9] P. V. C. Hough, Phys. Rev. **73**, 266 (1948), Eq. (1). The total cross section has been adjusted in the manner described by Hough, by multiplying by the ratio of the exact to the high energy differential cross section at the "midpoint," $E_+=E_-=k/2$.

[10] J. A. Wheeler and W. E. Lamb, Phys. Rev. **55**, 858 (1939); K. M. Watson, Phys. Rev. **72**, 1060 (1947); A. Borsellino, Helv. Phys. Acta **20**, 136 (1947); P. Nemirovsky, J. Phys. U.S.S.R. **11**, 94, (1947) treats energies<3 Mev.; V. Votruba, Phys. Rev. **73**, 1468 (1948).

to the absorption is nuclear photo-disintegration. The possible contribution of this process to the observed absorption cross section for copper will be discussed in the next section.

VI. COMPARISON BETWEEN THEORY AND EXPERIMENT

A comparison is given in Table III between the theoretical absorption cross sections and those observed experimentally. For the light elements, carbon and aluminum, the experimental and theoretical values agree within the statistical errors of 1.4 and 1.1 percent, respectively. This close agreement is secured only by taking into account the production of pairs in the field of the atomic electrons, since this process contributes 3.9 percent of the total cross section for carbon, and 2.8 percent for aluminum.

The experimental cross section for lead, the heaviest element measured, is 9.8 percent below the theoretical value, which far exceeds the statistical error of 0.6 percent. As mentioned above, this discrepancy is believed to result from the use of the Born approximation in the Bethe-Heitler calculation of pair production.[6] (See also references 4 and 5.) Since the condition for validity of the Born approximation is $Ze^2/\hbar v \ll 1$, where v is the velocity of the electron (or positron), it is not surprising to find a ten percent discrepancy for a heavy element. (For high energy electrons, this condition reduces to $Z/137 \ll 1$, which is certainly not very well satisfied for lead.)

The copper absorption cross section for 17.6 Mev gamma-rays is found to exceed the theoretical value by 2.9 percent, which is 5 times the standard statistical error. Although this discrepancy is too small to be very significant, it is not unreasonable to ascribe a part of it to nuclear photo-disintegration, which has a rather large cross section for copper, and which has not been included in the theoretical absorption cross section. If the error in the calculated pair cross section, arising from the use of the Born approximation, is proportional to Z^2,[5] then the absorption in copper by Compton scattering and pair production might be expected to be about 1 percent below the theoretical value of Table II. This means that the observed cross section is roughly 4 percent, or 0.14×10^{-24} cm^2, higher than might be "expected" without considering the nuclear photo-effect. Unfortunately, the cross section for this process has not been measured very accurately. Bothe and Gentner[11] give a value of $\sim0.05\times10^{-24}$ cm^2 for the $Cu^{63}(\gamma, n)Cu^{62}$ cross section at 17.6 Mev. However, recent measurements by Wäffler and Hirzel[12] give a value for the same energy of 0.16×10^{-24} cm^2. Other values which have been reported from betatron measurements are $\sim0.13\times10^{-24}$ cm^2,[13] and $\sim0.06\times10^{-24}$ cm^2.[14] The cross section for the $Cu^{65}(\gamma, n)Cu^{64}$ reaction involving the other copper isotope (abundance 30 percent) is even larger,[12] being about 1.5 times that for Cu^{63}. It thus appears that the photo cross section for copper may be large enough to account for the high absorption observed in the present experiment. (Compare also reference 4.)

It is also of interest to consider the possible contribution of the photo process to the absorption cross sections of the other elements investigated. This contribution is probably unimportant for the light elements, C and Al, since the photo cross section is very small at this energy in light elements.[12] (In fact, the threshold for the (γ, n) reaction in C is above 17.6 Mev.) It might contribute something like 0.3 percent for Al. In Sn and Pb, the photo cross sections may be comparable or even larger than that for Cu, but their effect is masked by the Born approximation error in the pair cross section.

The results of these experiments, in their relation to the theory, are very similar to those of Adams[4] at 11.04, 13.73, and 19.10 Mev, and of Lawson[5] at 88 Mev. One difference is that a 7 or 8 percent discrepancy with theory was found for Be by Lawson, whereas no discrepancy was observed in the present experiments for the light element, C.

An interesting conclusion regarding the "Born approximation discrepancy" for lead as a function of energy may be drawn from a comparison of the three experiments. This discrepancy, in percent, seems to be essentially constant between 11 and 88 Mev. If the entire discrepancy between the experimental and theoretical absorption cross sections is considered to represent an error in the theoretical pair cross section alone, then this error is approximately 12 percent at all the five energies which have been investigated between 11 and 88 Mev.*

Since exact calculations of Hulme and Jaeger[15] at 1.5 and 2.6 Mev give pair cross sections for lead *higher* than the Born approximation values, it would be interesting to measure this pair cross section at energies between 2 and 11 Mev.

VII. ACKNOWLEDGMENTS

I am indebted to Professor B. D. McDaniel for many discussions and continued interest in these measurements. This work was supported in part by the ONR.

[11] W. Bothe and W. Gentner, Zeits. f. Physik **106**, 236 (1937).

[12] H. Wäffler and O. Hirzel, Helv. Phys. Acta **21**, 200 (1948). The value $\sigma=0.12\times10^{-24}$ cm^2 published by Wäffler and Hirzel has been increased by them to 0.16×10^{-24} cm^2 by taking into account the fact that not all the lithium gamma-rays have an energy 17.6 Mev. The 14.8 Mev component is relatively less effective for the (γ, n) process.

[13] Skaggs, Laughlin, Hanson, and Orlin, Phys. Rev. **73**, 420 (1948).

[14] McElhinney, Hanson, Becker, Duffield, and Diven, Phys. Rev. **75**, 542 (1949).

* The energy dependence discussed by Adams for his data arises mainly from inaccuracies of a few percent in the theoretical cross sections used by him. These errors arise from a neglect of screening and from the use of the "usual" high energy integral formula for pair production. (See reference 1, p. 200, Eq. (15).) If Adam's data is compared to more accurate theoretical cross sections, the discrepancy for lead is found to be practically independent of the energy, as discussed above.

[15] H. R. Hulme and J. C. Jaeger, Proc. Roy. Soc. **153**, 443 (1936).

Capture Gamma-Ray Studies

H. E. KUBITSCHEK AND S. M. DANCOFF
Physics Department, University of Illinois, Urbana, Illinois and Argonne National Laboratory, Chicago, Illinois
(Received April 12, 1949)

Measurements are made of the maximum energies of gamma-rays emitted on neutron capture by a number of elements. Values so obtained are in rough agreement with semi-empirical formulas for neutron binding energies. Evidence is presented to show that gamma-rays carrying nearly the maximum energy are observed much more frequently than would be expected on statistical theories. The yield of gamma-rays on neutron capture is studied and found to show a variation, on the elements examined, of ±30 percent about a mean.

INTRODUCTION

THE earliest measurements of gamma-rays emitted upon neutron capture[1,2] were severely limited by the low intensities of natural sources, permitting only a rough estimation of the capture gamma-energies. With the higher fluxes obtainable from the D−D reaction, Kikuchi, Husimi, and Aoki[3] were able to determine capture gamma-energies from an end-point measurement. They were also able to make some estimates of the relative cross sections for gamma-excitation.

The greater fluxes available with the Argonne heavy water pile again made the study of capture gamma-rays expedient.[4] Higher intensities permit study of weak absorbers, and collimated neutron beams provide better geometry than was previously available.

The number of capture gammas emitted is a measure of the total radiation cross section $\sigma(n,\gamma)$, abbreviated in the following as σ_γ. Our experiments measured their intensity by observing the number of Compton electrons which they produced in an aluminum radiator, and the maximum energies of the gamma-rays were measured by the absorption method. Also, the geometry was good enough to permit discernment of the general features of the spectrum of capture gammas emitted.

Figure 1 shows the geometry used for detecting gamma-rays. The unmoderated neutron beam was incident on the target at 15° to the surface to give a large effective target thickness with a minimum multiple scattering. Capture gamma-rays produced at the target passed through a thick boron absorber before striking the aluminum radiator. Neutrons which were scattered off the target were prevented from entering the cylindrical shield directly by this 1-in. absorber, which had the constitution:

B^{10}: 2.16 g/cm²; B^{11}: 0.15 g/cm²; S: 0.96 g/cm².

The aluminum walls of the Geiger counters were 4.6 mils thick. These counters were used both singly and in coincidence; they resolved accidental coincidences separated by more than a microsecond. Irradiations were monitored by a fission counter mounted fully above the beam at the wall of the pile.

QUANTUM ENERGY MEASUREMENTS

Except for the light elements, the energy liberated on neutron capture is 6–10 Mev. This energy may be emitted in a single photon, or there may be a cascade involving several quanta of lower energy. The distribution of quanta among the various possible schemes of decay has been studied only very little. Some theoretical arguments, based on considerations of statistics, would indicate that the maximum energy is rarely, if ever, concentrated in a single quantum. If that were so, a measurement of the maximum energy in the spectrum would yield an energy considerably less than 6–10 Mev.

Previous measurements have been indecisive on this point because of the low intensities of, and the high backgrounds associated with, the sources. The energies which Kikuchi, Husimi, and Aoki found by the end-point method lay between 4 and 7 Mev. Although these values are undoubtedly low, they are, in general, greater than the corresponding values obtained through half-thickness measurements by Rasetti and by Fleischmann.

The technique of the present measurement corresponds closely to the measurements mentioned above for measuring gamma-ray energies by the method of the range of the recoils; successively thicker absorbers are interposed between the two G-M counters, and the thickness of absorber which would eliminate the coincidences altogether gives the energy of the hardest Compton electron.

All absorption curves show a steep decrease, breaking over abruptly into a tail of lesser slope. Our interpretation of the latter effect is that fictitious coincidences not associated with energetic gamma-rays or electrons may be generated in at least two ways: (a) A single gamma-ray may produce Compton electrons in both counters. (b) Brehmsstrahlung from a weak electron in the first counter may fire the second. In either case, the hard component is composed of soft gamma-rays and not hard electrons. The observed absorption coefficients for this component are consistent with gamma-rays of

[1] F. Rasetti, Zeits. f. Physik, **97**, 64 (1935).
[2] R. Fleischmann, Zeits. f. Physik, **103**, 113 (1936).
[3] Kikuchi, Husimi, and Aoki, Proc. Phys. Math. Soc. Japan **18**, 188 (1936).
[4] Such studies of gamma-rays from iron and cadmium were made by H. Lichtenberger using a beam from the original graphite pile, but because of the low intensities the results were only preliminary.

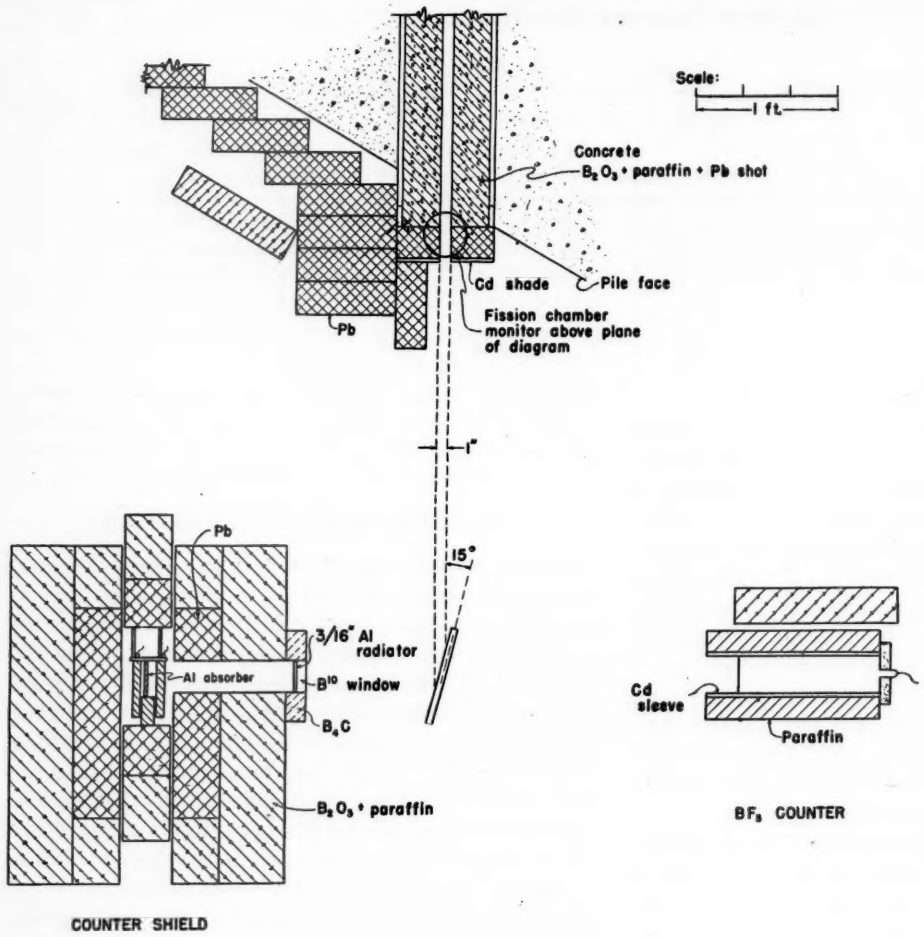

FIG. 1. Geometry for detecting capture γ-rays.

several hundred kev energy, although there is a rather large variation in this absorption coefficient among the various cases. Since in all cases the second component appears to be exponentially absorbed, the procedure has been to extrapolate it exponentially toward zero thickness, then subtract it from the total counting rate. The resultant curve is associated with the desired secondary radiation.

When the end point has been determined, there is added to it the thickness of two counter walls and the air between them (0.07 g/cm²). From the range so determined, the gamma-ray energy is obtained using the formula $R=0.46E$, where R is the range in Al in g/cm², and E is the gamma-ray energy in Mev. This formula fits, within experimental error, the data of Curran, Dee, and Petrzilka,[5] obtained over the range 2–17 Mev by a method similar to the one employed in this experiment.

For each absorber thickness, a subtraction of background must be made. Backgrounds are taken by interposing in the beam an enriched boron plug (approximately 2 g/cm² B^{10}) which stops the neutron beam but passes practically all the pile gamma-rays whose effect on the system is part of the background. Also, there is a

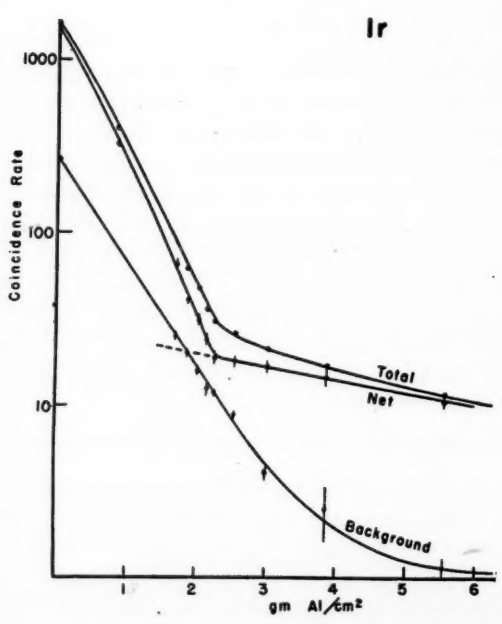

FIG. 2. Detailed absorption curve for the case of iridium. The upper curve indicates total counting rates with the iridium target in place, the lowest curve the measured background rate. The abscissa does not include counter wall thicknesses.

[5] Curran, Dee, and Petrzilka, Proc. Roy. Soc. **169**, 287 (1938).

TABLE I. Maximum energies of capture gamma-rays.

Target	Corrected range (g/cm² Al)	Gamma-ray energy (Mev)	Neutron binding energy	Probable capturing nucleus
S	3.50±0.2	7.6 ±0.4	9.1±0.9	(S^{32})
Cl	4.49±0.2	9.8 ±0.4	8.2±0.95	(Cl^{35})
K	3.32±0.2	7.2 ±0.4	7.1±0.9	(K^{39})
Mn	4.10±0.2	8.9 ±0.4	(7.0)	(Mn^{55})
Fe	3.60±0.3	7.8 ±0.7	8.3±1.6	(Fe^{56})
Co	3.52±0.1	7.7 ±0.2	(7.4)	(Co^{59})
Cu	3.52±0.2	7.7 ±0.4	(7.8)	(Cu^{63})
Ag	3.00±0.35	6.5 ±0.7	(6.9)	(Ag^{109})
Cd	3.22±0.1	7.0 ±0.2	(8.5)	(Cd^{113})
I	3.20±0.2	7.0 ±0.4	(6.2)	(I^{127})
Sm	3.03±0.15	6.6 ±0.3	(7.8)	(Sm^{149})
Gd	2.90±0.2	6.3 ±0.4	(8.6)	(Gd^{157})
W	3.27±0.2	7.1 ±0.3	(6.9)	(W^{186})
Ir	2.37±0.1	5.15±0.2	(6.1)	(Ir^{191})
Au	3.37±0.2	7.3 ±0.4	(6.9)	(Au^{197})
Hg	3.28±0.2	7.1 ±0.4	(6.6)	(Hg^{199})

negligible contribution due to the capture of neutrons in the Al target holder. Figure 2 shows a typical absorption curve, for the case of iridium, with subtraction of background detailed.

Table I summarizes the results as regards maximum gamma-ray energy. The second column gives the secondary electron end point plus 0.07 g/cm². The third column gives the gamma-ray energy derived from this. Estimated probable errors are given. These errors arise chiefly in the subtraction of the exponential tail.

The last column gives independent estimates of the neutron binding energies in the isotope assumed to do the capturing. For four elements (S, Cl, K, Fe) the relevant masses are sufficiently well known to permit the assignment of probable errors. In the remaining cases, the use of a semi-empirical mass formula must be resorted to. Such values, enclosed in brackets, were calculated from[6]

$$M(A,Z)+n-M(A+1,Z)$$
$$=0.01504+0.014[A^{\frac{2}{3}}-(A+1)^{\frac{2}{3}}]$$
$$+0.083\left[\frac{(A/2-Z)^2}{A}-\frac{((A+1)/2-Z)^2}{A+1}\right]$$
$$+0.000627Z^2[A^{-\frac{1}{3}}-(A+1)^{-\frac{1}{3}}]+\delta,$$

where

$$\delta=\mp 0.036A^{-\frac{3}{4}}; \qquad A \text{ even} \begin{cases} Z \text{ even} \\ Z \text{ odd} \end{cases}$$
$$=\pm 0.036(A+1)^{-\frac{3}{4}}; \quad A \text{ odd} \begin{cases} Z \text{ even} \\ Z \text{ odd} \end{cases}$$

and A is the mass number, Z the atomic number.

The maximum gamma-ray energies found in this experiment do not, on the whole, seem to be lower than the estimated neutron binding energies. In fact, considering the uncertainty attached to the two quantities being compared, one is tempted to say that they are identical. If this point of view is substantiated it will make possible the determination of mass differences in many cases where no other technique is available.

A comparison has also been made with the semi-empirical theory of Feenberg.[7] In this formulation, the neutron binding energy is written as $(Q_1+Q_2+Q_3)$. Q_1 is the binding energy that would exist for the nucleus of most stable Z for a given A, (Z_A^*), when even-odd differences are neglected. A plot of Q_1, taken from Feenberg's paper, appears in Fig. 3. Q_2 takes account of the displacement of Z from its optimum value:

$$Q_2=(80/A)(Z-Z^*_{A+\frac{1}{2}}) \text{ m}\mu.$$

Q_3 is a quantity similar to δ, in the Bohr-Wheeler formulation, but slightly different in numerical values.

From the measured gamma-ray energies, E_γ, and from the calculated values of Q_2 and Q_3, we obtain the quantity $(E_\gamma-Q_2-Q_3)$ which should be equal to Q_1 if E_γ is the same as the binding energy, and if the Feenberg theory is correct. The values obtained in this way are shown as the circled points in Fig. 3.

For comparison, we also plot values of $(E_\gamma-Q_2-Q_3)$ obtained in an analogous way from measurements of photo-neutron thresholds with the 22-Mev betatron.[8] All of the previous considerations apply if by A we now mean the atomic weight of the product nucleus. Such points are indicated by triangles.

Considering the experimental errors, the over-all agreement is not unreasonable, but there are several cases where the discrepancies are fairly marked, notably Fe^{53} and Mo^{93} on the high side, as well as Cd^{113}, Sm^{149}, Gd^{157}, and Ir^{191} on the low side. It is probably the case that considerations based on shell structure will be necessary to give a detailed account of neutron binding energies throughout the table.

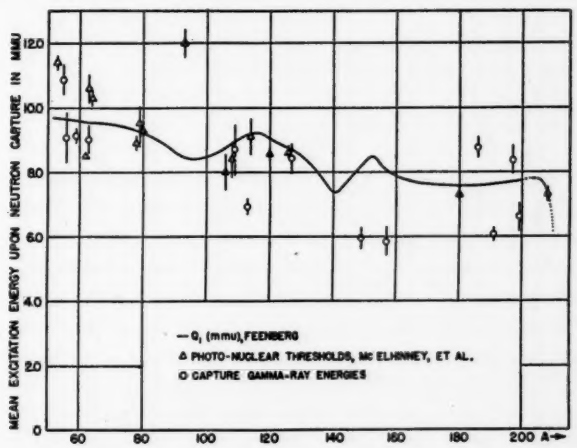

FIG. 3.

[6] N. Bohr and J. A. Wheeler, Phys. Rev. **56**, 426 (1939); G. B. von Albada, Astrophys. J. **105**, 393 (1947).

[7] E. Feenberg, Rev. Mod. Phys. **19**, 239 (1947).

[8] McElhinney, Hanson, Becker, Duffield, and Diven, Phys. Rev. **75**, 542 (1949).

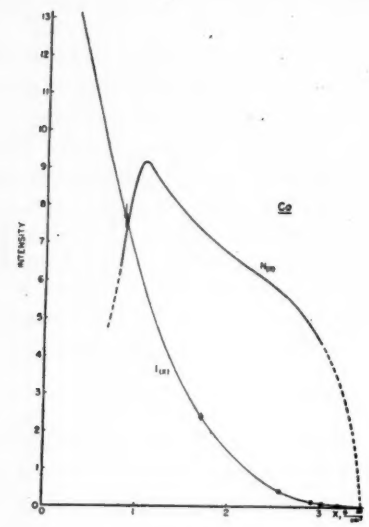

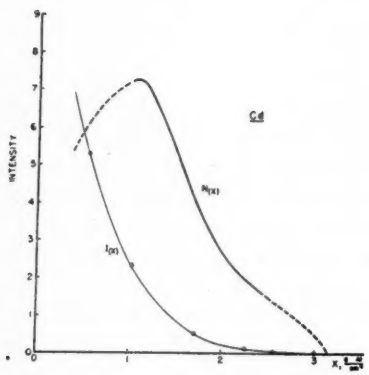

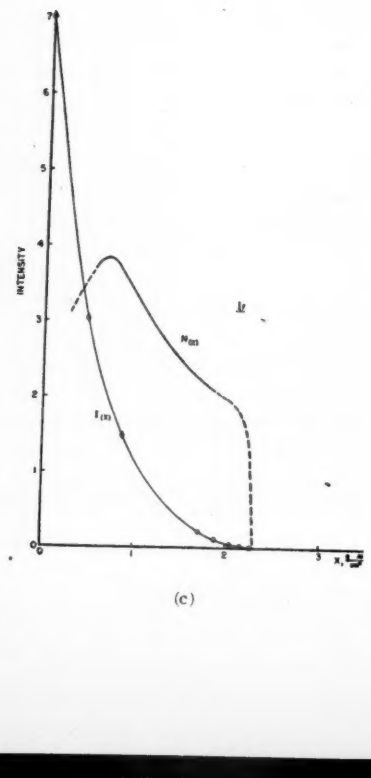

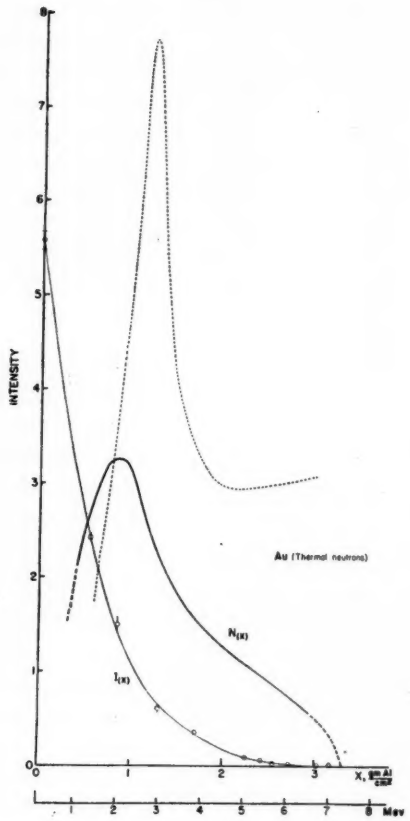

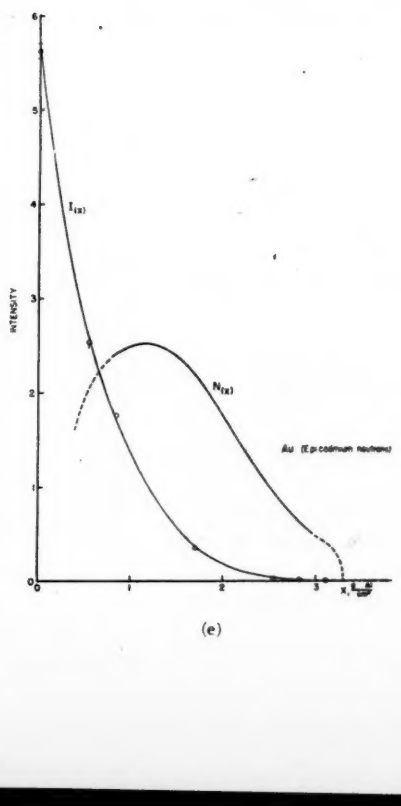

FIG. 4. Absorption curves $I(x)$ and spectral distributions $N(x)$ of capture gamma-rays assuming a sharp range. The dotted curve in Fig. 4(d) represents the spectral distribution on the assumption of linear absorption of secondary electrons.

SPECTRUM OF CAPTURE GAMMAS

The absorption method will, in principle, give some information as to the spectrum of gamma-rays emitted on neutron capture. The following analysis is based on idealized conditions only partially realized in our set-up.

For "high" geometry, the Compton recoils reaching the absorber and counters from the radiator will have been ejected in the forward direction. Let k be the gamma-ray momentum, measured in units mc, where m is the electronic mass. The corresponding range in g/cm² is $R(k)$. If $N(k)dk$ is the number of gamma-ray lines per capture within dk, then the number of electrons incident on the front face of the absorber is

$$I(0)=\int_0^\infty dkCN(k)\phi(k)R(k),$$

where $\phi(k)$ is the differential cross section for Compton scattering in the forward direction and C is a constant of the apparatus. As absorber is added the contribution of any particular k to the integral decreases linearly until absorber of amount $R(k)$ is reached. Hence, at absorber thickness x g/cm²,

$$I(x)=\int_{k_{\min}}^\infty dkCN(k)\phi(k)R(k)[1-x/R(k)]. \quad (1)$$

The lower limit is determined by $R(k_{\min})=x$.

Since $k_{\min}$ is a function of x,

$$d^2I/dx^2=CN(k_m)\phi(k_m)(dk_m/dx)$$

or, suppressing the subscript,

$$N(k)=[(d^2I/dx^2)]/[C\phi(k)(dk/dx)],$$

where $R(k)=x$. Experimentally we know that (dk/dx) is essentially constant in the range under consideration (1−8 Mev). $\phi(k)$ is obtained from the Klein-Nishina formula and is proportional to

$$\frac{1}{k+\frac{1}{2}}\left[1+\frac{1}{4(k+\frac{1}{2})^2}\right].$$

Using the formula previously quoted for the relation between energy and range, this becomes

$$N(k)=C'(x+0.118)[1+0.25(x+0.118)^{-2}]^{-1}d^2I/dx^2. \quad (2)$$

Formula (2) will be limited in its application because of the fact that electrons, particularly of low energy, do not have a sharp range. The effect of this will be to introduce a finite resolution to the spectral analysis. The resolution width will be that interval of k corresponding to the range straggling.

Other limitations are due to the non-exclusion of some recoils which must have originated elsewhere than in the radiator, and the contribution from pair electrons. These effects can be shown to be unimportant, to the accuracy of our analysis. The contributions from photo-electrons in this experiment were entirely negligible since the counter walls and air between them stopped all electrons below 0.15 Mev.

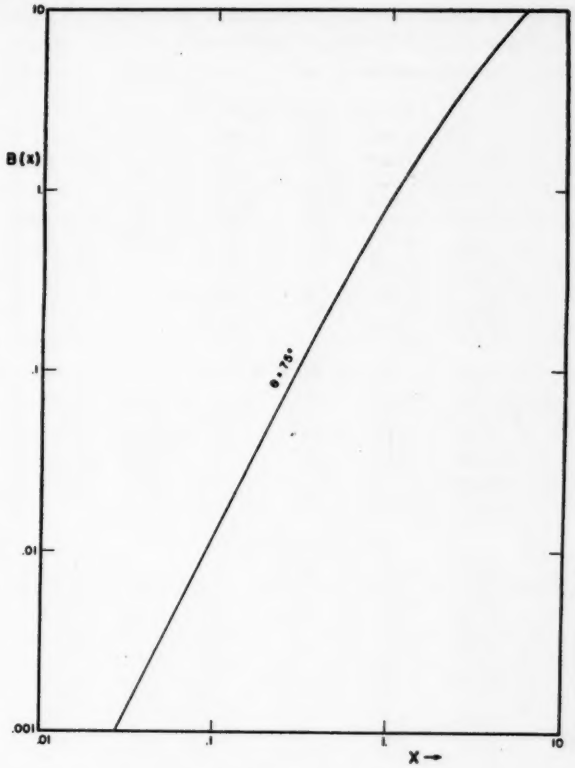

FIG. 5. $B(x)$ for $\theta=75°$.

Finally, the data must be very accurate and complete in order that the curve may be subjected to two differentiations with assurance. Only in a few cases did we consider the application of this method justified, and there only for distinguishing outstanding features of the spectral distribution. These absorption curves for the elements Cd, Ir, Au, and Co with their calculated distributions are shown in Fig. 4.

Within the above limitations we note that these elements have maxima between 1.5 Mev and 2.5 Mev. The positions of these maxima agree with those predicted by Bethe for the radiation emitted in the capture process itself.[9] Bethe's theory is based on the statistical theory of energy level density and on the assumption that the dipole moments for all possible transitions are of the same order. Because of the rapid increase of level density with energy on this model, transitions from the capture level all the way to the ground level (or nearly all the way) are highly improbable as compared to transitions of about a third that energy. This implies that the distribution curves $N(x)$ in Fig. 4 should show a high order of contact at the upper energy limit. However, the experimental distributions, in fact, show many quanta near the maximum energy. Thus, the

[9] H. A. Bethe, Rev. Mod. Phys. 9, 233 (1937).

TABLE II. Summary of experimental results.

Target	g/cm²	$\langle A\phi\rangle_{Av}$	σ_τ	σ_t	G_s/G_θ	Y	Δ%
			I. Very strong absorbers				
Rh	0.1115	0.243	110	115		1.13	4
Ag	0.0424	0.945	45	50		1.05	4
Cd	0.0222	0.055	2260	2266	All	1.41	3
Cd	0.01537	0.055	2260	2266	less	1.39	3
In	0.0229	0.89	140	145	than	0.96	4
Ir	1.092	0.062	300	300	0.001	0.89	4
Au	0.2632	0.246	72	78		0.993	3
Au	0.2632	0.246	72	78		0.992	3
Au	0.0566	0.89	72	78		1.010	3
Hg	0.2411	0.246	370	370		1.08	3
			II. Strong absorbers				
$C_{1/3}Cl$	0.591	0.055	25	30	0.020	1.46	8
Mn	0.532	0.246	9.4	11.9	0.011	1.23	4
Co	0.470	0.194	25	30	0.009	1.32	4
Ta	0.398	0.166	19	24	0.029	0.73	5
W	0.236	0.945	10	17.5	0.029	1.16	4
Pt	0.494	0.246	8.1	16.1	0.001	1.19	5
			III. Weak absorbers				
Mg	0.574	1.0	0.30	3.2	0.53	0.47	12
Al	0.850	1.06	0.17	1.6	0.19	1.05	11
S	0.726	0.246	0.4	1.9	0.09	1.52	7
Fe	0.474	1.06	1.9	12.9	0.15	1.53	7
Fe	0.989	0.246	1.9	12.9	0.18	1.53	7
Ni	0.709	0.246	3.3	18.8	0.12	1.86	6
Cu	1.50	0.246	3.0	10.8	0.08	1.34	5
Cb	0.0974	0.591	1.3	6.3	0.17	1.18	17
Sn	0.233	1.06	0.49	5.49	0.23	1.26	7
			IV. Very weak absorbers				
Pb	3.65	1.06	0.13	11.1	0.73	1.46	16

assumptions mentioned above are thrown seriously in doubt.

We could carry out an alternative analysis assuming that monokinetic electrons, instead of showing a sharp range, decrease linearly in penetrating the absorber. This assumption is known to describe fairly well the absorption of electrons of energy about 1 Mev. In the energy range being studied, the absorption would be intermediate in character between these two cases.

With the assumption of linear absorption, it is necessary to carry out three differentiations to obtain a spectral distribution. In general, the result is to emphasize the high energy end, moving the maximum slightly toward higher energies and strongly intensifying the number of quanta near the high energy limit (by about a factor of two compared to the number in the peak). The dotted curve in Fig. 4(d) gives this alternative distribution as derived from the data for Au.

While it is clear that quantitative conclusions regarding the spectral distribution can hardly be obtained, it is also clear that the number of high energy quanta present is far greater than the statistical theory of nuclear energy levels would predict.

Absorption curves for gold were made using thermal and epi-cadmium neutrons, respectively, and are shown in Figs. 4(d) and 4(e). Within experimental error the curves have the same shape and the same end point. The evidence is, therefore, that the decay of radioactive gold nuclei formed in the 5-ev resonance level involves the same radiative processes as for those gold nuclei formed by capture of thermal neutrons.

GAMMA-RAY YIELD MEASUREMENTS

Gamma-ray yield measurements were made in a survey of targets of a number of materials. A beam of neutrons of energy below the cadmium cut-off (hereafter called *thermal* for convenience) was permitted to fall on each target and the corresponding counting rates were observed in the Geiger counters inside the shield. These rates were compared with the rates of neutron capture calculated for the various targets from tabulated neutron cross sections. The ratio thus obtained is, as will be shown, approximately proportional to the total number of gamma-rays emitted on neutron capture. The constancy of this ratio would indicate a similarity in the spectra of capture gamma-rays for the various targets. However, some deviation from constancy is to be expected because of the variation of neutron binding energy among the substances studied.

For each target the following measurements were taken both with Geiger-Müller counters and with a boron trifluoride counter located directly adverse to the G-M counters and in a standard position about three feet from the target.

N_1: counting rate with the sample in open beam; sample mounted on and behind a thin aluminum holder,
N_2: holder alone in open beam,
N_3: sample in beam blocked off with Cd filter,
N_4: holder in Cd-filtered beam.

For thermal neutrons the significant rate for the G-M counters is

$$G_\theta=(N_1-N_2)-(N_3-N_4) \tag{3}$$

and may be compared with a calculated number

$$K=K_i+K_d+K_s. \tag{4}$$

K_i is the number of neutrons captured from the beam on first traversal of the target. K_d is the number of additional captures in the sample for neutrons scattered on first traversal, and is of significance only when the substance is such a weak absorber that a considerable thickness is necessary for counting. K_s is a contribution arising from neutrons scattered by the target which are subsequently captured in or near the shield producing detectable gamma-radiation. This contributes a fictitious absorption cross section and is dominant for a weak absorber such as graphite.

If a beam with flux ϕ falls on a target at an angle θ with the normal, then the rate of initial radiative capture is

$$K_i=A\phi\cos\theta(\sigma_\tau/\sigma_t)(1-\exp(-Nl\sigma_t\sec\theta)), \tag{5}$$

where N is the number of atoms/cm³, l is the thickness in cm, σ_τ is the radiative capture cross section, σ_t the total cross section, and A the area of the sample.

Furthermore, the secondary term K_d becomes for samples thin compared with a diffusion length (a valid approximation for all our samples),

$$K_d = A\phi \cos\theta[\kappa^2/(\nu^2-\kappa^2)]B(\nu), \quad (6)$$

where

$$\nu = N\sigma_t \sec\theta; \quad \kappa = N(3\sigma_r\sigma_t)^{\frac{1}{2}}(1-0.42\sigma_r/\sigma_t),$$
$$B(x) = (1-e^{-x})(0.71\times\sec.\theta-1)+x/2(1+e^{-x}).$$

A plot of $B(x)$ for $\theta = 75°$ is shown in Fig. 5.

Finally, the number of scattered neutrons leaving the target is $K_s = K_i(\sigma_s/\sigma_r)$ to very good approximation.

We define a yield Y as

$$Y = (G_\theta - G_s)/A\phi(K_i+K_d). \quad (7)$$

G_θ is the net Geiger counting rate, given by (3). G_s is that part of the Geiger counting rate due to neutrons scattered out of the beam by the target; shielding made this term small but not negligible. The numerator of (7) is therefore the counting rate due solely to captures in the target. The denominator is the predicted rate of captures, calculated from tabular cross sections.

The magnitude of the correction G_s was determined in two independent ways,

(A) We may write $G_s = mK_s$, with K_s calculated as above from tabular cross sections. m is a constant of the apparatus which may be determined empirically by using as a target an element whose capture cross section is so small that the observed count in our set-up is due to scattering entirely. Carbon is such an element. Carbon targets of various sizes were used to determine corresponding values of m above for each size and for each counter.

(B) We may also write $G_s = nB_\theta$, where B_θ is the net rate of counting of the BF_3 counter obtained, as in (3), by a difference of four measurements. B_θ is proportional to the actual number of scattered neutrons, hence to G_s, and n is another constant of the apparatus. Bismuth was used as the standard for this measurement. The values of n were found to be 0.200, 0.123, and 0.0394, for the fore singles counter, the rear singles counter, and the coincidences, respectively, for the standard foil. It follows that the effect of scattered neutrons was more important for the near counter than for the far one.

Any serious deviation between the values of G_s as determined by (A) and (B) would imply error either in the BF_3 counting or in the tabular cross sections. In fact, the agreement was reasonably good for almost all the cases. Our final tabulation of yield uses an average G_s, obtained as the average of (A) and (B). Deviation between the two values is taken account of in the probable error. Only in the case of aluminum is this the dominant contributing factor to the probable error.

The measurement of $\langle A\phi\rangle_{Av}$, the integrated neutron flux striking the target, was made by cutting Cd and brass dummies of the same areas as the various targets (which varied in size from a circle 1 in. in diameter for Cd to a rectangle $5\frac{1}{2}$ in.$\times$11 in. for Pb) and inserting these into the neutron beam. The highly emissive Cd dummy targets could be counted only with the pile operating at reduced intensity. These values of $\langle A\phi\rangle_{Av}$ were then referred to a standard value of unity for 4-in.$\times$9-in. targets, and are recorded in Table II in the appropriate column.

EXPERIMENTAL RESULTS

Table II summarizes the experimental results. The elements are divided into four groups according to the ascending importance of the scattering contribution G_s. However, this contribution is predominant in the last group only. The term K_d is negligible compared to K_i over most of the table, reaching a value about 10 percent of K_i only in the last group. The columns indicate the following:

Target: the element or compound used, normalized to one atom of the capturing element.

$\langle A\phi\rangle_{Av}$: the relative neutron flux intercepted by the target.

σ_r: the radiative capture cross section in barns, essentially taken from Table 9.5 of *The Science and Engineering of Nuclear Power*, Coryell, *et al.* (Addison-Wesley, 1947), and corrected to an assumed Maxwellian distribution at 400°K.

σ_t: tabular cross section in barns from the above table.

(G_s/G_θ): the fractional Geiger counting rate due to neutrons scattered out of target (average of two independent methods of determination).

Y: relative gamma-ray yield. This is the yield defined by (7), but referred for convenience to gold as having the value unity. Included here are the data from the fore singles counter, the rear singles counter, and the coincidence circuit; the yield as measured by each is divided by the corresponding one for gold and the three resulting numbers averaged with the coincidence data given half-weight.

Δ: the probable error in the relative gamma-ray yield.

DISCUSSION

With a few exceptions, the yields occupy the range of 0.9 to 1.6. That is to say, the variation about the mean is ± 30 percent; the chosen standard, gold, seems to have a yield considerably below the mean.

No marked correlations of yield with other parameters seem evident. Extreme cases are magnesium with a yield of 0.47 and nickel with 1.86.

Referring to the previous analysis and reasoning leading to Eq. (1), we see that the yield measured by this experiment is, to a fair approximation, proportional to the total number of gamma-rays emitted on neutron capture. In the expression for $I(0)$, the product $R(k)\phi(k)$ is about constant, and the quantity being measured becomes proportional to $\int dk N(k)$. This conclusion is independent of any special assumption as to the fashion in which the secondary electrons are absorbed.

PHYSICAL REVIEW VOLUME 76, NUMBER 4 AUGUST 15, 1949

Penetration and Diffusion of Hard X-Rays through Thick Barriers. I. The Approach to Spectral Equilibrium*

H. A. BETHE
Cornell University, Ithaca, New York

AND

U. FANO AND P. R. KARR
National Bureau of Standards, Washington, D. C.

(Received April 25, 1949)

When some of the secondary components of a complex radiation are barely softer than the primary, the process of formation and decay of these components alone governs the approach to equilibrium. It is then possible to determine the asymptotic trend of the total radiation intensity at great depths of penetration. Under broad assumptions, this trend is $x^{K_0}\exp(-\mu_0 x)$.

THE penetration of hard x- or γ-rays through thick barriers involves progressive simultaneous processes of energy degradation, multiple scattering and outright absorption. An adequate theoretical study of this phenomenon appears to require the application of a series of different approximation procedures, each of them appropriate to the treatment of one among the various effects which determine the course of the phenomenon. This note deals specifically with the effect of secondary components slightly less penetrating than the primary x-rays.

The generation of a softer secondary radiation component from a harder primary one usually leads, as is well known, to the establishment of "equilibrium" between the secondary and the primary. Equilibrium involves, in general, two different features, namely:

(a) The ratio of the *intensity* of the secondary to the intensity of the primary radiation, as a function of the depth of penetration, approaches asymptotically a maximum value.

(b) The *quality* of the secondary radiation also becomes independent of the depth of penetration.

These circumstances simplify the study of further penetration. The depth of penetration in a homogenous material required to approach equilibrium to a desired extent—e.g., such that the secondary-to-primary ratio attains 90 percent of maximum—is inversely proportional to the difference of the absorption coefficients of the primary and secondary radiation.

The penetration of hard x-rays presents a special problem with regard to the trend toward equilibrium. Some of the secondary x-rays arising from Compton scattering are only *infinitesimally softer* than the primaries, and they are deflected by an infinitesimal angle only. This circumstance does not merely slow down the approach to equilibrium; it actually suppresses the feature (a) in that the intensity ratio of the secondary to a monochromatic primary may grow beyond any limit.

Still, some sort of equilibrium should be attained among those secondary components which are substantially softer than the primary radiation. In fact, the spectral distribution of these components does become independent of the depth of penetration, as required by (b) above. The problem is therefore reduced to the treatment of the secondary x-rays whose frequency is not much lower than that of the primary. Once this problem is solved the rest should no longer offer the same difficulty.

This limitation of the frequency range affords an opportunity to treat the problem approximately by *expansion into powers* of the frequency change. Furthermore, the *deflections* of the secondaries may also be regarded as very *small*.

Note added in proof: The effect of angular deflections is not as small as one might surmise, even when the energy of the primaries is large. Further investigation, to be reported, indicates that the structure of the theory presented here is correct but that the effective value of the constant K_0 should be reduced by a substantial amount, owing to deflection effects.

CALCULATION

Within the limits of this approximation, that is disregarding deflection effects, the simultaneous penetration and energy degradation of a beam of x-rays in a material reduces to a one-dimensional problem. The number $N(\nu, x)d\nu$ of photons per unit volume traveling in the x direction, with a frequency between ν and $\nu+d\nu$ is governed by the equation

$$\partial N/\partial x = -\mu N + \int_{\nu}^{\nu_0} k(\nu', \nu)N(\nu')d\nu'. \qquad (1)$$

Here $\mu(\nu)$ is the total ("narrow beam") absorption coefficient for x-rays of frequency ν in the material under consideration, ν_0 is the highest x-ray frequency in the beam and $k(\nu', \nu)d\nu$ is the probability for a photon of frequency ν' to be Compton scattered per unit length in such a way that its frequency after scattering falls

* One of us (HAB) contributed to this paper while working as a Consultant to the Knolls Atomic Power Laboratory, Schenectady, New York. The work at the National Bureau of Standards is done under a contract with the Mathematics Branch of the ONR.

between ν and $\nu+d\nu$. The absorption coefficient μ of each photon may serve conveniently to characterize its frequency provided it is a monotonic function of the frequency (which is true only if one excludes the high frequencies where pair production is predominant). The frequency distribution in the beam may be described by the "integral spectrum" $I(\nu, x)=\int_{\nu}^{\nu_0} N(\nu', x)d\nu'$ rather than by N itself. Following these changes of variable, Eq. (1) takes the form:

$$\partial^2 I/\partial x\partial\mu=-\mu\partial I/\partial\mu+\int_{\mu_0}^{\mu} K(\mu', \mu)(\partial I/\partial\mu')d\mu', \quad (2)$$

where

$$K(\mu', \mu)=-k(\nu', \nu)d\nu/d\mu. \quad (2')$$

At this point we rely on the circumstance that our interest centers on a narrow spectral range corresponding to values of μ not much larger than μ_0. In this paper we limit ourselves to a first approximation in which the variations of the kernel $K(\mu', \mu'')$ in the range $\mu_0 \leq(\mu', \mu'')\leq\mu$ are disregarded altogether. The assumed constant value of the kernel will be indicated as K_0 and may be taken as equal to $K(\mu_0, \mu_0)$. Under this assumption Eq. (2) reduces to

$$\partial^2 I/\partial x\partial\mu=-\mu\partial I/\partial\mu+K_0 I. \quad (3)$$

If the primary radiation source is monochromatic, of frequency ν_0, is located at $x=0$ and emits radiation with a density of one photon per unit volume, the initial condition for I is

$$I(\mu, 0)=1 \quad \text{for} \quad \mu\geq\mu_0.$$

The solution of (3) reduces then to the product of an exponential and of a confluent hypergeometric, or Laguerre, function

$$I(\mu, x)=F(-K_0, 1, -(\mu-\mu_0)x)\exp(-\mu_0 x)$$
$$=L_{K_0}(-(\mu-\mu_0)x)\exp(-\mu_0 x). \quad (4)$$

The differential spectrum $\partial I/\partial\mu=(-d\nu/d\mu)\partial I/\partial\nu$ corresponding to this spectral distribution function is plotted in Fig. 1 for different values of the depth of penetration x, and for the representative value 1.5 of the parameter K_0 (see Fig. 2). The figure shows the trend of the spectral distribution toward equilibrium, as x and μ increase.

According to our introductory remarks equilibrium may be approached at a given depth x and for a spectral component whose absorption coefficient is μ when $(\mu-\mu_0)x$ is a large number. This condition does not require that μ be much larger than μ_0, provided $\mu_0 x$ is sufficiently large. The hypergeometric function in (4) may be expanded into inverse powers of $(\mu-\mu_0)x$.[1] The leading term for large values of $(\mu-\mu_0)x$ yields

$$I(\mu, x)\sim x^{K_0}(\mu-\mu_0)^{K_0}\exp(-\mu_0 x). \quad (5)$$

This expression describes an equilibrium distribution within the meaning of (b) above, since it consists of the product of a function of x and of a function of μ. The fact that the integral spectrum of an equilibrium distribution near its high energy limit μ_0 must behave as $(\mu-\mu_0)^{K_0}$ has been pointed out previously by Feshbach.[2] However, this result no longer holds, at least for a

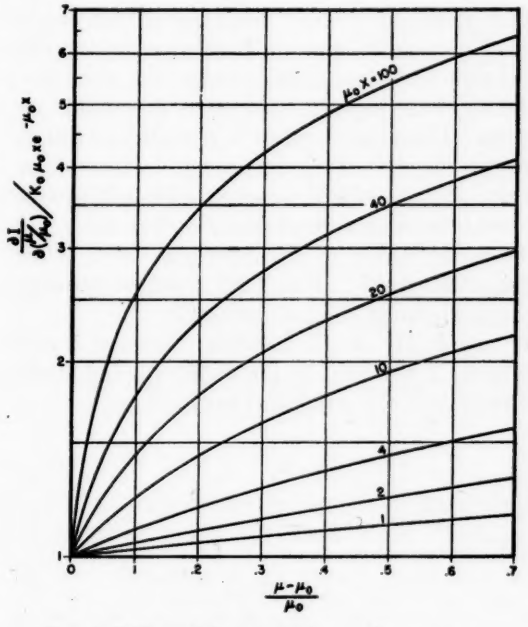

FIG. 1. Differential spectra of secondary x-rays, normalized to unity at $\mu=\mu_0$.

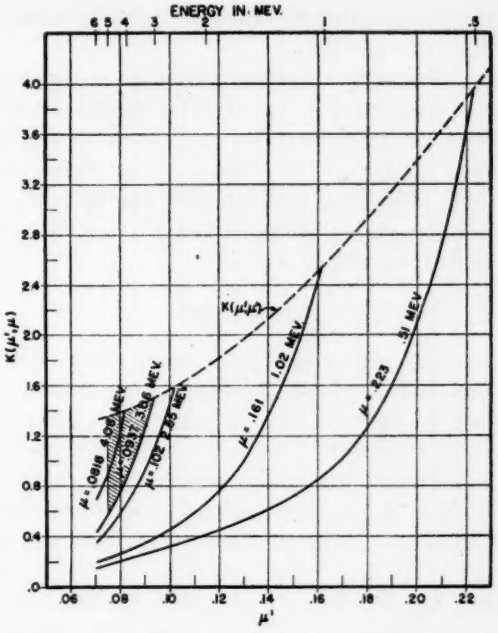

FIG. 2. The function $K(\mu', \mu)$ for aluminum.

[1] See Jahnke-Emde, *Tables of Functions* (B. G. Teubner, Leipzig, 1933 and Dover Publications, New York, 1943), p. 275.

[2] OSRD Rept. No. 4488, Vol. 4. Photostats available from U. S. Library of Congress.

monochromatic primary radiation, when μ is so close to μ_0 that $(\mu-\mu_0)x \leq 1$.

Since the density of primary photons at the depth x is $\exp(-\mu_0 x)$, the *ratio* of the total photon density to the primary density increases with the increasing depth according to the law x^{K_0}, that is, it increases beyond any limit. This result indicates that equilibrium within the meaning of (a) above is never attained or even approached asymptotically.

DISCUSSION

This work originates from a preliminary report by one of us (HAB), where a formula equivalent to (5) was obtained. In addition to some unnecessary approximations[3] the earlier work contains an arbitrary reduction of K_0 by a factor "1.5"/2 intended to compensate for variations of $K(\mu', \mu)$ in (2), variations that were disregarded when substituting (3) for (2). The actual values of $K(\mu', \mu)$ for aluminum are plotted in Fig. 2. If one intended to solve Eq. (2) in the energy interval from 5 to 3 Mev, the values of K involved in the integration would come from the shaded area. Their effective mean would in fact be lower than the value of 1.34 of $K(\mu_0, \mu_0)$ at 5 Mev by about 25 percent.

There remains to verify how accurate is the approximation introduced in (3)–(5), with $K_0 = K(\mu_0, \mu_0)$ or with a lower estimated effective value of K_0. This verification will be provided by further numerical work now in progress relying on better approximations where the variations of K are taken into account. The purpose of this note is primarily to point out the physical factors that control the approach to equilibrium and the analytical methods for treating them. For the time being, Eq. (5) must be understood to represent the integral spectrum of x-rays approximately, with the following restrictions:

(1) The lowest frequency ν considered should be sufficiently close to the primary frequency ν_0, so that $(\mu-\mu_0)/\mu_0 \ll 1$;

(2) The depth of penetration x considered should be sufficiently large so that $(\mu-\mu_0)x \gg 1$.

The restriction (1) should be removed by future work (now started) intended to determine the equilibrium spectral distribution in a form $f(\mu)$ that would be valid for all values of $\mu > \mu_0$ and $\nu < \nu_0$ and would reduce approximately to $(\mu-\mu_0)^{K_0}$ for $(\mu-\mu_0)/\mu_0 \ll 1$. Such a function will enable one to calculate by suitable integrations the quantities of practical importance such as the energy flux, the dose in roentgens or the total photon density at various depths. This future work should also indicate the choice of an optimum "effective value" for the exponent K_0 of x in (5).

The calculation performed in this note applies primarily to a monochromatic x-ray source. Any source may, of course, be treated as a superposition of monochromatic sources. However, when the primary x-rays arise from a thick target under electron bombardment, the secondary radiation is likely to approach equilibrium much faster than the secondary of a monochromatic spectrum. The reason is that the intensity spectrum of thick target primary x-rays already tends to zero at the peak energy where $\mu = \mu_0$ as the equilibrium spectrum (5) must eventually do, while the primary monochromatic (differential) spectrum consists of a sharp line just at $\mu = \mu_0$. This effect requires more detailed investigation. The progressive filtration of a non-monochromatic beam tends to make its attenuation curve steeper than $\exp(-\mu_0 x)$, while the addition of secondary x-rays scattered by a small angle tends to make this curve less steep. Owing to these opposite effects, an experimental attenuation curve may not be expected to differ very critically from $\exp(-\mu_0 x)$, in agreement with observation.

The entire treatment of this note assumes that the primary radiation is more penetrating than its secondaries. This condition is not fulfilled when the absorption is primarily due to pair production, since the pair production cross section increases as the photon energy increases. This case requires a separate investigation. From the standpoint of the present treatment, as the primary photon energy increases and pair production becomes increasingly important, the derivative $-d\mu/d\nu$ in the denominator of (2′) approaches zero. Then the coefficient K_0 in (3), (4) and (5) diverges showing that our approximation becomes unusable.

We thank Mr. J. C. Lamkin, National Bureau of Standards, X-ray Section, for his helpful and intelligent performance of the numerical calculations.

[3] General Electric Company Report HAB-1, A-4251, June 24, 1947. According to the report, the numerical values of the exponent K_0 (or a', as it was then called) is lower than one finds by taking $K_0 = K(\mu_0, \mu_0)$ for various reasons including: (a) Use of the extreme relativistic approximation for the Klein-Nishina cross section. The error due to this approximation amounts to about 10 percent at 5 Mev. (b) Failure to include the effect of pair production in the numerical evaluation of μ. This effect amounts to a factor of about 1.5 in aluminum at 5 Mev. (Notice that this effect depends on the derivative of the pair production cross section rather than on the cross section itself.)

Polarization Effects in $n-p$ and $p-p$ Scattering

LINCOLN WOLFENSTEIN
Carnegie Institute of Technology, Pittsburgh, Pennsylvania
(Received April 7, 1949)

Calculations have been made of the left-right asymmetry to be expected in neutron-proton scattering if polarized neutrons are used. The detection of such an asymmetry would be direct evidence of a tensor force interaction in the scattering. A 4 percent asymmetry might be expected at 100 Mev using a (p,n) exchange reaction as a source of 20 percent polarized neutrons. Effects are smaller in proton-proton scattering.

POSSIBLE methods for producing polarized beams of fast neutrons and protons have been discussed recently.[1-3] It has been hoped that such beams might provide a useful tool for studying the spin dependence of nuclear interactions. The present paper indicates the effect of using polarized incident beams in the experiments on the angular distribution of neutron-proton and proton-proton scattering. The same analysis, of course, also gives the polarization of the scattered particles when an unpolarized incident beam is used.

Three types of spin-dependent nucleon-nucleon interactions can be considered: (a) direct spin-spin coupling, which has the effect of differentiating the singlet and triplet interactions, (b) the tensor force interaction, and (c) the electromagnetic interaction of the magnetic moment of a nucleon with the Coulomb field through which it is moving. In order to detect the first of these by the use of polarized projectiles it is necessary either to use polarized target nuclei[4] or to detect the change in polarization[5] by an additional scattering. The tensor force, on the other hand, can produce a difference between the polarized and unpolarized angular distributions because it couples the spin with the orbital motion. It might be thought that this effect would also go to zero once one averages over the spin of the target nucleon; this is true, however, only to the Born approximation. An informal argument follows. The tensor interaction has a spin dependence of the form $(\sigma\cdot\mathbf{r}\ \ \sigma_N\cdot\mathbf{r})$, where σ_N is the spin of target nucleon. In the Born approximation this gives a scattered wave with the spin dependence

$$(\sigma\cdot\kappa\ \ \sigma_N\cdot\kappa)u_0, \tag{1}$$

where κ is parallel to the change in the momentum and u_0 is the initial spin state. Averaged over the directions of σ_N, this equals zero. However, if (1) is considered as an intermediate state in a second-order approximation, final states are found with a spin dependence

$$(\sigma\cdot\kappa'\ \ \sigma_N\cdot\kappa')(\sigma\cdot\kappa\ \ \sigma_N\cdot\kappa)u_0, \tag{2}$$

where $\kappa+\kappa'$ is parallel to the change in momentum. When averaged over the directions of σ_N, (2) yields a non-zero term dependent on the spin σ:

$$i\kappa\cdot\kappa'[\sigma\cdot(\kappa\times\kappa')]u_0.$$

The Born approximation is found to be so inaccurate for the case of the tensor force that such second order terms cannot be neglected.

The tensor force interaction for the case of $n-p$ scattering will be treated exactly using the general notation of Ashkin and Wu.[6] An incident triplet state is written

$$\psi_0 e^{ikz}=\sum_{m_s=-1}^{1} a_{m_s}\chi^{m_s}e^{ikz},$$

where χ^{m_s} are the triplet spin functions quantized along the z-axis (axis of incidence) and the a_{m_s} specify the polarization of the state. The scattered wave is

$$\psi_f(e^{ikr}/r)=\sum_{m_s'=-1}^{1}\chi^{m_s'}\sum_{m_s=-1}^{1}\mathcal{S}_{m_s'm_s}a_{m_s}(e^{ikr}/r),$$

with

$$\mathcal{S}_{m_s'm_s}=\frac{1}{2ik}\sum_{L,J}[4\pi(2L+1)]^{\frac{1}{2}}\{\exp(2i\delta_L{}^{Jm_s})-1\}\times(SLm_s-m_s'm_s'|SLJm_s)\times(SLJm_s|SLOm_s)Y_L{}^{m_s-m_s'}(\theta,\varphi),$$

where $\delta_L{}^{Jm_s}$ is the phase shift corresponding to an orbital angular momentum L and a total angular momentum J with z-component m_s, and $Y_L{}^m(\theta,\varphi)$ is a spherical harmonic function of the center-of-mass scattering angle θ and the azimuth angle φ. In matrix notation

$$\psi_0=a,\quad \psi_f=\mathcal{S}a$$

and the scattered intensity is given by

$$\psi_f{}^\dagger\psi_f=a^\dagger\mathcal{S}^\dagger\mathcal{S}a.$$

If the direction of initial polarization is taken as the y-axis,[7] this gives

$$\psi_f{}^\dagger\psi_f=\tfrac{1}{4}\,\mathrm{Tr}(\mathcal{S}^\dagger\mathcal{S})+\tfrac{1}{2}\bar{S}_y\,\mathrm{Tr}(S_y\mathcal{S}^\dagger\mathcal{S}),$$

where S_y is the indicated triplet spin operator, $\bar{S}_y$ is the

[1] J. Schwinger, Phys. Rev. **69**, 681 (1946).
[2] J. Schwinger, Phys. Rev. **73**, 407 (1948).
[3] L. Wolfenstein, Phys. Rev. **75**, 1664 (1949).
[4] M. E. Rose, Phys. Rev. **75**, 213 (1949).
[5] J. Schwinger and I. Rabi, Phys. Rev. **51**, 1003 (1937).
[6] J. Ashkin and T. Y. Wu, Phys. Rev. **73**, 973 (1948).
[7] Only polarization perpendicular to the axis of incidence can be detected (reference 3).

TABLE I. Maximum value of polarization effect I_P for $n-p$ scattering divided by unpolarized intensity I_0. θ is the scattering angle in the center-of-mass system for which I_P is a maximum. (I_P'/I_0) is given for the same angle.

Theory	Energy (Mev)	θ	I_P/I_0	I_P'/I_0
Neutral	15	120	−0.23	−0.0005
Charged	15	90	−0.19	−0.001
Symmetrical	15	120	−0.026	−0.0007
Half-exchange	15	45	0.011	−0.003
	15	135	−0.011	−0.0004
Symmetrical	100	35	0.24	−0.006
Half-exchange	100	35	0.19	−0.003
	100	145	−0.19	−0.0003

mean value of the y-component of the total spin in the initial state, and the triplet state is assumed to be normalized to $\frac{3}{4}$. Assuming a completely polarized neutron incident on an unpolarized proton, one finds that the polarization adds to the differential scattering cross section the term

$$I_P=\tfrac{1}{4}\,\mathrm{Tr}(S_y\mathcal{S}^\dagger\mathcal{S})$$

$$=\frac{1}{2\sqrt{2}}\,\mathrm{Im}\sum_{m_s=-1}^{1}\mathcal{S}_{m_s0}{}^*(\mathcal{S}_{m_s1}-\mathcal{S}_{m_s,-1}).$$

Since this is proportional to $\cos\varphi$, the effect of the polarization is to produce a left-right asymmetry in the scattered intensity relative to the initial direction of polarization.[3]

Values of I_P at 15 Mev have been calculated using the phase shifts computed by Rarita and Schwinger[8] under three assumed forms for the exchange interaction, designated "neutral," "charged," and "symmetrical." Calculations were also made for the "half-exchange" interaction which has been suggested to fit the high-energy scattering data.[9] The maximum values of I_P are given in Table I in the form of I_P/I_0 (for $\varphi=0°$), where I_0 is the differential cross section for unpolarized neutrons. The large effect for the "neutral" and "charged" theories is associated with the large p-wave scattering, which is predicted by these theories but is contrary to experiment. The other theories, which fit present data much better, give a much smaller effect.

The values of I_P at 100 Mev have been calculated using the phase shifts given by Ashkin and Wu[6] for a square-well potential. For the "symmetric" interaction

$$I_P=(1/k^2)\cos\varphi\sin\theta\{0.03+0.18\cos\theta+0.05\cos^2\theta+0.69\cos^3\theta+0.07\cos^5\theta\}$$

while for the "half-exchange" interaction

$$I_P=(1/k^2)\cos\varphi\sin\theta\cos\theta\times\{0.20+0.71\cos^2\theta+0.07\cos^4\theta\}.$$

In both cases (see Table I) the maximum value of I_P is about 20 percent of the theoretical unpolarized scattering (about 35 percent of the experimental unpolarized scattering). It follows that a 20 percent polarization of unpolarized neutrons can be accomplished by scattering from protons,[10] and thus an asymmetry of about 4 percent can be obtained in a double scattering experiment. A more practical possibility may be the scattering of high-energy neutrons produced in a (p,n) reaction. If this reaction can be viewed, in accordance with the general viewpoint of Serber,[11] as a single $p-n$ exchange collision it should exhibit the same polarization effects as $n-p$ scattering. In particular, assuming a "half-exchange" interaction the neutrons coming out at an angle of 35° should have a polarization of about 20 percent if 100 Mev unpolarized protons are incident. If these neutrons are then scattered from protons a left-right asymmetry of about 4 percent relative to the normal of the plane of the (p,n) reaction should be observed at a scattering angle of 35°.

The magnetic moment-Coulomb field interaction, which may be treated by the Born approximation,[2] adds another term to the angular distribution,[12]

$$I_P'=2(e/\hbar c)\mu\cot(\theta/2)\cos\varphi\,\mathrm{Im}g(\theta),$$

$$g(\theta)=\frac{1}{4k}\{\textstyle\sum_L(2L+1)\sin K_L e^{iK_L}P_L{}^0(\cos\theta)+\mathrm{Tr}\mathcal{S}\},$$

where μ is the magnetic moment of the neutron and K_L is a singlet phase shift. This term is found to be much less than 1 percent (see Table I) except at very small angles. Consequently any polarization effect that may be detected must be attributed to the tensor force interaction.

For the case of proton-proton scattering the analysis must be modified to account for the identity of the particles and the charge of the proton. At low energies the polarization effect is much less than for $n-p$ scattering because there is no s-wave triplet scattering and consequently the highest order terms entering I_P are interference terms between p-wave scattering and Coulomb scattering. At 100 Mev it is also considerably smaller; for the symmetric interaction neglecting Coulomb scattering completely

$$I_P=-(1/k^2)\cos\varphi\sin\theta\cos\theta\{0.10+0.08\cos^2\theta\}.$$

In the case of the "half-exchange" interaction the effect vanishes since there is no triplet $p-p$ scattering for this interaction.

I wish to express my thanks to Professor Edward Teller for many helpful discussions.

[8] W. Rarita and J. Schwinger, Phys. Rev. **59**, 556 (1941).

[9] Hadley, Kelly, Leith, Segrè, Wiegand, and York, Phys. Rev. **75**, 351 (1949). This interaction is written $(1+P)/2$, where P is the Majorana exchange operator. For odd values of L it gives zero scattering.

[10] The recoil protons, of course, are also polarized to the same extent.

[11] R. Serber, Phys. Rev. **72**, 1114 (1947).

[12] This interaction also contributes terms (not included in I_P') in the case of an unpolarized incident beam. These terms are also very small for the examples considered here.

Radiation from a Uniformly Accelerated Charge*

D. L. DRUKEY**
University of Minnesota, Minneapolis, Minnesota
(Received April 25, 1949)

It has been stated that there is no radiation from a charge moving in the relativistic equivalent of uniform acceleration. This proves to be not the case when means of measuring the radiation are used which are suitable to the infinite extent of the path.

The fields for a uniformly accelerated charge as deduced by conformal transformation from rest are found to correspond to one-half the sum of advanced and retarded potentials for two charges.

THE classical radiation from a charge in so simple a motion as uniform acceleration would hardly seem to merit attention at this time, but the fact remains that the published work on the relativistic equivalent of uniform acceleration contains a direct contradiction. The same theory, which states that a charge at rest, but accelerated, radiates at a rate $2e^2\ddot{x}^2/3c^3$, states that when this "rest system acceleration," a, is constant, the rate of radiation is not $2e^2a^2/3c^3$, henceforth called R_0, but zero.[1-3] It is the purpose of this note to show that the radiation rate R_0 is indeed correct, and that the arguments for the zero rate, though attractive, are not correct.

As stated above, the relativistic equivalent of uniform acceleration is a motion such that the acceleration, when viewed from a system in which the particle is instantaneously at rest, has some value, a, which is a constant of the motion. It must be noted that no single frame of reference exists in which the acceleration, a, is always found, but rather there is a different rest system for every instant: no single unaccelerated system can keep pace with the accelerated particle.

The equations of motion have been determined,[3,4] and the fields for a uniformly accelerated point charge have been calculated.[2,3] The mathematical expression for the fields constitutes the basis for one of the arguments for the zero radiation rate. In the special case that the acceleration is parallel to the velocity, the particle decelerates from the speed of light to rest, then accelerates back to the speed of light retracing its path. At the instant that the particle is at rest, the turning point, the magnetic field, vanishes everywhere. As a consequence, the energy flux, $\mathbf{E}\times\mathbf{H}/4\pi$, vanishes everywhere at this instant. At any instant, however, a suitable Lorentz transformation will bring the charge to rest so that there is never an instant when the energy flux is other than zero. It is thus concluded that there is never any radiation by an argument almost exactly parallel to that of Zeno, who once argued that an arrow in flight is at every instant at only one point, so that there is never an instant in which it is in motion. The specific fallacy in the argument here is that there is no single unaccelerated system in which the energy flux *remains* zero.

The same formulas for the fields used to construct the argument recounted above do, in fact, reveal that the rate of radiation is R_0 and not zero. The fields originating from the particle at some given time in the course of its motion will be found at some later time on the surface of a sphere centered on the point of origin and of a radius corresponding to the propagation of the signal with the speed of light. The fields from a slightly later point of the motion will be found at the same field time on the surface of a second sphere correspondingly smaller and centered on the second source point. All contributions to the radiation arising from the section of path between these two source points must then be contained in the eccentric spherical shell between the two spheres, Fig. 1. The energy density, $(E^2+H^2)/8\pi$, may be integrated over this shell for which the volume element proves to be:

$$dV=r^2(1-\beta\cos\theta)drd\phi d\cos\theta$$

with the polar axes about the velocity and β the ratio of the particles' velocity to that of light. Using the known fields to compute the energy density (reference 2, Eq. (244)) and doing the integration, it is found that there is a contribution, constant in that time, from that

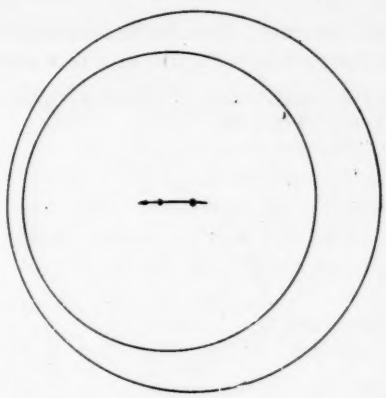

FIG. 1.

* From a thesis submitted in partial fulfillment of the requirements for the degree Master of Science.

** Atomic Energy Commission Fellow, University of Minnesota.

[1] H. A. Lorentz, Enc. d. Math. Wiss. sect. 5, Vol. 12, p. 168.
[2] W. Pauli, Enc. d. Math. Wiss. sect. 5, Vol. 19, pp. 648, 653.
[3] M. Born, Ann. d. Physik 30, 39 (1909).
[4] E. L. Hill, Phys. Rev. 72, 143 (1947).

section of the path. This contribution thus flows outward undiminished with the speed of light and is radiation. As might be expected, this contribution agrees with that calculated from the rate of radiation, R_0.

This same result is obtained if the Poynting vector, $\mathbf{E}\times\mathbf{H}/4\pi$ is computed and its normal component summed over the surface of a "light sphere" about some given source point correcting for the convection of energy due to the motion of the particle. The correction has the form, $1-\beta\cos\theta$.[5]

Finally, one may consider a finite motion composed of three parts: a gradual start from rest, as long a period of uniform acceleration as desired, and a gradual return to rest. It is then found that the beginning and ending portions can be made to contribute as little as desired to the radiation, and that the amount contributed by the uniformly accelerated portion is in accordance with the rate of radiation R_0. Since the motion in question is bounded, a sphere of sufficiently large radius can contain all of the currents of the problem and can be as far from them as desired, so that the usual method of evaluating the Poynting vector is justified. If the actual uniformly accelerated motion were to have a zero rate of radiation, it would thus be necessary to imagine complete destructive interference of the contributions from the finite and infinite portions of the path.

It may thus be shown by several devices specifically adapted to the nature of the problem that the radiation from a uniformly accelerated charge is not anomalous. The special devices have proven necessary because of the infinite extent of the path. They yield the same answers as more common methods when they are applied to ordinary problems. The prediction of zero radiation does not seem justified on the basis of classical field theory.

A second argument is cited[2] to demonstrate the nonexistence of radiation from the motion. It is stated that there is no radiation reaction force on a uniformly accelerated particle. Since the particle would do no work against the reaction, it could not emit energy by radiation.

This is not the case: Consider the expression derived by Lorentz for rate of radiation in a rest system.[1] The energy radiated during a given interval is:

$$\Delta E=\int_{t_1}^{t_2}\frac{2e^2\ddot{x}^2}{3c^3}dt.$$

This can be integrated by parts to give:

$$\Delta E=\left\{\frac{2e^2\dot{x}\ddot{x}}{3c^3}\right\}_{t_1}^{t_2}-\int_{t_1}^{t_2}\frac{2e^2\dot{x}\dddot{x}}{3c^3}dt.$$

The second term is the work done against the radiation reaction and vanishes for uniform acceleration, but the first term, the change in a quantity characteristic of the instantaneous state of the motion and called by Schott the acceleration energy, just accounts for the radiation previously predicted. This term, usually neglected because attention is generally confined to periodic motions or to those bounded in time, accounts for the entire energy in this problem.

Recently it has been suggested in another connection that uniform acceleration does not lead to radiation. In the course of his investigations of the application of the general conformal transformation to electrodynamics, Hill[6] has obtained the fields by conformal transformation from rest to uniform acceleration. The explanation as to the error in radiation rate leads to nothing new, but it is of interest to investigate the fields obtained by this method. One of the transformations takes a point at rest into one in uniform acceleration. Since the Maxwell equations are invariant under the transformation, the idea that the fields of a resting point charge might be transformed into those of a charge in uniform acceleration naturally presents itself for consideration, although its validity is by no means assured. In fact, the fields obtained prove to correspond to one-half of the sum of advanced and retarded potentials for two charges. The second charge is the reflection of the first, both in sign of charge and in position. The reflection is in a plane normal to the path and a distance c^2/a beyond the turning point where a is the rest acceleration and c the velocity of light.

I wish to thank Dr. J. W. Weinberg for suggesting the problem and for many helpful suggestions. I am indebted to Drs. E. L. Hill and C. L. Critchfield for many valuable discussions.

[5] Cf. Heitler, *Quantum Theory of Radiation* (Oxford University Press, New York, 1949), p. 20.

[6] E. L. Hill, Phys. Rev. 72, 148 (1947).

The Variation of the Adiabatic Elastic Constants of KCl, NaCl, CuZn, Cu, and Al with Pressure to 10,000 Bars*

DAVID LAZARUS
Department of Physics, University of Chicago, Chicago, Illinois
(Received April 4, 1949)

The adiabatic velocities of sound for longitudinal and transverse waves in single crystal specimens of five cubic solids have been measured as a function of pressure to 10,000 bars, using a pulse technique. The elastic constants calculated from these data in general agree well with previous measurements obtained for zero pressure elastic constants and compressibilities. With increasing pressure the anisotropy increases in crystals which are not closest-packed, but decreases in closest-packed structures. Consideration of the exchange force between nearest neighbors gives a qualitative explanation for this effect. Comparison of the present measurements with previous measurements of the variation of elastic constants with temperature indicates that the elastic moduli cannot be considered functions of volume alone but must also depend explicitly on the temperature.

INFORMATION derivable from a study of the variation of the elastic properties of solids as a function of hydrostatic pressure should be useful in the more general problem of formulating an equation of state for solids.[1] This paper presents results of measurements of the elastic constants of single crystal specimens of Cu, Al, CuZn, KCl, and NaCl subject to hydrostatic pressures to 10,000 bars.[2]

Previous measurements of the effects of pressure on the elastic properties of solids are limited to measurements of compressibility and shear modulus. Linear compressibilities have been determined for many solids by Bridgman and others using a dilatometric technique[3] based on measurement of the change in length of a specimen under pressure relative to the confining walls of the high pressure chamber. The observed data are plotted as a square-law curve, the first-order term giving the zero pressure compressibility, and the second-order term the change in compressibility with pressure. Since the compressibility of a solid is easily calculated from the elastic constants, measurements of the change of elastic constants with pressure give the *change* in compressibility as a *first-order* effect.

Birch[4] has measured the change in shear modulus with pressure to about 4000 bars for several polycrystalline metals, glasses, and minerals. His measurements were made by observing the resonant frequency of a cylindrical specimen excited in torsional oscillation. Viscosity effects were minimized in his measurements by use of nitrogen gas as a pressure fluid. This method and other techniques involving measurement of a set of resonant frequencies[5] are useful only for measurement of shear moduli over a somewhat limited pressure range. At high pressures measurement of compressional moduli would be impossible by such methods, since the large damping would preclude accurate determination of resonant frequencies.

The present investigation is made possible by the wartime development of pulsed circuits. Elastic constants are determined by a non-resonant method involving direct measurement of the transit time of a short pulse of ultrasonic energy through a solid. This technique, known as the pulsed ultrasonic method, or "reflectoscope" method, was first developed by Firestone[6] for detection of flaws in metals. More recently, the pulsed ultrasonic method has been employed by Huntington[7] and Galt[8] for measurement of the elastic constants of several cubic salts at atmospheric pressure.

For simplicity the present measurements are confined to cubic crystals, which have only three independent elastic constants. The specimens used represent the three principal groups of cubic crystals: simple cubic (NaCl, KCl), body-centered cubic (CuZn), and face-centered cubic (Cu, Al). These three designations, while not crystallographically correct, are useful in representing the lattice symmetry if differences between atoms are ignored. They represent extremes in packing of nearest neighbors, the simple cubic structure being least closely packed, and the face-centered cubic structure closest packed. In each of the extreme groups, two materials of considerably different degrees of anisotropy are investigated. By these choices it is hoped that some evaluation may be made of Zener's proposals[9] con-

* The research described here was performed in the High Pressure Laboratory of the Institute for the Study of Metals, University of Chicago, and was supported in part by the ONR under Contract N-6-ori-20-XX.

[1] For discussions of equations of state for solids see: P. W. Bridgman, Rev. Mod. Phys. **7**, 1 (1935); F. Seitz, *Modern Theory of Solids* (McGraw-Hill Book Company, New York, 1940), Chap. X; N. Mott and H. Jones, *Properties of Metals and Alloys* (Oxford University Press, London, 1936), Chap. I; K. Herzfeld and M. Goeppert-Mayer, Phys. Rev. **46**, 995 (1934); M. Born et al., Jour. Chem. Phys. **7**, 591 (1939); Proc. Camb. Phil. Soc. **36**, 160, 173, 454, 466 (1940); **37**, 34, 177 (1941); **38**, 61, 67, 82 (1942); **39**, 101, 104, 113 (1943); **40**, 151 (1944); R. Furth, Proc. Roy. Soc. **183**, 87 (1944).

[2] 1 bar = 10^6 dynes/cm^2 = 1.01972 kg/cm^2.

[3] P. W. Bridgman, *Physics of High Pressure* (The Macmillan Company, New York, 1931), Chap. 4.

[4] F. Birch, J. App. Phys. **8**, 129 (1937).

[5] L. Balamuth, Phys. Rev. **45**, 715 (1934).

[6] F. A. Firestone, J. Acous. Soc. Am. **18**, 200 (1946).

[7] H. B. Huntington, Phys. Rev. **72**, 321 (1947).

[8] J. K. Galt, Phys. Rev. **73**, 1460 (1948).

[9] C. Zener, *Elasticity and Anelasticity of Metals* (University of Chicago Press, Chicago, 1948), Chap. III; Phys. Rev. **71**, 846 (1947).

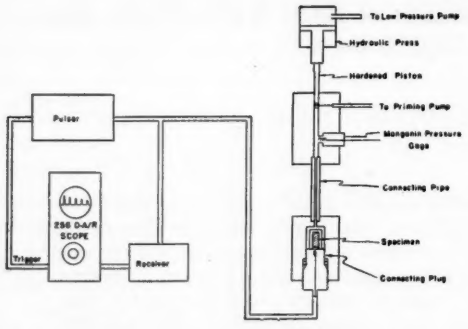

FIG. 1. Schematic arrangement of experimental apparatus.

cerning the effect of the short range exchange force between closed-shell ions on shear moduli. Zener pointed out that Fuchs' calculations[10] of the exchange contribution to the shear moduli of cubic crystals would indicate that in simple cubic lattices the shear modulus C_{44} might be expected to change much more slowly than the modulus $\frac{1}{2}(C_{11}-C_{12})$, or even in the opposite direction, with change in volume. According to this same viewpoint, the reverse effect might be expected in body-centered cubic lattices. In face-centered cubic lattices the modulus C_{44} would be expected to change slightly more slowly than $\frac{1}{2}(C_{11}-C_{12})$ with change in volume.

Since the elastic constants of all the above materials have been measured at zero pressure by a different method, a check is afforded on the accuracy of the present measurements. In addition, the elastic constants of three of these substances, KCl, NaCl,[11] and CuZn[12] have been measured as functions of temperature, so that some correlation may be obtained between the variation of elastic constants with temperature and with pressure.

The present measurements may also prove useful in comparison of the theories of finite strain proposed by several authors.[13] These theories all contain undetermined third-order constants. Unfortunately, all the third-order constants cannot be uniquely determined from pressure data alone. However, it may be possible to derive certain useful relationships between these quantities which will be helpful in evaluating the various theories.

EXPERIMENTAL METHODS

Measurement of elastic constants by the pulsed ultrasonic method involves determination of a set of velocities of sound in various directions in a crystal. By use of two crystals of a material with principal axes in the [100] and [110] directions, five velocities can be measured and the elastic constants computed with two

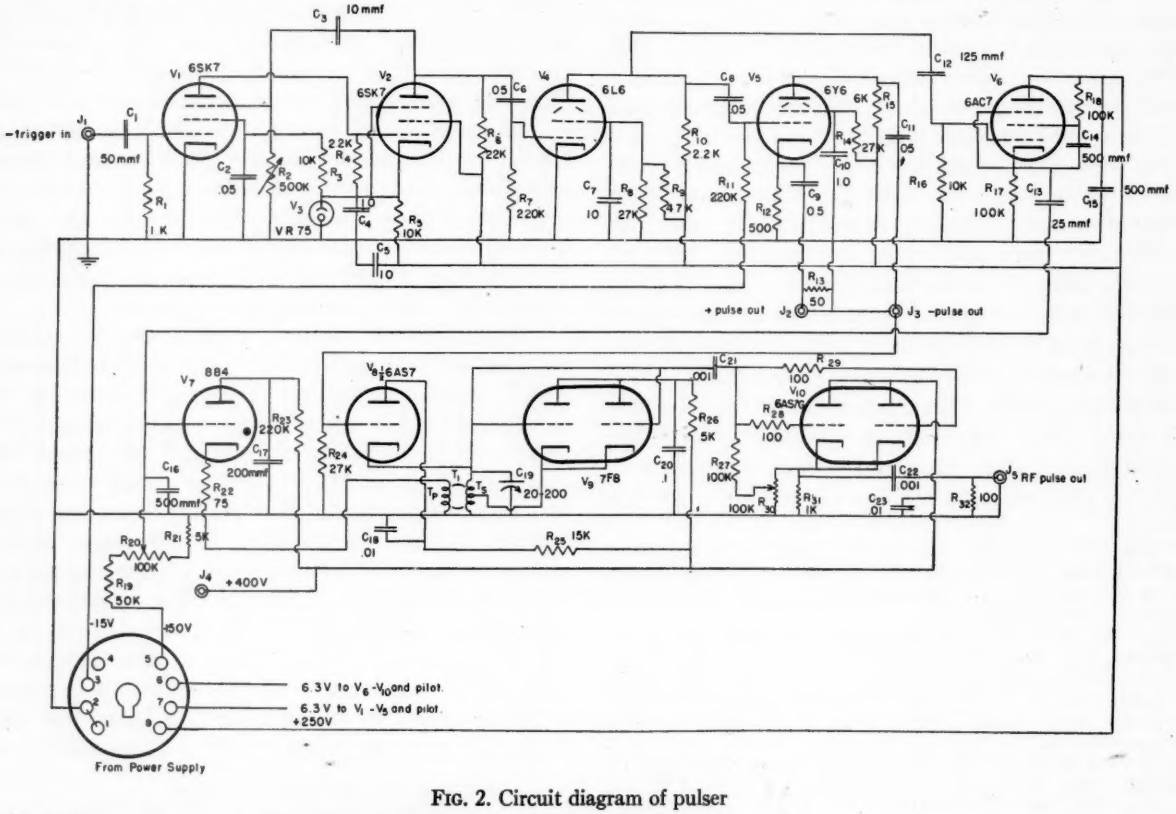

FIG. 2. Circuit diagram of pulser

[10] K. Fuchs, Proc. Roy. Soc. **151**, 585 (1935); **153**, 622 (1936); **157**, 444 (1936).
[11] M. A. Durand, Phys. Rev. **50**, 449 (1936); F. C. Rose, Phys. Rev. **49**, 50 (1936).
[12] W. A. Good, Phys. Rev. **60**, 605 (1941); J. S. Rinehart, Phys. Rev. **58**, 365 (1940).
[13] F. D. Murnaghan, Am. J. Math. **49**, 235 (1937); L. Brillouin, *Les Tenseurs* (Masson et Cie., Paris, 1938), Chap. X, XI; M. A. Biot, Phil. Mag. **27**, 468 (1939); F. Birch, Phys. Rev. **71**, 809 (1947).

internal checks. The velocities are expressible in terms of the elastic constants and the density ρ as shown below:[14]

$$\left.\begin{aligned}
&V_1=(C_{11}/\rho)^{\frac{1}{2}}=\text{velocity of longitudinal wave in (100) crystal in [100] direction.}\\
&V_2=[(C_{11}+C_{12}+2C_{44})/2\rho]^{\frac{1}{2}}=\text{velocity of longitudinal wave in (110) crystal in [110] direction.}\\
&V_3=(C_{44}/\rho)^{\frac{1}{2}}=\text{velocity of transverse wave in (100) crystal in [100] direction.}\\
&V_4=[\tfrac{1}{2}(C_{11}-C_{12})/\rho]^{\frac{1}{2}}=\text{velocity of transverse wave in (110) crystal in [1}\bar{1}\text{0] direction.}\\
&V_5=(C_{44}/\rho)^{\frac{1}{2}}=\text{velocity of transverse wave in (110) crystal in [100] direction.}
\end{aligned}\right\}\quad(1)$$

A schematic diagram indicating the arrangement of the various components involved in the present measurements is shown in Fig. 1. The apparatus consists of an electro-mechanical system for production of ultrasonic pulses and measurement of transit times, and a system for generation of high pressures.

I. The Electro-Mechanical System

The basic unit of the electrical system is a DuMont 256D-A/R oscilloscope. This instrument provides triggering pulses to an external pulser and means for accurate measurement of the time of travel of the ultrasonic pulse through the specimen. In operation the cycle is initiated by application of a triggering pulse to the pulser by the oscilloscope. The pulser then generates a short group of 12-mc waves. This signal is applied to a thin quartz crystal. The quartz crystal is in turn cemented to the specimen crystal, so that a short pulse of 12-mc acoustical waves is generated, and travels back and forth through the specimen several times before being completely damped. Each time the sound pulse passes through the quartz crystal an electrical pulse is generated which is applied to the receiver. After amplification and detection, the received set of pulses is displayed on the linear time base sweep of the oscilloscope. This cycle is repeated at a rate of about 2000 cps.

A. Oscilloscope—The oscilloscope contains precision delay circuits whereby the sweep may be initiated a measurable time after the triggering pulse. This delay circuit is set by means of a helical potentiometer, and can be calibrated to better than 0.1 percent by means of internal 10 microsecond crystal controlled range markers. These range markers have been checked by beating against station WWV, and found to be accurate to one part in 10^5. With adjustment of the delay time, the echoes can be made to move across the face of the oscilloscope and the 10 to 40 microsecond interval between echoes can be measured with considerable accuracy. The ultimate precision is largely limited by pulse distortion which makes accurate location of the leading edge of a pulse difficult.

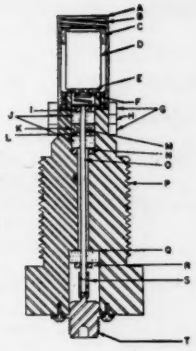

FIG. 3. Plug and specimen holder. *A*—screw cap; *B*—spring; *C*—retaining washer; *D*—specimen crystal; *E*—quartz crystal; *F*—spring contact; *G*—steel packing washers; *H*—lead washer; *I*—steel washer; *J*—bakelite washers; *K*—rubber washer; *L*—steel washer; *M*—steel ring; *N*—hardened steel washer; *O*—piano wire; *P*—body of plug; *Q*—bakelite spacer; *R*—nut; *S*—finger contact; *T*—type *N* connector.

B. Pulser—To minimize the effects of pulse distortion, some pains are taken in the design of the pulser circuit, shown in Fig. 2, to provide a steeply rising leading edge on the transmitted pulse. This is achieved first by the formation of a well-defined video rectangular pulse in the direct-coupled one-cycle multivibrator circuit of V_1 and V_2. This pulse is variable in width from 0.5 to 20 microseconds by setting rheostat R_2. After amplification, the negative rectangular pulse is applied to the grid of the clamp tube V_8, permitting oscillations to build up in the Hartley circuit of V_9. Simultaneously with the application of the negative pulse to V_8, a positive pulse is applied to the grid of thyratron V_7, which is normally biased beyond cut-off. Discharge of the thyratron sends a large surge of current through the close-coupled primary of the transformer T_1, causing oscillations to build up rapidly in the circuit $C_{19}T_8$. When the negative pulse is removed from the grid of clamp tube V_8 the oscillation decays rapidly because of the very low plate resistance of V_8. The resulting radio-frequency pulse is fed directly to the cathode-follower circuit of V_{10}, so that no high-Q tuned circuits are required between the oscillator and output. Use of two halves of a 6AS7G in parallel in the output cathode-follower results in an extremely small output impedance, so that the pulse shape is not distorted by the use of a

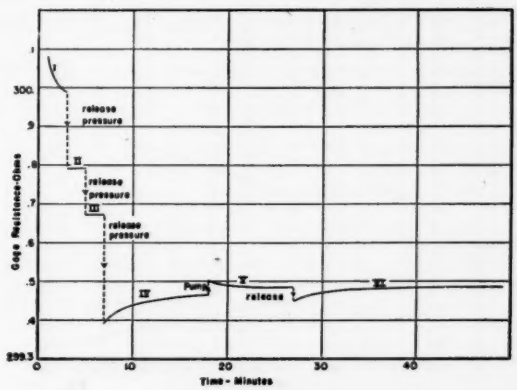

FIG. 4. Calibration of manganin pressure gage by determination of the freezing point of Hg at 0°C.

[14] W. G. Cady, *Piezoelectricity* (McGraw-Hill Book Company, New York, 1946), Chap. IV.

TABLE I. Densities and adiabatic velocities of sound for various hydrostatic pressures. (Densities in gm/cm³.)

Material	Velocity (km/sec.)	Pressure (bars) 0	2000	4000	6000	8000	10,000
KCl	V_1	4.541	4.646	4.752	4.845	4.914	5.044
	V_2	3.896	3.926	4.002	4.079	4.116	4.169
$\rho_0=1.986$	V_3	1.781	1.759	1.734	1.715	1.694	1.671
	V_4	2.921	2.990	3.069	3.135	3.201	3.282
	V_5	1.784	1.761	1.736	1.713	1.693	1.672
NaCl	V_1	4.766	4.875	4.947	5.041	5.140	5.230
	V_2	4.513	4.558	4.598	4.647	4.690	4.778
$\rho_0=2.162$	V_3	2.434	2.430	2.426	2.422	2.417	2.414
	V_4	2.920	2.987	3.039	3.099	3.156	3.208
	V_5	2.440	2.435	2.431			
CuZn	V_1	3.942	3.953	3.962	3.975	3.985	4.004
	V_2	4.931	4.945	4.954	4.971	4.985	5.011
$\rho_0=8.304$	V_3	3.151	3.164	3.171	3.180	3.187	3.192
	V_4	1.083	1.084	1.087	1.089	1.090	1.091
	V_5	3.152	3.162	3.170	3.179	3.180	3.187
Cu	V_1	4.373	4.383	4.393	4.403	4.405	4.415
	V_2	4.982	4.995	4.992	4.995	5.012	5.035
$\rho_0=8.941$	V_3	2.905	2.907	2.909	2.908	2.909	2.910
	V_4	1.621	1.623	1.626	1.629	1.633	1.637
	V_5	2.913	2.915	2.916			
Al	V_1	6.257	6.288	6.326	6.376	6.411	6.495
	V_2	6.409	6.468	6.479	6.487	6.520	6.562
$\rho_0=2.699$	V_3	3.252	3.269	3.286	3.306	3.334	3.357

relatively long 50-ohm coaxial lead between the pulser and the specimen.

C. Receiver—The pulse receiver is constructed by modification of an APS-15A 30 megacycle intermediate frequency amplifier. An additional radio-frequency stage was added and new coils wound to provide a tuned 12-mc receiver, with an over-all band width of about 3 cm between half-power points. The video amplifier stages of the receiver were unaltered and connected directly to the video amplifier of the oscilloscope. In practice, some increase in the accuracy of location of the leading edge of a pulse is obtained by deliberately overloading the receiver.

D. Transducer—The thin quartz transducer crystals[15] are gold sputtered for single-ended connection in the manner described by Huntington,[7] with an active area of about 1 cm². Longitudinal or transverse acoustical waves are excited in the specimen by use of *X* or *Y* cut quartz crystals, respectively. The quartz crystal must be fixed to the specimen with a binder permitting transmission of the sound pulse to the specimen.

An annoying problem was encountered in finding a satisfactory cement which would transmit shear waves through the specimen in the high pressure system. Phenyl salicylate, which was used by Huntington and Galt, is satisfactory for mounting the *X*-cut crystals, but dissolves rapidly in the pressure fluid at pressures above 500 bars and is thus unsuitable for mounting the *Y*-cut crystals. Similarly, all glues and resins soluble in hydrocarbons are unsatisfactory. Water-glass cements cannot be sufficiently dried even with appreciable baking to give adequate pulse transmission. DeKhotinsky wax proves satisfactory to about 5000 bars, but cracks at higher pressures. A satisfactory solution has been achieved by the use of red sealing wax. This wax is applied by heating the quartz crystal and specimen to about 150°C in a furnace. The surfaces of the specimen and quartz to be joined are then coated liberally with wax and placed together under a 500-gm weight. At this temperature the wax flows freely and uniform coats as thin as 0.001 in. can be obtained. This binder is usable over a pressure range of 12,000 bars. Unfortunately, the large difference in compressibilities between the quartz and the wax almost invariably results in shattering the quartz crystal during a high pressure measurement. Since the wax does not crack, this shattering does not in any way inhibit taking data, but does make it impossible to use the quartz crystal for a second run.

Since the acoustic pulse travels through the combined length of the specimen, transducer crystal, and cement film, the observed velocity is subject to a small correction for the thickness of the quartz and cement. This correction has been determined by measuring velocities

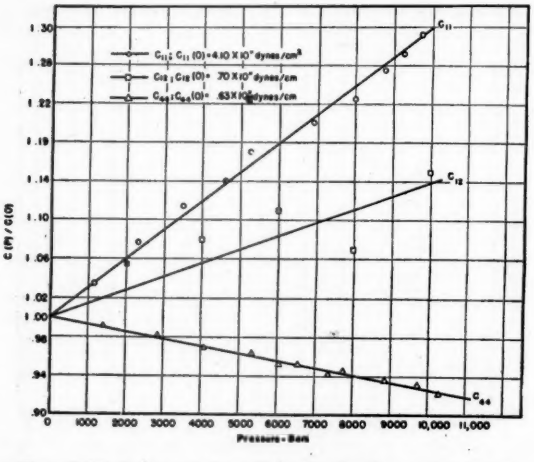

FIG. 5. Variation of the adiabatic elastic constants of KCl with pressure.

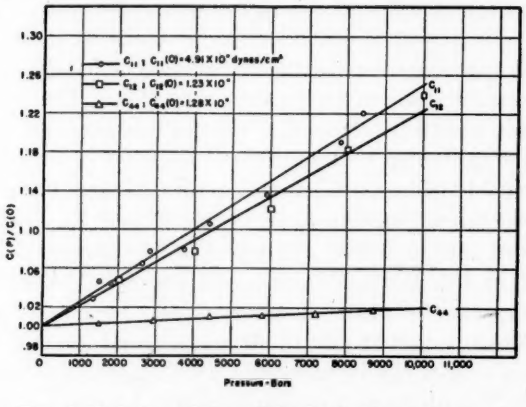

FIG. 6. Variation of the adiabatic elastic constants of NaCl with pressure.

[15] Purchased from James Knights Co., Sandwich, Illinois.

for longitudinal and transverse waves in specimens of different lengths, and is found to be 0.10–0.15 microseconds, depending on the thickness of the cement film and the quartz crystal used.

II. The High Pressure System

The specimen crystal, with quartz transducer attached, is mounted in a lower chamber by means of a special connecting plug, shown in detail in Fig. 3. This plug is designed to serve the dual purpose of providing a mount for the specimen and furnishing means for transmitting the electrical pulse to the quartz crystal. The cylindrical specimen, *D*, with quartz crystal, *E*, fixed at one end, is supported by means of the screw cap *A* and retaining washer *C*. Connection to the center of the quartz crystal is effected by the spring contact *F*. The outer conducting area of the crystal connects to ground through the outer shell of the plug.

The lower chamber is connected to the upper high pressure generating system by means of a pipe, the pressure being transmitted by the hydraulic fluid. The hydraulic fluid employed in the present measurements is petroleum ether, consisting principally of normal hexane, with a boiling point of 60°C. This fluid does not freeze at room temperature within the pressure range investigated.

The high pressure generating system is similar to that employed by Bridgman[16] and need not be separately described here. Pressure is determined by measurement of the change in resistance of a manganin resistance gage which is immersed in the pressure fluid.

The pressure gage used in the present measurements is a ten-foot length of No. 40 manganin wire, of about 300-ohms resistance, wound in a circular helix about $\frac{1}{2}$ in. in diameter and 1 in. long. The resistance of the coil is stabilized by heating to 150°C for about four hours. Before calibration the gage is "seasoned" by repeated cycling through a pressure range of at least 10,000 bars. After perhaps six such cycles, the zero pressure resistance is reproducible to better than one part in 10^5. The pressure gage is calibrated by determination of the freezing pressure of mercury at 0°C, using Bridgman's value of 7640 kg/cm², determined by a free piston gage, as a standard. For this measurement, hexane, which freezes at about 6000 bars at 0°C, is not a suitable pressure fluid. Normal pentane, which has a freezing point above 10,000 bars at 0°C, is employed. A typical calibration curve is shown in Fig. 4. The freezing point is found by approach from both sides, and can be located with a precision of 0.1 percent. As shown by Adams, Goranson, and Gibson,[17] the manganin pressure gage is sufficiently linear so that only a single calibration point is required for a 0.1 percent accuracy in determination of pressure.

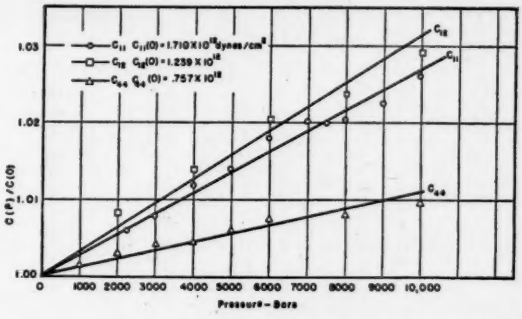

FIG. 8. Variation of the adiabatic elastic constants of Cu with pressure.

III. Preparation of Specimens

The single crystal specimens have been prepared in the shape of right circular cylinders of about 2-cm diameter and 2 to 3-cm length. A diameter large compared to the acoustical wave-length is used to insure that the sound pulse is transmitted as a plane wave, so that infinite-medium moduli are measured. This outer diameter is always at least twice the diameter of the active area of the quartz crystal. Measurements taken with polycrystalline samples of successively smaller diameters indicate no change in measured velocity as long as

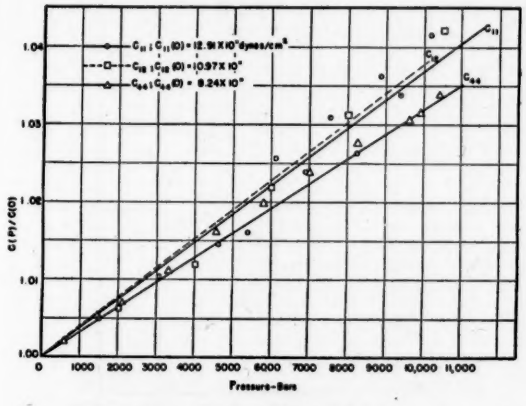

FIG. 7. Variation of the adiabatic elastic constants of CuZn with pressure.

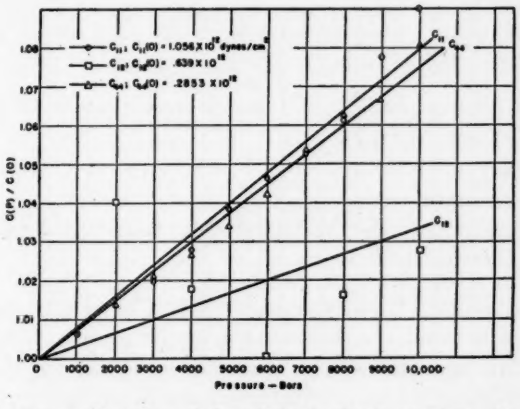

FIG. 9. Variation of the adiabatic elastic constants of Al with pressure.

[16] P. W. Bridgman, *Physics of High Pressure*, Chap. 2.

[17] Adams, Goranson, Gibson, Rev. Sci. Inst. 8, 230 (1937).

TABLE II. Variation of $(C_{12}-2P)/C_{44}$ with pressure for KCl and NaCl.

Pressure (bars)	0	10,000
Material		
KCl	1.119	1.05
NaCl	0.954	1.01

the specimen diameter is greater than that of the wave front, taken as equal to the diameter of the active area of the quartz crystal.

Single crystal specimens of beta-brass, copper, and aluminum have been prepared in this laboratory. The crystals were grown from the melts in graphite crucibles by lowering at a rate of about 1.5 cm per hour through a vertical tube furnace.

In preparation of the beta-brass melt, a considerable reduction in zinc loss is achieved by heating proper amounts of pure copper and zinc together with a small amount of fused borax. With increasing temperature the borax melts and forms a protective coating over the surface of the molten metal. Loss of zinc by oxidation is thus reduced to about five grams per kilogram.

The metal single crystals are grown about 3 cm in diameter and 10 cm in length so that sufficiently large sections of proper orientation can be cut from the large crystal. The orientations of the crystals are determined by means of back-reflection diffraction pictures. All crystals are cut with a water-cooled carborundum cut-off wheel. This method of cutting introduces very little strain in the crystal, judging from the sharpness of the Laue spots diffracted from such cut surfaces. After one face of a crystal has been properly oriented to within one or two degrees, the opposite face of the specimen is made accurately parallel to the first by mounting the crystal in a surface grinder. Successive 0.0005-inch cuts are taken with a water-cooled wheel until a flat parallel surface is obtained. After working, the finished specimens are annealed for 24 hours at about 400°C. No residual surface strains are detected by x-ray analysis after this treatment.

The metal specimens have been analyzed chemically and show the following compositions in weight percent:

Beta-brass crystals: Cu: 51.06; Zn: 48.94; Ag, B, Si, Pb, Al, Ca, Mg, Fe <0.01

Copper crystals: Cu: 99.99; Ca, Mg, Ag, Al, Si, Fe <0.01

Aluminum crystals: Al: 99.991; Mg: 0.003; Si, Fe, Cu, Ca <0.002.

The single crystal specimens of NaCl and KCl were purchased from the Harshaw Chemical Company. These crystals are oriented by Harshaw by cleaving along (100) planes. The orientations have been checked by back-reflections pictures and found to be accurate to within about a tenth degree. The alkali-halide crystals are also annealed before use.

RESULTS

I. Variation of Adiabatic Elastic Constants with Pressure

The observed velocities of sound for the various materials studied are indicated in Table I, together with the measured zero-pressure densities. Density values are obtained by hydrostatic weighing. The values V_1-V_5 refer to velocities of waves in various crystallographic directions as indicated in Eqs. (1). The velocities are computed from the relation

$$V_i=d_{0i}(1+\chi_T P)^{-\frac{1}{2}}t_i^{-1} \tag{2}$$

where d_{0i} is the zero-pressure path length as measured by a calibrated micrometer, χ_T is the isothermal cubic compressibility and t_i the observed transit time, corrected for the thickness of the cement and quartz crystal.

The elastic moduli of Eqs. (1) are calculated by the equation

$$m_i=\rho_0(1+\chi_T P)V_i^2 \tag{3}$$

where ρ_0 is the zero-pressure density. From Eqs. (2) and (3) it is evident that the compressibility enters explicitly in the computation of the elastic constants only through the factor $(1+\chi_T P)^{\frac{1}{2}}$. The value for χ_T used in the above relations can be easily calculated, in the absence of previous data, by a self-consistent solution since

$$\chi_T=\chi_s+(TV\alpha^2/C_P)$$
$$=[3/(C_{11_s}+2C_{12_s})]+TV\alpha^2/C_P \tag{4}$$

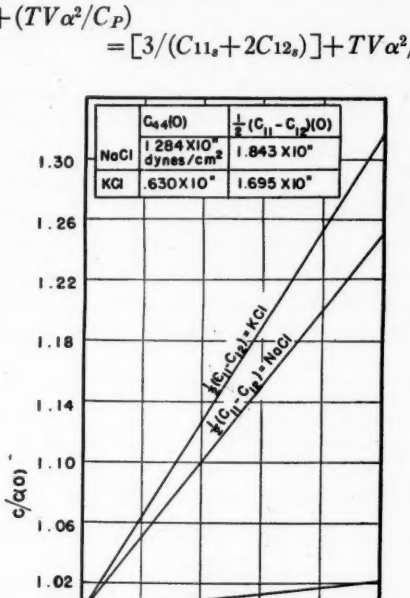

FIG. 10. Variation of the shear moduli of KCl and NaCl with pressure.

where T is the absolute temperature, V the molal volume, α the cubic thermal expansion coefficient and C_P the molal specific heat at constant pressure. The subscript s refers to adiabatic moduli. For most solids, χ_T is small, and a fairly large error in the assumed value for the compressibility introduces only a small error in the calculated value for the elastic constants.

In the case of aluminum, data are not given in Table I for the (110) shear velocities V_4 and V_5. For this specimen it has not been possible to resolve the two normal modes of vibration by positioning of the Y-cut quartz crystal. This anomaly presumably arises as a result of the very small anisotropy of aluminum, previous measurements[18] indicating that the velocities V_4 and V_5 should differ by only a few percent. With inevitable imperfections present in the metal crystal, some cross-coupling between normal modes must be anticipated. In anisotropic materials the cross-coupling is small if the transducer crystal is properly oriented. However, in aluminum the effect is evidently sufficiently large so that only a single average shear velocity is observed for a (110) crystal.

The adiabatic elastic constants calculated by Eqs. (1) and (3) are plotted as functions of pressure in Figs. 5–9.

All measurements are taken at room temperature, nominally 25°C. Changes in pressure are made sufficiently slowly so that temperature equilibrium is maintained. The change in viscosity of the pressure fluid with temperature may be presumed to have no observable effect. At 10,000 bars hexane has a viscosity of about 3 poises,[19] roughly the same as that of glycerin at zero pressure. Measurements taken for both compressional and shear waves in specimens immersed in air, hexane, and glycerin at atmospheric pressure have shown no detectable differences in velocities for the various media.

As can be seen from the graphs, the precision in the measurements for transverse waves is somewhat better than that for longitudinal waves. This difference results from the rather large radiation damping encountered at high pressures with longitudinal waves which limits the number of distinct echoes observable. This source of error is most serious for the alkali-halides, since the amount of energy radiated to the pressure fluid is proportional to the ratio of the compressibility of the solid to that of the liquid. Although the zero pressure constants, measured in air, are accurate to about ±0.2 percent, the accuracy in the high pressure values for C_{11} is probably no greater than ±1.0 percent for the alkali-halides, ±0.6 percent for Al and ±0.4 percent for Cu and CuZn. The accuracy of the shear measurements is about the same as at zero pressure. Since the constant C_{12} is obtained by difference, the precision of this value at high pressures is about ±4 percent for NaCl, ±6 percent for KCl, ±0.5 percent for CuZn, and ±1 percent for Cu.

[18] E. Goens, Ann. Phys. **17**, 233 (1933).
[19] P. W. Bridgman, *Physics of High Pressure*, Appendix.

TABLE III. Comparison of zero-pressure adiabatic elastic constants with previous values (units—10^{11} dynes/cm²).

Material	Present C_{11}	Present C_{12}	Present C_{44}	Previous C_{11}	Previous C_{12}	Previous C_{44}	Reference
KCl	4.095	0.705	0.630	4.00	0.6	0.625	*
NaCl	4.911	1.225	1.284	4.99	1.31	1.26	*
CuZn	12.91	10.97	8.24	5.20	3.35	17.3	**
Cu	17.10	12.39	7.56	16.98	12.26	7.53	***
Al	10.56	6.39	2.853	10.82	6.22	2.84	****

* M. A. Durand, Phys. Rev. **50**, 449 (1936).
** W. A. Good, Phys. Rev. **60**, 605 (1941).
*** E. Goens, Ann. Phys. **17**, 233 (1933).
**** E. Goens and J. Weerts, Physik. Zeits. **37**, 321 (1936).

For Al, the value of C_{12} must be obtained by taking a double difference, owing to the impossibility of measuring the shear modulus $\frac{1}{2}(C_{11}-C_{12})$ directly. The high pressure values for C_{12} are thus subject to an error of about ±3 percent for this material.

Since a considerable number of independent readings were taken for each curve, and no systematic error was noted, the slopes of the lines for C_{11} and C_{44} should be accurate to within ±0.5 percent. In no case is there apparent justification for assuming a relation other than linear between the elastic constants and pressure.

II. Variation of Anisotropy with Pressure

Several interesting effects can be noted by comparison of the rates of change of the two independent shear moduli C_{44} and $\frac{1}{2}(C_{11}-C_{12})$, as shown in Figs. 10 and 11. For the materials whose crystal structures are not closest-packed, the anisotropy increases with increasing pressure. The originally larger shear modulus, $\frac{1}{2}(C_{11}-C_{12})$ for the alkali-halides, C_{44} for beta-brass, increases with pressure at about the same rate as C_{11}, while the smaller modulus increases more slowly, or in the case of KCl, actually decreases. Face-centered-cubic copper, which has a closest-packed structure shows the reverse effect, the anisotropy decreasing with pressure.

The effects noted for the alkali-halides are in excellent agreement with Zener's predictions regarding the effects of exchange forces on the shear moduli. The supposition

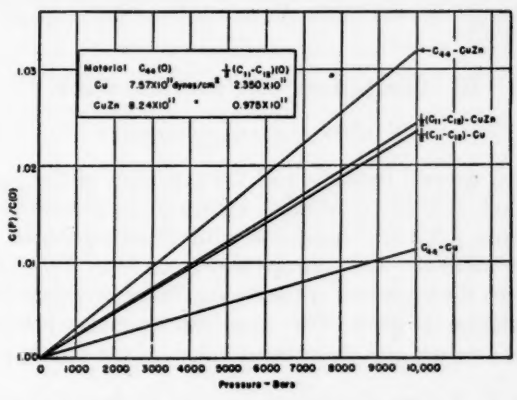

FIG. 11. Variation of the shear moduli of CuZn and Cu with pressure.

TABLE IV. Comparison of present computed isothermal compressibilities with previous values. (Units of a are 10^{-7} bar^{-1}, $b-10^{-12}$ bar^{-2}.)

Material	Present a	Present b	Previous a	Previous b	Reference
KCl	56.8	72.4	56.3	74.4	*
NaCl	43.1	49.6	42.6	51	**
CuZn	9.06	2.30	9.11	0.99	***
Cu	7.38	1.36	7.29	1.6	***
Al	13.49	4.6	13.65	4.9	***

* J. C. Slater, Proc. Am. Acad. **61**, 135 (1926).
** P. W. Bridgman, Proc. Am. Acad. **64**, 33 (1929).
*** P. W. Bridgman, Proc. Am. Acad. **70**, 285 (1935).

that the difference in rates of change of the two moduli results from the exchange repulsion is further verified by the marked decrease in C_{44} for KCl. Since the potassium ion is somewhat larger than the sodium ion, the exchange force would be expected to be larger for KCl than for NaCl, and thus the effect on C_{44} of decreasing the inter-atomic distance larger for KCl.

The difference in rates of change of C_{44} and $\frac{1}{2}(C_{11}-C_{12})$ for copper are also qualitatively explained by consideration of exchange forces. According to Fuchs' results for this material, the exchange contribution is about 90 percent of the modulus $\frac{1}{2}(C_{11}-C_{12})$ and 75 percent of C_{44}. On this basis the former would be expected to change more rapidly with pressure than the latter, in agreement with the observed result.

In the case of beta-brass, the difference in rates of change of the two moduli, while significant, is much smaller than that anticipated on the basis of consideration of exchange forces alone. According to Zener's calculations a marked decrease in $\frac{1}{2}(C_{11}-C_{12})$ with pressure would be expected, rather than a small increase in this modulus.

At zero pressure the Cauchy relation[20] $C_{12}=C_{44}$, derived from the assumption of central forces between ions, is approximately realized for the alkali-halides. Love[21] has shown that under an external pressure P, the Cauchy relation is given by $C_{44}=C_{12}-2P$. The ratio $(C_{12}-2P)/C_{44}$ for KCl and NaCl is given in Table II.

The Cauchy relation is evidently satisfied somewhat better at high pressures than at zero pressure for both materials.

III. Comparison with Previous Data

A. Zero-pressure constants

As a general indication of the precision of the pulse method, it is worth while to compare the present zero-pressure adiabatic constants with those measured by other methods. This comparison is made in Table III.

With the exception of the constants for beta-brass the correlation is good. The large discrepancies between Good's values and the present values of the elastic constants of beta-brass were noted in a recent paper.[22] The differences probably result from a gross error in Good's measurement of C_{44}, resulting from the presence of impure modes in his resonant sample. Good's values for C_{11} and C_{12} were computed from Rinehart's[12] values for Young's modulus using this value for C_{44}. Values for Young's modulus computed from the present elastic constants correlate well with Rinehart's data.

TABLE V. Comparison of present value for change of shear modulus with pressure with previous values.

Material	Present $\left(\frac{\partial \ln C_{44}}{\partial P}\right)_T$	Present $\left(\frac{\partial \ln \frac{1}{2}(C_{11}-C_{12})}{\partial P}\right)_T$	Previous $\left(\frac{\partial \ln G}{\partial P}\right)_T$
Cu	1.13×10^{-5} bars^{-1}	2.45×10^{-5}	2.76×10^{-5}
Al	7.49×10^{-5}		7.76×10^{-5}

B. Compressibility

In Table IV the values for isothermal compressibility computed from the present data by Eq. (4) are compared with those previously reported by Bridgman and Slater. The coefficients a and b in the table refer to Bridgman's usual expression for the change in volume with pressure,

$$-[(V(P)-V_0)/V_0]=aP-bP^2 \qquad (5)$$

where $V(P)$ is the volume at pressure P and V_0 the zero-pressure volume.

Bridgman's and Slater's values for a and b are corrected for Bridgman's most recent value for the compressibility of iron.[23]

The agreement is generally good for both first and second-order coefficients. Because of the low precision in the present high-pressure value of C_{12} for Al, the agreement in b coefficients for this material, while fortuitous, is probably not very significant. In the case of beta-brass, the present b coefficient is appreciably larger than that reported by Bridgman. The discrepancy is well beyond the experimental error of the present measurements. Bridgman's low value of b may have resulted from the use of rapidly quenched polycrystalline specimens in his measurement, or possibly from differences in composition between his specimens and those used in the present investigation.

C. Shear modulus

Values of the pressure variation of the shear moduli C_{44} and $\frac{1}{2}(C_{11}-C_{12})$ of Cu and Al are compared in Table V with those observed by Birch[4] for polycrystalline specimens.

Birch's somewhat larger value for copper may be due to grain boundary effects.

[20] A. E. H. Love, *Mathematical Theory of Elasticity* (Cambridge University Press, Cambridge, 1934), p. 100.
[21] See Reference 20, p. 619.
[22] D. Lazarus, Phys. Rev. **74**, 1726 (1948).
[23] P. W. Bridgman, Rev. Mod. Phys. **18**, 1 (1946).

D. Correlation with temperature data

The elastic modulus M of a crystal may be regarded as both an implicit function of temperature, through its volume V, and as an explicit function. Thus

$$M=M(V, T),$$

and

$$d\ln M=(\partial \ln M/\partial V)_T dV+(\partial \ln M/\partial T)_V dT.$$

The measured variation of M with temperature is evidently given by

$$\frac{d\ln M}{dT}=\left(\frac{\partial \ln M}{\partial P}\right)_T\left(\frac{\partial V}{\partial P}\right)_T^{-1}\frac{dV}{dT}+\left(\frac{\partial \ln M}{\partial T}\right)_V=-\frac{\alpha}{\chi_T}\left(\frac{\partial \ln M}{\partial P}\right)_T+\left(\frac{\partial \ln M}{\partial T}\right)_V.$$

Solving for $(\partial \ln M/\partial T)_V$, one obtains

$$(\partial \ln M/\partial T)_V=\alpha/\chi_T(\partial \ln M/\partial P)_T+(d\ln M/dT). \quad (6)$$

The value of $(\partial \ln M/\partial T)_V$ compared with the observed $(d\ln M/dT)$ gives a measure of the explicit dependence of the modulus on temperature, since evidently the left-hand term of Eq. (6) vanishes if $M=M(V)$.

The previous measurements of the temperature variation of the adiabatic elastic moduli are compared with the present pressure measurements in Table VI. Comparison is made for the bulk modulus $\frac{1}{3}(C_{11}+2C_{12})$ using Bridgman's values for $(d\ln M/dT)$. For the alkali-halides the comparison is also made for the moduli C_{11}, $\frac{1}{2}(C_{11}-C_{12})$, and C_{44}, using Rose's and Durand's values for $(d\ln M/dT)$. For beta-brass, the present results are compared with those of Rinehart for the Young's moduli $E_{[100]}$, $E_{[110]}$, and $E_{[111]}$ rather than with Good's values for the elastic constants, for reasons noted above. The Young's moduli are calculated from the elastic constants by the relations[24]

$$E_{[100]}^{-1}=\frac{\chi_s}{9}+\left[3\frac{(C_{11}-C_{12})}{2}\right]^{-1},$$

$$E_{[110]}^{-1}=\frac{\chi_s}{9}+(4C_{44})^{-1}+\left[12\frac{(C_{11}-C_{12})}{2}\right]^{-1}, \quad (7)$$

$$E_{[111]}^{-1}=\frac{\chi_s}{9}+(3C_{44})^{-1}.$$

[24] C. Zener, Phys. Rev. **71**, 846 (1947).

TABLE VI. Comparison of present data with previous measured changes in adiabatic elastic constants with temperature.

Material	Modulus (M)	$(\partial \ln M/\partial P)_T$	$(d\ln M/dT)$	$(\partial \ln M/\partial T)_V$
KCl	$\frac{1}{3}(C_{11}-2C_{12})$	2.609×10^{-5} bar^{-1}	-5.10×10^{-4} deg. C^{-1}	-0.45×10^{-4} deg. C^{-1}
	C_{11}	2.99	−9.80	−4.47
	$\frac{1}{2}(C_{11}-C_{12})$	3.16	−11.49	−5.85
	C_{44}	−0.74	−2.68	−4.00
NaCl	$\frac{1}{3}(C_{11}+2C_{12})$	2.46	−8.51	−1.66
	C_{11}	2.49	−7.60	−0.67
	$\frac{1}{2}(C_{11}-C_{12})$	2.53	−11.70	−4.66
	C_{44}	0.21	−2.50	−1.92
CuZn	$\frac{1}{3}(C_{11}+2C_{12})$	0.382	−5.37	−2.49
	$E_{[100]}$	0.249	+2.23	+4.41
	$E_{[110]}$	0.282	+0.93	+3.06
	$E_{[111]}$	0.384	−4.34	−1.44
Cu	$\frac{1}{3}(C_{11}+2C_{12})$	0.280	−4.17	−2.15
Al	$\frac{1}{3}(C_{11}+2C_{12})$	0.507	−4.69	−1.99

It appears from Table VI that any assumptions that elastic moduli are unique functions of volume are evidently invalid, especially in the case of shear moduli.

In this connection it was thought advisable to ascertain whether compositional differences between the beta-brass crystals used in the present measurements and those employed by Rinehart might not be involved in the large positive values for $(\partial \ln M/\partial T)_V$ for $E_{[100]}$ and $E_{[110]}$. Since the predominant terms in these moduli arise from the shear modulus $\frac{1}{2}(C_{11}-C_{12})$ the latter value has been checked roughly between room temperature and −100°C. The measured shear modulus is found to decrease with decreasing temperature in essential agreement with Rinehart's observation.

ACKNOWLEDGMENTS

The author wishes to express his gratitude to his sponsor, Professor A. W. Lawson, for his many constructive suggestions during the course of this research; to Professor C. M. Zener for several enlightening conversations; to Dr. W. Bergmann for his kindness in preparing the Cu and Al crystals, and to Messrs. S. Mayburg, F. Bruce, K. Lindholm, and N. D. Nachtrieb for assistance in the construction and manipulation of the equipment.

Cathode Field in Diodes under Partial Space-Charge Conditions

HENRY F. IVEY
Westinghouse Electric Corporation, Bloomfield, New Jersey
(Received March 16, 1949)

A method for calculating the electric field at the cathode of a diode for any condition of current flow in the diode is presented. A "universal" curve gives the cathode field as a function of diode current. The equation for this curve is

$$\frac{I}{I_s}=\frac{1}{2}\left[1\pm\left\{1-\frac{27}{4}\left(\frac{E}{E_0}\right)^2\left(1-\frac{E}{E_0}\right)\right\}^{\frac{1}{2}}\right],$$

where I is the diode current, I_s is the saturation current corresponding to the applied anode voltage as calculated from the Child-Langmuir equation, E is the cathode field, and E_0 is the value of E in the absence of current flow.

The only restrictions on the derivation are those of an equipotential, smooth cathode, and negligible initial velocities of emission. Only plane and cylindrical diodes have been considered, but the results are believed to be applicable to any geometry. Application of the results to the study of thermionic cathodes in the Schottky emission region is very straightforward.

The variation of the cathode field as a function of anode voltage is also discussed. A method for calculating the potential distribution in a plane diode for any value of diode current is given in the Appendix.

I. INTRODUCTION

THE characteristics of diodes under conditions of complete space charge, i.e., space-charge density so great that the electric field at the cathode is zero, were calculated long ago. The results are expressed by the familiar Child-Langmuir equations for plane[1,2] and cylindrical[2,3] geometries,

$$J_s=(1/9\pi)(2e/m)^{\frac{1}{2}}V^{\frac{3}{2}}/d^2, \tag{1}$$

and

$$I_s'=(2/9)(2e/m)^{\frac{1}{2}}V^{\frac{3}{2}}/r_a\beta^2, \tag{2}$$

respectively. β^2 is the usual Langmuir-Blodgett function[3] which has been tabulated as a function of the ratio of electrode radii, r_a/r_c, V is the anode voltage, J indicates current density, and I' indicates current per unit axial length.

The problem of the diode under partial space-charge conditions has, however, received little attention. Most textbooks, for example, contain only a simple statement that as the current, and therefore the space-charge density, in a diode with constant anode voltage is increased from zero to the saturation value, the field at the cathode decreases continuously from that in the absence of space charge to zero. In many cases, and in particular the study of electron emission from cathodes in the Schottky region,* a knowledge of the field actually existing at the cathode of the experimental diode under all conditions is necessary. This paper presents a solution of this problem.

The discussion is restricted to cases where initial velocities of emission can be neglected. This condition is not, however, a real limitation, since the anode voltages employed in practical investigations of the Schottky effect are so high that the initial energies of a few tenths of an electron volt are indeed negligible. The cathode is also assumed to be equipotential and ideally smooth (i.e., the surface roughness is neglected).

II. THE PLANE DIODE

For simplicity, consider first a diode consisting of infinite parallel plane electrodes separated by a distance d. Let the space potential U and the distance x be measured from the cathode so the $U=0$ at $x=0$. The distribution of the potential in the space between the electrodes is determined by Poisson's equation, which in this case involves only the coordinate x,

$$\nabla^2U=d^2U/dx^2=4\pi\rho, \tag{3}$$

where ρ is the electron space-charge volume density (considered a positive quantity). As auxiliary relations one has also the current flow equation,

$$J=\rho v, \tag{4}$$

where J is considered positive for electron flow, and the conservation of energy,

$$mv^2/2=eU, \tag{5}$$

where v is the electronic velocity at the point x and the initial velocities of emission have been assumed negligible.

With the aid of these equations ρ and v can be eliminated and a new equation obtained giving the relation between U and J,

$$d^2U/dx^2=aU^{-\frac{1}{2}}, \tag{6}$$

where

$$a=4\pi(m/2e)^{\frac{1}{2}}J. \tag{7}$$

The variable "a" can be further simplified by substituting from Eq. (1),

$$a=\frac{4J}{9J_s}\cdot\frac{V^{\frac{3}{2}}}{d^2}=\frac{4I}{9I_s}\cdot\frac{V^{\frac{3}{2}}}{d^2}. \tag{8}$$

If Eq. (6) is multiplied by the factor $2(dU/dx)$ it may be integrated directly to give

$$(dU/dx)^2=4aU^{\frac{1}{2}}+C_1. \tag{9}$$

[1] C. D. Child, Phys. Rev. **32**, 492 (1911).
[2] I. Langmuir, Phys. Rev. **2**, 450 (1913).
[3] I. Langmuir and K. B. Blodgett, Phys. Rev. **22**, 347 (1923).
* By Schottky emission is meant thermionic emission under conditions such that the potential barrier at the emitter surface is lowered significantly by the electric field at the cathode.

The magnitude of the electric field, dU/dx, at the cathode ($x=0$, $U=0$) is designated by E. Using this as a boundary condition, $C_1=E^2$, and one can rewrite Eq. (9) as

$$dx=(E^2+4aU^{\frac{1}{2}})^{-\frac{1}{2}}dU. \tag{10}$$

This can be integrated to give[4]

$$x=-(1/6a^2)(E^2-2aU^{\frac{1}{2}})(E^2+4aU^{\frac{1}{2}})^{\frac{1}{2}}+C_2. \tag{11}$$

The constant of integration can be determined from the requirement that $U=0$ at $x=0$, or $C_2=E^3/6a^2$. Substituting this value and rearranging terms,

$$x=\frac{2V^{\frac{1}{2}}}{3a^{\frac{1}{2}}}\left(\frac{U^{\frac{1}{2}}}{V^{\frac{1}{2}}}+\frac{E^2}{4aV^{\frac{1}{2}}}\right)^{\frac{1}{2}}\left(\frac{U^{\frac{1}{2}}}{V^{\frac{1}{2}}}-\frac{E^2}{2aV^{\frac{1}{2}}}\right)+\frac{E^3}{6a^2}. \tag{12}$$

This equation expresses the potential distribution in the diode. It can be put into more useful form by introducing the new dimensionless variable,

$$u=\frac{E^2}{4aV^{\frac{1}{2}}}=\left(\frac{I_s}{I}\right)\left(\frac{3E}{4E_0}\right)^2, \tag{13}$$

where E_0, the field in the absence of space charge ($I=0$), is given by

$$E_0=V/d, \tag{14}$$

and rearranging to obtain[5]

$$\left(\frac{x}{d}\right)\left(\frac{I}{I_s}\right)^{\frac{1}{2}}=\left[\left(\frac{U}{V}\right)^{\frac{1}{2}}+u\right]^{\frac{1}{2}}\left[\left(\frac{U}{V}\right)^{\frac{1}{2}}-2u\right]+2u^{\frac{1}{2}}. \tag{15}$$

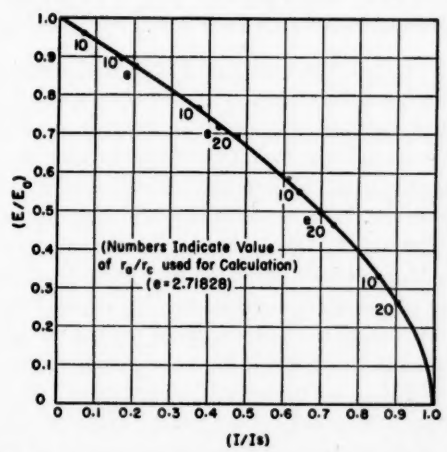

FIG. 1. Cathode field in a diode as a function of diode current.

[4] Equation (11) has also been integrated to essentially the same form by Stern, Gossling, and Fowler, Proc. Roy. Soc. **A124**, 699 (1929) in a study of field emission.

[5] Equation (15) and data for the curve of Fig. 1 were also obtained by R. Cockburn, Proc. Phys. Soc. London **47**, 810 (1935), who also considered the effect of initial velocities, but the data was not plotted in the manner of Fig. 1. Cockburn's work was not known to the author at the time this paper was first written (12/23/48). In the discussion resulting when this paper was presented at the M.I.T. Electronics Conference (April 7, 1949), it developed that the case of the plane diode has also been treated by Mr. Esterson of the English Electric Valve Company, by Professor Dow of the University of Michigan, and by Mr. W. M. Brubaker of the Westinghouse Research Laboratories. None of these workers investigated the cylindrical diode, however, and none has published his work.

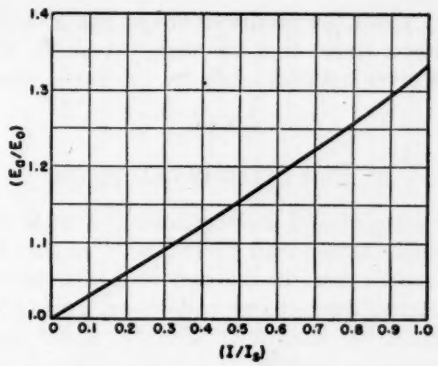

FIG. 2. Variation of anode field with current in a plane diode.

In the Appendix it is shown how this equation can be utilized to determine the potential distribution in the diode.

By definition, $U=V$ when $x=d$. When this substitution is made in the expression above one obtains the relation

$$(I/I_s)^{\frac{1}{2}}=(1+u)^{\frac{1}{2}}(1-2u)+2u^{\frac{1}{2}}. \tag{16}$$

This expression and Eq. (13) may be considered as a parametric representation of the relation between (I/I_s) and (E/E_0), where u is the parameter. However, these equations can be combined to give the explicit relation[6]

$$\frac{I}{I_s}=\frac{1}{2}\left[1\pm\left\{1-\frac{27}{4}\left(\frac{E}{E_0}\right)^2\left(1-\frac{E}{E_0}\right)\right\}^{\frac{1}{2}}\right]. \tag{17}$$

Here the negative sign is to be used for values of (E/E_0) greater than $\frac{2}{3}$, and the positive sign for values less than $\frac{2}{3}$.

Values of cathode field as a function of diode current calculated by this method are plotted in Fig. 1 as the solid curve. It is seen, as might be expected, that the major portion of the drop in cathode field occurs in the region close to complete space-charge saturation. Thus, for a current density which is one-half of the saturation value, the cathode field has fallen only to two-thirds of its zero-current value; for a current density 90 percent of the saturation value, the cathode field is still 27 percent of the zero-current value.

It is of interest also to investigate the field at the anode of a plane diode under conditions of partial space charge. From Eq. (10) one may write

$$E_a=(dU/dx)_{x=d}=(E^2+4aV^{\frac{1}{2}})^{\frac{1}{2}}. \tag{18}$$

Substituting the value of "a" from Eq. (8) and introducing E_0 from Eq. (14) gives the resulting expression

$$E_a/E_0=[(E/E_0)^2+(16/9)(I/I_s)]^{\frac{1}{2}}. \tag{19}$$

Use of the data obtained above for (E/E_0) as a function

[6] First pointed out to the author by Mr. Esterson of the English Electric Valve Company. Also obtained by Mr. Brubaker of the Westinghouse Research Laboratories.

of (I/I_s) yields the results shown in Fig. 2. Inspection of the figure shows that the variation of (E_a/E_0) with (I/I_s) is given approximately by the linear relation

$$E_a/E_0=1+\tfrac{1}{3}(I/I_s). \tag{20}$$

III. THE CYLINDRICAL DIODE

Most experimental investigations are made in cylindrical diodes rather than plane diodes, so that this is a very practical case. In the case of a cylindrical diode under partial space-charge conditions, Poisson's equation cannot be integrated directly. Rose[7] has used series expansion methods to investigate the field at the cathode of such a diode but the results are not easy to apply. Crank, Hartree, Ingham, and Sloane,[8] however, have made a numerical investigation of the potential distribution in such diodes with the aid of the differential analyzer. The data of their Table I may be utilized to find the electric field at the cathode.[9] In their notation,

$$U=1667(rI')^{\frac{1}{2}}\Phi, \tag{21}$$

and

$$\frac{dU}{dr}=1667\left(\frac{I'^2}{r}\right)^{\frac{1}{3}}\left(\frac{d\Phi}{d\xi}+\frac{2}{3}\Phi\right), \tag{22}$$

where

$$\xi=\log_e(r/r_c). \tag{23}$$

In Table I they give values of Φ (which may be considered as a reduced voltage variable) as a function of ξ for the boundary conditions $\Phi=0$ at $r=r_c$ and for various values of $(d\Phi/d\xi)_{r=r_c}$, that is, the potential distribution in the diode for various values of diode current.

Since we require $U=0$ at $r=r_c$, Eq. (21) shows that $\Phi=0$ at $r=r_c$ and Eq. (22) may therefore be written

$$E=1667(I'^2/r_c)^{\frac{1}{3}}(d\Phi/d\xi)_{r=r_c}. \tag{24}$$

E_0, the value of E for zero current (i.e., in the absence of space charge) is given from electrostatics as

$$E_0=V/r_c\cdot\log_e(r_a/r_c). \tag{25}$$

The anode voltage, V, is given by Eq. (21) as

$$V=1667(r_aI')^{\frac{1}{2}}\Phi. \tag{26}$$

Combination of these three expressions gives

$$\frac{E}{E_0}=\left(\frac{r_c}{r_a}\right)^{\frac{1}{2}}\log_e\left(\frac{r_a}{r_c}\right)\cdot\frac{1}{\Phi}\left(\frac{d\Phi}{d\xi}\right)_{r=r_c}. \tag{27}$$

Equation (26) shows that for a given diode at a given anode voltage, the quantity $(I'^{\frac{1}{2}}\Phi)$ is a constant, so that

$$I'/I_s'=I/I_s=(\Phi_0/\Phi)^{\frac{1}{2}}, \tag{28}$$

where Φ_0 is the value of Φ corresponding to complete space-charge saturation, i.e., $E=0$ and $(d\Phi/d\xi)=0$ from Eq. (24). Φ_0 is given in the second column of Table I in the reference cited.

Equations (27) and (28) permit calculation of corresponding values of (E/E_0) and (I/I_s). Such calculations have been made for cylindrical diodes with various values of r_a/r_c, and a few points are shown plotted as circles in Fig. 1. The values of r_a/r_c used are shown. It is seen that these points fall on the curve obtained for the planar diode, a fact that was not expected beforehand.

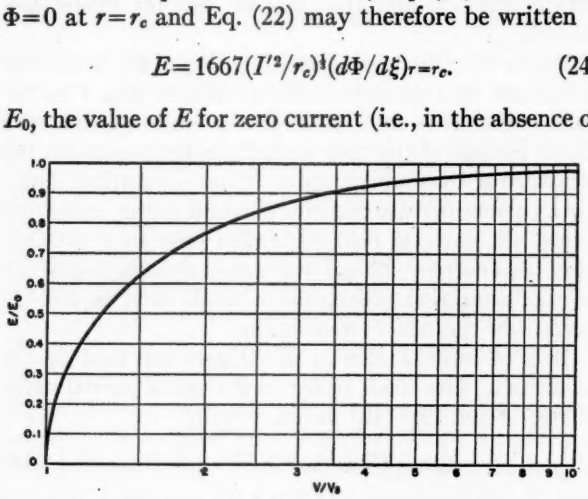

FIG. 3. Maximum cathode field in a diode as a function of anode voltage.

IV. UNIVERSAL NATURE OF THE CATHODE FIELD CHARACTERISTIC AND ITS APPLICATION

The fact that the curve of Fig. 1, relating the two dimensionless ratios (E/E_0) and (I/I_s), applies to both plane and cylindrical diodes is very interesting and leads one to believe that this characteristic is of even wider application. Apparently the effect of geometry is entirely taken into account by the two normalizing factors E_0 and I_s, one of which is obtained from the solution of Laplace's equation and the other from the solution of Poisson's equation for complete space charge. Although a rigorous proof cannot be given for the statement, it is believed that the cathode field characteristic of Fig. 1 is "universal" and applies also to other geometries, including those with external cathodes. Indeed, it seems to be a direct consequence of Poisson's equation. Probably the only restrictions on its application are those of negligible initial velocities and an equipotential cathode—the same conditions imposed on the generalized space charge law.[10] The calculated value of E assumes that the cathode is ideally smooth.

The universal cathode field characteristic can be applied very simply to electron emission measurements in the Schottky region. Here the current I, in a diode, is measured as a function of the anode voltage V. For purposes of analysis it is desired to know the current as a function of the electric field at the cathode. The

[7] M. E. Rose, Bartol Research Foundation, Contract OEMsr-385, First Progress Report, Supplement I (November 1942).

[8] Crank, Hartree, Ingham, and Sloane, Proc. Phys. Soc. (London) 51, 954 (1939).

[9] H. M. Schwartz, of the Bartol Foundation (communication from W. E. Danforth), has also suggested use of the data of Crank *et al.*

[10] I. Langmuir and K. T. Compton, Rev. Mod. Phys. 3, 251 (1931).

saturation current I_s corresponding to the applied voltage V can be calculated from the Child-Langmuir equation or from an extrapolation of an experimental Child-Langmuir plot, and the value of the cathode field in the absence of space charge, E_0 can be determined from the usual formulas of electrostatistics. The existing value of E can then be obtained directly from Fig. 1 and the measured value of the current I. No approximations are involved, and it is not necessary to sum a complicated series expansion.

As a further extension of the universal cathode field characteristic, consider now a diode with an emitter for which the Schottky effect is negligible so that for values of anode voltage V above the saturation voltage V_s corresponding to the temperature-limited emission I_0, the current is constant and equal to I_0. It is desired to find the variation in cathode field E as a function of V. For V less than V_s, the diode is completely space charge limited and E is zero. For V greater than V_s, the current I_0 is always less than the current I_s which would flow under complete space-charge limitation and is related to I_s by

$$I_s/I_0=(V/V_s)^{\frac{1}{2}}. \tag{29}$$

Here I_0 is analogous to I, the current flowing in the diode, of the previous considerations, so that

$$V/V_s=(I/I_s)^{-\frac{1}{2}}, \tag{30}$$

and (E/E_0) can be calculated as a function of (V/V_s) from the data of Fig. 1 giving (E/E_0) as dependent on (I/I_s).

The results of this calculation are given in Fig. 3. It is seen that under these conditions an anode voltage 5.4 times the saturation voltage is required to bring the cathode field to within 5 percent of its space-charge-free value, while the value to attain 98 percent of the zero-current field is ten times V_s.

In this section it has been assumed thus far that the saturation is ideal and that the Schottky effect (and also field emission) is negligible. If this is not the case, then the diode current will be increased over the value I_0 and the cathode field will always be less than that predicted by Fig. 3. This figure should therefore be interpreted in this case as giving the maximum cathode field which can exist in a diode as a function of the ratio of anode voltage to the voltage required to obtain maximum space-charge-limited emission (the "*MSCLE* point"). The exact value can be obtained, of course, from Fig. 1 as a function of the diode current.

V. SUMMARY

A method has been presented for calculating the electric field at the cathode of a diode under conditions of partial space charge. The results are shown by the "universal" characteristic of Fig. 1, which gives the cathode field as a function of the diode current and is in a particularly convenient form for use. An analytical expression has also been given for this universal characteristic (Eq. 17). The derivation has been applied only to plane and cylindrical diodes, but the results are believed to be applicable to any geometry. The only restrictions are an equipotential, smooth cathode and negligible initial velocities of emission. No approximations are involved in the derivation.

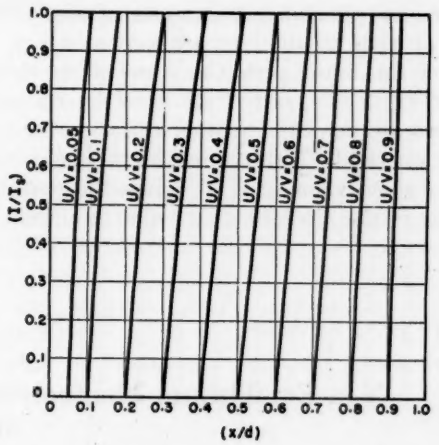

FIG. 4. Potential distribution in a plane diode.

The maximum cathode field is also plotted in Fig. 3 as a function of anode voltage. If the current saturation in the diode is ideal, this curve gives the correct value of the cathode field, but if this is not the case, the real value of field is less than that indicated.

Variation of the electric field at the anode of a plane diode with the diode current is shown in Fig. 2. The potential distribution in a plane diode under partial space-charge conditions can be obtained from Fig. 4 (see Appendix).

ACKNOWLEDGMENTS

This investigation of the cathode field in diodes was suggested by an approximate solution of the problem by Dr. J. G. Buck.[11] The writer is indebted to Dr. J. W. McNall, of this laboratory, for his advice and criticism concerning the presentation of the results.

APPENDIX

Potential Distribution in a Plane Diode

The analysis above also permits determination of the complete potential distribution in a plane diode. The quantity B, defined as

$$B=(x/d)^2(I/I_s), \tag{31}$$

may be calculated from Eq. (15) as a function of u with the quantity (U/V) as a parameter. For $(U/V)=1.0$, by definition $(x/d)=1.0$, so that this case gives values of (I/I_s) corresponding to the various values of u. The position of a point x in the diode, expressed as (x/d), corresponding to given values of (U/V) and (I/I_s) can

[11] Coomes, Buck, and Petrauskas, Third Progress Report, Contract NObsr-30028, Physics Department, University of Notre Dame (March 19, 1948).

therefore be calculated by means of Eq. (31). The results of such calculations are shown in Fig. 4. The curves of this figure permit any one of the three variables (x/d), (U/V), and (I/I_s) to be determined if the other two are known. The intersection of the contours of constant (U/V) with the horizontal line corresponding to a given value of (I/I_s) gives the potential distribution in the diode for that value of current.

Note Added in Proof: Since this paper was submitted for publication it has been found that as early as 1920 G. Jaffe (Ann. d. Phys. **63**, 145) considered the plane diode under partial space-charge conditions and obtained an equation identical, except for notation, to Eq. (17) above. However, Jaffe did not express his results in the convenient manner of Fig. 1 nor did he consider the cylindrical diode.

PHYSICAL REVIEW VOLUME 76, NUMBER 4 AUGUST 15, 1949

Non-Equilibrium Phenomena in a Bose-Einstein Gas. I. Transmission of Second Sound

WILLIAM BAND
The Institute for the Study of Metals, The University of Chicago, Chicago, Illinois
(Received April 27, 1949)

A model Bose-Einstein gas is considered in which numerical perturbations in the population of the lowest state have a relaxation time that is long compared with the relaxation time for perturbations in the symmetry of the velocity distribution in the excited states. Oscillations of the population of the lowest state about its equilibrium value are transmitted as second sound waves. The velocity of transmission is found as a function of temperature below the lambda-point and compared with that of second sound in liquid helium. In the gas there is a temperature dependent coupling between pressure waves and thermal waves; the normal modes of propagation are mixed. The high speed mode is pure pressure wave near T_λ but goes over gradually to pure thermal wave as T goes down towards 0°K; the low speed mode is pure thermal wave near T_λ but goes over gradually to pure pressure wave as T goes down towards 0°K. For $T \ll T_\lambda$ the thermal wave has a higher speed of propagation than the pressure (ordinary sound) wave.

INTRODUCTION

In a recent paper[1] the formal first order perturbation theory of transport phenomena in a Bose-Einstein gas was considered. In that theory it was assumed that at every point in the gas the numerical populations of the various energy states accessible to the gas atoms remain equal to their equilibrium populations. In other words the regression of numerical fluctuations was assumed to be rapid compared with that of asymmetry fluctuations in the velocity distribution. This assumption is implicit in most applications of first-order perturbation theory in statistical mechanics and is probably valid in general. However, in the degenerate Bose-Einstein gas below a certain transition temperature the number of atoms in the lowest state becomes comparable with the total number of atoms in the gas. The general theory of fluctuations[2] then leads one to expect that the numerical fluctuations in the population of the lowest state become of major importance below the transition temperature. This may be seen in the following way.

The standard deviation Δn of the population of any one state from the mean population $\bar{n}$ is given by

$$\text{Fermi-Dirac gas} \quad \Delta n/\bar{n}=(1/\bar{n}-1)^{\frac{1}{2}},$$
$$\text{Bose-Einstein gas} \quad \Delta n/\bar{n}=(1/\bar{n}+1)^{\frac{1}{2}}.$$

At very low temperatures in the Fermi-Dirac gas $1/\bar{n}\rightarrow 1$ and the fluctuations tend to vanish as T approaches absolute zero. In the Bose-Einstein gas, on the other hand, the fluctuations remain of the order unity; in particular the lowest state has a population $n_0\rightarrow N$ as $T\rightarrow 0$ where N is the total number of atoms in the gas, and $\bar{n}_0$ is comparable with N immediately below the transition temperature T_λ. Thus

$$\Delta n_0/\bar{n}_0=1 \text{ for all } T<T_\lambda.$$

These finite fluctuations at low T would be of no importance if all the states had similar populations and were closely spaced in the energy spectrum; it could then be supposed that there would be no correlation between the fluctuations of neighboring states so that in any appreciable energy range there would be no appreciable fluctuation in the total population in that range. But if the system contains one state or one degenerate set of states, in the present case the single lowest state, with a population comparable with that of the whole gas and, therefore, enormous compared with the population of any other state, the finite value of $\Delta n_0/\bar{n}_0$ becomes extremely serious. For example, if a Gaussian distribution is assumed for the actual deviations of the population from its mean value, the fact that $\Delta n_0/\bar{n}_0=1$ means that the number of atoms in the lowest state may be 20 percent above or below the mean value for roughly 23 percent of the time. At tem-

[1] W. Band, Phys. Rev. **76**, 1937 (1949).
[2] R. H. Fowler, *Statistical Mechanics* (Cambridge University Press, London, 1936), Chapter 20.

peratures not more than 40 percent below T_λ there are already over one-half the atoms of the gas involved in this uncertainty.

The foregoing equations are exact only so long as $\bar{n}_0 \ll N$ because the fundamental theorems of statistical mechanics are exact only under this restriction. As soon as $\bar{n}_0$ becomes comparable with N it would be more appropriate to treat the lowest state as a separate phase and the above conclusions can hardly be accurate. The approximation is still good, however, if we are not too far below T_λ and comparatively large fluctuations are to be expected even well below the transition. Because the condensation into the lowest state occurs only in momentum space, these very large fluctuations have only secondary effects on the density of the same order of magnitude as the classical fluctuations near the critical point of a vapor.[3] Perhaps for this reason these large fluctuations in the Bose-Einstein gas have hitherto been regarded more as a mathematical curiosity than a physical reality. But if, for some reason, the relaxation time for these fluctuations happens to be long compared with the relaxation time for asymmetrical perturbations of the velocity distribution, then it is clear that such a situation would place the problem completely outside the scope of ordinary first-order perturbation theory and alter the whole character of transport phenomena to be expected in the assembly.

To make the mathematical problem as simple as possible, consider a quasi-ideal Bose-Einstein gas in which the lowest state is separated by a finite energy gap, say e_z from the next state, and let e_z be large (by a factor of the order 10) compared with the average spacing between adjacent levels.

With such a model it may reasonably be assumed that the relaxation time for re-adjustments of equilibrium following an imposed change in the populations of the lowest state is comparatively long.* We shall call this the population relaxation time. It will further be assumed that the model has the following convenient properties: let there be three relaxation times, τ_0 the population relaxation time for the lowest state, τ_a the asymmetry relaxation time for the velocity distribution in the whole gas, and τ_1 the mean population relaxation time for the individual excited states; it is assumed only that

$$\tau_0 \gg \tau_a \gg \tau_1. \qquad \text{(A)}$$

Under (A) there may conceivably occur physical processes for which significant times t lie well within the range $\tau_0 > t > \tau_a$. For such processes, which will be called "t-processes," the atoms in the lowest state will behave as an almost independent assembly having no appreciable interaction with the remainder of the gas, while the latter, which will be called the "high energy component," remains separately in equilibrium with respect to all external perturbations because of the relation $t > \tau_a \gg \tau_1$.

For t-processes this Bose-Einstein gas model behaves like a mixture of two fluids similar to the two fluid model proposed by Tisza[4] for his phenomenological theory of helium II.

The conditions under which this two-fluid model is applicable to the Bose-Einstein gas are, therefore, the following: first, there must exist three relaxation times of the type described under assumption (A), and secondly, (B) the mean population of the single low energy state or degenerate group of states must be large compared with that of any other single state.

Any physical system that conforms to conditions (A) and (B) will be superfluid for t-processes if the states of lowest energy can include particle transport.[5] Such a system may conform to (A) and (B) because it is a Bose-Einstein gas of the model here described. But there may be other physical systems that conform to (A) and (B) for entirely different reasons. In particular, electrons are known not to obey Einstein-Bose statistics, and yet assemblies of electrons can, under appropriate conditions, become superfluid. The statistics are evidently not in themselves basically decisive, but rather conditions (A) and (B) enunciated above, and it has to be determined in each case of superfluidity why the particular assembly happens to satisfy these conditions.

The calculations to be reported in the present paper were undertaken with the familiar idea that helium II may possibly happen to satisfy conditions (A) and (B) because the statistics applicable to the gas phase influence the behavior of the liquid phase in some way not yet fully understood. The results, namely the existence of second sound propagation of thermal waves in the Bose-Einstein gas, would appear to add to the gradually accumulating evidence that tends to support this point of view.

The proof that this model also yields supercon-

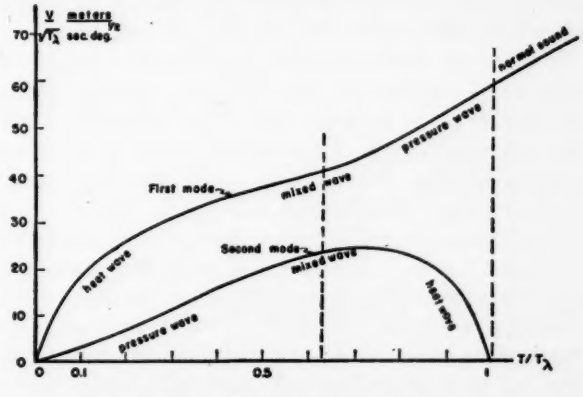

FIG. 1. Sound modes in B.-E. gas.

[3] L. I. Schiff, Phys. Rev. **57**, 844 (1940).

* In other words, it is assumed that the large energy gap reduces the transition probability between the lowest state and the other states, while no such anomaly on average exists between other pairs of adjacent states.

[4] L. Tisza, Phys. Rev. **72**, 838 (1947); Phys. Rev. **75**, 885 (1949).

[5] Compare K. Mendelssohn, Proc. Phys. Soc. London **LVII**, 371 (1945), and N. F. Mott, Phil. Mag. **40** 61 (1949).

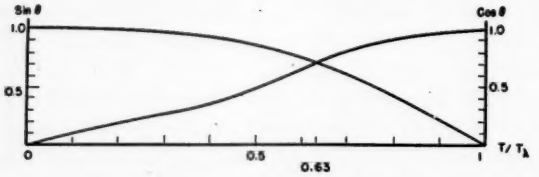

FIG. 2. Phase relation between superfluid and high energy component displacements in the normal modes of sound in B.-E. gas.

ductivity for heat of the same general character as that observed in helium II is reserved for a later paper.

In the first section of this paper some of the thermodynamic functions of the high energy component of the Bose-Einstein gas are calculated on the assumption that there does exist an equilibrium parameter λ_n and a temperature T_n defining the distribution in energy among the excited states, but that there does not exist any necessary relation between these parameters and the ratio ρ_s/ρ. In other words, three independent variables exist as required for t-processes in describing the assembly as a mixture of high and low energy components.

In the second section the Lagrangian for oscillatory t-processes is expressed in terms of the above thermodynamic functions with special reference to oscillations that carry the state of the assembly back and forth through an equilibrium center that would, if the ordered kinetic energy could be removed, correspond to an internal thermodynamic equilibrium. The Euler equations for this Lagrangian are the wave equations for first and second sound.

In the third section the velocities of propagation of the two modes of propagation are evaluated as functions of mean temperature, and in the last section the velocity of propagation of ordinary sound above the lambda-point is shown to be continuous with the curve for first sound at the lambda-point. Figure 1 shows the two curves calculated for the gas whose atoms are equal in mass to the helium atom. Both the shape of the curve and the magnitude of the velocity for second sound are remarkably like those observed in liquid helium.

It turns out that when the Lagrangian is expressed in terms of the most obvious variables—velocity of the mass center of the mixture and relative velocity between the two components, respectively—there is a strong coupling between the two. In other words, the normal modes of wave propagation are not in general pure pressure waves (mass center oscillations) and pure concentration waves (relative velocity oscillations). The coupling is removable formally by transforming to other variables, and mathematically this is equivalent to treating the two modes as plane polarized components that can each be resolved into two "directions," one a pure pressure and the other a pure concentration wave. Figure 2 shows the "polarizing angle" as a function of temperature. The first sound mode at T_λ is pure pressure wave and the second mode has zero phase velocity. As T drops below T_λ the "plane of polarization" of the first mode rotates gradually until at $T_1=0.63T_\lambda$ it is 45° which means that here the first mode involves both pressure and concentration changes in equal proportions. Below T_1 the first mode becomes predominantly concentration wave and as $T\to 0$ the proportion of pressure oscillation approaches zero. The second mode on the other hand starts at just below T_λ as almost pure concentration wave, passes through the neutral mixture at T_1 and becomes predominately pressure wave as T approaches zero.

This would mean, for example, that if a source of either pure pressure or pure heat oscillations were present in the gas, the latter would act like a doubly-refracting medium; in particular, if the temperature were near T_1, the two modes would carry roughly equal shares of the transmitted energy, and a "beat" phenomenon between the two might be possible.

It is particularly interesting to note that below T_1 the heat wave would propagate most of its energy in the high speed first mode, while the pressure wave would be found predominately in the lower speed second mode of propagation, thus reversing the relationship existing near the lambda-point.

If one tries to fit the Bose-Einstein gas model more closely to helium II by arbitrarily assigning to (ρ_n/ρ) a $(T/T_\lambda)^6$ law in place of the ideal $(T/T_\lambda)^4$ law, the present calculations yield the somewhat surprising result that second mode of propagation then has a pure imaginary phase velocity. In other words, such a model might simulate liquid helium in its C_v-curve, but it would fail to give second sound propagation.

NON-EQUILIBRIUM THERMODYNAMIC FUNCTIONS

Under conditions (A) of the last section, the high energy component of the Bose-Einstein gas below T_λ, considered separately, forms an assembly in internal equilibrium and the number of atoms in volume V is

$$N_n=V(2\pi mkT_n)^{\frac{3}{2}}h^{-3}\Lambda_n(1,\tfrac{3}{2}). \tag{2.1}$$

In this equation the expression $\Lambda_n(1,\frac{3}{2})$ is the same as $\Lambda(1,\frac{3}{2})$ of the previous paper,[1] written in terms of T_n and λ_n instead of T and λ; T_n is the temperature appropriate to the normal component separately, and λ_n is its logarithmic free energy. The expression $\Lambda_n(1,\frac{3}{2})$ is a series in powers of λ_n whose coefficients depend only on the quantity e_z/kT_n.

If the whole gas were in equilibrium, the low energy component would have the same λ and T. Actually the low energy component must always have $\lambda=1$. The radius of convergence of the λ_n-series in the expression $\Lambda_n(1,\frac{3}{2})$, however is at

$$\lambda_n=1/(1-e_z/kT_n)>1 \tag{2.2}$$

so that it is possible for λ_n to oscillate both above and below its equilibrium value of unity. It is interesting that the existence of the finite energy gap e_z is formally nec-

essary to permit oscillations about equilibrium, for if e_s were zero, λ_n would only vary *below* unity. The temperature and λ-values for the low energy component do not have to appear formally: given N/V, T_n and λ_n, the population N_s of the low energy state can always be calculated from the identity

$$N=N_n+N_s. \tag{2.3}$$

The energy per unit volume in the normal component is

$$E_n/V=(\tfrac{3}{2})kT_n(2\pi mkT_n)^{\frac{3}{2}}h^{-3}\Lambda_n(2, 5/2). \tag{2.4}$$

where $\Lambda_n(2, 5/2)$ is another λ-series defined in the first paper[1] and here expressed in terms of λ_n and T_n. The energy per excited particle is obtained from (2.4) and (2.1):

$$E_n/N_n=(3/2)kT_n\Lambda_n(2, 5/2)/\Lambda_n(1, 3/2). \tag{2.5}$$

It is clear that if both T_n and λ_n vary in such a way as to keep N_n constant, the energy E_n will vary, alternatively E_n could be kept fixed but then N_n will vary. In equilibrium λ_n would be determined at unity. Here fluctuations about equilibrium are being considered and evidently λ_n-1 may be regarded as a measure of departure from equilibrium.

The entropy of the high energy component may be defined as

$$S_n=k\sum_r \ln(1-\lambda_n e^{-\epsilon_r/kT_n})^{-1}+E_n/T_n-N_nk\ln\lambda_n \tag{2.6}$$

where the sum over ϵ_r extends from the lowest normal state upward. Since the state $\epsilon_0=0$ is excluded, the logarithm may be expanded

$$\ln(1-\lambda_n e^{-\epsilon_r/kT_n})^{-1}=\sum_{j=1}(1/j)\lambda_n{}^j e^{-j\epsilon_r/kT}$$

and it is easy to show that in terms of the notation used previously

$$S_n=kV(2\pi mkT_n)^{\frac{3}{2}}h^{-3}\Lambda_n(1, 5/2)\cdot +E_n/T_n-N_nk\ln\lambda_n. \tag{2.7}$$

The extra "j" factor in the denominator yields $\Lambda_n(1, 5/2)$ in place of $\Lambda_n(1, 3/2)$. Neglecting $N_nk\ln\lambda_n$ because λ_n is almost unity for all $T<T_\lambda$, (2.7) can be rewritten in the form

$$S_n/V=k(2\pi mkT_n)^{\frac{3}{2}}h^{-3}\{\Lambda_n(1, 5/2)+(3/2)\Lambda_n(2, 5/2)\}. \tag{2.8}$$

The entropy per excited particle, later needed, is obtained from (2.8) and (2.1), namely:

$$\sigma=S_n/N_n=k\{\Lambda_n(1, 5/2)+(3/2)\Lambda_n(2, 5/2)\}/\Lambda_n(1, 3/2). \tag{2.9}$$

This is a function both of T_n and λ_n; and again these two quantities may vary in such a way as to keep N_n constant, when of course σ will vary; or vice-versa T_n and λ_n may vary in such a way as to keep σ constant, when N_n will vary. Incidentally the value of σ under equilibrium for the whole gas, $T_n=T$ and $\lambda_n=1$ is

$$\sigma=\sigma_e=k\{\Lambda_e(1, 5/2)+(3/2)\Lambda_e(2, 5/2)\}/\Lambda_e(1, 3/2). \tag{2.10}$$

Here the Λ_e expressions are evaluated at $\lambda=1$, but they are still functions of T. Thus under equilibrium σ becomes a function of T only*** while in the absence of equilibrium both T_n and λ_n must be known to find σ.

The most obvious variables to choose in specifying a non-equilibrium state of the whole system are N/V, T_n, and λ_n. However, by using (2.9) and (2.1) all functions can be expressed at least formally in terms say of the three variables ρ, $x=\rho_n/\rho$, and σ, where $\rho_n=mN_n/V$ and $\rho=mN/V$.

THE LAGRANGIAN EQUATIONS FOR OSCILLATORY t-PROCESSES

In the foregoing argument an additional independent variable has been introduced which becomes dependent on the true thermodynamic state variables under the proper conditions. For convenience the ratio $x=\rho_n/\rho$ may be chosen as this new variable. Let S and V be the thermodynamic state variables and consider a three-dimensional space (S, V, x). The equilibrium dependency of x on S and V:

$$x=x(S, V). \tag{3.1}$$

Let the surroundings be such that the gas can be supplied heat or work without altering the temperature T or the pressure P of the surroundings, no matter how rapidly the exchanges may be effected. For slow changes the gas will also be kept at T and P, and the energy exchange is

$$\Delta_e E=T\Delta S-P\Delta V, \tag{3.2}$$

where ΔS and ΔV refer to the gas. During this displacement the representative point of the gas in (S, V, x)-space remains on the surface (3.1). Now consider an oscillatory exchange in which the surroundings lose entropy to the gas by an amount that fluctuates $\pm\Delta S_0$ while its volume varies $\pm\Delta V_0$. If this oscillation is at sufficiently low frequency the representative point of the gas traces out a curve in (3.1); but if the frequency is rapid enough it will trace out a curve that lies outside of this surface, intersecting it only at the "equilibrium center." The energy of the gas at one extreme of this oscillation can be expressed in terms of the three displacements ΔS, ΔV, Δx to second-order terms

$$\begin{aligned}\Delta E_1=&(\partial E/\partial S)_{xv}\Delta S+(\partial E/\partial V)_{xs}\Delta V+(\partial E/\partial x)_{sv}\Delta x\\&+\tfrac{1}{2}(\partial^2E/\partial S^2)_{xv}\Delta S^2+\tfrac{1}{2}(\partial^2E/\partial V^2)_{xs}\Delta V^2\\&+\tfrac{1}{2}(\partial^2E/\partial x^2)_{sv}\Delta x^2+(\partial^2E/\partial x\partial V)_s\Delta x\Delta V\\&+(\partial^2E/\partial x\partial S)_v\Delta x\Delta S+(\partial^2E/\partial S\partial V)_x\Delta S\Delta V.\end{aligned} \tag{3.3}$$

On the other hand the energy received from the surroundings is exactly

$$\Delta E_2=T\Delta S_0-P\Delta V_0, \tag{3.4}$$

*** The expressions Λ_e and therefore σ_e depend on T because e_s/kT differs from zero. If we neglect the energy gap, the entropy per particle σ becomes independent of T below the transition temperature, and for a first approximation in numerical calculation it is sufficiently accurate to replace (2.10) by

$$\sigma=(5/2)k\sum_{j=1}^{\infty}1/j^{5/2}\div\sum_{j=1}^{\infty}1/j^{3/2}=1.285k.$$

where $\Delta V_0 = -\Delta V$ exactly. The second-order terms in ΔE_2 are absent because under the "bath" conditions assumed in the surroundings T and P are independent of the displacements.

The additional work needed to drive the gas through the displacement $(\Delta S, \Delta V, \Delta x)$ is

$$\Delta W = \Delta E_1 - \Delta E_2. \tag{3.5}$$

This, in practice, must be obtained from the ordered kinetic energy present in the gas as it passes through the equilibrium center in the course of the oscillations. It is clear that the equilibrium center must, by definition, be such that the first order terms in ΔW vanish identically when ΔS, ΔV, ΔX are measured from that center. Thus,

$$-T\Delta S_0 + P\Delta V_0 = (\partial E/\partial S)_{xv}\Delta S + (\partial E/\partial V)_{xs}\Delta V + (\partial E/\partial x)_{sv}\Delta x. \tag{3.6}$$

This is essentially a projective relation between two vectors in (S, V, x)-space, one in the surface (3.1) and one lying in a direction intersecting that surface. The relation tells us the point on the surface towards which the gas in the non-equilibrium state $(\Delta S, \Delta V, \Delta x)$ tends to relax. In the present paper this relaxation question will not be discussed.

Using (3.6) in (3.5) remembering (3.3) we have

$$\Delta W = \tfrac{1}{2}(\partial^2 E/\partial S^2)_{xv}\Delta S^2 + \tfrac{1}{2}(\partial^2 E/\partial V^2)_{xs}\Delta V^2 + \tfrac{1}{2}(\partial^2 E/\partial x^2)_{sv}\Delta x^2 + (\partial^2 E/\partial x \partial V)_s \Delta x \Delta V + (\partial^2 E/\partial x \partial S)_v \Delta x \Delta S + (\partial^2 E/\partial S \partial V)_x \Delta S \Delta V. \tag{3.7}$$

To make use of this it is first necessary to transform the variables to σ, ρ and x in place of S, V, and x, $\sigma = S/x$ and $\rho = 1/V$. The calculation is elementary and it is found that

$$\Delta W = \tfrac{1}{2}(\partial^2 E/\partial \sigma^2)_{x\rho}\Delta\sigma^2 + \tfrac{1}{2}\{(\partial^2 E/\partial \rho^2)_{x\sigma} + (2/\rho)(\partial E/\partial \rho)_{x\sigma}\}\Delta\rho^2 + \tfrac{1}{2}(\partial^2 E/\partial x^2)_{\sigma\rho}\Delta x^2 + \{(\partial^2 E/\partial x \partial \sigma)_\rho - (1/x)(\partial E/\partial \sigma)_{\rho x}\}\Delta x \Delta\sigma + (\partial^2 E/\partial x \partial \rho)_\sigma \Delta x \Delta\rho + (\partial^2 E/\partial \sigma \partial \rho)_x \Delta\sigma \Delta\rho. \tag{3.8}$$

The present paper considers only the high frequency limit when $S \propto N_n$ so that $\Delta\sigma = 0$, implying absence of transitions between the two components. Thus

$$\Delta W = \tfrac{1}{2}\{(\partial^2 E/\partial \rho^2)_{x\sigma} + (2/\rho)(\partial E/\partial \rho)_{x\sigma}\}\Delta\rho^2 + \tfrac{1}{2}(\partial^2 E/\partial x^2)_{\sigma\rho}\Delta x^2 + (\partial^2 E/\partial x \partial \rho)_\sigma \Delta x \Delta\rho. \tag{3.9}$$

This has been written out on the assumption of complete absence of transitions between the two components, but in calculating the coefficients appearing in (3.9) full equilibrium will be assumed. This is the same approximation as used by Tisza[2] in his first derivation of second sound in helium II; in that work an error of some 15 percent resulted.[6] In the present problem the error will be similar with the difference between σ and σ_e; it vanishes with e_s/kT. On this understanding first approximations will be obtained for the various terms appearing in (3.9), writing E_n for E.

[6] W. Band and L. Meyer, Phys. Rev. **74**, 386 (1948).

To the approximation here accepted the Λ-sums in (2.1), (2.4) and (2.9) can also be regarded as constants. Then from (2.1)

$$x = \rho_n/\rho = (T_n/T_\lambda)^3 \doteqdot (T/T_\lambda)^3, \tag{3.10}$$

while from (2.4) $E_n\rho \propto T_n{}^{5/2}$. Therefore,

$$E_n \propto x^{5/3}/\rho, \tag{3.11}$$

where the constant of proportionality depends only on the mass of the atom, etc. From this relation

$$(\partial E_n/\partial \rho)_x = -E_n/\rho \quad \text{and} \quad (\partial^2 E_n/\partial \rho^2)_x = 2E_n/\rho^2,$$

so that

$$\tfrac{1}{2}(\partial^2 E_n/\partial \rho^2)_x + (1/\rho)(\partial E_n/\partial \rho) = 0. \tag{3.12}$$

Also, $(\partial E_n/\partial x)_\rho = (5/3)E_n/x$ so that

$$(\partial^2 E_n/\partial x^2)_\rho = (10/9)E_n/x^2, \tag{3.13}$$

and

$$(\partial^2 E_n/\partial x \partial \rho) = -(5/3)E_n/x\rho. \tag{3.14}$$

Let the displacement of the mass center of the mixture of low energy and high energy components be $\mathbf{Y}$ and that of the high energy component relative to the mass center be $\mathbf{X}$. Then make the transformation

$$\mathbf{Z} = (\rho_n/\rho_s)^{\frac{1}{2}}\mathbf{X}, \tag{3.15}$$

where ρ_s means the partial density, or mass per cm^3 due to the low energy component. Then the complete Lagrangian for unit mass of the mixture, namely, L = K.E. per gm$-\Delta W$ becomes:[6]

$$L = \tfrac{1}{2}\dot{\mathbf{Y}}^2 + \tfrac{1}{2}\dot{\mathbf{Z}}^2 + f(\nabla\cdot\mathbf{Y})^2 + g(\nabla\cdot\mathbf{Z})^2 + h(\nabla\cdot\mathbf{Y})(\nabla\cdot\mathbf{Z}), \tag{3.16}$$

where the coefficients f, g, h are constants expressed in terms of the partial derivatives (3.12)–(3.14) as follows:

$$\left.\begin{aligned} f &= -\tfrac{1}{2}\rho^2(\partial^2 E_n/\partial\rho^2)_x - \rho(\partial E_n/\partial\rho)_x - \tfrac{1}{2}x^2(\partial^2 E_n/\partial x^2)_\rho, \\ g &= -\tfrac{1}{2}x(1-x)(\partial^2 E_n/\partial x^2)_\rho, \\ h &= -[x(1-x)]^{\frac{1}{2}}\rho(\partial^2 E_n/\partial x \partial\rho) - 2x[x(1-x)]^{\frac{1}{2}}(\partial^2 E_n/\partial x^2)_\rho. \end{aligned}\right\} \tag{3.17}$$**

Using (3.12)–(3.14) in these relations

$$\left.\begin{aligned} f &= -5E_n/9 = -(5/6)P/\rho, \\ g &= -(5/6)[(1-x]P/\rho, \\ h &= -(5/6)[(1-x)/x]^{\frac{1}{2}}P/\rho. \end{aligned}\right\} \tag{3.18}$$

The h-term represents coupling between density and thermal fluctuations and it is evident that it is not generally small. It is, therefore, necessary to transform (3.16) so that the second quadratic form becomes diagonal while the kinetic energy form remains invariant. This can be done by means of a simple rotation in $\mathbf{Y}-\mathbf{Z}$ space:

$$\mathbf{Y} = \mathbf{Y}^* \cos\theta - \mathbf{Z}^* \sin\theta, \quad \mathbf{Z} = \mathbf{Z}^* \cos\theta + \mathbf{Y}^* \sin\theta, \tag{3.19}$$

where θ is a constant for a given equilibrium tem-

** See Eq. (C9) of reference 6 where the term in $(\partial E/\partial\rho)_x$ was inadvertently omitted.

perature and pressure, namely,

$$\tan 2\theta = h/(f-g). \tag{3.20}$$

The Lagrangian then becomes

$$L=\tfrac{1}{2}\dot{\mathbf{Y}}^{*2}+\tfrac{1}{2}\dot{\mathbf{Z}}^{*2}+F(\nabla\cdot\mathbf{Y}^{*})^2+G(\nabla\cdot\mathbf{Z}^{*})^2, \tag{3.21}$$

where

$$\begin{aligned} F&=f\cos^2\theta+g\sin^2\theta+h\sin\theta\cos\theta,\\ G&=g\cos^2\theta+f\sin^2\theta-h\sin\theta\cos\theta. \end{aligned} \tag{3.22}$$

THE TWO MODES OF SOUND PROPAGATION

The Lagrangian (3.21) gives Euler equations in the form of two-wave equations, one in terms of $\mathbf{Y}^*$ and the other in terms of $\mathbf{Z}^*$. The former will be called first sound, and roughly corresponds to normal sound; it has a velocity of propagation V_n given by

$$V_n^2=-2F, \tag{4.1}$$

and this happens to coincide with the velocity of normal sound at the lambda-transition, as will be proved later. The other form of wave propagation will be called second sound and has a velocity of propagation V_s given by

$$V_s^2=-2G. \tag{4.2}$$

The expressions (3.22) and (3.20) have to be examined to find the temperature dependence of the two velocities. After some manipulation it is found that

$$\left.\begin{aligned} F&=\tfrac{1}{2}(f+g)+\tfrac{1}{2}((f-g)^2+h^2)^{\frac{1}{2}},\\ G&=\tfrac{1}{2}(f+g)-\tfrac{1}{2}((f-g)^2+h^2)^{\frac{1}{2}}. \end{aligned}\right\} \tag{4.3}$$

Using (3.18) these can be expressed as follows:

$$\left.\begin{aligned} F&=-(5/12)(P/x\rho)\{1+(1-3x(1-x))^{\frac{1}{2}}\},\\ G&=-(5/12)(P/x\rho)\{1-(1-3x(1-x))^{\frac{1}{2}}\}. \end{aligned}\right\} \tag{4.4}$$

The following asymptotical expressions are of interest:

$$\left.\begin{aligned} T\to T_\lambda\quad & F\to-(5/6)P/\rho,\\ & G\to-(5/8)(1-x)P/\rho\to 0. \end{aligned}\right\} \tag{4.5}$$

$$\left.\begin{aligned} T\to 0\quad & F\to-(5/6)P/x\rho\to 0,\\ & G\to-(5/8)P/\rho\to 0. \end{aligned}\right\} \tag{4.6}$$

Figure 1 shows the two curves.

Just below T_λ first sound is almost pure pressure wave, but (3.19) and (3.20) show that as T falls, the proportion of thermal wave present in first sound increases until the temperature at which $f=g$, or $2\theta=\frac{1}{2}\pi$, $Y^*=(Y+Z)/\sqrt{2}$. This temperature is given by writing $f=g$ in (3.18): thus say $T=T_1$ when $(1-x)/x=1$, or $x=\frac{1}{2}$: $T_1=0.63T_\lambda$. Below this temperature first sound becomes predominately heat wave, while second sound becomes predominately pressure wave. The values of $\cos\theta$ and $\sin\theta$ as functions of temperature are plotted in Fig. 2.

The relation (3.19) is identical with that between two polarized components of light waves in an optically active medium. The difference of velocity between the two polarized components in the present case is, however, comparable with the velocity of both, instead of being small. If pure pressure fluctuations were produced by a source in the gas at some temperature in the neighborhood of T_1 it would split up into two "polarized" components on transmission in the gas, which would recombine at a receiver either as heat waves or as pressure waves, or as some mixture of the two, depending on the phase relation of the two components, i.e., on the length of the path at the receiver. A receiver sensitive only to thermal waves that could be moved along the direction of propagation, could be used to measure the coupling by observation of the "beats" between the two waves. The heat wave in this case would be of the type that carries only the kinetic energy of relative motion between the two fluid components alternately hotter and colder than the equilibrium temperature.[7]

It has occasionally been suggested that by suitable modification of the density of the lower energy states the Bose-Einstein gas could be made to behave more like He II in respect to the temperature dependence of the normal fluid concentration, namely to make

$$x=(T/T_\lambda)^k, \tag{4.7}$$

where k has a value somewhere in the neighborhood of 5 or 6. It is of interest to see what such a relation as this would do to the transmission of second sound in such a modified gas.

In order to simulate the equilibrium thermal properties of liquid helium it would also have to be assumed that the energy spectrum did not modify the relation

$$E_n\rho\propto xT$$

so that, using (4.7)

$$E_n\propto x^{(1+1/k)}/\rho \tag{4.8}$$

in place of (3.11). By the same type of argument as used before, it is now quite easily shown that

$$\begin{aligned} f=-\tfrac{1}{2}(1+k)E_n/k^2,\quad g=-\tfrac{1}{2}(1+k)(1-x)E_n/xk^2,\\ h=-(1+k)(2-k)[(1-x/x)]^{\frac{1}{2}}E_n/k^2. \end{aligned} \tag{4.9}$$

The discriminant of the quadratic form is $-\frac{1}{4}h^2+fg$ and if this is negative, the form reduces to two straight lines and is no longer positive definite; the velocity of transmission of the second sound would become purely imaginary. This restricts k to the range

$$3\geqslant k\geqslant 1.$$

The value 5.5 for k required to simulate the equilibrium properties of liquid helium would eliminate the possibility of second-sound transmission in the model.

Incidentally by choosing a model in which $k=2$ it is seen from (4.9) that coupling between the two modes would be zero, and first sound would be pure pressure waves and second sound would be pure heat waves at all temperatures. Second sound would have a higher velocity of transmission below T_1 than first sound,

[7] W. Band and L. Meyer, Non-Equilibrium States in He II, (communicated to Phys. Rev., April 4, 1949).

however, so that it would still be true that heat waves would travel faster than pressure waves at such low temperatures.

VELOCITY OF NORMAL SOUND ABOVE T_λ

To complete the study of this model it is desirable to know the behavior of the velocity of normal sound V just above T_λ. defined by the equation

$$V^2=(\partial P/\partial\rho)_S. \tag{5.1}$$

Neglecting the effect of the energy gap,

$$N/V=(2\pi mkT)^{\frac{3}{2}}h^{-3}\sum_{j=1}^{\infty}\lambda^j/j^{\frac{3}{2}}, \tag{5.2}$$

$$P=kT(2\pi mkT)^{\frac{3}{2}}h^{-3}\sum_{j=1}^{\infty}\lambda^j/j^{5/2}, \tag{5.3}$$

$$S=Nk\left\{(5/2)\sum_{j=1}^{\infty}\lambda^j/j^{5/2}\div\sum_{j=1}^{\infty}\lambda^j/j^{\frac{3}{2}}-\ln\lambda\right\}. \tag{5.4}$$

One needs to compute

$$(\partial P/\partial\rho)_S=(\partial P/\partial\rho)_T+(\partial P/\partial T)_\rho(dT/d\rho)_S. \tag{5.5}$$

Write (5.2) in the form

$$\sum_{j=1}^{\infty}\lambda^j/j^{\frac{3}{2}}=(\rho h^3/m)(2\pi mkT)^{-\frac{3}{2}},$$

then one can easily obtain the partial derivatives

$$(\partial\lambda/\partial\rho)_T=(\lambda/\rho)\sum_{j=1}^{\infty}\lambda^j/j^{\frac{3}{2}}\div\sum_{j=1}^{\infty}\lambda^j/j^{\frac{3}{2}}, \tag{5.6}$$

$$(\partial\lambda/\partial T)_\rho=-(3\lambda/2T)\sum_{j=1}^{\infty}\lambda^j/j^{\frac{3}{2}}\div\sum_{j=1}^{\infty}\lambda^j/j^{\frac{3}{2}}. \tag{5.7}$$

Using (5.6) one then derives from (5.3)

$$(\partial P/\partial\rho)_T=(kT/m)\Lambda(\tfrac{3}{2})/\Lambda(\tfrac{1}{2}), \tag{5.8}$$

and using (5.7) similarly obtains

$$(\partial P/\partial T)_\rho=(P/T)\times\{5/2-(3/2)\Lambda(3/2)^2/\Lambda(5/2)\Lambda(\tfrac{1}{2})\}. \tag{5.9}$$

Because

$$(dT/d\rho)_S=-(\partial S/\partial\rho)_T\div(\partial S/\partial T)_\rho \tag{5.10}$$

it follows from (5.4) that

$$(dT/d\rho)_S=-(\partial\lambda/\partial\rho)_T/(\partial\lambda/\partial T)_\rho=2T/3\rho. \tag{5.11}$$

Finally substituting (5.11), (5.9) and (5.8) into (5.5) after using (5.2) and (5.3) in the following form:

$$(kT/m)=(P/\rho)\Lambda(3/2)/\Lambda(5/2) \tag{5.12}$$

one finds

$$(\partial P/\partial\rho)_S=5P/3\rho,$$

or

$$V^2=(5/3)P/\rho. \tag{5.13}$$

This curve coincides with the velocity of first-sound at the lambda-point and has the same gradient.

It is of interest that isothermal sound, if it could exist, would theoretically have a velocity given by

$$V_{is}^2=(\partial P/\partial\rho)_T=(kT/m)\Lambda(\tfrac{3}{2})/\Lambda(\tfrac{1}{2})=(P/\rho)\Lambda(\tfrac{3}{2})^2/\Lambda(5.2)\Lambda(\tfrac{1}{2}). \tag{5.14}$$

But because $\Lambda(\frac{1}{2})$ diverges, as T goes down to T_λ the isothermal velocity would vanish at the lambda-point. Physically this is clear because at this temperature the pressure ceases to depend on the density and becomes a function only of the temperature: "*isothermal*" would then mean "*constant pressure*" and so would eliminate pressure waves.

The writer is very grateful to Dr. Lester Guttman and to Dr. Lothar Meyer for their helpful discussions.

Letters to the Editor

PUBLICATION of brief reports of important discoveries in physics may be secured by addressing them to this department. The closing date for this department is five weeks prior to the date of issue. No proof will be sent to the authors. The Board of Editors does not hold itself responsible for the opinions expressed by the correspondents. Communications should not exceed 600 words in length.

An Extension of the Theory of Mason and Matthias to the Low Temperature Transitions in $BaTiO_3$

H. J. WELLARD
H. H. Wills, Physical Laboratory, University of Bristol, England
June 3, 1949

THE notation of the original paper by Mason and Matthias[1] is here followed except that β_x, β_y, β_z are used to denote the Lorentz factors for the x, y, z crystallographic directions, and P_x, P_y, P_z always refer to permanent polarizations.

Mason and Matthias use the Boltzmann principle to derive the expression (Eq. (17) of their paper)

$$P_z=\frac{N\mu\sinh[(E_z+\beta_zP_z/1-\beta_z\gamma)\mu/kT]}{2+\cosh[(E_z+\beta_zP_z/1-\beta_z\gamma)\mu/kT]}$$

leading to the conclusion that for $E_z=0$ solutions other than $P_z=0$ can occur only if the function $A_z=[(\beta_zN\mu^2/1-\beta_z\gamma)1/kT]\geqslant 3$ giving the "Curie" temperature T_c.

They further derive a similar expression for P_y in the presence of the resulting spontaneous P_z (Eq. (40)) but go on to suggest after replacing the hyperbolic sine by its argument and the hyperbolic cosine by unity (Eq. (71) but replacing E_y by E_z) that no non-zero solutions are possible in the absence of an external field. However, if we consider the more exact Eq. (40) and put $E_y=0$ we obtain

$$P_y=\frac{N\mu\sinh[(\beta_yP_y/1-\beta_y\gamma)\mu/kT]}{1+\cosh[(\beta_zP_z/1-\beta_z\gamma)\mu/kT]+\cosh[(\beta_yP_y/1-\beta_y\gamma)\mu/kT]}. \quad (1)$$

We may write

$$A_y=\left[\left(\frac{\beta_yN\mu^2}{1-\beta_y\gamma}\right)\frac{1}{kT}\right],\quad A_z=\left[\left(\frac{\beta_zN\mu^2}{1-\beta_z\gamma}\right)\frac{1}{kT}\right] \text{ as above.}$$

$$\therefore\ \frac{P_y}{N\mu}=\frac{\sinh(A_yP_y/N\mu)}{1+\cosh(A_zP_z/N\mu)+\cosh(A_yP_y/N\mu)}\simeq\frac{\sinh(A_yP_y/N\mu)}{3\cdot6+\cosh(A_yP_y/N\mu)},$$

since

$$\cosh(A_zP_z/N\mu)\simeq 2\cdot6. \quad (2)$$

Hence solutions for $P_y\neq 0$ can occur if $A_y\geqslant 4$.

If we assume that $\beta_y=0.123$, we find that the critical temperature for the occurrence of a further spontaneous polarization P_y when P_z already exists is $T_2\simeq 275°K$.

We shall here assume that the system takes on the form given by the symmetrical solution $P_y=P_z$ and $A_y=A_z\geqslant 4$ as this is in accord with recent x-ray determinations of the symmetry of single crystals.[2] This implies an initial drop in P_z to about $\frac{3}{4}$ of its former value in order that Eq. (2) may remain unchanged. We have further

$$P_z=\frac{N\mu\sinh[(\beta_zP_z/1-\beta_z\gamma)\mu/kT]}{\cosh[(\beta_zP_z/1-\beta_z\gamma)\mu/kT]+\cosh[(\beta_yP_y/1-\beta_y\gamma)\mu/kT]+\cosh[(\beta_zP_z/1-\beta_z\gamma)\mu/kT]}.$$

Assuming that the mean value of β varies in accordance with Mason and Matthias, Fig. 11, that $A_y=A_z=4.1$ and that $P_y=P_z$ remains $\frac{3}{4}$ of the room temperature value we obtain

$$\frac{P_z}{N\mu}=\frac{\sinh(A_zP_z/N\mu)}{6\cdot4+\cosh(A_zP_z/N\mu)},\quad \text{where}\quad A_z=[(\beta_zN\mu^2/1-\beta_z\gamma)1/kT].$$

Hence there are solutions for $P_z\neq 0$ if $A_z\geqslant 4.8$, so that $T_3\simeq 180°K$ giving the critical temperature for occurrence of P_z. However, if we determine the critical temperature for three equal mutually perpendicular polarizations from the equation

$$P_z=\frac{N\mu\sinh[(\beta_zP_z/1-\beta_z\gamma)\mu/kT]}{3\cosh[(\beta_zP_z/1-\beta_z\gamma)\mu/kT]},$$

we find $T_3'\simeq 150°K$ using the same β-curve. This determines the temperature of break up of the rhombohedral form when heated from lower temperatures and would be expected to be greater than that calculated for the same transition on cooling and it therefore seems likely that the average value of β falls off slightly less rapidly as the temperature is lowered than Mason and Matthias indicate. A value of $\beta\simeq 0.11$ at 180°K gives agreement between the two values of $T_3\simeq(180°K)$.

The above solutions are the symmetrical ones and would presumably be the stable ones for an infinite single domain crystal but in any real crystal twinning and boundary effects will result in slight variations of the local field in different domains and even within a domain and this may well result in stability of slightly asymmetric solutions (i.e., $P_y=P_z+\delta P$, etc.) which would account for the diffuseness observed in x-ray reflections at low temperatures, particularly from polycrystalline specimens. This is confirmed by very accurate parameter measurements on "single" crystals in the region +18°C–40°C by the present author where it is found that the variations in spacing are essentially confined to the y–z plane of the above notation. These measurements will be published in detail subsequently.

It may be noted here that the theory depends essentially only on the existence of a dipole array having the assumed symmetry properties, the question as to whether this is the result of a titanium or oxygen ion shift or other charge displacement (e.g., covalent bonds) being irrelevant. The exact treatment when two or more polarizations occur together requires the solution of simultaneous equations; nevertheless the above simplified theory gives very satisfactory agreement with experiment.

[1] W. P. Mason and B. T. Matthias, Phys. Rev. **74**, 1622 (1948).
[2] Kay, Vousden, and Wellard, Nature **163**, 636 (1949).

A Note on Plasma Oscillation

J. R. PIERCE
Bell Telephone Laboratories, Murray Hill, New Jersey
July 1, 1949

IT is interesting to note that some of the plasma oscillation effects recently described in papers by Bohm and Gross[1,2] have been observed in vacuum tubes and were explained by a similar analysis.[3] Particularly, oscillations sometimes occur in the electron beams of traveling-wave tubes because of the presence of positive ions. The oscillations have discrete frequencies in the range of the estimated plasma frequencies of the ion clouds.

These oscillations were described in terms of an equation, (16) of reference 3, which is the one dimensional form of (7) of reference 1. An expansion similar to that of (10) of reference 1 was used in connection with the velocity distribution. While the effect of ion velocity on the rate of increase of the wave was considered, collisions were not taken into account in the analysis.

A case of a finite beam filling a tube and confined by a magnetic field was also analyzed. In such a case, the electron beam can excite not only plasma oscillations of the ions, but oscillations of ions in the magnetic field as well. These oscillations would usually have a lower frequency than plasma oscillations, and they were suggested as an explanation for lower frequency fluctuations which had been observed.

[1] D. Bohm and E. P. Gross, Phys. Rev. **75**, 1851 (1949).
[2] D. Bohm and E. P. Gross, Phys. Rev. **75**, 1864 (1949).
[3] J. R. Pierce, J. App. Phys. **19**, 231 (1948).

Note on Meson Production

H. W. LEWIS
University of California, Berkeley, California
May 6, 1949

IN an earlier paper,[1] formulas were derived, on the basis of the pseudoscalar meson theory, which describe the multiplicity and angular distribution of mesons produced in nuclear collisions involving extremely high energies. It is the purpose of this note to rewrite these formulas in such a way that they can somewhat more justifiably be applied to the region of intermediate primary energies (5–15 Bev). In this connection, we have in mind, in particular, comparison with the cloud-chamber experiments of Fretter.[2]

In this range one must consider the difference between γMc^2, the energy of the primary nucleon in the center of mass system, and ϵ, the largest energy it can lose in that system through meson production (called ϵ_{max} in M). We take $\epsilon=(\gamma-\alpha)Mc^2$, where α is a parameter which must probably be chosen between 1 and 2, and which represents, roughly, the energy below which a nucleon ceases to radiate mesons effectively. The only reason for the appearance of such a parameter is the high energy approximation made in M, and one can expect that a more careful theoretical calculation, expressly intended for the intermediate energy region, should serve to determine the best value of α, in the approximation in which one can make the cut-off in this crude way.

The multiplicity is, then, proportional to $\epsilon^{\frac{1}{4}}$, hence to $[(1+\gamma_0)^{\frac{1}{2}}-2^{\frac{1}{2}}\alpha]^{\frac{1}{4}}=F(\gamma_0)$, where $\gamma_0 Mc^2$ is the energy of the primary nucleon in the laboratory system.* To obtain the multiplicity, one must multiply this by a factor estimated in M to be about 4, and whose explicit expression is given there. $F(\gamma_0)$ is plotted in Fig. 1,

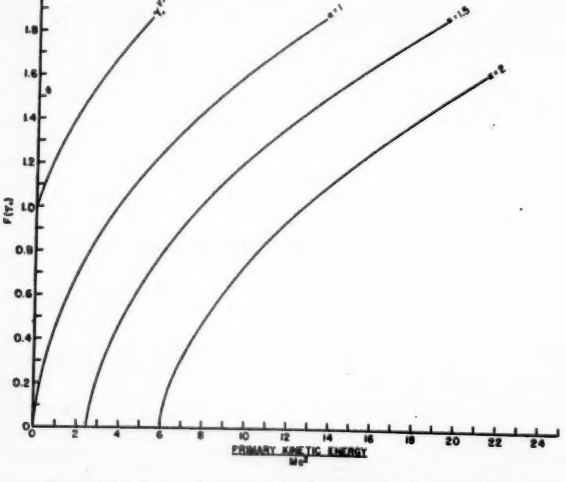

FIG. 1. $F(\gamma_0)$ as a function of primary kinetic energy. The most probable multiplicity is $\sim 4F(\gamma_0)$.

for three values of α, along with the asymptotic form $\gamma_0^{\frac{1}{4}}$. The failure of the asymptotic approximation, even for moderately high primary energies, should be noted.

The calculation of the mean square angular spread of the mesons leads to a number of superficial complications in integration. One can, however, obtain a rough estimate without undue effort, and finds $\overline{\vartheta^2}\approx 2/(1+\gamma_0)[1+\ln 2\gamma_0]$, with an accuracy of around 25 percent. An interesting feature of this result is its independence (to this approximation) of ϵ, and of the multiplicity, hence of α. One must be careful in applying this to a practical case, since the major contribution to the angular spread comes from slow mesons. Thus, for $\gamma_0=5$, if one were to leave out the contributions from mesons with kinetic energy below around 125 Mev, the factor in square brackets would be reduced to unity. This should be considered in the interpretation of an experiment.

It does not seem worth while to carry these calculations any further, particularly since the formulas given in M were not intended for the intermediate energy region, but also because of the inherent uncertainty of the underlying theory.

* $\gamma_0=2\gamma^2-1$.

[1] Lewis, Oppenheimer, and Wouthuysen, Phys. Rev. **73**, 127 (1948) hereinafter referred to as M.
[2] W. B. Fretter, Phys. Rev. **76**, 511 (1949).

Proximity Effects in the Measurement of Magnetic Susceptibility

M. C. STEELE
Naval Research Laboratory, Washington, D. C.
June 27, 1949

EXPERIMENTS have been performed to determine the effect of interaction between particles in measuring the magnetic susceptibility of suspensions containing superconducting spheres. The susceptibility was determined from the changes produced in the self-inductance of an air-core measuring coil when the suspension was introduced into the coil. The specimens were prepared from four different size-ranges of lead spheres (purity 99.9+ percent) dispersed in vaseline to give lead concentrations ranging from 1.7 percent to 9.3 percent by volume. All the samples were contained in Pyrex test tubes 5 cm long and 0.6 cm i.d. The magnetic field of the coil was parallel to the axis of the test tube in all cases. The diameter of the lead spheres ranged from 4.9×10^{-2} to 17.5×10^{-2} cm, so that the effect of penetration depth could be neglected.

The results are shown in Fig. 1, where χ/χ_0 is plotted as a

FIG. 1. Relation between χ/χ_0 and volume concentration. The points ⊡, △, ⊗ and ⊙ correspond to samples in which the diameter of the spheres ranged from 4.9 to 7.1×10^{-2} cm; 7.1 to 8.4×10^{-2} cm; 8.4 to 10.0 $\times10^{-2}$ cm; and 16.5 to 17.5×10^{-2} cm, respectively.

function of the lead volume concentration. χ is the apparent susceptibility of the lead spheres as obtained from the changes in self-inductance of the coil and χ_0 is the susceptibility of an ideal spherical superconductor when interaction is negligible.[1] It is to be noted that the line in Fig. 1 was made to pass through $\chi/\chi_0=1$ for zero percent volume, since this is a requirement for any curve relating these quantities. The deviation of each point from the line *drawn* in Fig. 1 is smaller than the over-all uncertainty in the corresponding experimental observations.

The relation between χ/χ_0 and concentration seems to be independent of the size of the spheres over the range used. Thus, it should be possible to utilize these results to correct the susceptibility measurements on samples containing much smaller spheres. For example, if the radius of the spheres was of the order of λ, the penetration depth, an appropriate correction could be made by determining the "effective" volume concentration. This "effective" concentration could be estimated by means of the London theory[2] if the radius of the spheres, R, and the order of the magnitude of λ are known.

[1] See D. Shoenberg, Proc. Roy. Soc. **A175**, 49 (1940).
[2] F. London, Physica **3**, 450 (1936).

Thermionic Electron Emission from Carbon

HENRY F. IVEY
Westinghouse Electric Corporation, Bloomfield, New Jersey
July 8, 1949

GLOCKLER and Sausville[1] have recently determined the thermionic constants for carbon, in the form of an extruded filament, as 4.35±0.06 ev for the electronic work function and 48±25 amp/cm² deg² for the Richardson constant, A. They state that these values are in good agreement with "the most recent determination reported in the literature," i.e., that of Reimann[2] (ϕ=4.34 ev, A=30 amp/cm² deg²). The purpose of this letter is to compare these results with other values published since Reimann's work and also with results obtained in this laboratory[3] on similar carbon filaments.

Braun and Busch[4] investigated the thermionic emission from a graphite rod and found ϕ=4.39 ev and A=15 amp/cm² deg². Using a graphite tube, Bhatnagar[5] found ϕ=4.84 ev but did not determine the A value. Bhatnagar also makes the interesting observation that the initial measurement of work function resulted in ϕ=3.4 ev, but that with continued heat treatment (100 hours) the value increased and approached 4.84 ev assymptotically. It should be noted that this final value is considerably higher than the other figures quoted above.

In the experiments here, a filament 0.0295-in. in diameter[6] was first outgassed in a separate tube by heating to a maximum temperature of 2525°K. At this temperature the vapor pressure[7] of carbon is about 2×10^{-4} mm Hg and in twenty minutes the walls of the tube were appreciably coated. This outgassing temperature is several hundred degrees hotter than that used by previous investigators. Following this treatment the filament was removed and mounted in a conventional tube with a cylindrical tantalum collector and guard rings for emission measurements. This tube was continually pumped and, after baking and outgassing the vacuum, was always at least a factor of ten better than the figure of 10^{-5} mm Hg reported by Glockler and Sausville for their tube which contained a ground-glass joint.

Three Richardson plots were made after the filament had been heated to various temperatures. The results are shown in Table I.

TABLE I. Thermionic constants as determined from three Richardson plots.

No.	Maximum Temperature (°K)	ϕ (ev)	A (amp/cm² deg²)
I	1610	4.44	22
II	2125	4.61	45
III	2335	4.59	48

The constants were calculated by the method of least squares. The temperature was measured with an optical pyrometer and the spectral emissivity was assumed to be 0.85. This is a good approximation to the temperature scale of Prescott and Hincke[8] used by Reimann and by Glockler and Sausville. As a matter of fact, the choice of spectral emissivity has very little effect on the value of the work function, but does affect the A value. For example, if uncorrected brightness temperatures are used to calculate the constants for measurements III above, the results are ϕ=4.61 ev and A=81 amp/cm² deg².

The last two measurements above, i.e., those taken after heating at a high temperature, agree very closely and give average values of ϕ=4.60 ev and A=46 amp/cm² deg². These values are considered to be a reliable determination of the thermionic constants of carbon. This value of work function lies about halfway between that of Bhatnagar and those of Reimann, Braun and Busch, and Glockler and Sausville, while the value obtained from measurement I at lower temperatures is closer to the latter values. This increase in work function with heat treatment is consistent with Bhatnagar's results, although it is to be noted that 200° increase in seasoning temperature between measurements II and III had little effect. It is also to be recalled that the filament had been pre-treated at an even higher temperature prior to the measurements.

It is also of interest to compare the emission current density obtained by the various investigators at some particular temperature. The results for 1500°K and 2000°K are tabulated in Table II where the emission from tungsten has been included for comparison. The emission measured here is lower than that obtained in any of the other investigations. This may be a result of the severe heat treatment used.

TABLE II. Comparison of the emission current density of carbon obtained by various investigators at 1500°K and 2000°K.

Investigator	ϕ (ev)	A (amp/cm² deg²)	J(μa/cm²) at T=1500°K	J(ma/cm²) at T=2000°K
Glockler and Sausville	4.35	48	0.28	2.2
Reimann	4.34	30	0.19	1.5
Braun and Busch	4.39	15	0.064	0.58
Ivey	4.60	46	0.039	0.50
Bhatnagar	4.84	—	—	—
(Tungsten)	(4.52)	(60)	(0.094)	(1.00)

In conclusion it may be of value to point out that Braun and Busch have interpreted their measurements as indicating that carbon is a degenerate excess semiconductor whose surface barrier lies 4.56 ev above the bottom of the conduction band and which has approximately 1×10^{20} defects/cm³. If the data for measurement III above are analyzed in a similar manner, the corresponding values are 4.77 ev and 7×10^{20} defects/cm³, or about one defect for 160 atoms.

[1] G. Glockler and J. W. Sausville, J. Electrochem. Soc. **95**, 292 (1949).
[2] A. L. Reimann, Proc. Phys. Soc. London **50**, 496 (1938).
[3] The experiments referred to were performed under Contract No. W-36-039-sc-33643 with the U. S. Army Signal Corps Engineering Laboratories and carried out during February, 1949.
[4] A. Braun and G. Busch, Helv. Phys. Acta **20**, 33 (1947).
[5] A. S. Bhatnagar, Proc. Nat. Acad. Sci. India **A14**, 5 (1944).
[6] These filaments were obtained from the F. J. Rooney Electrical Supply Company, Hoboken, New Jersey.
[7] W. Espe and M. Knoll, *Werkstoffkunde der Hochvakuumtechnik* (Verlag. Julius Springer, Berlin, 1936), p. 359.
[8] C. H. Prescott and W. B. Hincke, Phys. Rev. **31**, 130 (1928).

Beta-Ray Spectra

H. J. LIPKIN
Palmer Physical Laboratory, Princeton University, Princeton, New Jersey
June 27, 1949

THE following unsuccessful attempt was made to account for the prevalence of beta-ray spectra, experimentally found to have the allowed shape, in cases where the *ft*-value would indicate a forbidden transition:

Consider a third order transition having the following inermediate states:

1. Emission of an electron and a neutrino with the nucleus going to an excited state of the residual nucleus of such spin and parity that the transition is allowed.
2. Emission of a photon as the nucleus goes to the ground state.

The transition to the final state is achieved by absorption of the photon by the electron.

A rough calculation, using non-relativistic wave functions, was made for the case $\Delta J=3$, with $\Delta J=1$ for the transition to the first intermediate state and $\Delta J=2$ for the transition from the first to the second. The spectrum obtained for this process differed from the allowed spectrum by a factor of p^4, where p is the momentum of the emitted electron. Thus the number of electrons emitted with kinetic energy between E and $E+dE$ would be proportional to the allowed spectrum multiplied by the factor p^4. This spectrum is shifted toward the high energy end, and differs considerably from the experimentally measured spectra.

The writer wishes to express his appreciation to Professor E. P. Wigner for his assistance and suggestions.

Two-Component Wave Equations

C. W. KILMISTER
Queen Mary College, London, England
July 6, 1949

IN a recent letter Jehle[1] has considered a two-component wave equation; it is of interest to know the relationship of such equations to Dirac's equations. The object of this letter is to show that by modifying Eddington's[2] method of deriving Dirac's equations we can obtain an equation additional to Dirac's and simpler in form, which may, under certain circumstances, be put in two-component form. This differs somewhat from Jehle's equation, but its derivation suggests that it is the two-component equation most likely to have physical interest.

It is convenient to use quaternion notation; f_i, $(i=1, 2, 3)$, are the usual quaternion units, and $f_0=i$. For a quaternion q, where

$$q=q^k f_k,$$

we write

$$Sq=q^0 f_0, \quad Vq=q-Sq.$$

When the position quaternion,

$$q=x^k f_k \tag{1}$$

undergoes the orthogonal transformation

$$q'=aqb, \quad (|a|=|b|=1), \tag{2}$$

a "wave quaternion," ψ, is defined as one which undergoes the transformation,

$$\psi'=a\psi.$$

If φ is any other quaternion and

$$p=V\cdot\psi\varphi, \quad q=V\cdot\varphi\psi, \tag{3}$$

the obvious identities

$$p\psi=\psi q, \quad \varphi p=q\varphi, \tag{4}$$

are equivalent to Eddington's[3] simple wave equation; and their covariance under (2) is equivalent to

$$P'=apa^{-1}, \quad q'=q, \quad \overline{\varphi}'=a\overline{\varphi}, \tag{5}$$

where $\overline{\varphi}$ is the conjugate quaternion to φ.

The divergence of a mixed (see Silberstein[4]) quaternion, j, is the invariant

$$\mathrm{div} j=S(\partial j/\partial x^0-\nabla j); \tag{6}$$

since the four quaternions,

$$j(\alpha)=S\cdot(\psi f_\alpha\varphi)+V\cdot\psi\varphi, \quad (\alpha=0\cdots3), \tag{7}$$

are mixed, the identification of one of them with the four-dimensional probability vector is suggested. Using (6) leads to the equations

$$\nabla\psi-(\partial\psi/\partial x^0)f_\alpha=M\psi, \quad \varphi\nabla'-f_\alpha(\partial\varphi/\partial x^0)=-\bar{M}\varphi, \tag{8}$$

where M is a linear quaternion function of a quaternion, $\bar{M}$ its conjugate (Hamilton[5]) and under field-free conditions M, $\bar{M}$ have special forms so that iteration produces the second-order wave equation. *If $\alpha\neq0$, these are identical with Dirac's equations* as written by Conway,[6] and are well known to admit a 4×4 matrix representation. *If* $\alpha=0$, *however*, the ψ-equation, for instance, becomes

$$\nabla\psi-i(\partial\psi/\partial x^0)=M\psi, \tag{9}$$

or, it may be written

$$f^k(\partial\psi/\partial x^k)=-M\psi, \tag{10}$$

where

$$f^k=g^{k\lambda}f_\lambda=\bar{f}_k, \quad \tfrac{1}{2}(f^k\bar{f}^\lambda+f^\lambda\bar{f}^k)=S(f^k\bar{f}^\lambda)=-g^{k\lambda}. \tag{11}$$

The special form of the left-hand side of (10) allows of a 2×2 matrix representation of the f^k, and ψ is then represented as a two-component column matrix. Such a representation of M is not, in general, possible, but when it is, a two-component equation is true. One such possibility, suggested by considering the case when ψ has real quaternion components (i.e., $S\cdot\psi f_i$), $(i=1\cdots3)$, $S\cdot\psi$, real), is the equation, where now f^k and λ, μ, ψ represent matrices,

$$f^k(\partial\psi/\partial x^k)=\lambda\psi+\mu\psi^*. \tag{12}$$

Under field-free conditions iteration must give the usual wave equation; this requires $\lambda=0$, and if we choose the representation

$$f_1=\begin{pmatrix} i & \cdot \\ \cdot & -i \end{pmatrix}, \quad f_2=\begin{pmatrix} \cdot & -1 \\ 1 & \cdot \end{pmatrix}, \quad f_3=\begin{pmatrix} \cdot & -i \\ -i & \cdot \end{pmatrix}, \tag{13}$$

then

$$\mu=\nu f_2,$$

where ν is a scalar. Writing now

$$f^2 f^k=\gamma^k, \quad \lambda=\lambda_k\gamma^k, \tag{14}$$

we find that

$$\overline{\gamma}^k=-\gamma^k \text{ for } k\neq2, \quad \overline{\gamma}^2=\gamma^2,$$

and the γ^k obey the same rules as the f^k. The equation becomes

$$\gamma^k[(\partial/\partial x^k)-\gamma_k]\psi=\nu\psi^*,$$

where the λ_k describe the applied field. Jehle's choice of a special form for s^k, involving complex conjugates, restricts the λ_k to the form, $i\varphi_k$, which he considers; however, Eddington[7] has remarked that, in Dirac's theory, this is an unnecessary survival of Hermitic conditions from the Schrödinger theory, and it seems as if the same should apply here.

[1] H. Jehle, Phys. Rev. **75**, 1609 (1949).
[2] Sir A. S. Eddington, *Relativity Theory of Protons and Electrons* (Cambridge University Press, London, 1936), §8.2.
[3] Reference 2, §5.4.
[4] L. Silberstein, Phil. Mag. (6) **23**, 798 (1912), Eq. (13).
[5] Sir W. R. Hamilton, *Elements of Quaternions* (Longmans Green and Company, New York, 1866).
[6] A. W. Conway, Proc. Roy. Soc. **(A)162**, 147) 1937).
[7] Reference 2, p. 131.

On the Temperature Dependence of Counter Characteristics in Self-Quenching G-M Counters*

OM PARKASH
E.P.U. Physics Department, Government College, Hoshiarpur (E.P.), India
July 5, 1949

IT has been reported[1] that the self-quenching counters, usually employing argon or some other gas mixed with some organic vapor, show a temperature dependence of their counting rate which can be sometimes troublesome. Korff, Spatz, and Hilberry[2] during their experiments on argon-alcohol counters found a marked dependence of the counting rate on temperature. They also found that the plateau disappeared at lower temperatures. Putman,[3] in trying to eliminate variations of counting rate with temperature, found that there is a bodily shifting of the plateau towards high operating potentials as the temperature was increased. In his case, however, when the plateau was flattened with an external quenching circuit, the counting rate became largely independent of temperature.

The temperature dependence of the counting rate has been explained in terms of the action of the quenching vapors in a counter. Most of the organic compounds are vapors at room temperature. At lower temperature, however, some of these will condense out with the following result: (1) There may be insufficient quenching vapor left. Under such conditions, the number of vapor molecules and consequently the effect of quenching will depend on temperature. (2) The liquid might condense near the electrodes in such a way as to cause semi-conducting paths across the insulating material between the wire and the cylinder. Leakage across such paths can manifest itself as spurious counts. It is therefore very important to know the range of temperatures within which we can safely use the G-M counters, and the present investigation was undertaken to this effect.

Two counters were chosen, one with internal and the other with external cathode. The counter with internal cathode, prepared in this laboratory, is a usual type of glass enveloped counter with a thin oxidized copper cylinder cathode, filled with commercial

argon at 8.5 cm and absolute alcohol (100 percent pure) at 1.5 cm, to a total pressure of 10 cm of mercury, the temperature at the time of filling being 33–34°C. The second is a thin walled glass counter[4] of the self-quenching type with external cathode consisting of a thin layer of graphite. (This counter was brought by Dr. P. S. Gill from Paris and was given to Dr. H. R. Sarna of the East Punajb University. The author is grateful to Dr. Sarna for lending this counter for the present investigation.) The counters could be heated or cooled in a suitable enclosure to different temperatures and maintained constant within ±0.2°C by means of a simple thermostat constructed in this laboratory. The total range of variation extended from 8°C to 60°C. A number of plateau curves were obtained at different temperatures for the two tubes (Fig. 1).

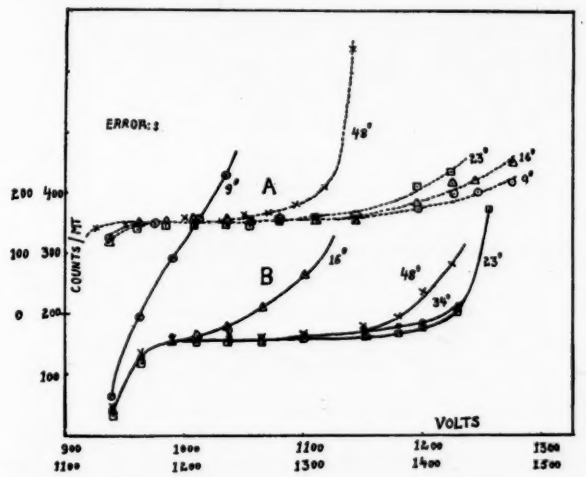

FIG. 1. The temperature dependence of the plateau curves for (A) external cathode and (B) internal cathode G-M counters.

It is clear from the figure that in the case of a counter with external cathode, there has been practically no change in the counting rate within this temperature range, while with the other counter with internal cathode there has been a marked effect near the lower temperatures. In the latter case as well, the counting rate remains independent within about 18° to 60°C; however, below 18°C the plateau has decreased and disappeared at about 9°C. Further it is also clear that the plateau curve becomes flatter at lower temperatures, while there is a definite increase in slope of the plateau at higher temperatures together with a decrease in over-all width of the plateau, possibly due to increase in the number of spurious counts at higher temperatures. (This point is being investigated.) The decrease in plateau width and its disappearance at lower temperatures in the case of a counter with internal cathode might be explained on the supposition that some of the quenching vapor condenses forming semi-conducting paths between the cathode and the central wire, thus giving rise to spurious counts. In the case of the counter with external cathode there is no possibility of such conducting paths and hence no such effect. The extent to which the decrease in the partial pressure of the quenching vapor is responsible for this change will be discussed and a full account of the present investigation published later.

The author is very grateful to Dr. P. L. Kapur, Reader in Physics, Delhi University, Delhi, India, who provided all the facilities for this work. Without his help this work would not have been possible.

* The work was completed in the Delhi University Physics Laboratories, Delhi, India.

[1] S. A. Korff, *Electron and Nuclear Counters* (D. Van Nostrand Company, Inc., New York, 1948).
[2] Korff, Spatz, and Hilberry, Rev. Sci. Inst. **13**, 127 (1948).
[3] J. L. Putman, Proc. Phys. Soc. London **61**, 312 (1948).
[4] Roland Maze, J. de phys. et rad. **7**, 164 (1946).

On the Latitude Dependence of Nuclear Disintegrations and Neutrons at 30,000 Feet*

J. A. SIMPSON, JR. AND R. B. URETZ
Institute for Nuclear Studies, University of Chicago, Chicago, Illinois
July 5, 1949

PRELIMINARY measurements of the change in the rate of production of low energy nuclear disintegrations between geomagnetic latitudes 40°N and 55°N have been made at 30,000 feet pressure altitude in a B-29 aircraft using electron collection ionization pulse chambers. Since both fast and thermal neutrons in the atmosphere at this altitude display a latitude dependence much larger (Fig. 1) than for other components observed in the

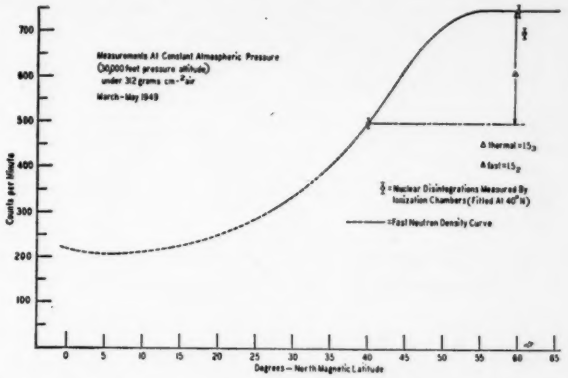
Measurements At Constant Atmospheric Pressure
(30,000 feet pressure altitude)
under 312 grams cm⁻² air
March–May 1949
Δ thermal = 15%
Δ fast = 15%
= Nuclear Disintegrations Measured By Ionization Chambers (Fitted At 40° N)
= Fast Neutron Density Curve
Counts per Minute
Degrees — North Magnetic Latitude

FIG. 1. Comparison of the latitude dependence of nuclear disintegrations and neutrons at 30,000 feet.

cosmic radiation,[1,2] a measurement of nuclear disintegration rates may indicate the extent to which the observed neutrons are associated with these nuclear disintegrations or "star" events.

Two identical thin wall ionization chambers filled with 6 atmospheres of highly purified argon (similar to those used at Los Alamos and by Bridge, Rossi, and co-workers[3]) were operated using fast, linear amplifiers with their output pulses mixed in a non-loading circuit before sorting pulse sizes in a multi-channel pulse height analyzer. The ionization chambers were separated so that the probability of a nuclear event being simultaneously detected in both chambers was negligible.[3] Three G-M counter trays were located to cover a shower area of 1.5 m² including the area occupied by the ionization chambers. They were connected to a three-fold shower recording circuit, and this circuit was, in turn, connected to one of the ion chamber pulse height discriminator channels to form four-fold coincidences.

To determine the absolute energy loss in a chamber due to a nuclear event, the maximum pulse size from a retractable polonium alpha-particle source in the chamber was used as a standard to calibrate the pulse discriminator circuits. A linear oscilloscope deflection system and electronic pulsing circuit provided bias calibrations from 0.8 to 2.0×Po alpha-pulse maximum. The system was recalibrated in intervals of not more than two hours with consequent discriminator bias drifts less than ±5 percent. All data were recorded both manually and by photographic film recording. Test intervals to search for spurious pulses due to vibration or electrical pick-up showed that no spurious pulses were observed on any of the flights.

The results at 40°N geomagnetic latitude in Table I show the reproducibility of results over the period of several weeks in which the flights occurred. The same kind of measurements are given in Table II for latitudes greater than 55° (the aircraft was flown to 65°N). It will be noted that Flight No. 3 gives consistently lower values than Flight No. 4. This might be explained as the kind of variation in time previously found for the fast neutrons.[2]

The latitude factor of increase between 40° and 55° has been calculated separately for Flight No. 3 and Flight No. 4 in Table III.

TABLE I. Nuclear disintegrations at 30,000 feet pressure altitude (312 gms air) at 40° magnetic latitude.

Mev energy loss in chambers	Flight No. 2 Total no. of events	Flight No. 2 Events per hour	Flight No. 6 Total no. of events	Flight No. 6 Events per hour	Flight No. 7 Events per hour	Average events per hour
>4.2	···	···	···	···	1412±38	1412±38
>5.8 }	834	535±19	1024	512±15	525±23 }	514±11
>5.8 } two channels	816	523±18	955	477±15	··· }	
>6.9	525	338±14	653	326±13	334±19	332±9
>8.0	418	268±13	479	239±11	···	252±8
>10.6	252	162±10	···	···	140±12	153±8

TABLE II. Nuclear disintegrations at 30,000 feet pressure altitude (312 gms air) at magnetic latitudes greater than 55° north.

Mev energy loss in chambers	Flight No. 3 Total no. of events	Flight No. 3 Events per hour	Flight No. 4 Total no. of events	Flight No. 4 Events per hour
>5.8	1893	644±15	1588	794±20
>5.8	2028	689±15	1520	760±19
>6.9	1371	467±12	1023	511±16
>8.0	1050	357±11	···	···
>10.6	566 in 134 min.	253±11	458	229±10

TABLE III. Factor of increase L of nuclear disintegration rate between 40° and 55°N magnetic latitude at 30,000 ft. pressure altitude.

Integral Mev energy loss in chambers	Using flight No. 3 and table C	Using flight No. 4 and table C	Fast or slow neutrons
	L	L	
>5.8	1.30	1.49	
>6.9	1.41	1.54	1.5
>8.0	1.42	···	
>10.6	1.65	1.51	

In addition to these measurements the production of showers was measured by covering the chambers with lead hemi-cylinders 2.5 cm thick corresponding approximately to the optimum thickness for maximum electronic shower production.[4] The number of events observed with lead over the chamber divided by the number of nuclear events without the lead may be called R; R at 55° has an average value of 1.9 and at 40° has a value of 2.4. Using these ratios and the observed latitude factor of increase for nuclear events from Table III, it is found that the number of events produced by the lead shows little or no decrease in going from 55° to 40°. This is in substantial agreement with the observed three-fold shower coincidences and present knowledge of the latitude dependence of electronic showers.[5] It was shown by measurements with additional absorbers around the ion chambers that the contribution of nuclear disintegrations in the lead to the chamber counting rate was negligible.

The dependence of nuclear bursts upon *altitude* at 55° was in agreement with the burst measurements of Bridge[3] and the production of neutrons in air.[1]

Measurements of both thermal neutrons and moderately fast neutrons were made concurrently with the ion chamber measurements. Since these neutrons were slowed down before detection they are incoherent; therefore, a comparison of the latitude factors for neutrons and for nuclear disintegrations is only significant when a wide range of energy losses in the chambers is measured at the different latitudes. Thus, the integral rates have been used in Tables I, II and III.

In Fig. 1 the ion chamber data have been fitted to the fast neutron latitude curve at 40°. This curve is characteristic of a nucleonic component in the cosmic-radiations particularly with respect to the factor of increase of 1.4 to 1.5 between 40° and 55°N at 30,000 feet. Although recently Tongiorgi[6] has found that neutrons are produced in extensive showers, the present experiment indicates that the most predominant process for the formation of most of the neutrons in the atmosphere with energies below 20 Mev appears to be the emission of neutrons and protons from nuclear disintegration or "star" events. These star events, in turn, may be produced predominantly by higher energy nucleons.[1]

Additional flights to the magnetic equator were not entirely successful due to equipment failures at the low latitudes. However, more than a three fold-increase in nuclear disintegration rate between 0° and 55°N magnetic latitude has been obtained and is to be compared with a factor of 3.5 for the neutron densities. Measurements at the low latitudes are being repeated.

The authors wish to thank Mr. Stanley Molner for assisting on the flights. The excellent cooperation of the U. S. Air Force personnel, particularly Major W. Gustafson, was greatly appreciated.

* Supported in part by the ONR.

[1] J. A. Simpson, Phys. Rev. **73**, 1389 (1948).
[2] Simpson, Baldwin, and Uretz, Phys. Rev. **76**, 165 (1949).
[3] Bridge, Hazen, Rossi, and Williams, Phys. Rev. **74**, 1083 (1948).
[4] B. Rossi, Rev. Mod. Phys. **20**, 537 (1948).
[5] H. L. Kraybill and P. J. Ovrebo, Phys. Rev. **72**, 351 (1947) and private communication.
[6] V. Cocconi Tongiorgi, Phys. Rev. **75**, 1532 (1949).

The Penetration of High Energy Electrons in Aluminum*

F. L. HEREFORD† AND C. P. SWANN
Bartol Research Foundation of The Franklin Institute, Swarthmore, Pennsylvania
July 8, 1949

PREVIOUS determinations of the range of monoenergetic electrons in matter have extended up to electron energies of 2.6 Mev. These data as well as measurements of the end points of beta-ray spectra have served as the basis for various empirical range-energy relations.[1-3] In the absence of experimental data at higher energies Fowler, Lauritsen, and Lauritsen[4] have carried through a calculation extending these results to 25 Mev. They integrate the theoretical energy loss in aluminum adjusting the integration constant to yield normalization with Bleuler and Zunti's semi-empirical relation at 3 Mev.[2] Despite the fact that radiation losses introduce straggling at higher energies, the concept of maximum range in the region which they consider remains defined. For moderate energies ($<800/Z$ Mev) an appreciable fraction of electrons will not experience radiative collisions and hence will penetrate to the maximum depth allowed by ionization losses. Though the curve given by Fowler, *et al.* is for maximum range (R_0) *versus* electron energy, they also give an expression for the *practical* maximum range (R_p). This latter quantity, which is obtained by straight line extrapolation of the linear portion of the absorption curve of a monoenergetic electron beam is the most conveniently measurable range in practice. According to Bleuler and Zunti it is less than the maximum range (R_0) of a monoenergetic beam by 0.14 g/cm² Al.

In order to check the calculations of Fowler, *et al.*, we have carried through measurements of the absorption in aluminum of monoenergetic electrons in the range from 3 to 12 Mev. To this end we have used the B^{12} beta-spectrum (produced through the $B^{11}(d,p)B^{12}$ reaction) analyzed by the 90 degree magnet normally used for the Van de Graaff beam (resolution ~4 percent). Using a triple coincidence train of G-M counters, absorption curves in aluminum of the analyzed beam were obtained. Calibration of the magnetic analyzer was checked by running the B^{12} momentum spectrum and matching the distribution with that given by Hornyak, Dougherty, and Lauritsen.[5] A Kurie plot of the data yielded an end point at total energy 27.3 m_0c^2 (13.4 Mev). The excellent agreement with the result of Hornyak, *et al.* (27.30 m_0c^2) is added assurance that the energy values subsequently used in the range measurements are correct.

In determining the absorption curves threefold (1, 2, 3) and twofold (1, 2) coincidences were recorded simultaneously with the aluminum absorbers placed immediately in front of counter 3 (Fig. 1). The twofold coincidence rate was employed to monitor

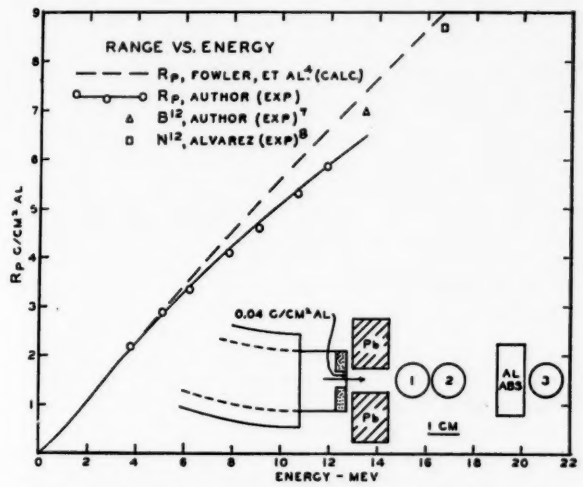

FIG. 1. The practical maximum range in aluminum (R_p) *versus* electron energy. The counter arrangement relative to the magnetic analyzer is shown in the lower right corner.

the electron beam emerging through the 0.04 g/cm² aluminum window of the spectrometer. The results yielded a family of absorption curves (corrected for counter wall thicknesses) for various electron energies selected by the spectrometer. The shape of these curves agreed well with that of computed curves[4] and the linearity near the end point allowed accurate determination of the practical maximum range. These values of R_p are shown in Fig. 1 plotted against the corresponding electron energies.

It is seen that in the high energy region the experimental points indicate a practical range somewhat less than that expected on the basis of the theoretical energy loss (dotted line). It seems likely that this may be due to two factors: (1) several cloud chamber investigations[6] have provided evidence that the energy loss of electrons traversing thin foils is greater than that predicted by theory by as much as 40 percent in the region of energy involved here, (2) multiple scattering effects have been shown to give rise to actual path lengths through absorbers which are appreciably greater than the absorber thickness.[6]

Corrected to maximum range ($R_0=R_p+0.14$ g/cm²), the solid curve should be satisfactory for energy measurements of monoenergetic gamma-rays by coincidence absorption as outlined in reference 4. However, the data do not necessarily furnish a range-energy curve suitable for end point measurements of beta-ray spectra. It is difficult to correlate the maximum range as determined here with that obtained by extrapolation of a logarithmic plot or by a Feather analysis. In this connection the end point ranges of B^{12} [7] and N^{12} [8] have been indicated in Fig. 1 plotted at energy values corresponding to the spectrometrically determined end point for B^{12} and to that expected from the atomic masses and (p,n) threshold for N^{12}. The good agreement of these points with the modified Feather formula given by Glendenin and Coryell[3] is evidence for the validity of that relation for absorption measurements of high energy beta-rays.

* Assisted by the Joint Program of the ONR and the AEC.
† Now at University of Virginia; Charlottesville, Virginia.
[1] N. Feather, Proc. Cambr. Phil. Soc. **34**, 599 (1938).
[2] E. Bleuler and W. Zunti, Helv. Phys. Acta **19**, 376 (1946).
[3] L. E. Glendenin, Nucleonics **2**, No. 1, 12 (1948).
[4] Fowler, Lauritsen, and Lauritsen, Rev. Mod. Phys. **20**, 237 (1948).
[5] Hornyak, Dougherty, and Lauritsen, Phys. Rev. **74**, 1727 (1948).
[6] For a review of these results see M. M. Slawsky and H. R. Crane, Phys. Rev. **59**, 1203 (1939).
[7] F. L. Hereford, Phys. Rev. **74**, 574 (1948).
[8] L. W. Alvarez, Phys. Rev. **75**, 1815 (1949).

Hyperfine Structure of Te^{125}

G. R. FOWLES
Department of Physics, University of California, Berkeley, California
June 27, 1949

HYPERFINE structure in the spectrum of singly ionized Te^{125} has been observed with a Fabry Perot etalon. Using 20 mg of 80 percent enriched isotope in a water-cooled Schuler tube, photographs were obtained in three to five minutes on Eastman 103a-F plates. About a dozen lines in the region from 4000 to 6000A show hyperfine structure, all of them giving only two components. The average separation of the components is about 0.2 cm^{-1}. In some of the lines, for example λ5666, the intensities of the two components have the ratio 3:1, with corresponding displacements relative to the single component of the even isotopes. Thus it can be concluded that the spin of Te^{125} is ½. The ratio of intensities in the line λ5708 corresponds to a j value of ⅜ which does not agree with the classication $6s\ ^2P_{\frac{1}{2}}$ given by Rao and Sastry[1] for the lower level of this line.

[1] K. R. Rao and M. Gourinatha Sastry, Ind. J. Phys. **14**, 423 (1940).

Spurious Counts in Geiger Counters and the Pretreatment of the Electrodes

J. D. LOUW AND S. M. NAUDÉ
National Physical Laboratory, South African Council for Scientific and Industrial Research, Pretoria, South Africa
June 30, 1949

GEIGER-MÜLLER counters and point counters are found under certain conditions to give spurious counts which cannot be attributed to photoelectric emission. It has been found by various observers[1,2] that newly made counters show a marked activity of this kind, which decreases with time until finally the normal background count only remains. Because of this phenomenon, various recipes for the preparation of counter cathodes have been proposed and some workers[1,2] have put forward explanations for this behavior in terms of the conditions existing on the surface of the cathode. In a recent letter to *The Physical Review*, Wiedenbeck and Crane[3] described a very interesting experiment with counters which showed nearly similar effects after having been operated at voltages above the pleateau. These authors concluded that the effect which they observed could be attributed to delayed emission of electrons from the cathode. In view of their method of pretreatment of the cathodes made from various metals (dry polishing with fine steel wool) it seems possible that a connection may exist between their observations and that of J. Kramer.[4] He maintains that the disturbances observed in newly made counters offer a new method for investigating the surfaces of metals, as regards their structure and stability. He concludes from his experiments that electrons are emitted by metals during exothermal processes.

As a result of a previous private communication of Kramer with one of the authors (S.M.N.), in which he proposed the Geiger-Müller counter or the Geiger point counter as new tools for studying metal surfaces, a series of experiments were conducted by the authors as a repetition of those by Kramer, and they were able to confirm his findings for the effects which were tried. The effects studied can briefly be stated as follows:

(1) Metal surfaces which have been ground or polished exhibit strong counting activity when placed in a counter. This activity diminishes with time according to the severity of the pretreatment and differing also in extent for various metals.
(2) On heating such a metal surface inside the counter after the activity has died down to the level of the normal background, a gradual, steep rise in counting rate may set in above a certain temperature. The behavior of the metal depends on the nature of the pretreatment, the time elapsed since treatment, and the particular metal.

Typical curves obtained by us illustrating these two phenomena are given in Figs. 1 and 2.

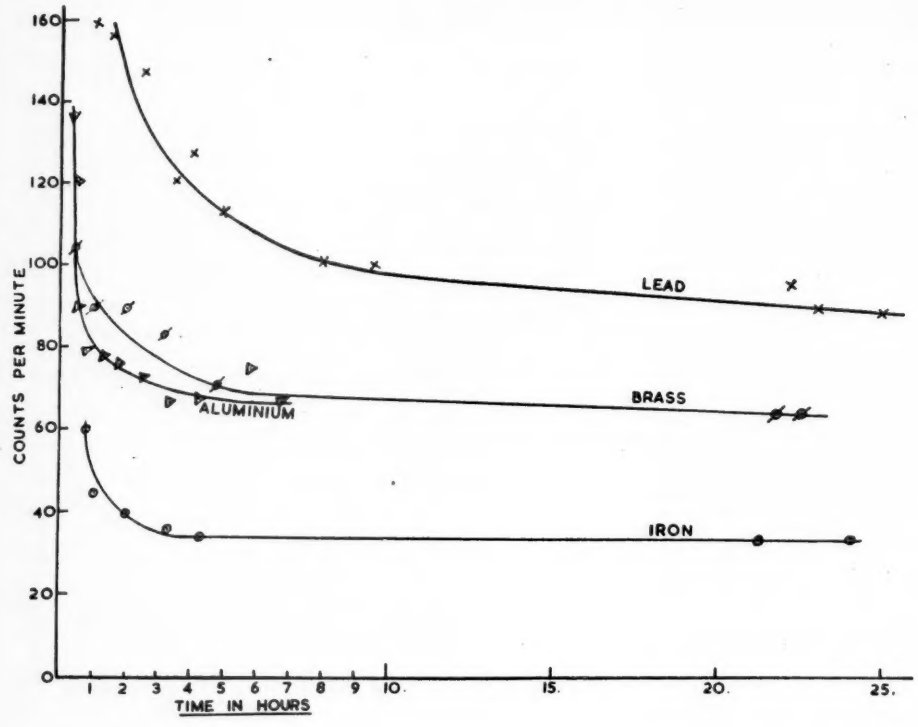

FIG. 1. Decay curves of the counting rate for sandpapered metal surfaces.

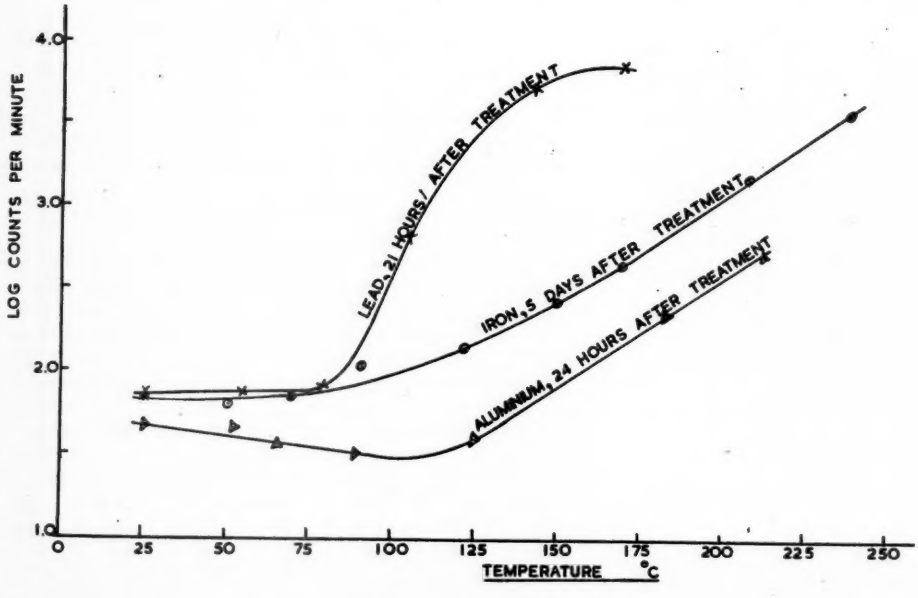
LOG COUNTS PER MINUTE
TEMPERATURE °C
LEAD, 21 HOURS AFTER TREATMENT
IRON, 5 DAYS AFTER TREATMENT
ALUMINIUM, 24 HOURS AFTER TREATMENT

FIG. 2. The temperature effect. Metals sandpapered and tested for temperature effect after periods indicated. Tests started at room temperature.

In these experiments a glass Geiger point counter was used with a colloidal graphite cathode and a platinum point. The metal under test was placed opposite the point on a stage which was fixed to a ground glass stopper so that it could easily and quickly be removed or replaced. Provision was made for heating and measuring the temperature of the test metal inside the counter. The point was operated at a positive voltage which ranged from 1000 to 1500 volts and the cathode and test metal were earthed. The counter was filled with 9 cm argon and 1 cm alcohol vapor. Due precautions were taken against the possible effects of photoelectric emission and stray radioactivity by carefully shielding the counter by means of a lead jacket.

Work is now in progress with the object of investigating the nature of the emission causing the high counting rate. For this purpose a special cloud chamber is being constructed in which the ionizing agent sets off the cloud chamber, and in this way makes visible its own track, so that the apparatus will actually be a combination of a cloud chamber and a point counter. It is hoped in this way to identify the emitted ionizing agent, as well as to obtain a verdict on the nature of the structure of the surface layers of the pretreated metals.

The authors wish to thank the South African Council for Scientific and Industrial Research for the permission to publish this letter.

[1] W. Kutzner, Zeits. f. Physik **23**, 117 (1924).
[2] W. B. Lewis and W. E. Bureham, Proc. Camb. Phil. Soc. **32**, 503 (1936).
[3] M. Wiedenbeck and H. R. Crane, Phys. Rev. **75**, 1268 (1949).
[4] J. Kramer, Zeits. f. Physik **125**, 739 (1949).

Radioactivity of Mo^{91} and Mo^{93} *

R. B. DUFFIELD AND J. D. KNIGHT
Department of Physics, University of Illinois, Urbana, Illinois
June 24, 1949

THREE radioactive decay periods have been reported in the literature which might be assigned to either Mo^{91} or Mo^{93}. These have half-lives of 6.7 hours, approximately 17 minutes and 73 seconds.[1] Recent work of Kundu and Pool[2] indicates that the 17-minute period is probably Mo^{91}, but the mass asignments of the other two are still uncertain. We wish to report some of our observations on the properties of these isotopes as deduced from betatron experiments.

The irradiation of molybdenum with betatron x-rays produces the 17-minute period by a (γ,n) reaction, the threshold energy being 13.5 Mev.[3] This is higher than that calculated for either of the reactions $Mo^{94}(\gamma,n)$ or $Mo^{92}(\gamma,n)$ on the basis of Feenberg's nuclear energy surface. It is somewhat more reasonable for the latter however, since Mo^{92} contains the magic number 50 neutrons, a configuration which is especially stable.[4]

In order to establish the identity of these periods we have irradiated samples of molybdenum oxide enriched in Mo^{92} and Mo^{94} with 23-Mev betatron x-rays and examined the radioactive products.[5] The intensity of the 17-minute period has been found to be proportional to the Mo^{92} content of the irradiated samples, confirming its assignment to Mo^{91}. Our experiments gave a half-life of 15.5 minutes, in agreement with the determination of Wäffler and Hirzel.

The radiation characteristics are shown in Table I and Figs. 1 and 2. Positron emission was verified by following the decay with

TABLE I. Radiation characteristics.

Isotope	Made by	Half-life	Radiation
Mo^{91}	$Mo^{92}(\gamma, n)$	15.5±0.5 min.	β^+ 3.7±0.1 Mev no γ
Mo^{91}	$Mo^{92}(\gamma,n)$	75.0±5.0 sec.	β^+ 2.6±0.2 Mev γ 0.3 Mev

the source in the field of a permanent magnet with proper field orientation. The particle energy was estimated by a Feather analysis of the aluminum absorption curve of a sample of molybdenum metal using as a standard a P^{32} source mocked up to resemble the molybdenum in self-absorption.

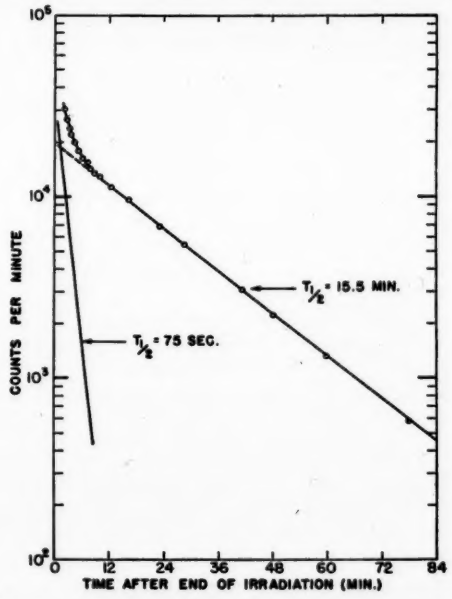

FIG. 1. Decay of Mo^{91} formed by 23 Mev x-rays on molybdenum containin 95.5 percent Mo^{92}.

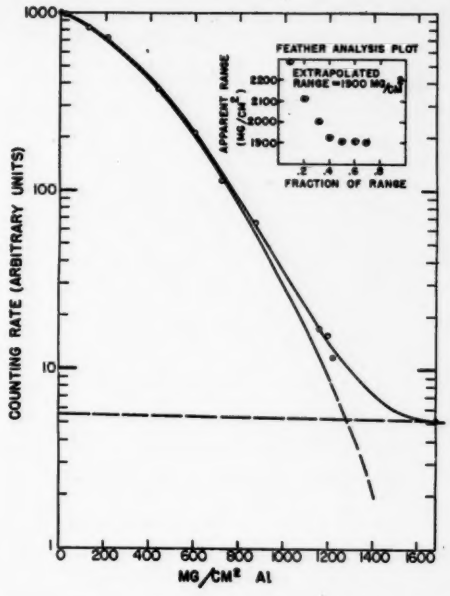

FIG. 2. Aluminum absorption curve of radiation from 15.5-minute Mo^{91}.

A chemical separation was done to verify that the activity observed was really molybdenum and not columbium produced by $Mo(\gamma,p)$, or by growth from a short-lived molybdenum parent. The columbium was carried down by a ferric hydroxide precipitate from alkaline ammonium molybdate solution and the molybdenum then precipitated as ammonium phosphomolybdate from acid solution. Over 99 percent of the 15.5-minute activity was found in the molybdenum fraction. The 68-minute Cb^{97}, formed by $Mo^{98}(\gamma,p)$, was found quantitatively in the columbium fraction.

By similar techniques the 75-second positron emitter was found to be due to Mo^{91} made by $Mo^{92}(\gamma,n)$. Characteristics of its radiations are shown in Table I and Figs. 1 and 3. It is apparent that

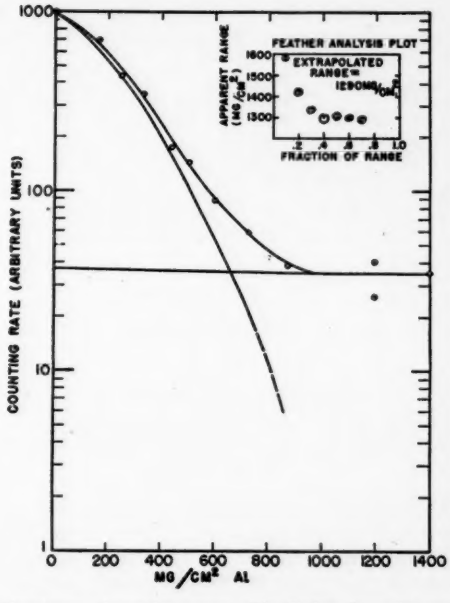

FIG. 3. Aluminum absorption curve of radiation from 75-second Mo^{91}.

this period did not grow from the 15.5-minute activity by isomeric transition, but we have not excluded the possibility that the 15.5-minute period was formed at least in part by decay of the 75-second period.

We have not observed the 6.7-hour activity to be formed by $Mo^{94}(\gamma,n)$ as can be seen from Fig. 4. If this reaction occurs to produce the 6.7-hour period, its cross section with 23 Mev x-rays must be less than 0.0005 that of the (γ,n) reactions for the other molybdenum isotopes. A further search for this activity was carried out on samples of enriched Mo^{92} and Mo^{94} which had been irradiated with slow neutrons in the pile at the Argonne National Laboratory. No evidence of decay with this half-life could be found.

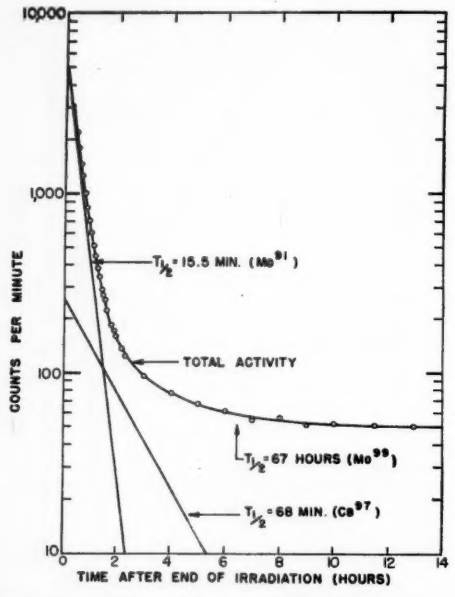

FIG. 4. Decay of total activity formed by 23 Mev x-rays on molybdenum containing 79.1 percent Mo^{94}

It is interesting that the existence of the two isomers reported for Mo^{91} means that there are two well-established isomers for all the 49-neutron nuclei with even atomic number from 34 to 42. The prevalence of nuclear isomerism near the end of closed shells has been pointed out by Mrs. Mayer.[6]

* Assisted by the joint program of the ONR and the AEC.

[1] For a summary of previous work see G. T. Seaborg and I. Perlman, Rev. Mod. Phys. 20, 585 (1948), also H. Wäffler and O. Hirzel, Helv. Phys. Acta 21, 200 (1948).

[2] D. N. Kundu and M. L. Pool, Phys. Rev. 76, 183 (1949).

[3] G. C. Baldwin and H. W. Koch, Phys. Rev. 67, 1 (1945).

[4] M. G. Mayer, Phys. Rev. 74, 235 (1948).

[5] The Mo^{92} and Mo^{94} samples used in this investigation were supplied by Carbide and Carbon Chemicals Corporation, Y-12 Plant, Oak Ridge, Tennessee, and obtained on allocation from the Isotopes Division of the AEC.

[6] M. G. Mayer, Phys. Rev. 76, 185 (1949).

Beta-Decay of In^{115*} ‡

P. R. BELL, B. H. KETELLE, AND J. M. CASSIDY
Oak Ridge National Laboratory, Oak Ridge, Tennessee
June 30, 1949

A SCINTILLATION spectrometer and a magnetic lens spectrometer have been used to investigate the decay of In^{115*}. This substance decays mostly by isomeric transition to In^{115} ground state but a beta-spectrum has also been observed.

A sample of cadmium metal was bombarded in the pile for some hours and allowed to decay for 24 hours to remove the 4-hour cadmium activity. Cadmium and indium were then separated chemically after the addition of indium carrier. The indium fraction was discarded and indium activity allowed to grow from the 2.3-day cadmium parent. After 16 hours a few milligrams of indium carrier were added and the indium fraction separated. The indium as hydroxide was mounted on 0.5 mg/cm² polyethylene and measured in the anthracene scintillation spectrometer.

A plot of pulse counting rate in a small height interval against pulse height is shown as curve *A* in Fig. 1.

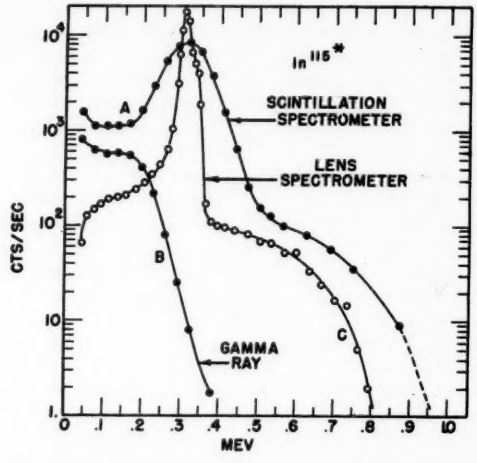

FIG. 1. Pulse counting rate as a function of pulse height.

The scale of pulse height was calibrated in Mev by using the 630-kev conversion line of Cs^{137}. The conversion line at 312 kev can be seen and also a beta-ray group containing about 1/10 as many electrons. Curve *B* is the Compton electron distribution produced by the gamma-ray when the electrons are cut off by an absorber. The curve shows evidence of only one strong gamma-ray group. All parts of curves *A* and *B* decay with the same 4.5-hour half-life. In order to make sure that the "β-ray" was not a defect in the scintillation spectrometer, a large sample was prepared and run in a magnetic lens spectrometer. The results, converted to a distribution as a function of energy rather than of momentum, are shown as curve *C* on Fig. 1. The β-ray is still seen and has about the same intensity (0.13) relative to the conversion line.

A Kurie plot of the lens spectrometer data above the conversion line is shown in Fig. 2. The plot is fairly straight and the endpoint seems to be 830±20 kev. If the 338-kev gamma-ray transition goes to the ground state of In^{115} and the 830-kev β-ray transition goes to the ground state of Sn^{115}, the energy difference between the two ground states would be 490 kev with In^{115} as the unstable member of the pair.

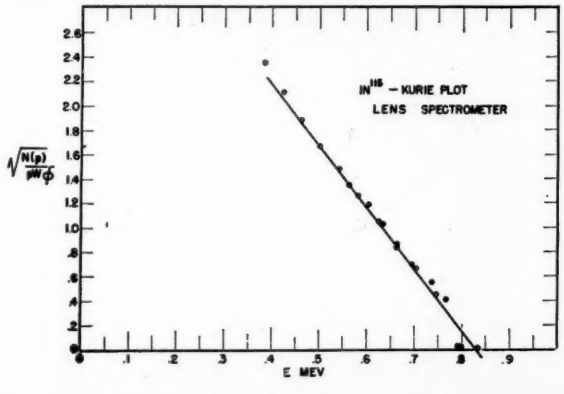

FIG. 2. Kurie plot of the lens spectrometer data.

‡ This document is based on work performed under Contract No. W-7405, eng. 26 for the Atomic Energy Project at Oak Ridge National Laboratory.

A New Germanium Photo-Resistance Cell

J. N. SHIVE
Bell Telephone Laboratories, Murray Hill, New Jersey
June 27, 1949

THE various photoelectric properties of the semi-conductor germanium have been studied by a number of investigators. Bray and Lark-Horovitz[1] observed both photo-conductive and photo-e.m.f. effects in germanium crystal rectifiers. Benzer has observed a "photo-diode" effect[2] due to the illumination of an N-P barrier in series with a rectifying contact, and has studied both the photo-behavior of rectifying germanium-to-metal contacts in the presence of applied bias voltages[3] and the rectification behavior of such contacts in the presence of light.[4] The spectral response and quantum efficiency of the photo-e.m.f. effect at N-P boundaries in germanium were determined by Goucher.[5]

The purpose of the present letter is to report a device utilizing a photo-conductive property of germanium which combines high spatial resolving power with an over-all quantum efficiency greater than unity. These features are obtained in one construction with an electrode geometry which is similar to that of the double-surface transistor.[6] In the double-surface transistor the characteristics of the collector are modified by the injection of charge into the neighboring semiconductor from a nearby emitter electrode. In the present photo-cell the characteristics of the collector are modified by the photo-liberation of charge in the neighboring semiconductor. Figure 1 shows an illustrative drawing of

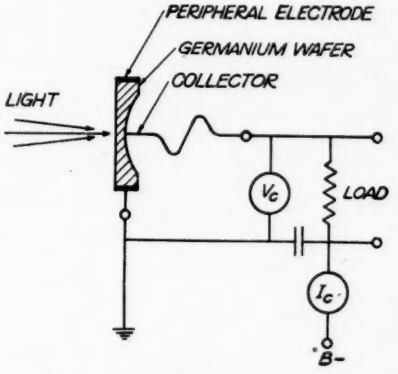

FIG. 1. Diagram of photo-cell showing electrical connections for testing and typical use.

such a photo-cell, in which the germanium has the dimpled pill-shape used in the Kock-Wallace transistor mounting.[7] The preparation of the (N-type) germanium wafer and the electrical forming treatment of the collector contact are described elsewhere.[8]

The area of the germanium wafer over which incident light affects the cell resistance is confined to a region a few hundredths sq. mm in extent on the illuminated side immediately opposite the collector contact. The responsive areas of a number of cells have been explored with a small spot of light from the vertical illuminator attachment of a metallurgical microscope. When the resulting current response of a typical cell is plotted *vs.* distance along a line passing through the center of the responsive area, an error-function-shaped curve is obtained whose breadth at half-maximum, corrected for the diameter of the exploring light spit, is about 0.2 mm. Allowing light to fall uniformly all over the wafer surface not only wastes light, but avoids the realization of the spatial resolving power of which the cell is capable. In the measurement of the characteristics reported below a condensing lens was used to focus an image of the light source substantially within the responsive area of the cell under test.

In operation the collector is biased negatively with respect to the peripheral contact through a load resistance of from 5000 to 30,000 ohms. This polarity corresponds to the blocking direction of diode rectification of metal against N-type germanium at the collector contact. A family of static collector current *vs.* collector voltage curves for several different values of steady light flux is shown in Fig. 2. By selecting suitable battery voltage and load

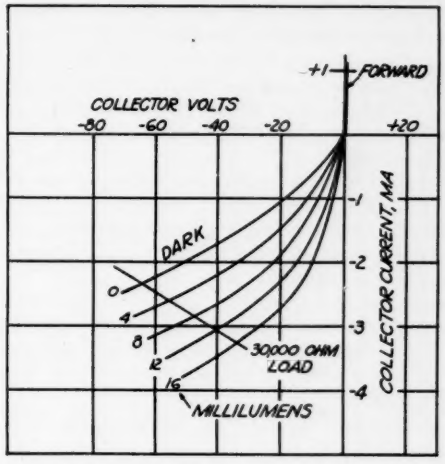

FIG. 2. Static characteristics of photo-cell.

resistance values, drawing the corresponding load line across this family of characteristics, and analyzing, in the usual way, for the performance of the circuit, load power responses of the order of several tenths milliwatt per millilumen can be deduced. The response of the cell to different frequencies of modulation of the incident light is substantially flat to the highest frequency studied, about 200 kc per second.

Preliminary measurements of the spectral distribution of the sensitivity of the photo-cell have been made in collaboration with H. B. Briggs. The response rises slowly from visible yellow to a peak at about 1.5μ and decreases rapidly beyond 1.6μ. The shape of this response *vs.* wave-length relationship is practically identical with that determined by Goucher and Briggs for the photo-e.m.f. effect at N-P junctions in germanium. The breadth of the forbidden band in germanium, obtained from the intrinsic region of the resistivity-temperature relationship, corresponds to about 1.75μ. Detectable responses have been found for some germanium cells as far as 1.9μ.

Measurements of the over-all quantum efficiency of this cell show that with 1.5μ radiation, current increments corresponding to 3 or 4 electrons per incident quantum are realized. The seat of this effect is believed to be a current-multiplication occurring at the collector barrier in the process of collecting the primary charge already produced photoelectrically. The above current amplification is about the same as that ordinarily observed between emitter and collector in transistors.

[1] R. Bray and K. Lark-Horovitz, Phys. Rev. **71**, 141 (1947).
[2] S. Benzer, Phys. Rev. **72**, 1267 (1947).
[3] S. Benzer, Phys. Rev. **73**, 1256 (1948).
[4] S. Benzer, Phys. Rev. **69**, 683 (1946).
[5] F. S. Goucher, Phys. Rev. **75**, 1625 (1949).
[6] J. N. Shive, Phys. Rev. **75**, 689 (1949).
[7] W. E. Kock and K. L. Wallace, Jr., Elec. Eng. **68**, 222 (1949).
[8] J. Bardeen and W. H. Brattain, Phys. Rev. **74**, 230 (1948); also H. C. Torrey and C. A. Whitmer, *Crystal Rectifiers* (McGraw-Hill Book Company, Inc., New York, 1948), Ch. X.

Neutron Induced Radioactivities in V^{52}, Mo^{99}, and W^{185}

J. M. CORK, H. B. KELLER, AND A. E. STODDARD
University of Michigan, Ann Arbor, Michigan
June 30, 1949

ON exposing specimens of vanadium, molybdenum, and tungsten to neutron capture in the Argonne and Oak Ridge piles, certain new radioactivities are found to be produced. While

our principal interest has been the spectrometric determination of gamma-rays by conversion electrons, observations are also made of the half-life and the energy of penetrating gamma-rays by absorption.

Vanadium. Since a single isotope of stable vanadium of mass 51 occurs in nature, the isotope formed by neutron capture should have the mass 52. The decay as observed showed clearly 2 half-lives; one of 16 hours and another of about 635 days. A half-life of 600 days had previously been reported for V47, which isotope could not possibly be produced here. Conversion electrons indicate the existence of gamma-rays of energy 80.5 and 119.3 kev for the long-lived emitter.

Molybdenum. A single radioactive isotope of molybdenum of probable mass 99, having a half-life of 68.3 hours, is produced. By absorptions in lead there appears to be a gamma-ray of energy about 0.78 Mev and conversion electrons indicate gamma-energies of 139.6, 167.6, and 179.3 kev.

Tungsten. The decay curve of tungsten is complex, showing a half-life of 25.0 hours (previously reported 24.1) and a long-lived emitter of half-life 76 days. Associated with the latter activity are two electron lines which, if interpreted as an *L–M* combination, yield a single gamma-ray at 133.7 kev.

This investigation is supported jointly by the ONR and the AEC.

Photo-Disintegration of Deuterium by Seven- to Twenty-Mev X-Rays*

EVERETT G. FULLER
Physics Department, University of Illinois, Urbana, Illinois
July 5, 1949

A PRELIMINARY study has been made of the angular distributions and distribution in energy of the protons arising from the photo-disintegration of deuterium by the continuous x-ray spectrum from 20.8 Mev electrons in the betatron. The x-rays were collimated into a beam having a full angular width of forty-six minutes by means of a laminated lead collimator placed between the coil boxes of the betatron. The collimated x-ray beam passed through a scattering chamber filled with deuterium gas. Ilford, type C-2, one hundred micron nuclear emulsions were placed inside the scattering chamber to one side of the x-ray beam to detect the protons resulting from the photo-disintegration of the deuterium gas in the beam. Plates were exposed with three atmospheres of deuterium to emphasize the high energy end of the spectrum, with one atmosphere of deuterium to emphasize the low energy end, and with one and three atmospheres of hydrogen. The exposures made with the chamber filled with hydrogen were used to determine the background due to the photo-neutrons coming from the lead collimator and shielding. At all energies this background was a small effect and at high energies it was completely negligible.

To date the analysis has been completed of about four square centimeters of the plates exposed with the chamber filled with three atmospheres of deuterium and the corresponding hydrogen background plates. The energy of each proton track as it entered the plate was determined from the range-energy relations for the Ilford emulsions.[1] These energies were then corrected for the range of each track in the gas of the chamber before it reached the emulsion. From the known geometry of the plates with respect to the x-ray beam and angular measurements made on each track it was possible to determine the angle each track made with respect to the direction of the incident quanta. Angles could be determined between 20 and 160 degrees in the laboratory system. The quantum energy corresponding to each track was calculated from the measured angle and energy of each track in the laboratory system.

Using the intensity spectrum of the betatron as determined by Koch and Carter,[2] Fig. 1 shows the relative cross section as a function of quantum energy for the photo-disintegration of deuterium as determined from these data. The scale on the left is in arbitrary units while that on right has been normalized such that the cross section at seven Mev is $11.7(10)^{-28}$ cm², the value given by the Bethe-Peierls expression. The dashed curve is the Bethe-Peierls expression for the cross section as a function of energy. The solid curve, which seems to fit the data at the high energy end, is for a cross section which varies as $1/(E)^{\frac{1}{2}}$, where E is the energy of the incident quantum. The various theoretical values calculated at 17.5 Mev by Rarita and Schwinger[3] have also been plotted.

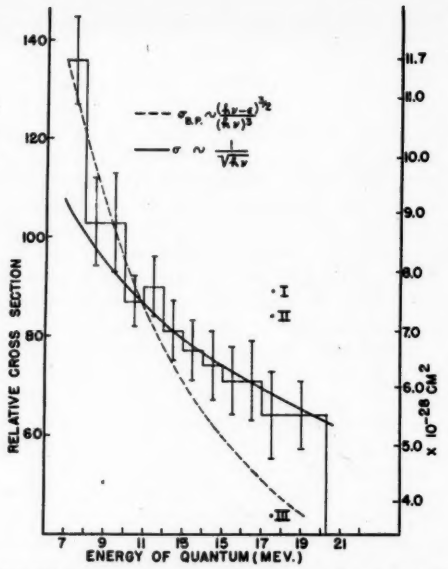

FIG. 1. Relative cross section for photo-disintegration of deuterium. Scale on right normalized to give cross section of $11.7(10)^{-28}$ cm² at 7 Mev. Points calculated by Rarita and Schwinger: *I* symmetrical theory, *II* charged theory, *III* neutral theory.

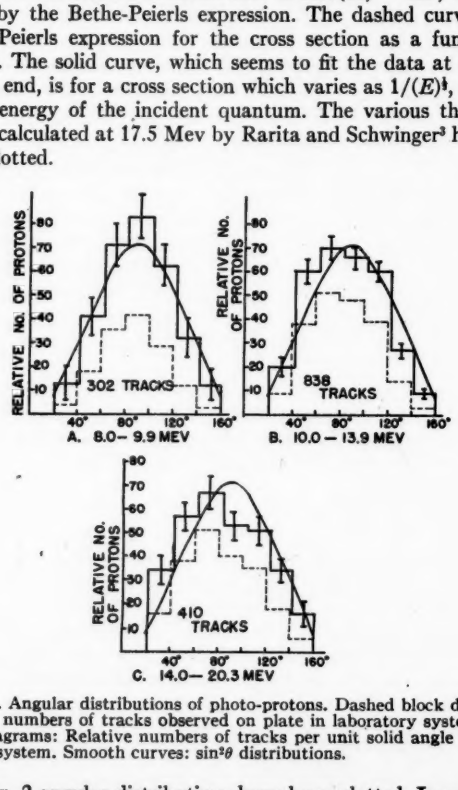

FIG. 2. Angular distributions of photo-protons. Dashed block diagrams: Relative numbers of tracks observed on plate in laboratory system. Solid block diagrams: Relative numbers of tracks per unit solid angle in center of mass system. Smooth curves: $\sin^2\theta$ distributions.

In Fig. 2 angular distributions have been plotted. In each case the dashed block diagram represents the observed distribution on the plate after correction for background. The solid block diagrams represent the distributions per unit solid angle normalized to the same area after conversion to the center of mass system. The smooth curve in each figure represents a $\sin^2\theta$ distribution. These data seem to indicate a possible forward asymmetry in the angular

distribution for high energies. It is not felt that the statistics at the present time are sufficient to make any definite statements about this asymmetry. The amount of this asymmetry, however, is of the order of that given by the theory of Rose and Goertzel,[4] i.e., in their notation $A_0(u)=(L/\zeta^4)^2 \sin^2\theta$. A rough calculation at ten and twenty Mev of the cross section by this theory, however, gives an energy dependence which is slightly steeper than that given by the Bethe-Peierls expression.

The author is grateful for the encouragement and advise of Professor A. O. Hanson who initiated this work. He also wishes to acknowledge the helpful discussions of the work held with Professors S. M. Dancoff and Mr. J. S. Blair.

* Assisted by the joint program of the ONR and AEC.
[1] Lattes, Fowler, and Cuer, Nature **159**, 301 (1947).
[2] H. W. Koch and R. E. Carter, Phys. Rev. **75**, 1950 (1949).
[3] W. Rarita and J. Schwinger, Phys. Rev. **59**, 556 (1941).
[4] M. E. Rose and G. Goertzel, Phys. Rev. **72**, 749 (1947).

The Thermal Neutron Absorption Cross Section of K^{39}

JOHN L. HANSEN AND JOHN E. WILLARD
Department of Chemistry, University of Wisconsin, Madison, Wisconsin
June 27, 1949

THE thermal neutron capture cross section for natural potassium (93.3 percent K^{39}, 0.012 percent K^{40}, 6.7 percent K^{41})[1] has been measured by Lapointe and Rasetti[2] by determining the concentration of boron in a water solution of boric acid necessary to produce the same intensity decrease in thermal neutrons as that produced by a solution of potassium fluoride of known concentration. The thermal neutron capture cross section for the reaction $K^{41}(n,\gamma)K^{42}$ has been determined to be 1×10^{-24} cm² by Seren, Friedlander, and Turkel[3] by measuring the K^{42} activity induced in potassium by a thermal neutron irradiation of known flux and duration. A direct determination of the capture cross section of K^{39} by measurement of induced K^{40} activity has not been reported, probably because the long half-life[4] of K^{40}, together with the necessity of counting the induced activity against the background of the natural K^{40} activity, require very intense irradiation of long duration to produce a measurable amount of activity.

We have determined the ratios of the counting rate of K^{40} in samples of KCl which have received neutron exposures of 1.3×10^{18}, 2.3×10^{18} and 8.1×10^{19} neutrons/cm²[5] to the counting rate of ordinary KCl under identical conditions. From these ratios, the neutron exposures, and the percentage abundance of K^{40} and K^{39} in natural K a value for the thermal neutron absorption cross section of K^{39} has been obtained.

The irradiated KCl samples were rigorously purified with respect to Cl^{36}, S^{35} and P^{32} activities produced by the $Cl^{35}(n,\gamma)Cl^{36}$ $Cl^{35}(n,p)S^{35}$ and $Cl^{35}(n,\alpha)P^{32}$ reactions. Other radioactive nuclear species originally present were sufficiently short-lived to decay before the measurements of K^{40} activity were made. The most difficult activity to remove was the S^{35}, which was present at a specific activity more than 10^6 times as great as the K^{40} in the most active sample and which before removal gave rise to a high counting rate of brehmsstrahlung produced by the absorption of its weak (0.17 Mev) beta-particles in the thick KCl samples used.

The last step of purification was always the precipitation of the potassium as KCl by bubbling HCl gas into the aqueous solution. This salt was then fused, powdered and placed in a brass cup 3.8 cm in diameter and 1 cm deep. An absorption curve for the radiation of the sample was determined with the aid of a mica window Geiger-Mueller counter and aluminum absorbers. An absorption curve of an unexposed sample of reagent grade KCl of the same weight, fused, powdered, and mounted in the same way was determined in the same position under the same counting tube.

An irradiated sample was considered to be radiochemically pure when its absorption curve was parallel to the curve for an identical sample of KCl which had not been irradiated. The ratio of the ordinate of the curve for the irradiated sample to that for the unirradiated sample at any absorber thickness is equal to the factor by which the irradiation increased the K^{40} content of the irradiated sample, there being no need for knowledge of the absolute counting efficiency of the equipment. Following the counting of the solid samples they were dissolved to make solutions of equal concentration which were counted by placing them in an annular jacket around a thin glass-walled Geiger-Mueller counter tube.[6]

Absorption curves for the most active purified irradiated sample of KCl and for a duplicate unirradiated comparison sample are given in Fig. 1. A summary of the results from this sample is given in Table I. The values in the third column for the counting

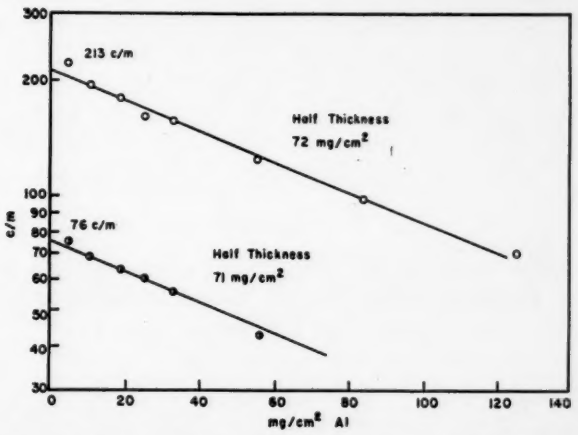

FIG. 1. Absorption curves taken on KCl samples. Upper curve: after neutron irradiation and subsequent purification from radioactive species other than K^{40}. Lower curve: KCl which was not irradiated.

TABLE I. Determination of thermal neutron absorption cross section of K^{39} (using 0.60 gram of a KCl sample irradiated with 8×10^{19} neutrons per cm²).

KCl sample	Type of sample counted	Counts per minute	σ of K^{39} (cm²$\times10^{24}$)
Irradiated	Solid	213	2.9
Not irradiated	Solid	76	
Irradiated	Solution	147±2.2	2.6
Not irradiated	Solution	56±2.7	

rates of the solid samples have been obtained by extrapolating the absorption curves of Fig. 1 to zero absorber. The values of the individual points making up the absorption curves have been determined with a statistical counting error of less than ±4 percent at the 0.95 reliability level. The 0.95 error of the solution counts is included in column 5 of Table I.

The calculated value of the cross section of K^{39} depends upon the value used for the neutron exposure and for the abundance of K^{40} in natural K. The value for the neutron exposure is believed to be accurate to ±25 percent,[5] and that for the abundance of K^{40} has been stated to have a probable error of ±10 percent.[1] Self-shielding probably made the average neutron exposure of the sample about 0.8 of the maximum (the sample of KCl exposed was about 0.9 cm thick, 10 cm long and weighed 10 g). It seems reasonable, therefore, to assign a value of $3\pm1.5\times10^{-24}$ cm² to the capture cross section of K^{39} for the pile neutrons with which these samples were bombarded.

This value is in agreement with the value of 3.9×10^{-24} cm² obtained from the total absorption cross section value of Lapointe and Rasetti[2] if the latter is corrected for the changed value of the cross section of boron, for the absorption due to K^{41},[3] and for the abundance of K^{39}.

Five samples purified from KCl which had received neutron exposures of 1.3×10^{18} and 2.3×10^{18} neutrons/cm^2 gave an average value in agreement with that obtained from the more active sample, but the increase in counting rate as a result of irradiation in these experiments was in the range of only 5–15 counts per minute so the accuracy with which it could be determined was relatively low.

This work was supported in part by the University Research Committee with funds made available by the Wisconsin Alumni Research Foundation.

[1] A. O. Nier, Phys. Rev. **50**, 1040 (1936).
[2] C. Lapointe and F. Rasetti, Phys. Rev. **58**, 554 (1940). The value of 3.2×10^{-24} cm^2 which they give is based on the assumption that the thermal neutron absorption cross section of boron is 600×10^{-24} cm^2. If the more recent value of 703×10^{-24} cm^2 for boron is used the value obtained by these authors for potassium would be 3.7×10^{-24} cm^2. Way and Haines, United States AEC Declassified Document 2138, cite a value of 2.5×10^{-24} cm^2 for the natural potassium cross section.
[3] L. Seren, H. N. Friedlander, and S. H. Turkel, Phys. Rev. **72**, 888 (1947).
[4] L. B. Borst and J. J. Floyd, Phys. Rev. **74**, 989 (1948). Other references are given in this paper.
[5] The samples, obtained from the Oak Ridge National Laboratory of the U. S. AEC, were the result of irradiations made for the purpose of producing high specific activity Cl^{36}. The values for neutron exposures were kindly furnished by J. A. Cox of the Isotopes Office of the Oak Ridge National Laboratory.
[6] Further details of these determinations are given in a M.S. thesis field with the University of Wisconsin library in August, 1948, by John L. Hansen.

Investigation of the Attractive Forces between the Persistent Currents in a Superconductor and the Lattice*

E. U. Condon and E. Maxwell
National Bureau of Standards, Washington, D. C.
June 29, 1949

We have investigated the behavior of a superconducting sphere in a magnetic field in order to answer the question of whether the persistent surface currents can move with respect to the metal or are rigidly bound to it. An early experiment of Tuyn's[1] has been interpreted as indicating that the supercurrents are in fact rigidly fixed in the superconductor. Since Tuyn employed a hollow sphere, one would expect the intermediate state to set in and produce a strong frozen-in moment. Therefore his experiment is not conclusive.

It also appears that the hypothesis of currents rigidly bound to the metal is incompatible with the Meissner effect. Since

$$\mathbf{B}=\mathbf{H}+4\pi\mathbf{I}, \tag{1}$$

we may regard the condition $\mathbf{B}=0$, the Meissner effect, as resulting from the building up of a $4\pi\mathbf{I}$ in the metal which is everywhere equal to $\mathbf{H}$ and oppositely directed to it, inasmuch as (1) is a vector equation and $\mathbf{I}=-\mathbf{H}/4\pi$ vectorially. If we were now to regard the surface currents, or what amounts to the same thing, the magnetization $\mathbf{I}$, as fixed to the metal sphere, then on turning the sphere in a magnetic field, the vector $\mathbf{I}$ would rotate with respect to $\mathbf{H}$, and therefore the condition $\mathbf{H}+4\pi\mathbf{I}=0$ could not be fulfilled.

We have investigated this matter experimentally by suspending a tin spheroid of radius 1.8 cm in a magnetic field and observing the period of oscillation of the resulting torsion pendulum as a function of the field strength. Observations have been made at temperatures down to 1.74°K and at field strengths sufficiently below the critical field to avoid the appearance of the intermediate state. The earth's field was compensated to within one or two milligauss before cooling so as to avoid the possibility of frozen-in moments.

If the currents were rigidly fixed to the sphere, then we should have, in addition to the restoring torque of the suspension, a torque of $\mathbf{H}^2/4\pi$ dyne-cm/rad. cm^3 due to the interaction between the currents and the applied field. We have observed no torques greater than about 1 percent of this quantity and therefore conclude that except for effects of the order of 1 percent or less, the currents do not remain bound to the metal.

We have, however, observed a restoring torque which is 1 percent or less of the value $\mathbf{H}^2/4\pi$ and which is an interesting function of the applied field strength. Since we used a rather soft suspension (approximately 130 dyne-cm/rad.) these effects were well within the precision of measurement. A typical result is plotted in Fig. 1

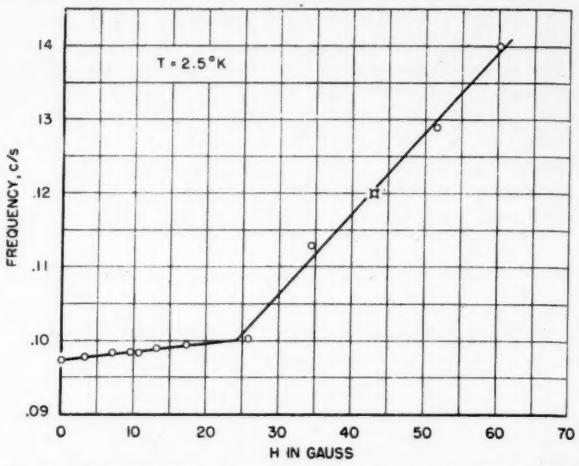

FIG. 1. Relation between frequency of oscillation and magnetic field for tin spheroid. ⊙ Points taken with ascending magnetic field. × Point taken with descending field.

which gives the frequency of oscillation *vs.* the applied field for a temperature of 2.5°K. Note the curious discontinuity in the slope at 24 gauss. The same general behavior has been observed at other temperatures. No hysteresis is apparent as long as we do not exceed the critical field.

The experiments are still in a preliminary stage so that it is entirely possible that the effect we observe is due to small departures from true cylindrical symmetry or other secondary features. We have some indication of dependence on the relative orientation of field and spheroid and are investigating this point further. It is also planned to measure the torque under static conditions, to extend the measurements to other superconductors, and possibly to study the effect using a long cylinder with circumferential persistent currents.

After we observed these phenomena it was brought to our attention that effects of this sort have been observed and briefly reported on by Mendelssohn.[2]

* Supported by the ONR.
[1] W. Tuyn, *Quelques essais sur les courants persistants*, Leiden Comm. No. 198.
[2] K. Mendelssohn, *Report of an International Conference on Fundamental Particles and Low Temperatures* (Physical Society, Cambridge, 1946), p. 128.

Thresholds for Photo-Neutron Reactions in Mn, Zn, Zr, Mo, Cd, Pr, Nd, Au, Hg, Tl and Pb

A. O. Hanson, R. B. Duffield, J. D. Knight, B. C. Diven, and H. Palevsky
Physics Research Laboratory, University of Illinois, Champaign, Illinois
June 27, 1949

Measurements on thresholds for photo-neutron reactions, using x-rays from the 22-Mev betatron, have been extended to include a number of other elements. The experimental arrangements are similar to those already described.[1] The energy scale is again determined relative to the threshold for the 10-minute activity from the $Cu^{63}(\gamma,n)Cu^{62}$ reaction which is taken as 10.9 Mev.

The thresholds for the production of characteristic radioactivities were measured in samples which varied from a single 10-mg sample enriched in Zn^{70} to a number of large cylindrical samples of the more common elements. Metallic samples were used in all cases with the exception of the Zn^{70}, Pr, and Nd which were in the form of oxides.

The thresholds for the production of neutrons from various elements were obtained by irradiating samples, of the order of 200 grams, placed just outside the x-ray donut. The neutron yields from these materials were determined by the use of rhodium foils placed near the samples. In order to reduce the background of neutrons from the x-ray target a special tube was used with Ag or Al probe targets placed at a position 90° away from the injector structure. The materials were in the form of laminated metal samples with the exception of the Zr which was in the form of the oxide.

The excitation functions near threshold in nearly all cases could be represented by parabolas which makes it possible to estimate the threshold from a linear extrapolation of the square root of the yield plotted as a function of the x-ray energy.

The results are shown in Table I. It is assumed that the

TABLE I. Thresholds for photo-neutron reactions.

Parent isotope	Activity detected	Observed threshold (Mev)	Previous work (Mev)	Empirical binding energy (Mev) Eq. 3[1]	Feenberg
$_{25}Mn^{55}$	Neutrons	10.15±0.20		10.9	10.3
$_{30}Zn^{64}$	38 min. β^+	11.80±0.20	11.6±0.4†	11.7	11.9
$_{30}Zn^{70*}$	52 min. β^-	9.20±0.20		9.0	9.1
$_{40}Zr^{90}$	4.5 min.	12.48±0.15	12.0±0.2††	10.1	10.4
$_{40}Zr^{91}$	Neutrons	7.20±0.40		7.5	7.1
$_{42}Mo^{92}$	15.5 min. and 75 sec. β^+	13.28±0.15	13.5±0.4†	10.8	11.6
$_{42}Mo^{97}$	Neutrons	7.10±0.30		7.1	6.2
$_{48}Cd^{113}$	Neutrons	6.44±0.15		6.8	6.6
$_{50}Sn^{119}$	Neutrons	6.51±0.15		6.6	7.1
$_{50}Sn^{124}$	40 min. β^-	8.50±0.15		7.3	8.1
$_{59}Pr^{141}$	3.5 min. β^+	9.40±0.10	9.8±0.3††	8.4	8.2
$_{60}Nd^{150}$	1.7 hr. β^-	7.40±0.20		7.2	7.5
$_{79}Au^{197}$	Neutrons	8.00±0.15		7.4	8.0
$_{80}Hg^{201}$	Neutrons	6.25±0.20		5.9	6.5
$_{81}Tl^{205}$	Neutrons	7.48±0.15		7.0	7.6
$_{82}Pb^{207}$	Neutrons	6.85±0.20	6.9†††	5.9	6.5

* Supplied by the Y-12 Plant, Carbide and Carbon Chemicals Corporation, through the Isotope Division, US-AEC, Oak Ridge, Tennessee.
† G. C. Baldwin and H. W. Koch, Phys. Rev. 67, 1 (1945).
†† W. E. Ogle, Nuclear Sci. Abstracts 2, 363 (1949).
††† K. Way, Phys. Rev. 75, 1448 (1949).

thresholds defined by the neutron yields are those for the isotope of the highest odd mass number of the element irradiated. The binding energies as obtained from semi-empirical relations[1] are shown in the table for comparison. It can be seen that there is fair agreement between the observed and calculated thresholds with the exception of the Zr^{90}, Mo^{92}, and Pr^{141} which have been pointed out as being exceptionally stable nuclei having closed shells of 50 and 82 neutrons.[2] The recent assignment of the 17 (15.5)-minute activity in Mo to Mo^{92} [3] serves to explain one of the large discrepancies between the observed and semi-empirical thresholds reported in the earlier work.

We wish to acknowledge the assistance of Mr. D. E. Riesen and Mr. B. A. Smith, who aided materially in obtaining these data. The work was assisted by the joint program of the Office of Naval Research and the Atomic Energy Commission.

[1] McElhinney, Hanson, Becker, Duffield, and Diven, Phys. Rev. 75 542 (1949).
[2] M. G. Mayer, Phys. Rev. 74, 235 (1948).
[3] D. N. Kundu and M. L. Pool, Phys. Rev. 76, 183 (1949); R. B. Duffield and J. D. Knight (private communication)

Analysis of the Temperature Coefficient of Shear Modulus of Aluminum

T'ING-SUI KÊ
Institute for the Study of Metals, University of Chicago, Chicago, Illinois

June 6, 1949

THE shear modulus G of a specimen of cubic symmetry may be regarded as an implicit function of temperature (through its volume V) and as an explicit function. Thus, $G=G\{V(T), T\}$. The temperature coefficient of this modulus will, therefore, contain two terms, namely,

$$d\ln G/dT=(\partial \ln G/\partial \ln V)_T\cdot d\ln V/dT+(\partial \ln G/\partial T)_V. \quad (1)$$

The purpose of this note is to estimate the contribution of each term to the total temperature coefficient for an aluminum crystal which is fairly isotropic and for which sufficient experimental data are available. Such a study has recently been made by Lazarus for a number of cubic crystals.[1]

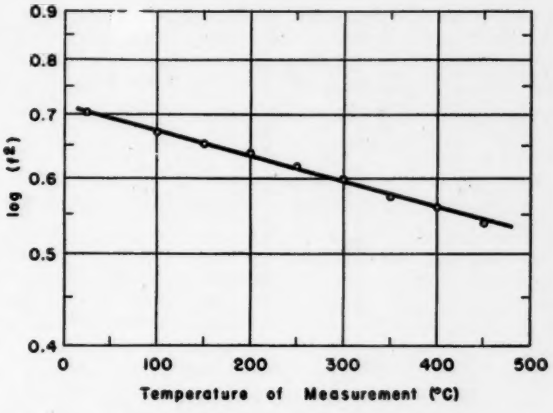

FIG. 1. Variation of the logarithm of the square of the frequency of vibration as a function of temperature.

In order to determine the left-hand term of Eq. (1), the shear modulus of an aluminum single crystal of commercial purity was determined by measuring the frequency of torsional vibration of the wire carrying a small torsional bar. The apparatus and the experimental procedure used in the measurement have been previously described.[2] Figure 1 plots the logarithm of the measured value of the square of the frequency of vibration as a function of temperature. From this curve, which is a straight line, the value of $d\ln G/dT$ was computed, due allowance being taken of the change of volume with thermal expansion, an allowance which increases the value by 13 percent. This gives

$$d\ln G/dT=-6.8\times10^{-4}\ \text{deg.}^{-1}.$$

It is to be pointed out that this value has been found to be the same for polycrystalline aluminum at temperatures when the grain boundary relaxation does not occur.[2] This indicates that the temperature variation of the shear moduli of aluminum along various crystallographic directions is similar.

The value of $(\partial \ln G/\partial \ln V)_T$ was computed from the measured values of $(\partial \ln G/\partial P)_T$ by Birch[3] and by Lazarus[1] and of $(\partial \ln V/\partial P)_T$ by Ebert[4] and by Bridgman[5] for commercial aluminum at 30°C and one atmospheric pressure. This gives

$$(\partial \ln G/\partial \ln V)_T=-5.64.$$

Upon combining this value of $(\partial \ln G/\partial \ln V)_T$ with the average volume expansion coefficient of commercially pure aluminum for the temperature range 20°C to 400°C, which is $8.0\times10^{-5.6}$ we obtain -4.5×10^{-4} as the first term in the right-hand side of Eq. (1), and hence, -2.3×10^{-4} for the second term $(\partial \ln G/\partial T)_V$. It is seen that the explicitly temperature-dependent term contributes more than one-third of the total temperature coefficient. This indicates that even for a first approximation, the shear modulus cannot be regarded as a sole function of volume, and this is in corroboration with Lazarus' observations for other cubic crystals and other types of elastic moduli.

[1] David Lazarus, Phys. Rev., this issue.
[2] T. S. Kê, Phys. Rev. 71, 533 (1947).
[3] F. Birch, J. App. Phys. 8, 129 (1937).
[4] H. Ebert, Zeits. f. Physik 36, 388 (1935).
[5] P. W. Bridgman, Proc. Am. Acad. 70, 285 (1935).
[6] P. Hidnert, Sci. Papers Bur. Stand., No. 497 (1925).

Infra-Red Absorption of Hydrogen and Carbon Dioxide Induced by Intermolecular Forces

H. L. WELSH, M. F. CRAWFORD, AND J. L. LOCKE*
McLennan Laboratory, University of Toronto, Toronto, Canada
July 5, 1949

ROTATION-vibrational infra-red absorptions forbidden for the free molecules have recently been observed by us in oxygen and nitrogen at high densities.[1] We now report similar absorptions in gaseous hydrogen and carbon dioxide. As in the previous cases, for pure gases the absorption coefficients for all points in the bands vary as the square of the pressure. Enhancement of the hydrogen absorption by foreign gases (helium and nitrogen) has been observed and is proportional to the partial pressure of the foreign gas. Thus these absorptions must be induced by the forces acting during molecular collisions and support the belief that induced absorption is a general molecular phenomenon. The contours of the new bands, especially the hydrogen band for which the rotational structure is partially resolved, confirm the rotational selection rule $\Delta J=0, \pm 2$.

The absorption in hydrogen was obtained with an absorbing path length of 85 cm and gas pressures up to 100 atmospheres. The most prominent maximum (Q-branch) of the band occurs at the vibrational frequency of the H_2 molecule, 4155 cm^{-1}. Two additional maxima, only one of which is clearly resolved, occur at the frequencies predicted for the first two lines in the S-branch. The relative intensities of the O- and S-branch lines calculated from the Raman effect matrix elements are indicated by the vertical lines in Fig. 1. If the experimental half-width of the Q-branch, 250

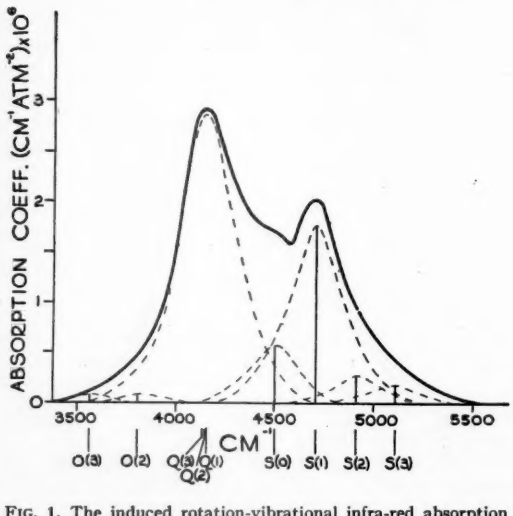

FIG. 1. The induced rotation-vibrational infra-red absorption of gaseous hydrogen.

cm^{-1}, is assumed for the theoretical components of the O- and S-branches the observed contour is reproduced. The energy levels, although greatly broadened by the collisions, are not displaced by more than ± 10 cm^{-1}, the error in our frequency calibration. The ratio of the sum of the intensities of the O- and S-branches to the total intensity in the hydrogen band is 0.4; the corresponding ratios for nitrogen and oxygen are 0.6 and 0.7, respectively. Although the maximum absorption coefficient for hydrogen is of the same order as those for oxygen and nitrogen, the integrated absorption coefficient is about four times greater because of the broadness of the band. Thus the intensity of the hydrogen band relative to that of either oxygen or nitrogen does not appear to be simply related to the polarizabilities or the derivatives of the polarizabilities of the molecules.

In the previous note it was suggested that induced transitions might be responsible in part for the overtone absorptions observed in hydrogen by Herzberg.[2] Since the half-width of the lines of the induced absorption is greater by several orders of magnitude than the half-width of the lines observed by Herzberg, this suggestion is no longer plausible. An induced overtone absorption could produce at most only a continuum underlying the narrow lines arising from the quadrupole transitions.

The symmetrical frequency of carbon dioxide, normally forbidden in the infra-red, was observed with a path length of 85 cm and gas pressures up to 25 atmospheres, and with a path length of 11 meters and pressures up to 6 atmospheres. The band has two maxima at 1286 cm^{-1} and 1388 cm^{-1}. The two components arise from the Fermi resonance interaction of the symmetrical vibration and the overtone of the doubly degenerate vibration. The intensity ratio of the components is 0.8 whereas the ratio obtained in the Raman effect is 0.6.[3]

The induced absorption in oxygen at low pressures (1–10 atmos.) has been re-examined with an 11-meter path length. It was found that over this range the absorption coefficient is accurately proportional to the square of the pressure. These more accurate results prove that the slight departure from linearity of the curve in Fig. 1 of our first note is not real. There is, therefore, no evidence of quadrupole or magnetic dipole absorption.

* Holder of a scholarship under the Ontario Research Council, 1947–1949.
[1] Crawford, Welsh, and Locke, Phys. Rev. **75**, 1607 (1949).
[2] G. Herzberg, Nature **163**, 170 (1949).
[3] A. Langseth and J. R. Nielsen, Phys. Rev. **46**, 1057 (1934).

The Alpha-Particles Emitted in Fission

L. L. GREEN
George Holt Physics Laboratories, University of Liverpool, England
AND
D. L. LIVESEY
Wellington College, Berkshire, England
June 27, 1949

IN a recent paper in the Physical Review,[1] Dr. L. Marshall made several misleading comments on the results of our experiments on the emission of light particles in fission, as briefly reported in Nature.[2] We should like to draw attention to a detailed account of the work which was published in the Philosophical Transactions[3] of the Royal Society in August, 1948, in which the problem of nuclear recoils is fully dealt.

Confusion seems to have arisen in that we reported observations on a further group of short range particles first observed by Cassels, Feather, Dainty, and Green[4] in addition to the long range alpha-particles with which Dr. Marshall's paper is concerned. Our abundance figure for this group of long range alpha-particles is roughly in agreement with Dr. Marshall's.

Recent experiments by Allen and Dewan[5] fully substantiate the main conclusions of our paper.

[1] L. Marshall, Phys. Rev. **75**, 1339 (1949).
[2] L. L. Green and D. L. Livesey, Nature **159**, 332 (1947).
[3] L. L. Green and D. L. Livesey, Phil. Trans. **A241**, 323 (1948).
[4] Cassels, Dainty, Feather, and Green, Proc. Roy. Soc. **A191**, 428 (1947).
[5] K. W. Allen and J. T. Dewan, Phys. Rev. **76**, 181 (1949).

Magnetic Moments and Eddy Current Damping in Spherical Superconductors*

J. J. FRITZ, O. D. GONZALES, AND H. L. JOHNSTON
Cryogenic Laboratory and Department of Chemistry, Ohio State University, Columbus, Ohio
June 27, 1949

THE magnetic moments of six spherical specimens of pure tin have been measured between 1.2°K and 3.6°K in fields up to and including those producing the intermediate state. The magnetic moments were observed in terms of the effect of magnetic fields upon the period of oscillation of the specimen suspended from a torsion wire. No magnetic moment was detected when the specimens were cooled from above the transition temperature in zero field. However, after the superconductivity had

been destroyed, below the transition temperature, by application of magnetic fields above two-thirds the critical value, a magnetic moment remained upon removal of the field.

The observed magnetic moments were independent of the measuring field provided the latter was not sufficient to put the material in the intermediate state. They depended on the temperature and upon the geometry of the specimen. For the solid spheres, the observed moments corresponded to 1 to 3 percent of the induction present at the critical field, and apparently were due solely to "frozen-in" moment. For the hollow spheres considerably larger moments were found.

Upon entry into the intermediate state, the magnetic moments increased sharply. Apparently magnetic induction set up in very small normal regions was "trapped" in its original position because of a long relaxation time required for reorientation of the normal regions. This abrupt increase in magnetic moment could be used to determine the field at which entry into the intermediate state occurred; the results were consistent with previous measurements of the critical fields for tin.

Large field-dependent damping effects were observed in the intermediate state, due to the appearance of normal areas in the superconductor. Small field dependent damping effects were observed at lower fields for the specimens with magnetic moment, but were absent when there was no moment present. This can be explained if one assumes that the moment interacts with the applied field in such a way as to produce small normal regions even at low fields.

The effects observed were reversible so long as the measuring field was less than that required to cause entry into the intermediate state. Pronounced hysteresis and relaxation effects were observed in the transition between the superconducting and intermediate states.

* Supported by a sub-contract with the Curtiss-Wright Corporation, which in turn was a part of Contract No. W33-038-ac-14161 with the Army Air Forces.

Tidal Effects in the F Layer*

M. W. JONES AND J. G. JONES
Geophysical Observatory, University of Alaska, College, Alaska
June 30, 1949

A PERIODIC variation of the semi-thickness, τ, of the F layer, noted at College, Alaska,[1] was submitted to harmonic analysis. In addition to the diurnal change in the thickness (the solar diurnal wave) of the ionized layer due to the sun's ionizing radiation, waves resulting from the contractions and expansions of the layer due to solar and lunar gravitational forces were extracted. The important gravitational tidal variations are the solar semi-diurnal wave, whose amplitude was approximately 60 percent of the solar diurnal wave, and the lunar diurnal wave, whose amplitude varied from 0.1 to 1.6 times the amplitude of the solar semi-diurnal tide during the winter of 1948–49 (October–March). A semi-diurnal lunar wave is usually found in geophysical phenomena, but the incidence of a significant lunar diurnal wave at College can be explained by simple tidal theory.[2] The vertical component of the tide-producing force has a diurnal term proportional to

$$\sin 2Y \sin 2D \cos t,$$

where Y is the latitude of the station, D is the moon's declination, and t is the hour angle of the moon, and a semi-diurnal term

$$\cos^2 Y \cos^2 D \cos 2t.$$

Hence at a high latitude (for College, $Y=64°\ 52'$) the semi-diurnal term becomes insignificant while the diurnal term is relatively large.

An example of the lunar diurnal wave is shown in Fig. 1. The lunar diurnal wave

$$L_1 = 3.1 \sin(t+25°)$$

found in the harmonic analysis is the solid curve, while the points

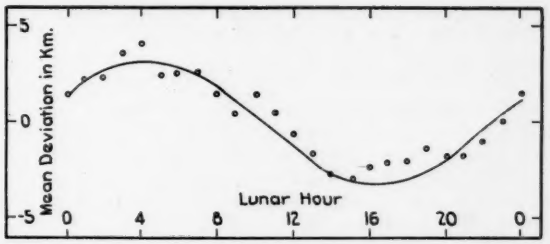

FIG. 1. Mean lunar variation of τ for December, 1947, at College, Alaska.

are the lunar-hourly means of the lunar variation of τ for December, 1947, extracted from the data.

The lunar diurnal wave is shown to be that predicted above in that the sign of the diurnal oscillation corresponds to the sign of the moon's declination (see Fig. 2).

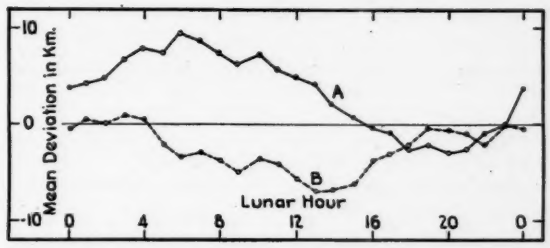

FIG. 2. Mean lunar variation of τ for intervals in December, 1947, at College, Alaska. Curve A for the days when the moon's declination was positive; curve B for the days when the moon's declination was negative.

* This work was supported in part by Contract No. W28-099-ac-445 with the U. S. Air Force, through sponsorship of the Geophysical Research Directorate, Air Materiel Command.

[1] Geophysical Research Directorate of the Cambridge Field St., A.M.C., U. S. Air Force, "State of the earth's atmosphere in the Arctic," Research Report No. 3 (February 17, 1949).

[2] P. Schureman, *Manual of Harmonic Analysis and Prediction of Tides* (United States Government Printing Office, Washington, 1941).

Gamma-Radiation from Deuteron Bombardment of Be^9

V. K. RASMUSSEN, W. F. HORNYAK, AND T. LAURITSEN
Kellogg Radiation Laboratory, California Institute of Technology, Pasadena, California
June 27, 1949

THE bombardment of beryllium with deuterons leads to the following reactions:

a. $Be^9+D^2 \rightarrow B^{10}+n^1+4.31$ Mev.
b. $\rightarrow Be^{10}+H^1+4.52.$
c. $\rightarrow Li^7+He^4+7.09.$
d. $\rightarrow Be^8+T^3+4.53.$

In cases a, b, and c, excited states of the residual nuclei are known to be formed, and the energies of some of the resulting gamma-rays have been determined.[1–3] This and the following letter summarize the results of some further measurements of the gamma-ray spectra; a more complete report will be presented at a later date.

As in the previously reported work, the gamma-ray energies have been determined from the photo-electrons produced in thorium converters, using a magnetic lens spectrograph. A vacuum connection to an electrostatic accelerator permits deuteron bombardment of targets within the spectrometer.[4] A part of the observed electron distribution is reproduced in Fig. 1, where the Compton electron spectrum from a thick beryllium converter is also shown. Other parts of the spectrum are shown in references 1 and 3, and in the following letter.

The results of a number of runs, using a thick target with a deuteron energy of 1.2 Mev, are collected in Table I. The gamma-

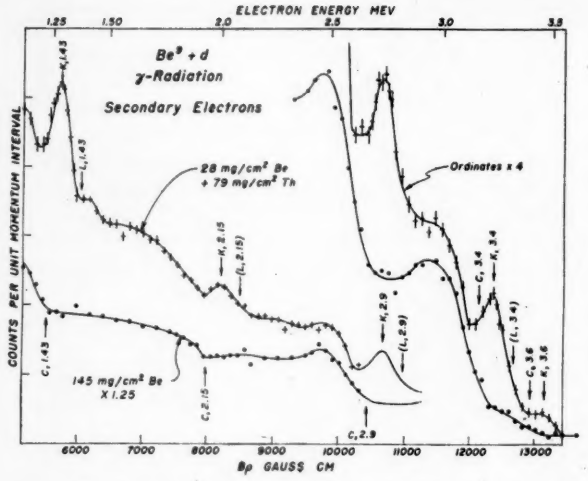

FIG. 1. Part of the momentum spectrum of secondary electrons produced in the converters noted by the gamma-radiation resulting from the bombardment of beryllium with deuterons.

ray energies are calculated from the photo-line peaks, applying corrections for converter thickness. In deducing the corresponding level transition energies given in column 5, allowance has been made for the Doppler effect due to the center of mass motion. This correction is modified somewhat at the lower energies because of the angular distribution of photo-electrons and the effects of scattering in the converter and is uncertain to about 50 percent for energies less than about 1 Mev. The relative gamma-ray intensities in column 3 have been estimated from the observed areas under the peaks, using the total photoelectric cross sections given by Hulme *et al.*,[5] and may be in error by as much as a factor of two, again because of the effect of the variation with energy of the angular distribution of the photo-electrons and of scattering and energy loss in the converter. The neutron intensities are those calculated by Evans, Malich, and Risser[6] from the data of Bonner and Brubaker obtained with 0.9 Mev (peak a.c.) deuterons

From considerations discussed in reference 1, it is believed that at least part of the radiation at 414, 717, 1433, 2150, and 3600 kev corresponds to transitions from excited levels directly to the ground state of B^{10}. Including the Doppler shift corrections, the excitation energies of these levels are 412, 713, 1424, 2138, and 3580 kev. The 1022 kev line is most easily accounted for by cascade from the 1424 kev level to that at 412; the absence of a corresponding neutron group suggests a similar explanation for the 2853 kev line, although the existence of levels at either of these two energies cannot be excluded. The 472 kev radiation is clearly associated with the d,α-reaction, and the 3380 kev radiation is almost certainly from the known level in Be^{10} as observed in the $Be^9(d\,p)Be^{10}$ reaction.[7]

Inspection of the table reveals several interesting features: the most conspicuous of these is that a number of the transition energies are integral multiples of 713 kev to an accuracy of the order of 0.5 percent, as exhibited in the last column. It seems somewhat unlikely that such close correspondence should be entirely fortuitous. It may also be observed that the neutron transitions to the higher states are relatively much more numerous than the corresponding gamma-transitions to the ground state, indicating that cascades must be the rule rather than the exception. It is of some interest that the 411 kev state is apparently involved in only one such cascade, that from the 1424 kev state.

This work was assisted by the joint program of the ONR and the AEC.

TABLE I. Results of a number of experiments in which a thick target of Be^9 is bombarded with deuterons of 1.2-Mev energy.

Nucleus	E_γ	I_γ	I_n	$E_{\text{transition}}$	$n\times713$
B^{10*}	413.5±1	14	53	412±1.5	
B^{10*}	716.6±1	56		713±1.5	713
B^{10*}	1021.6±2	13		(1016±2)‡	
B^{10*}	1432.9±5	8.7	†	1424±5	1426
B^{10*}	2152.0±15	2.9	22	2138±15	2139
B^{10*}	2871.0±15	4.6		(2853±15)‡	2852
B^{10*}	3604.0±30	1.5	25	3580±30	3565
Li^{7*}	(472)††	15		(476.6±0.8)††	
Be^{10*}	3380±15	6.2		3359±15	

† A neutron group corresponding to this level is observed but has been attributed to the $D^2(dn)He^3$ reaction.
‡ Weak neutron groups corresponding to levels in B^{10} at these energies cannot be ruled out.
†† The breadth and asymmetry of the photoelectron peak from $Be^9(d\alpha)Li^{7*}$ (see reference 3) is such as to make an energy determination more or less meaningless. The level energy quoted is from $Be^7(K)Li^{7*}$.

[1] Lauritsen, Fowler, Lauritsen, and Rasmussen, Phys. Rev. **73**, 636 (1948).
[2] Lauritsen, Dougherty, and Rasmussen, Phys. Rev. **74**, 1566A (1948).
[3] Rasmussen, Lauritsen, and Lauritsen, Phys. Rev. **75**, 199 (1949).
[4] Hornyak, Rasmussen, and Lauritsen, Phys. Rev., to be published.
[5] Hulme, McDougall, Buckingham, and Fowler, Proc. Roy. Soc. **149**, 131 (1934).
[6] Evans, Malich, and Risser, Phys. Rev. **75**, 1161 (1949).
[7] W. W. Buechner and E. N. Strait, Phys. Rev. **76**, 168 (1949).

High Energy Gamma-Radiation from Be^9+D^2

C. Y. CHAO, T. LAURITSEN, AND V. K. RASMUSSEN
Kellogg Radiation Laboratory, California Institute of Technology, Pasadena, California
June 27, 1949

IN a study of the reaction $Be^9(d\,n)B^{10}$ ($Q=4.31$ Mev), Evans, Malich, and Risser[1] have found evidence for a new neutron group with $Q=-0.74$ Mev, corresponding to an excited state of B^{10} at 5.0 Mev. At a bombarding energy of 1.4 Mev this group is stated to account for about 30 percent of the total neutron emission, if an isotropic distribution is assumed. However, their total gamma-ray yield does not indicate the appearance of additional gamma-radiation corresponding to this group.

Using a magnetic lens spectrometer arranged as described in the preceding letter, we have examined the high energy end of the gamma-ray spectrum in some detail. The source assembly consisted of several layers of beryllium metal foil, aggregating about 300 kev energy loss at the deuteron energy used, 25 mg/cm² of thorium metal foil to stop the deuterons and 250 mg/cm² of beryllium metal as a Compton electron source. This assembly was suspended in the spectrometer by a fine wire, to avoid extraneous scattering and conversion effects, and bombarded by a 1.50 Mev deuteron beam.

The resulting momentum distribution of the secondary Compton electrons is shown in Fig. 1, where the abscissa scale is proportional to the current in the lens coils, and hence to the momentum of the focused electrons (10,000 gauss cm = 27.4_8 mv). Above the 3.38 and 3.60 Mev lines reported in the preceding letter, there appear distinct breaks in the curve, indicating three higher energy gamma-rays. The energies and approximate relative intensities of these gamma-rays have been determined by comparison with the Compton electron distribution from similar converters re-

TABLE I. Energies and intensities of gamma-rays from Be^9 bombarded with deuterons.

E_γ (Mev)	2.89±0.04†	3.35±0.05†	3.56±0.06†
Relative‡ intensity	2.9	1.8	1.0
E_γ (Mev)	3.97±0.08	4.47±0.07	5.20±0.1
Relative‡ intensity	0.1	0.14	0.04

† From this experiment only. Compare with previous letter.
‡ May be in error by as much as a factor of two.

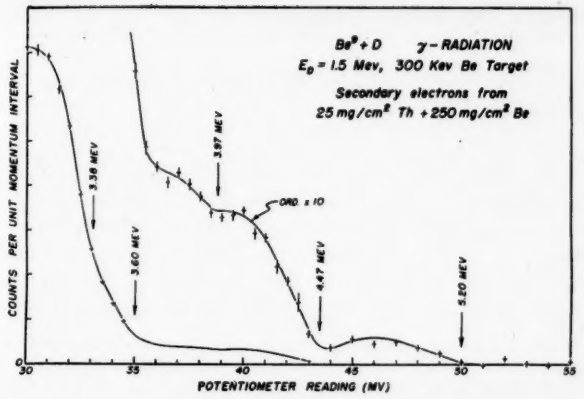

FIG. 1. Compton electrons ejected from 250 mg/cm² of beryllium by the high energy gamma-radiation produced in the bombardment of beryllium with deuterons. The abscissae are proportional to the current in the lens coil, and therefore proportional to the magnetic field and to the momentum of the focused electrons.

sulting from the 3.11-Mev gamma-ray from $C^{12}(d\,p)C^{12*}$ [2] and the 6.15-Mev gamma-ray from $F^{19}(p\,\alpha)O^{16*}$.[3] The results are given in Table I. The total intensity of the three higher energy lines is less than about 2 percent of the total gamma-intensity from the $Be^9(d\,n)B^{10}$ reaction under the conditions of the present experiment.

The assignment of these gamma-rays to particular nuclei is complicated by the fact that B^{10}, Be^{10}, Be^8 and Li^7 may all be formed by the deuteron bombardment of Be^9 as highly excited residual nuclei. Because of the agreement of the energy of the highest line with the value expected from the Q of the new neutron group it seems reasonable to associate this line with a level in B^{10}, the low intensity of the line implying that the state decays primarily either by emitting a series of lower energy gamma-rays or by heavy particle emission to Li^6+He^4 (Q=0.84 Mev). The fact that the total gamma-ray yield does not reflect the appearance of the neutron group would indicate that the latter mode of disintegration may be preferred in spite of the rather low energy of the alpha-particles. The 4.47-Mev line may represent a level in B^{10} for which the neutron group has not yet been observed or which is reached only by cascade from the 5.2 Mev level. The 3.97 Mev line could then result from the transition from this level to the known 0.411 Mev level. Alternatively, the 4.47 Mev line could represent a transition from the 5.2 Mev level to the known 0.713 Mev level leaving the 3.97 line still to be accounted for.

This work was assisted by the joint program of the ONR and the AEC.

[1] Evans, Malich, and Risser, Phys. Rev. **75**, 1161 (1949).
[2] Dougherty, Hornyak, Lauritsen, and Rasmussen, Phys. Rev. **74**, 712 (1948).
[3] Rasmussen, Hornyak, and Lauritsen, Phys. Rev. **75**, 1462A (1949).

On the Origin of Heavy Cosmic-Ray Particles

LYMAN SPITZER, JR.
Princeton University Observatory, Princeton, New Jersey
July 7, 1949

IT has been suggested by F. Zwicky[1,2] that supernovae might produce cosmic rays, with expulsion of high-speed atoms from the stellar surface. Another mechanism, apparently not considered hitherto, is the acceleration of small solid particles, or dust grains, by the pressure of supernova radiation. The velocities reached are close to that of light. The high-speed grains would gradually disintegrate into cosmic-ray particles of the heavier elements, primarily O, Mg, and Fe. The computed density of these particles in space is consistent with the observed flux of heavy nuclei in cosmic radiation.

The absolute brightness of a supernova, according to W. Baade,[3] is 5×10^7 suns, or 2×10^{41} ergs/sec. if the surface temperature of a supernova equalled that of the sun. Interstellar grains further away than about 10^{16} cm (0.01 light year) would be heated to less than 1000°K and Fe and Mg compounds would not evaporate. A grain of radius 10^{-5} cm at this distance initially would be accelerated to a velocity of about 3×10^9 cm/sec. within a few weeks; this gives a kinetic energy of about 0.01 Bev per nucleon.

This velocity is a minimum value, since, according to R. Minkowski,[4] the actual surface temperature of a supernova is apparently much higher than 6000°. With increased temperature the total flux of radiation is greater. In addition, the wave-length, λ_m, of maximum radiation flux is decreased; the acceleration is greatest for grains whose radius is about $\lambda_m/2\pi$, and with decreasing λ_m grains of less mass per area can be more effectively accelerated. If a surface temperature of 100,000° is assumed, the minimum distance at which a grain will not evaporate becomes about 10^{17} cm (0.1 light year) and the final kinetic energy becomes about 1 Bev per nucleon for a grain of radius 10^{-6} cm.

These high-speed grains would not last long, provided that they are retained in the galactic plane by a strong magnetic field, as postulated by E. Fermi,[5] and verified by the observations of Hiltner[6] and Hall[7]—see Spitzer and Tukey.[8] In a few thousand years such a grain will collide with a low-speed grain in an interstellar cloud. Even if a grain could survive such an impact, encounters with H atoms would knock all the atoms off the surface of a high-speed grain every few thousand years, giving a relatively rapid evaporation.

To compute the density of the individual high-speed atoms produced we shall assume that all the grains between 10^{17} and 2×10^{17} cm of a supernova are accelerated, and that the resultant nuclei are retained within a cylindrical volume of our galaxy 30,000 light years in radius, and 600 light years thick. Since interstellar matter is apparently confined to spiral arms, which occupy perhaps a fifth of this volume, the mean density of interstellar matter in this cylinder may be taken as 0.2 H atom per cm³. An Fe nucleus, moving with a kinetic energy of about 1 Bev per nucleon, will lose half its energy to the interstellar H atoms in about 2×10^7 years. The frequency of supernova in the spiral arms of the galaxy we take as one per 100 years; this rate, about five times that found for external galaxies, seems warranted both by the large size of our galaxy and by the number of supernovae observed nearby. The average space density of the relevant grains, each 10^{-6} cm in radius and containing 10^6 atoms, is highly uncertain. We assume here that this density is 10^{-11} per cm³; the true value may lie anywhere between 10^{-10} and 10^{-14}. On these assumptions, the computed average density of high-speed atoms in the galaxy is 5×10^{-14} per cm³, yielding a particle flux of about 10^{-4} atom per cm² per steradian. This result is consistent with the corresponding observed particle fluxes in the cosmic radiation which, according to B. Peters,[9] are 1.0×10^{-4} for $10<Z<28$, and 4.3×10^{-4} for O, C, and N.

While this mechanism may apparently produce an appreciable fraction of the heavy-particle cosmic radiation, it may not be capable of generating particles with energies greater than a few Bev per nucleon. Possibly the mechanism proposed by E. Fermi[5] may be important in accelerating particles further, although the injection energies required for this mechanism apparently exceed 5 Bev per nucleon for Fe. Further observational and theoretical study of the energy spectrum seems needed. Detailed abundances of the different elements in cosmic radiation would also provide a check on the further theoretical work planned. I am much indebted to Professor John Wheeler for illuminating discussions.

[1] F. Zwicky, Phys. Rev. **55**, 986 (1939).
[2] F. Zwicky, Proc. Nat. Acad. Sci. **25**, 338 (1939).
[3] W. Baade, Astrophys. J. **88**, 285 (1938).
[4] R. Minkowski, Publ. Astr. Soc. of the Pacific **53**, 224 (1941).
[5] E. Fermi, Phys. Rev. **75**, 1169 (1949).
[6] W. A. Hiltner, Science **109**, 165 (1949).
[7] J. S. Hall, Science **109**, 166 (1949).
[8] L. Spitzer, Jr. and J. W. Tukey, Science 109, 461 (1949).
[9] B. Peters, informal communication.

Proceedings of the American Physical Society

MINUTES OF THE MEETING AT THE UNIVERSITY OF WASHINGTON, AT SEATTLE, WASHINGTON
JUNE 27–29, 1949

THE 294th meeting of the American Physical Society was held at the University of Washington, Seattle, on June 27–29, 1949. About 160 members of the Society registered and the attendance at the various sessions varied up to a maximum of about 250. The local arrangements were excellent and there were several interesting social functions including a theater party at the famous Showboat Theater of the University of Washington and a well-attended luncheon of the Society on June 29. The principal speaker at the luncheon was Dr. K. K. Darrow who presented an interesting account of the development of the Society during its first 50 years. Many of the members took advantage of the excellent opportunities for excursions in this beautiful part of the country. The growth of the science of physics in the Pacific Northwest was well demonstrated at this meeting and the success of this meeting should make many future summer meetings in this region highly desirable and profitable.

The Tuesday afternoon session of invited papers was a joint session with the Astronomical Society of the Pacific. The Wednesday afternoon session was a joint session with the American Association of Physics' Teachers. Two post-deadline papers were accepted. The first one, by R. F. Christy of the California Institute of Technology, was presented by R. F. Taschek following the latter's invited paper. Dr. Christy's paper dealt with the theoretical aspects of the experimental results reported by Dr. Taschek. The second paper was a report on "Gamma-Radiation from Capture of Protons by Deuterons," by A. V. Tollestrup, W. A. Fowler, and C. C. Lauritsen, presented by W. A. Fowler.

The presiding officers at the various sessions were: Professors C. L. Utterback, E. A. Uehling, J. E. Henderson, and D. H. Loughridge of the University of Washington; Professor H. Margenau of Yale University; Professor J. Kaplan of the University of California, Los Angeles; Professor W. Weniger of Oregon State College and Dr. K. K. Darrow.

J. KAPLAN, *Local Secretary for the Pacific Coast*
UNIVERSITY OF CALIFORNIA
LOS ANGELES, CALIFORNIA

Invited Papers on the General Programme

Recent Developments in Electron Microscopy. L. MARTIN, *National Bureau of Standards, Washington, D. C.*

Recent Advances in Quantum Electrodynamics. R. P. FEYNMAN, *Cornell University, Ithaca.*

High Energy Gamma-Rays from the Cyclotron Target. BURTON J. MOYER, *University of California, Berkeley.*

Proton-Proton Scattering. WOLFGANG K. H. PANOFSKY, *University of California, Berkeley.*

Recent Theoretical Work at the Radiation Laboratory. M. L. GOLDBERGER, *University of California, Berkeley.*

Nuclear Spectroscopy. W. A. FOWLER, *California Institute of Technology, Pasadena.*

Isotopes in Stellar Atmospheres. ANDREW MCKELLAR, *Dominion Astrophysical Laboratory.*

Scattering and Reactions of Protons on Tritons. R. F. TASCHEK, *Los Alamos Scientific Laboratory.*

Direct Crystal Spectroscopy of Gamma-Radiation. DAVID A. LIND, *California Institute of Technology, Pasadena.*

An Infra-Red Recording Spectrograph of High Resolution and High Precision. EDSON PECK, *Northwestern University, Evanston.*

Solar Activity Variations and Their Apparent Consequences. WALTER O. ROBERTS, *Harvard University, Cambridge.*

The New California Institute Electrostatic Generator. J. E. PERRY, *California Institute of Technology, Pasadena.*

Theory and Applications of the Shock Tube. OTTO LAPORTE, *University of Michigan, Ann Arbor.*

Contributed Papers

A1. Forbidden Oxygen Lines in Afterglows.* S. KASH AND J. KAPLAN, *University of California, Los Angeles.*—A remarkable luminescence which appears to be associated with the green oxygen auroral line has been reported by Vegard and Kvifte[1] and by Jenkins, Bowtell, and Strong.[2] This appears to be the same effect which was first observed by one of us[3] in an unusually strong green line afterglow in nitrogen-oxygen mixtures. The spectrum published in 1942 shows a continuous shading on the short wave-length side of the green line. This shading was not present in the vicinity of the forbidden oxygen

line 2972. Current studies of intensity variations in this strong green line afterglow have shown clearly that the green line and the associated line 2972 follow a different intensity-time relationship than does the forbidden nitrogen line 3467 in the same afterglow. The two oxygen lines decay much more slowly than do all other features of the afterglow spectrum. The continuous spectrum which accompanies the green line shows the same intensity-time behavior as do the two forbidden lines which originate on the $^1S_0$ level. Further studies of these effects in other oxygen forbidden line sources are in progress.

* This work is being carried on under an ONR contract.
[1] L. Vegard and G. Kvifte, Nature, No. 2, 967 (1948).
[2] Jenkins, Bowtell, and Strong, Nature, **163**, 401 (1949).
[3] J. Kaplan, Nature, **149**, 273 (1942).

A2. Propagation Rate of Streamers in High Pressure Sparks. B. A. JACOBSOHN, *University of Washington.*—The formative time for sparks at high pressures and large gap lengths is related to the rate of propagation of the streamer head back to the cathode. The propagation mechanism, which has been described by Loeb,[1] depends on photo-ionization near the streamer tip by ultraviolet photons of short mean free path. The crude model for streamer advance to be presented here includes the effect of those photons emitted in all directions. Thus the advance of the streamer head is governed by a diffusion equation which takes into account the "random walk" performed by the photons and the efficiency of each absorbed photon in eventually producing g new photons. If g is only slightly greater than one (small overvoltage), the region in which a critical positive ion density exists is not extended for some time after the passage of the first electron avalanche; after this delay time, the streamer propagates with high velocity. This is to be contrasted with models which lead to uniform streamer tip velocities.

[1] L. B. Loeb, Rev. Mod. Phys. **20**, 151 (1948).

A3. Transients in the Phenomena of Nuclear Induction. E. A. UEHLING, *University of Washington.*—The influence of the thermal relaxation time T_1 on the character of nuclear induction signals has been exhibited frequently as the time of approach to steady-state conditions when a change has been made in $\Delta\omega$, the difference of Larmor and exciting frequencies. In order to obtain a more quantitative examination of this phenomenon, transient solutions of the nuclear induction equations, valid for excitation amplitudes which are not arbitrarily small, but for modulation amplitudes which are much less than the line widths have been obtained. These solutions exhibit two types of approach to equilibrium: an approach without oscillation at a time constant nearly equal to T_1, and an approach with oscillation at a frequency determined by the final state and at a time constant nearly equal to the transverse relaxation time T_2. Under appropriate conditions, the solution dependent essentially on T_1 may be exhibited separately providing the radiofrequency field amplitude is greater than $1/\gamma(1/T_2-1/T_1)$, where γ is the gyromagnetic ratio.

A4. Nuclear Induction Proton Signals Below Noise Level from Gases at One Atmosphere.* F. BLOCH AND DAVID H. GARBER,** *Stanford University.*—A photographic method has been developed for observing nuclear induction signals with magnitude below the noise level of the associated detection and amplification stages. The signal together with the accompanying camouflaging noise is displayed in the usual manner on a cathode-ray oscillograph with linear sweep. A time exposure of several thousand traces is taken; the random nature of the noise contributes a horizontal, more-or-less uniform ribbon most dense in the middle, with the small recurrent signal observable at the top and bottom edges of the ribbon. The contrast obtained is enhanced by use of a high contrast film and by further contrast copying. Optimum or experimentally limiting conditions will be discussed for choice of contrast, exposure time, vertical sharpness of CRO beam, and band width of amplifier. Proton signals will be shown, obtained from samples of propane and of hydrogen gas, at one atmosphere pressure. A new design is employed for splitting the r-f transmitter coils which surround the receiver coil and sample; this eliminates difficulties of tuning and re-assembly previously accompanying changes of samples.

* Assisted by the ONR and the Research Corporation.
** Now at the University of Washington.

A5. Nuclear Resonances in Rotating Magnetic Fields.* E. H. ROGERS AND H. H. STAUB, *Stanford University.*—The sign dependence of the nuclear induction phenomenon has been observed by obtaining proton signals in purely rotating radiofrequency magnetic fields. It will be recalled[1] that the nuclear induction effect demands a radiofrequency field rotating about the direct current field in a direction which corresponds to the direction of Larmor precession of the nucleus under consideration. Ordinarily the rotating field is obtained from one rotating component of an oscillating field. As a consequence the direction of rotation of the precessing nuclei cannot be determined. In this new device the required field was produced by two pairs of coils oriented at right angles to one another and fed by two r-f currents differing in phase by 90°. Proton signals appeared and disappeared according to the direction of rotation of the r-f field around the d.c. field. By setting up elliptically polarized fields, various combinations of signal magnitudes were observed according to expectation. The device was constructed for and is currently being used to make a direct comparison of the signs of the magnetic moments of the neutron and the proton. The method for observing neutron resonances is similar to that described previously.[2]

* Assisted by the Joint Program of the ONR and AEC.
[1] F. Bloch, Phys. Rev. **70**, 460 (1946).
[2] Bloch, Nicodemus, and Staub, Phys. Rev. **74**, 1025 (1948).

A6. Collision Theories of Pressure Broadening of Spectral Lines.* J. H. VAN VLECK, *Harvard University,* AND HENRY MARGENAU, *Yale University.*—It is shown that in the calculation of absorption in the Lorentz collision theory, it is essential to include the work done impulsively by the electric field during the sudden change of position at collision. This work was implicitly included in the theory of Van Vleck and Weisskopf, but they did not give the breakdown into work done between and at collision. It is verified that the shape of spectral lines for a classical harmonic oscillator, and also a Debye slow rotator, are the same in absorption and spontaneous emission, provided the energy density obeys the Rayleigh-Jeans law. The usual proofs of equilibrium simply establish equality of the integrated absorption and emission, without examining the detailed balancing at individual frequencies, not necessarily near resonance.

* Supported in part by the ONR.

A7. Pressure Dependence of the Inversion Frequency of NH_3.* HENRY MARGENAU, *Yale University.*—Several experiments (Bleany and Penrose, Weingarten) on the shape of the inversion lines of NH_3 have indicated an effective decrease in the inversion frequency with increasing pressure of the gas. This is to be expected on theoretical grounds, as was suggested in a forthcoming publication. The interaction of two NH_3 molecules causes the doublet levels to change their spacing. It is shown that *two* transitions of different frequencies occur when the molecules approach each other, one smaller and one larger than the normal value and given by $\nu_0[(1+\lambda^2)^{\frac{1}{2}}\mp\lambda]$. Here λ is the dipole interaction energy divided by the normal doublet spacing. When transition probabilities are calculated it is seen that the smaller frequency gains in strength upon approach of the molecules, at the expense of the other. The

pressures at which the reduction in the resonance frequency is observed correspond to the distances of separation between molecules at which the effect here calculated sets in.—The preceding comments have reference to non-rotating molecules. Our calculation includes the rotation and shows that the deformation described is superposed upon the interaction (Margenau and Warren) previously discussed.

* Supported in part by the ONR.

A8. Waves Guided by a Single Surface. F. J. ZUCKER, *Electronics Research Laboratories*, USAF. (*Introduced by R. E. Hiatt.*)—Among the many possible modes known in electromagnetic theory, there is one type which enables energy to be propagated along a smooth or periodic interface between two media. This mode is characterized by the very rapid attenuation of the amplitude away from the guiding surface. Energy is transported along flow lines undulating from one medium into the other and back again, the relative amount of time spent in each depending on their constitutive parameters. A general discussion of the theory in its mathematical aspects is followed by a brief enumeration of several optical phenomena in which the mode arises (total internal reflection, Wood's anomalies in diffraction gratings,* reflection from metal mirrors), and of its connection with other fields of physics (molecular beams, acoustics). The type of mode in question has applications in microwave physics as well. It enables energy to be transported along single sheets or rods, both smooth or corrugated. Structures of this type lend themselves as radiators. Experimental verification of the theory will be displayed in several illustrative examples.

* U. Fano, Ann. d. Physik 5, 32/5 (1938).

A9. The Measurement of Electrical Anisotropy of High Polymers at Microwave Frequencies. T. M. SHAW AND J. J. WINDLE, *Western Regional Research Laboratory.**—Techniques are described for measuring the electrical anisotropy of natural and synthetic high polymers at microwave frequencies. A cylindrical cavity resonator operating in the TM_{010} mode at 3000 mc/sec. is used to determine the dielectric constant of the polymer for various orientations with respect to the electric field of the cavity. Appropriate procedures permit the method to be applied to solids of practically any form. Specific examples are given of measurements on fibers, films, and cylindrical rods.

* Bureau of Agricultural and Industrial Chemistry, Agricultural Research Administration, U. S. Department of Agriculture.

A10. Solenoidal Beta-Ray Spectrometer with Uniform Magnetic Field. F. H. SCHMIDT, *University of Washington.*—The theory of the ring focus has recently been discussed.[1,2] The results of a different approach to the focusing problem are here reported. An offset ring baffle[2] is used. For a point source the resolution is found to be a maximum at 55° 20′ emission angle. The inverse momentum resolution is then $\Delta p/p = 6.5(\Delta\Phi)^2$, where $\Delta\Phi$ is the fractional solid angle transmitted. The resolution is quite flat and decreases by only 20 percent at emission angles of 40° and 68°. For a source of finite surface area perpendicular to the axis of the instrument, the optimum emission angle is 43°±1° under conditions of constant luminosity (source area times solid angle). The resolution at constant luminosity decreases by only 10 percent at angles 32° and 60°. By adopting the resolution criterion of DuMond,[2] and equating the aberration due to finite disk source to that due to the finite solid angle, the following optimum conditions at 43° are obtained: $\Delta p/p = 12(\Delta\Phi)^2$, source diameter $= 1.16R\Delta p/p$, where R = maximum distance between trajectories and axis of the instrument. Thus, a $\Delta p/p$ of ½ percent should be obtainable with a 2 percent $\Delta\Phi$. Such an instrument is under construction and will be described.

[1] E. Persico, Rev. Sci. Inst. **20**, 191 (1949).
[2] J. W. M. DuMond, Rev. Sci. Inst. **20**, 160 (1949).

C1. Neutron Polarization. J. FLEEMAN AND H. H. STAUB, *Stanford University.*—The time-of-flight method has been used to obtain a monoenergetic beam of neutrons in order to determine the cross section for the polarization of neutrons by magnetized iron. We obtain the following results: (1) The measured values of p as a function of the velocity of the neutrons are in good agreement with those obtained by Hughes;[1] they are roughly 6 percent smaller than the calculated values of Steinberger and Wick,[2] using the 3d wave function with zero slope at the atomic radius. (2) The velocity spectrum of the neutron beam was measured and we find that it deviates somewhat from a Maxwell-Boltzmann distribution at room temperature, as expected. From these measurements, the modification of the spectral composition of the neutron beam upon passage through iron can be calculated. From measurements of the single-transmission effect at thicknesses ranging from 0.6 cm to 5.0 cm it is found that the average value of p, for the spectrum used in the present experiment, is 2.33±0.10 barns in agreement with previous results.[3] The dependence of magnetic saturation upon H is also in satisfactory agreement with previous magnetic measurements.[3]

[1] Hughes, Wallace, and Holtzmann, Phys. Rev. **73**, 1277 (1948).
[2] J. Steinberger and G. C. Wick, Phys. Rev. **74**, 1207 (1948).
[3] Bloch, Hamermesh, and Staub, Phys. Rev. **64**, 47 (1943); Bloch, Condit, and Staub, Phys. Rev. **70**, 972 (1946).

C2. Proton Induced Activities in Tantalum. J. W. BURKIG AND J. REGINALD RICHARDSON, *University of California, Los Angeles.*—When tantalum is bombarded with 12-Mev protons, the following activities are observed: one or possibly two periods in the range 15 to 20 minutes, an activity of eight hours half-life, and a long period activity. Excitation functions have been obtained indicating a very steep rise of the eight-hour period with increasing proton energy, and a threshold at six Mev. This corresponds to the reaction $Ta^{181}(p, pn)Ta^{180}$, except that the threshold is somewhat lower than that reported for the (γ, n) reaction and may indicate the presence of some (p, d) reaction. In the case of the long period, however, the excitation function is less steep with an ill-defined threshold below 4 Mev. This corresponds to the reaction $Ta^{181}(p, n)W^{181}$. The half-life of W^{181} is 140 days.[1] The energy spread of the proton beam has been checked by the usual foil-wheel technique. The width at half maximum of the current *vs.* energy curve is 0.5 Mev. The excitation function of the short period activity is complex. This may indicate the presence of two activities of approximately this period. This work was supported in part by the joint program of the ONR and the AEC.

[1] G. Wilkinson, Nature **160**, 864 (1947).

C3. The Q Value for $B^{10}(p\alpha)Be^7$. C. Y. CHAO, C. C. LAURITSEN, AND A. V. TOLLESTRUP, *California Institute of Technology.*—From the Q values for $B^{10}(p\alpha)Be^7$ and $Li^7(pn)Be^7$ and the energy of the first excited state of Li^7, the Q values for $B^{10}(n\alpha)Li^7$ and $B^{10}(n\alpha)Li^{7*}$ can be calculated. The energy of this latter group of α-particles is of particular interest since, together with their range determined by Bøggild[1] and also by others, it gives a fixed point in the range-energy relation for slow α-particles. From threshold measurement, the Q value of $Li^7(pn)Be^7$ has been determined to be 1.646±0.002 Mev[2] while several recent investigations have yielded 0.478±0.001 Mev for the energy of the first excited state of Li^7. The α-particles from $B^{10}(p\alpha)Be^7$ have been studied by bombarding a thin evaporated layer of B^{10} enriched B_2O_3 with protons from an electrostatic generator. The α-particles emerging from the target at a mean angle of 137.8° with the incident beam were analyzed by a double focusing magnetic spectrograph

and detected with a scintillation counter. The Q value for $B^{10}(p\alpha)Be^7$ is found to be 1.148 ± 0.005 Mev which is somewhat higher than the value 1.05 ± 0.07 found by Burcham and Freeman.[3] Our value leads to 2.794 ± 0.006 Mev for the Q value of $B^{10}(n\alpha)Li^7$ and 2.316 ± 0.006 Mev for that of $B^{10}(n\alpha)Li^{7*}$. This work was assisted by the joint program of the ONR and the AEC.

[1] J. K. Bøggild, Kgl. Danske Vid. Sels. Math.-fys. Medd 23, No. 4, 1 (1945).
[2] Herb, Snowdon, and Sala, Phys. Rev. 75, 246 (1949).
[3] W. E. Burcham and J. M. Freeman, Nature 163, 167 (1949).

C4. Magnetic Analyzer for Electrostatic Generators. D. B. DUNCAN, *California Institute of Technology.*—A magnetic analyzer has been constructed for use with the new electrostatic generator. The beam from the generator is deflected through 90° with a radius of curvature of 16 in. An "H type" cross section is employed so that the return path for almost all of the flux is in iron, thereby minimizing the interference of the stray field with nearby apparatus. By shaping the pole pieces so that the field varies as $r^{-\frac{1}{2}}$ point for point focusing properties are obtained.[1,2] A parallel beam is focused 17 in. from the magnet where slits are located to give energy resolution. The field is measured with a null-reading fluxmeter.[3] The 125 amperes necessary are obtained from selenium rectifiers, the current being regulated by supplying the input to saturable core reactors from the electronically amplified potential drop across a series resistor. This work was assisted by the joint program of the ONR and the AEC.

[1] Svartholm and Siegbahn, Arkiv. f. Mat. Astr. o. Fys. 33A, No. 21 (1946).
[2] Snyder, Lauritsen, Fowler, and Rubin, Phys. Rev. 74, 1564 (1948).
[3] C. C. Lauritsen and T. Lauritsen, Rev. Sci. Inst. 19, 916 (1948).

C5. Application of Proportional Counter to $p-\alpha$ Reactions at 100 Kev. A. W. SCHARDT, E. J. WOODBURY, AND W. A. FOWLER *California Institute of Technology.*—A β-ray mica window counter is used either with original filling or with 20- to 30-cm Hg of a mixture of 90 percent A and 10 percent CO_2. The amplifier[1] has a gain of 10^4 to 10^5 with the shortest time constant 1.6 μsec. The high voltage on the counter is derived from a shunt regulated power supply (600 to 1500 volts) which drifts less than 1.5 volts after initial warm-up. If wide apertures are desired 4 percent to 6 percent of a sphere the pulse heights are not uniform. However 100 percent α-counting is possible in presence of strong β- and γ-ray background. The mica window of the counter is 1.8 mg/cm^2. It is coated with 0.2 mg/cm^2 of aluminum. Thus no scattered protons enter the counter. With 100 μamp. of protons on a clean brass target 1 background count per minute is observed. Investigations are being made on the $N^{15}(p\alpha)C^{12}$ reaction which is of special interest since it is part of the stellar cycle.[2] The target (TiN^{15}) is mounted on an air-cooled brass support. Special care has to be taken to eliminate surface films which can mask completely the true reaction. An improved design of the r-f ion source[3] gives reliably 100 μamps. of protons through a 0.095-in. aperture mounted in front of the target. Preliminary results will be discussed. This work was assisted by the joint program of the ONR and the AEC.

[1] W. H. Jordon and P. R. Bell, Rev. Sci. Inst. 18, 703 (1947).
[2] H. A. Bethe, Phys. Rev. 55, 434 (1939).
[3] R. N. Hall, Rev. Sci. Inst. 19, 905 (1948).

C6. Operation of a Linear Electron Accelerator.* G. E. BECKER AND D. A. CASWELL *Stanford University.*—The traveling wave linear electron accelerator[1] constructed at Stanford has been extended in length to 14 ft. The increase has been made in steps of approximately 2 ft., and at each new length the dependence of the energy spectrum on the frequency power input and injection voltage has been investigated. The energy spectrum is monochromatic in character in that there is a single peak in the curve of electron current *vs.* electron energy. With a length of 14 ft. the peak occurs at 5.7 Mev with a half-width of 1 Mev. The width of the peak is less for shorter lengths and is probably caused in part by the fact that the filling-time for a length of 14 ft. is an appreciable fraction (nearly $\frac{1}{2}$) of the pulse length. The current reaching the target remains of the same order of magnitude as the length is increased. The frequency sensitivity increases with length, but the energy spectrum remains good within a frequency range of ±0.5 mc/sec. Variations of 10 kv from the design injection voltage of 80 kv produce no significant changes in the output.

* Assisted by the ONR.
[1] Ginzton, Hansen, and Kennedy, Rev. Sci. Inst. 19, 89 (1947).

C7. A High Intensity Cyclotron. E. J. LOFGREN, *University of California, Berkeley.*—Preliminary experiments have been carried out on the use of a cyclotron as an injector for the Bevatron. We have obtained 20 ma of 1-mev protons circulating in pulses with a duty cycle of 1:1000. It has been possible to deflect 7 ma and by the use of a wedge-shaped magnetic field to bring $\frac{3}{4}$ ma to a focal spot about $\frac{1}{2}$ in.$\times1\frac{1}{2}$ in. 8 ft. from the cyclotron. The source is a cold cathode arc inside of a $\frac{1}{2}$-in. diameter tube whose axis is parallel to the field. The ions are withdrawn from a vertical slot in the tube by a pair of slits mounted on one dee. A large change of radius during the first turn is necessary so that the ions shall not strike the source. This condition is met by a magnetic field of 7000 gauss and 70 to 100 kv r-f between dees. A deflector with a longitudinal channel has been successfully used. It makes the deflector insensitive to positional or voltage adjustment since ions deflected too far feel a reduced electric field and move in again. Many suggestions were made by E. O. Lawrence including the channel deflector. This work was sponsored by the AEC.

C8. Total Cross Sections of Nuclei for 40-Mev Neutrons. R. H. HILDEBRAND AND C. E. LEITH, *University of California, Berkeley.*—The measurement of the 40-Mev neutron total cross sections of various nuclei will be described. The 40-Mev neutron beam is produced in the 184-in. cyclotron by the stripping[1] of 90-Mev deuterons in a $\frac{1}{2}$-in. thick Be target. The method of detection is that used by Cook, McMillan, Peterson, and Sewell[2] in making similar measurements for 90-Mev neutrons. The neutron intensity is measured by counting the 20.5-min. C^{11} positron activity resulting from the $C(n, 2n)$ reaction in carbon disks. The threshold for this reaction is about 20 Mev. The cross sections at 40 Mev will be compared to those at other energies. In the region of O, Mg, and Al the cross sections are only slightly smaller than those measured at 14 Mev[3], whereas, for nuclei heavier than Sn, the cross sections are closer to those measured at 90 Mev.[2] This work was sponsored by the AEC.

[1] R. Serber, Phys. Rev. 72, 1008 (1947).
[2] L. J. Cook, *et al.*, Phys. Rev. 75, 7 (1949).
[3] E. Amaldi, *et al.*, Nuovo Cimento 3, 15, 203 (1946).

C9. Range-Energy Relations for High Energy Protons in Photographic Emulsions. H. BRADNER, A. S. BISHOP, W. H. BARKAS,* *University of California, Berkeley.*—Range-energy relations for protons in the region of 30 Mev in nuclear emulsions are of particular interest for the calculation of the mass of artificially produced mesons. The range-energy relations of Lattes, Fowler, and Cüer[1] for protons of energies up to 13 Mev in Ilford B-1 emulsion have been extended to approximately 35 Mev using protons in the 184-in. Berkeley cyclotron. A check point was obtained with the Berkeley linear accelerator. Preliminary measurements at 33.4 Mev yield a range of 4597 μ in 200 μ emulsion evacuated for 6 hours. The range of 32-Mev protons in the glass of Ilford plates has been found to be 18 percent greater than in C-2 emulsion. Sixteen-Mev tracks were 3 percent shorter in 100 μ C_2 emulsion which had been evacuated for 6 hours, than in emulsion which had been kept at

~80 percent humidity for 6 hours, and then evacuated for 5 minutes. Thirty-three-Mev tracks in 200-μ C_2 emulsion showed an 8 percent difference in the same direction. This work was sponsored by the AEC.

* ONR, San Francisco.
[1] Nature 159, 301 (1947).

C10. Improved Mass Values for π^-, π^+, and μ^+ Mesons. A. S. BISHOP, H. BRADNER, AND F. M. SMITH, *University of California, Berkeley.*—The two major sources of error in the previously reported values[1] of π^-, π^+, and μ^+ mesons are (a) the uncertainty in the absolute value of the magnetic field of the 184-in. cyclotron and (b) the error in the range-energy relationship for mesons in Ilford C-2 emulsions. Two independent methods of minimizing these errors are being pursued. The most obvious method involves a redetermination of the magnetic field strength by the method of nuclear induction, together with a direct measurement[2] of the range-energy relationship in Ilford C-2 emulsion of protons from 13 to 40 Mev (corresponding to meson energies from 2 to 7 Mev). The second procedure is that of comparing the mass of the meson to that of the proton, when the apparent mass of the latter is also determined by $H\rho$ and range. In this way, approximate cancelation of the above errors can be achieved merely by selecting for measurement those protons with the same velocity as the mesons being measured. Results from both methods of measurement will be reported. This work was performed under the auspices of the AEC.

[1] A. S. Bishop, Phys. Rev. 75, 1468 (1949).
[2] Bradner, Bishop, and Barkas (accompanying abstract).

C11. Yield of Negative π-Mesons Produced by High Energy Protons as a Function of Proton Energy.* STANLEY B. JONES AND R. STEPHAN WHITE, *University of California, Berkeley.*—A study is now in progress to find the relative numbers of negative π-mesons created by protons of various energies. The energies were obtained by placing the targets at different radii in the 184-in. Berkeley cyclotron. The study is limited to star-producing mesons with energies of approximately 2–6 Mev emitted within $\pm 45°$ of the forward direction from a $\frac{1}{32}$-in. carbon target. Eastman type NTB Plates were used to record the mesons. Preliminary data are given in Table I. Column 1 gives the energy of the bombarding protons; column 2, the numbers of mesons actually counted; and column 3, the numbers of mesons relative to the number at 340 Mev, corrected for beam current, plate thickness, and area scanned.

TABLE I.

Beam energy (Mev)	No. of mesons	Corrected relative yield
340	75	100 percent
306	126	44 percent
272	46	19 percent
238	19	6 percent
204	3	0.8 percent
170	0	0 percent

* This work was performed under the auspices of the AEC.

C12. Temperature Dependence of Structure of Thin Silver Films.* GERALD W. JOHNSON, *State College of Washington.*—Single crystals of silver of thickness 100–1000A grown by thermal distillation of silver upon cleaved rocksalt single crystals were heat-treated at various temperatures in the range 100–500°C. Such films supported by the rocksalt substrate were examined optically under bright field illumination and polarized light at high magnification. No structural changes were noted up to 400°C. In the temperature range of 400–500°C structural changes took place whose nature depended upon the film thickness. For the thinnest films the formation of small nuclei occurred which were similar in appearance to the spherulites observed by Andrade and Martindale.[1] In films of intermediate thickness, rectangular holes appeared with the sides oriented along the 110 direction of the rocksalt. In still thicker films, systems of straight lines were observed which intersected at right angles and were directed along the 110 directions. In the thickest films (1000A) no changes were apparent. All films disintegrated at temperatures above 500°C. The formation of the holes and of the straight lines is attributed to local rupture of the film under tension arising from the difference in expansion of silver and rocksalt.

* Supported by ONR.
[1] E. N. Da. C. Andrade, and J. G. Martindale, Phil. Trans. Roy. Soc. 235 (A), 69 (1936).

C13. Surface Self-Diffusion of Silver on Thin Single Crystals.* GERALD W. JOHNSON AND T. WATANABE, *State College of Washington.*—Single crystals of silver of thicknesses in the range of 500–1000A were produced by thermal distillation of silver upon the surface of a freshly cleaved rocksalt single crystal using a technique similar to that of Brück.[1] Subsequently silver enriched with Ag^{110} was deposited in a strip across the previously deposited single crystal which gives then two single crystals in contact with the same orientation. The change in distribution of the radioactive silver was then measured as a function of temperature and time for films of different thicknesses. A scanner was constructed to permit the ready determination of the distribution without destroying the film. Diffusion coefficients will be given.

* Supported by ONR.
[1] v. L. Brück, Ann. d. Physik 26, 233 (1936).

E1. Experimental Method for Determining Relative Stopping Power.* JOHN G. TEASDALE, *University of California, Los Angeles. (Introduced by J. R. Richardson.)*—To make use of the small external proton beam (12 Mev) of the 37-in. cyclotron at UCLA for stopping power measurements, a differential ionization chamber and electrometer tube was used. The chamber is arranged so that ions having opposite sign coming from two sections are collected on the grid of a G.E. 5674 electrometer tube. If the beam is very near the end of its range in the differential chamber the grid current is sensitive to energy variations but not to intensity changes. Foils to be compared are alternately inserted into the beam and the thicknesses adjusted so that no change in grid current results from substitution. A sensitivity enabling detection of 0.1 ma/cm^2 at differences between foils has been used although a greater sensitivity is possible. At this sensitivity the background radiation from the cyclotron is of no consequence. A preliminary check of the relative stopping power per electron for silver, palladium, tantalum, gold, and platinum gives results higher than those reported by E. L. Kelly† (for example ten percent higher for silver). This is not inconsistent with the higher velocity of the particles used.

* This work was in part supported by the joint program of the ONR and AEC.
† E. L. Kelly, Phys. Rev. 75, 1006 (1949).

E2. Branching Ratio in Be^7 Decay. C. M. TURNER, *University of California, Berkeley.*—A new measurement has been made of the branching ratio in the K capture decay of Be^7 in which about 90 percent of the decays go directly to the ground state of Li^7 and about 10 percent[1] go to the 475 kev excited level with subsequent emission of a γ-ray. This ratio is of interest since it can give information about the selection rules effective in β-decay. The method used is as follows: (1) Geometrically identical samples of Be^7 and C^{11} are made with the proton beam from the Van de Graaff generator using the reactions $Li^7(p, n)Be^7$ and $B^{11}(p, n)C^{11}$. The ratio of activities induced in a manganese bath by the neutrons gives the ratio of the number of activated atoms in the two samples. (2) The targets containing the Be^7 and C^{11} are counted in

identical geometry with respect to a Geiger counter with sufficient absorber to convert the positrons from C^{11} decay to annihilation quanta. The annihilation quanta have essentially the same energy as the Be^7 decay quanta and serve to calibrate the counter. Preliminary results indicate that the ratio lies close to 0.1. This work was sponsored by the AEC.

[1] Phys. Rev. **54**, 657 (1938).

E3. Angular Distribution of 10.8 Mev Deuterons Scattered by Deuterons. E. J. STOVALL, JR., J. C. ALLRED, K. W. ERICKSON, AND J. L. FOWLER, *Los Alamos Scientific Laboratory.*—Cross sections for the elastic scattering of deuterons by deuterons have been measured for incident energy of 10.8 Mev at laboratory angles from 17.5° to 57° at 2.5° intervals. The deuteron beam from the Los Alamos cyclotron was focused on a thin target containing deuterium, and the scattered deuterons were detected in a proportional counter. A selsyn controlled foil shutter mounted in front of the counter prevented He^3, and H^3 at angles greater than 40°, from entering the counter. H^1, and H^2 at the smaller angles, were discriminated against by using a ten-channel pulse amplitude analyzer. Typical values of the elastic scattering cross section at 10.8 Mev in barns per unit solid angle are given in the table for several angles in the center of mass system. The standard error of these values is estimated to be ±3 percent. The experimental curve is symmetrical about 90° in the center of mass system.

θ	35°	40°	50°	60°	70°	80°	90°
σ	0.283	0.235	0.158	0.127	0.109	0.099	0.094

E4. On the Theory of Neutron Reflectors for Chain-Reacting Spheres.* G. M. VOLKOFF, *University of British Columbia.*—An expression for the fractional reduction ϵ in the critical radius of a homogeneous neutron multiplying sphere of multiplication constant $k>1$ due to an infinite reflector of multiplication constant $0\leq k'<1$ has been obtained on the basis of elementary neutron diffusion theory and of the following assumptions. The chain reaction is sustained by thermal neutrons. The scattering and slowing-down properties of the reflector are identical with those of the core at all neutron energies. The difference in the resonance escape probability within and outside the core affects only the values of k and k' but does not affect the slowing down process. The problem is formulated as an integro-differential equation which is solved by a method based on the Hopf-Wiener solution of Milne's integral equation. For a general model of the slowing-down process and in particular for the "age-velocity" model a formal approximate solution has been found valid from $k\approx 1$ up to high values of k. The approximation has been checked by finding the exact solution for a special ("synthetic kernel") model of slowing-down which in a certain limit reduces to the "age-velocity" model. The contributions to ϵ of thermal and of fast neutrons have been evaluated separately.

* Based on unclassified reports CRT 391 and 392 of the AEP, National Research Council, Chalk River, Ontario.

E5. Precision Measurement of Half-Lives.* LORNA M. SILVER, *University of British Columbia. (Introduced by G. M. Volkoff.)*—A number of decay periods have been measured using a differential ionization chamber with a vibrating reed condenser electrometer and feed-back amplifier. The sensitivity of this instrument enables the activity to be followed over 12 periods and hence permits the detection of, and correction for any weak long period background activity. The accuracy of the method for a simple decay, as estimated by the method of least squares, is about 0.4 percent. The whole apparatus was operated continuously in an underground room at fairly constant temperature and humidity. Periods of activated materials were found as follows:

Cu^{64}	12.88	±0.03 hr.
Cu^{66}	4.34	±0.03 min.
Ni^{65}	2.564	±0.005 hr.
Au^{198}	2.69	±0.01 days
In^{116}	53.93	±0.13 min.

* This work was carried out at the Chalk River Laboratories of the National Research Council.

E6. Absorption of Alpha-Particles in Gases.* G. G. EICHHOLZ AND N. J. HARRICK, *University of British Columbia.*—A shallow ionization chamber has been used to measure the range of alpha-particles from a thin Polonium source in gases at atmospheric pressure. A chamber of depth 3 mm was used with a preamplifier which formed an integral part of the assembly and preceded a balanced main amplifier. The stopping power of the gases relative to air was obtained from the extrapolated number-distance range using Holloway and Livingston's[1] value for air of 3.897 cm as standard. The following results were obtained:

Gas	Extrapolated range	Stopping power
Argon:	4.185±0.009 cm;	0.931
Deuterium:	16.509±0.029 cm;	0.236
Methane (C.P.):	4.556±0.010 cm;	0.853

* This work was supported by the National Research Council of Canada.
[1] Holloway and Livingston, Phys. Rev. **54**, 18 (1938).

E7. The Half-Life of the Positive π Meson. E. A. MARTINELLI, *University of California, Berkeley.*—Data for the half-life of the positive π-meson has been obtained using essentially the method employed by Richardson* for the determination of the half life of the negative π-meson. This consists of determining the decrease in number beyond geometrical factors of the mesons reaching 180° and those which reach 540° or 900° from the target. Simultaneous exposure of plates at 180° and at one of the other positions is accomplished by utilizing the helical paths of the mesons in the nearly uniform field of the cyclotron. The mesons are produced by proton bombardment of a carbon target in the 184-in. cyclotron. Several refinements in the method have been introduced which will enable the geometry of the apparatus to be determined to a higher degree of accuracy and also a third point on the decay curve will be determined. Preliminary scanning of the plates shows a half life in agreement with that of Richardson, within the statistics of track counting. This work was sponsored by the AEC.

* J. Reginald Richardson, Phys. Rev. **74**, 1720 (1948).

E8. $N-P$ Scattering Experiments at 280 Mev.* E. KELLY, C. LEITH, C. WIEGAND, *University of California, Berkeley.*—The total $n-p$ cross section and the angular distribution of the scattered protons have been studied with the same method used at 90 Mev.[1] The total cross section is approximately 0.03 barn. The angular distribution will be shown. It varies from about 0.013 barn per steradian at 180° to 0.002 barn per steradian at 90° in the cm system.

* The work described was sponsored by the AEC.
[1] J. Hadley *et al.*, Phys. Rev. **75**, 351 (1949).

E9. Nuclear Cross Sections for 95 and 270 Mev Neutrons (Measured with Bismuth Fission Chambers).* J. DEJUREN, N. KNABLE, B. MOYER, *University of California, Berkeley.*—Total and inelastic nuclear cross sections for 95 and 270 Mev neutrons have been measured using bismuth fission chambers. The 95 and 270 Mev neutrons are produced by bombarding a Be target with 190 Mev deuterons and 350 protons respectively in the 184-in. cyclotron. Total cross sections were measured using good geometry, and a special geometry was devised

so that inelastic and total cross sections could be measured simultaneously. The total cross sections of the elements measured from deuterium to tin at 270 Mev are all 0.57 to 0.58 times their values at 95 Mev. The ratio of inelastic to total cross sections was about 0.40 for heavy elements at 95 Mev. At 270 Mev, σ_i/σ_t is nearly 0.50 for both Cu and Pb, which is the value obtained for opaque nuclei at "low" neutron energies.

* This work was sponsored by the AEC.

E10. Total Cross Sections of Nuclei for 280 Mev Neutrons. R. Fox, C. Leith, K. McKenzie, L. Wouters, *University of California, Berkeley.*—The measurement of 280 Mev neutron cross sections of various nuclei will be described. The neutron beam used results from 350 Mev protons in the 184-in. cyclotron striking a 2-in. Be target. The neutron detector consists of a double coincidence anthracene scintillation counter telescope which counts recoil protons scattered at 15° from a paraffin cylinder placed in the collimated neutron beam. A 2-in. Cu absorber placed between the two counters assures that only protons of energy greater than 250 Mev are counted. The cross sections for all nuclei measured from Li to Pb are smaller than the corresponding cross sections measured at 90 Mev[1] by factors between 0.5 and 0.6. This work was sponsored by the AEC.

[1] Cook *et al.*, Phys. Rev. 75, 7 (1949).

E11. The Energy Dependence of Several Organic and Inorganic Counters. R. H. Davis and J. D. Graves, *Naval Radiological Defense Laboratory.*—The energy dependence of naphthalene, anthracene, stilbene, $CaWO_4$, KI(Tl), KBr(Tl), and the 1P21 photomultiplier tube has been determined in the energy ranges from 30 to 185 effective kv x-radiation and for radium gamma-radiation. The sensitivity of thalium activated potassium iodide shows a broad maximum in the energy range from 85 to 175 kv effective of about 40 times the gamma-ray sensitivity. Potassium bromide shows a sensitivity relative to the gamma-radiation of about 5 in the range from 45 to 190 kv effective, having a maximum of about 8 at 60 kv effective. Calcium tungstate is nearly energy independent in the region from 60 to 185 kv effective, having a sensitivity of about 16 relative to radium gamma-rays. Anthracene exhibits a generally increasing sensitivity relative to the gamma-radiation from about 1 to 3 in the energy region from 30 to 160 kv. In this same range the relative sensitivity of naphthalene increases from about 1 to 2 and that of stilbene from about 2 to 7. The response of the 1P21 relative to gamma-radiation is about 42 at 55 kv and decreases to about 5 at 190 kv.

E12. Temperature Dependence of a Scintillation Counter Using Several Organic and Inorganic Phosphors. G. E. Koch and J. D. Graves, *Naval Radiological Defense Laboratory.*—The temperature dependence of the gamma-counting efficiency of stilbene, calcium tungstate, thalium activated potassium iodide, and potassium bromide has been investigated in the region between −196°C and +50°C. The total current output from the 1P21 Photomultiplier was measured by metering the plate current in a direct coupled amplifier. The temperature and response for the end point and maxima and minima of the curves for these materials are shown in Table I using arbitrary response scales.

Table I.

Material	Temperature	Maximum	Minimum
Stilbene	−196°C		40 (end point)
	−100°C	225	
	+40°C		80 (end point)
Calcium Tungstate	−196°C		35 (end point)
	−30°C	110	
	+60°C		63 (end point)
Potassium Iodide	−76°C		50 (end point)
	−15°C	150	
	+35°C		100
	+50°C	145 (end point)	
Potassium Bromide	−76°C	63 (end point)	
	−35°C		40
	+60°C	100 (end point)	

E13. A Calibrated X-Ray Film Badge Dosimeter. E. Tochilin, R. H. Davis, J. Clifford, HMC, USN. (*Introduced by R. I. Condit.*)—An x-ray film badge dosimeter has been developed which will allow a quantitative interpretation of roentgen dose received for effective energies of 15 kv to 150 kv. The dosimeter is able to cover a range of intensities from 0.1 r to 2.0 r. Both duPont type 552 insensitive film and Eastman radiatized type DF-7 dental film have been calibrated for use with the dosimeter. The film is covered by an echelon of three metal shields plus an open window region. Tables are presented in which the ratio of film densities between two adjacent shields determine a factor which, when multiplied by the net density under a given shield, gives the radiation received directly in roentgen units. Data are also included which allow the dosimeter to be used to determine the effective energy of x-radiation, direct or scattered, striking the film badge. Proper processing of exposed film is accomplished by a one-point calibration check and consists of developing a pre-exposed "Density Standard" film for various developing times until a net density of 1.5 ± 0.15 is obtained. The films can be developed in any commercially available x-ray developer.

E14. The RCA 1P21 Photo-multiplier Tube as a Gamma-Ray Detector. J. D. Graves and G. E. Koch, *Naval Radiological Defense Laboratory.*—The characteristics of the 1P21 photo-multiplier tube used as a gamma-radiation detector have been studied. The response of the tube has been determined by metering the total current output. The range of radium gamma-intensities observed have been from 0.001 r to 100 r per hour. The response of the tube is linear throughout this range. The tube exhibits no directional dependence in the plane perpendicular to its axis. In the plane containing the axis of the tube a 28 percent variation in response is observed for a point source 40 cm from the tube. Minimum response occurs for the gamma source on the axis of the tube. A 0.6 percent per degree centigrade decrease in response is observed with increasing temperature in the region of room temperature. A one percent increase in applied voltage results in a 10 percent increase in response.

F1. A Portable High Intensity Magnet and Cloud Chamber for Use in Cosmic-Ray Research.* D. S. Potter, J. E. Henderson, C. E. Miller, and Jay Todd, Jr., *University of Washington.*—Two identical relatively light weight electro magnets with cloud chambers for use in high altitude cosmic-ray research have been constructed. The magnets can be used independently or in combination. The total weight including the frame-work is 5000 pounds, of which 2000 pounds is copper while the steel casing and core weigh 2000 pounds. This weight meets the requirement for use in a B-29 bomb-bay. At 10,000 gauss the current density is 5000 amperes per square inch in the copper, and the power consumption is 50 kw while at 8000 gauss the power consumption is 25 kw. The Joule heat is removed by oil flowing at 60 g.p.m. through each magnet. The temperature is regulated to within 0.01C° and the field is uniform to one percent over the entire illuminated region of the chamber. The 17-cm cloud chamber has an illuminated depth of 2.5 cm. Expansion takes place through a two-inch tube in the core of the magnet. The chamber is

photographed through a hole in the other core. The magnet and automatic chamber control units are conventional. To date this equipment has been utilized at sea level and 3.4 km at Climax, Colorado.

* Supported by Bureau of Ordnance, USN, under the technical supervision of the ONR.

F2. Cosmic-Ray Protons at 3.4 Km.* JAY TODD, JR., J. E. HENDERSON, C. E. MILLER, AND D. S. POTTER, *University of Washington.*—Of 18,000 counter-controlled cloud-chamber photographs taken at Climax, Colorado (elevation 3.4 km) at field strengths of 8,000 and 10,000 gauss, approximately 200 protons which are unaccompanied by other time-coincident tracks have been identified (by means of ionization and momenta). In addition, about a fifth as many protons accompanied by one or more lightly ionizing time-coincident particles have been found. With no absorber above the chamber single identifiable proton tracks constitute two percent of all single tracks. Since the momentum spectrum is not distorted above 350 Mev/c by failure of the protons to trip the lower counter, and the ionization below 500 Mev/c is sufficiently high to make identification fairly certain, this interval provides a good basis for estimating the percentage of protons in the penetrating component in this momentum range. This value is estimated to be about ten percent.

* Supported by Bureau of Ordnance, USN, under the technical supervision of the ONR.

F3. The Penetrating Component of Cosmic-Rays at 3.4 Km.* C. E. MILLER, J. E. HENDERSON, D. S. POTTER, JAY TODD, JR., *University of Washington.*—Using the knowledge of the momentum spectrum of protons and the momentum spectrum of all ionizing particles, an analysis of the penetrating component of cosmic rays at 3.4 km into protons and mesons can be made. A momentum spectrum for all ionizing particles similar to that found by Adams *et al.* at 30,000 feet has been found. A meson maximum has been found at a momentum of about 500 Mev/c, which is about the value of the proton peak of reference 1. The 3.4-km data indicate a proton peak at a higher momentum. The protons which form the strong maximum at about 500 Mev/c at 30,000 feet would be absorbed before reaching 11,000 feet (neglecting production). This interpretation of the 3.4 km no-lead absorber spectrum is also consistent with our results obtained under absorbers of 5 and 20 cm of lead.

[1] R. V. Adams *et al.*, Rev. Mod. Phys. **20**, 334 (1948).
* Supported by Bureau of Ordnance, USN, under the technical supervision of the ONR.

F4. A Precision Determination of the Energy of the 1.1 and 1.3 Mev Gamma-Radiations from Co^{60} by Direct Crystal Diffraction. D. A. LIND, J. R. BROWN, J. W. M. DUMOND, *California Institute of Technology.*—Recent improvements in the focusing curved crystal gamma-ray spectrometer have extended its energy range and yielded much better luminosity and resolving power than obtained initially. These are: (1) new crystal holder—aperture 1.7×2 inches, focal length 196 cm, resolution 0.05 x.u. giving twofold gains in both luminosity and resolving power; (2) new collimator—24 die-cast tapering lead partitions 30 inches long with 25 tapering spacers, thickness of both partitions and spacers 40 mils at entry end. Geometrically this can accept the diffracted beam and block the transmitted beam for angular differences between them as small as 8 minutes giving a calculated (theoretical) upper working limit of 3 Mev, a threefold improvement over previous collimator. Wave-lengths and energies of two gamma-rays emitted following β-decay of Co^{60} have been measured with this new equipment using a source of 50 mc and found to have values of 9.308 x.u. $\pm$0.005 and 10.580 x.u. $\pm$0.005 corresponding to 1.3316$\pm$0.0010 Mev and 1.1715$\pm$0.0010 Mev, respectively. The lines appear to have equal intensities. The integrated reflection coefficient of the (310) planes of the curved quartz crystal appears to follow a λ^2-dependence on wavelength down to 9 x.u., the shortest so far observed.

F5. Study of Ions Formed in a Hg Resonance Cell Containing N_2. R. H. BROWN, *University of Washington.*—When sufficiently pure N_2 is admitted into a Hg resonance cell excited by unreversed λ2537, ions may be formed in sufficient quantity to produce image forces of several dynes/cm^2 on a metal foil. The foil forms one plate of a capacitor in an IF bridge which permits detection of a shift of as little as 0.2A in the average position of the foil. By illuminating with λ2537 from a pulsed RF-excited electrodeless Hg discharge, ion decay data are obtained. The observed image forces are a maximum for roughly 12 cmHg of N_2. On extinction of the exciting radiation the square root of the image force decays exponentially for less than one cmHg of N_2 and hyperbolically for greater than four cmHg of N_2. The exponential decay constants conform with diffusion to the walls as the principal means of ion decay. The image forces are directly proportional to the intensity of the exciting radiation, appear only when ions are formed at a metal surface in the cell, and are unobservable unless great precautions are taken to remove H_2 and H_2O from the N_2. The linear force relationship and the hyperbolic decay have not been satisfactorily accounted for.

F6. Work Functions of Gas-Coated Silver Surfaces. G. L. WEISSLER AND T. N. WILSON, *University of Southern California.*—Average electronic work functions of silver surfaces, subjected to glow discharges in various gases, were determined by a method first suggested by C. W. Oatley.[1] The procedure used was similar to the one described earlier for gas coated surfaces of Ta and W.[2] By measuring the contact potential between a cold cylinder and a concentric hot W-filament one can obtain the work function of the cylinder surface assuming the filament has a known work function. When the cylinder surface was subjected to glow discharges in various gases, positive or negative ions were driven onto the surface and formed a gas film over a vacuum evaporated silver layer. Results will be presented for the following gas treatments: Ag+He; Ag+A; Ag+N_2; Ag+H_2; Ag+O_2; Ag+H_2O; Ag+Freon 12. Oxygen and freon, both forming negative ions, produced the most significant changes in work functions by increasing them by about 1.4 ev. Gas films of these gases seemed very stable even to strong positive ion bombardment with A or He;—both N_2 and H_2 showed a decrease of the work function by a few tenths ev, whereas A and He did not seem to affect the surface. Water vapor, when admitted to the baked-out system on a freshly prepared Ag layer, showed a slight increase in the work function. Further work on Au and other surfaces is in progress.

[1] C. W. Oatley, Proc. Phys. Soc. London, **51**, 318 (1939).
[2] G. L. Weissler and R. W. Kotter, Phys. Rev. **73**, 538A (1948).

F7. Thermal Noise at Very High Frequencies. A. VAN DER ZIEL, *University of British Columbia.*—In his well-known paper on thermal noise Nyquist[1] found for the available noise power P_a in a frequency interval $\Delta\nu$:

$$P_a = kT\Delta\nu.\quad \frac{h\nu}{kT}(e^{h\nu/kT}-1)^{-1},$$

from thermodynamical considerations. L. Burgess[2] found the same formula for the available noise energy of an antenna enclosed in a hollow sphere of uniform temperature T. It will be shown that the latter result can be obtained from a very simple argument. From the electron theory Spenke[3] found $P_a = kT\Delta\nu$ even for frequencies for which $h\nu/kT \geqq 1$; it will be shown that this is due to the fact that the interaction between

the motion of the electrons in the lattice and the lattice vibrations was not fully taken into account.

[1] H. Nyquist, Phys. Rev. **32**, 110 (1928).
[2] R. Burgess, Proc. Phys. Soc. **53**, 293 (1941).
[3] E. Spenke, Wiss. Veroff Siemens Werken **18**, 55 (1939).

F8. Some Results in the Scattering Theory of the Dirac Equation. G. PARZEN, *Stanford University.*—While treating the problem of investigating the charge distribution in heavy nuclei by means of 1 Bev electron scattering, the following results have been obtained. Let $g_L(r)$, $f_L(r)$ be the radial parts of the wave function,[1] $g_L(r) \to \cos(kr+\eta_L) = \sin(kr - L\pi/2 + \delta_L)$, and let $g_L(r) = (E^2+1)^{\frac{1}{2}} S_L + \bar{S}_L$, $f_L(r) = (E^2-1)^{\frac{1}{2}}(S_L - \bar{S}_L)/i$, then an approximate expression for the phase shifts equivalent to the Born Approximation is (in relativistic units) $(e^{2i\delta_L}-1)/2i = \frac{1}{2}(E+1)(\Delta_L + k^2/(E+1)^2 \cdot \Delta_{L+1})$ and $(e^{2i\delta_{-L-1}}-1)/2i = \frac{1}{2}(E+1)(\Delta_L + k^2/(E+1)^2 \cdot \Delta_{L-1})$, where $\Delta_L = -2k\int_0^\infty j_L^2(kr) V(r) r^2 dr$. By means of a variational principle, two other approximate expressions f or η_L were found. Let s_L, $\bar{s}_L$ be solutions for the potential $V_0(r)$ with the phase shifts η_L^0, then we have $\eta_L - \eta_L^0 = -(E/k)\cdot\int_0^\infty (V-V_0)(s_L\bar{s}_L + (s_L^2+\bar{s}_L^2)/2E) dr$. This result for $V_0(r) \equiv 0$, reduces to the BA except that $(e^{2i\delta_L}-1)/2i$ is replaced by δ_L. A second variational result is

$$\eta_L - \eta_l = a\sin\varphi - a\sin(2(\eta_l - \eta_L^0) + \varphi) - (E/k)\int_0^\infty (V-V_0)(s_L\bar{s}_L + (s_L^2+\bar{s}_L^2)/2E) dr,$$

where $ae^{i\varphi} = \int_0^\infty ((L+1)/r + iV/k) s_L^2 dr$ and $\cos(2(\eta_l - \eta_L^0) + \varphi) = 1/2a$. For high energies the two variational results approach each other.

[1] N. F. Mott, Proc. Roy. Soc. 124, 426 (1929).

F9. Potential and Gradient Distributions in Parallel Plane Diodes at Currents below Space Charge Limited Values. WILSON M. BRUBAKER, *Westinghouse Research Laboratories.*—The equations for electron motion in a plane diode under the influence of space charge are integrated. The solution is expressed in terms of four dimensionless numbers, normalized so that their range is from zero to unity. The gradients at the cathode and at the anode are expressed as functions of the current density as it varies from zero to space charge limited values. Space distributions of potential and gradient are given in terms of the location of the plane of interest between the cathode and the anode for a number of specific current densities. Evidence is shown of the existence of a plane for which the gradient is essentially independent of the current density.

F10. A Logical Extension of the Field Equations of General Relativity. CORNELIUS LANCZOS, *National Bureau of Standards* and *University of California, Los Angeles.*—Consider a Riemannian space, controlled by an action principle which is quadratic in the curvature components. The resultant field equations, if expressed in the g_{ik}, are complicated differential equations of fourth order, and the objection can be raised that simpler invariant field equations of only second order—the Einsteinian field equations—may be found. The same variational problem is now approached from a modified mathematical angle, considering the curvature components R_{iklm} as the basic field quantities. The resulting algebraic minimum problem is restricted by the Bianchi identity, which in specifically four dimensions takes the form of a divergence equation. The method of the Lagrangian multiplier gives rise to a new field tensor of third order $H_{ik}^{\ m}$, antisymmetric in i, k, in remarkable analogy to the curvature tensor $\Lambda_{ik}^{\ m}$ of Einstein's theory of "distant parallelism." The resultant field equations are now of only second order and appear as a generalized system of gravitational equations. The Einsteinian field equations represent a special subclass of the general solution. The place of electromagnetism in this theory cannot be decided without studying the behavior of the fields of second order. The present investigation does not go beyond the first order approximation.

F11. An Electrodynamic Examination of the Hydrogen Atom. DAN MCLACHLAN, JR., *University of Utah.*—In an attempt to devise a classical model of the hydrogen atom which fulfills two requirements, (a) only discreet energy states are stable, and (b) energy is not lost by radiation while in a stable state, it is assumed that the positive and negative charges are mutually sources and sinks for one another's radiation. It is assumed that the variation of the effective index of refraction in the space between the charges is such as to focus the radiation from one charge to its partner. The two conclusions deduced from this model are (a) the optical path lengths between the electron and the proton in the hydrogen atom are restricted to multiples of one-half wave-length of the standing wave between them, and (b) the high indexes of refraction required for focusing results in an elongation of the standing waves by a factor in the neighborhood of 2000 upon escape from the atom into free space. Since the introduction of this concept of index is the chief contribution, methods for calculating it are described using a doublet to explore the field.

F12. On the Theory of the Establishment of Flow in Water Entry.* EUGENE P. COOPER, *U. S. Naval Ordnance Test Station, Pasadena Annex.*—When a solid object passes across an air-water interface, a complex flow, whose most obvious manifestation is the phenomenon of splash, is established in the water. The mathematical description of this flow-establishment involves potential theory primarily. However, classical potential theoretic methods are not directly applicable because the requirement that the pressure be constant at the water surface is, in terms of velocity potential, only an implicit boundary condition. A particular type of entry situation is considered, namely, oblique entry of a half-plane of infinite inertia. An attempt is made to obtain an approximate solution in the form of a time-parametric steady state solution. This attempt is shown to lead to divergences. The transient nature of the phenomenon must be explicitly included in the mathematical description. Methods are developed for solving the problem by iterative numerical procedures. The most important characteristics of the observed flow are shown to be in good agreement with the theory.

* This investigation was supported by the ONR.

F13. Infra-Red Studies with the Perkin-Elmer Spectrometer. A. M. CROOKER, *University of British Columbia.*—A comparison has been made between the different methods of calibrating a model 12-B Perkin-Elmer spectrometer to the NaCl limit at 15 μ. There appears to be a small shift in calibration probably due to temperature variation, so that for accurate frequency determinations one must calibrate the unknown absorption frequencies from internal standards. Experience with several calibration procedures indicates that a power series with cubic terms can be fitted to the internal standards rapidly and with residuals of the order of the reproducibility of instrument readings. Results on observations in the absorption spectra of CS_2 and the isomers of decalin will be presented.

F14. Handedness in Space-Time and the Nature of Magnetic Poles. M. AVRAMY MELVIN, *Eastsound, Washington.*—Handedness transformations, or odd numbers of reversals of the base vectors of a standard set, in 3+1 dimensional space-time fall naturally into four types: two reducing to the familiar mirrorings, and inversions through a point, of pre-relativistic physics; and the other two involving reversal of time components of space-time objects. Since ordinary regions of space-time are free from any intrinsic handedness (except possibly for

time-asymmetry), any physical theory should be invariant under handedness transformations (except possibly for time-reversals). Dirac's new theory of magnetic poles is not at all handedness-invariant. In trying to set up a theory of unisolated atomistic particles, which yet have statistical macroscopic manifestations, we may be able to make symmetry deductions from the latter. This is the case with the theory of magnetic poles: To insure handedness-invariance, one or the other, charges or poles, in the Maxwell-Heaviside equations with which the theory begins, must have pseudoscalar symmetry. What is pseudoscalar is also determinate. Reviving, in relativistic form, an old argument of Curie and Voigt from the general Symmetry Principle and phenomena in crystal physics, it is shown that the magnetic pole is the pseudoscalar entity.

Author Index to Papers Presented at the Seattle Meeting

Becker, G. E., and D. A. Caswell—No. C6
Bishop, A. S., H. Bradner, and F. M. Smith—No. C10
Bloch, F., and David H. Garber—No. A4
Bradner, H., A. S. Bishop, and W. H. Barkas—No. C9
Brown, R. H.—No. F5
Brubaker, Wilson M.—No. F9
Burkig, J. W. and J. Reginald Richardson—No. C2
Chao, C. Y., C. C. Lauritsen, and A. V. Tollestrup—No. C3
Cooper, Eugene P.—No. F12
Crooker, A. M.—No. F13
Davis, R. H. and J. D. Graves—No. E11
Duncan, D. B.—No. C4
DeJuren, J., N. Knable, and B. Moyer—No. E9
Eichholz, G. G. and N. J. Harrick—No. E6
Feynman, R. P.—No. B1
Fleeman, J. and H. H. Staub—No. C1
Fowler, W. A.—No. D1
Fox, R., C. Leith, K. McKenzie, and L. Wouters—No. E10
Goldberger, M. L.—No. B4
Graves, J. D. and G. E. Koch—No. E14
Hildebrand, R. H. and C. E. Leith—No. C8
Jacobsohn, B. A.—No. A2
Johnson, Gerald W.—No. C12
Johnson, Gerald W. and T. Watanabe—No. C13
Jones, Stanley B. and R. Stephan White—No. C11
Kash, S. and J. Kaplan—No. A1
Kelly, E., C. Leith, and C. Wiegand—No. E8
Koch, G. E. and J. D. Graves—No. E12
Lanczos, Cornelius—No. F10
Laporte, Otto—No. G4
Lind, David A.—No. D4
Lind, D. A., J. R. Brown, and J. W. M. DuMond—No. F4
Lofgren, E. J.—No. C7
McKellar, Andrew—No. D2
McLachlan, Jr., Dan—No. F11
Margenau, Henry—No. A7
Martin, L.—No. A11
Martinelli, E. A.—No. E7
Melvin, M. Avramy—No. F14
Miller, C. E., J. E. Henderson, D. S. Potter, Jay Todd, Jr.—No. F3
Moyer, Burton J.—No. B2
Panofsky, Wolfgang K. H.—No. B3
Parzen, G.—No. F8
Peck, Edson—No. G1
Perry, J. E.—No. G3
Potter, D. S., J. E. Henderson, C. E. Miller, and Jay Todd Jr.—No. F1
Roberts, Walter O.—No. G2
Rogers, E. H. and H. H. Staub—No. A5
Schardt, A. W., E. J. Woodbury, and W. A. Fowler—No. C5
Schmidt, F. H.—No. A10
Shaw, T. M. and J. J. Windle—No. A9
Silver, Lorna M.—No. E5
Stovall, Jr., E. J., J. C. Allred, K. W. Erickson, and J. L. Fowler—No. E3
Taschek, R. F.—No. D3
Teasdale, John G.—No. E1
Tochilin, E., R. H. Davis, and J. Clifford—No. E13
Todd, Jay, Jr., J. E. Henderson, C. E. Miller, and D. S. Potter—No. F2
Turner, C. M.—No. E2
Uehling, E. A.—No. A3
van der Ziel, A.—No. F7
Van Vleck, J. H. and Henry Margenau—No. A6
Volkoff, G. M.—No. E4
Weissler, G. L. and T. N. Wilson—No. F6
Zucker, F. J.—No. A8